

CRANFIELD UNIVERSITY

Mehmet Akarcay

An Experimental Study on Oil-Water Slug Flow in Export  
Pipelines with Shallow Inclined Elevations

School of Water, Energy and Environment (SWEE)  
Energy and Power

PhD

Academic Year: 2019 – 2022

Supervisor: Dr Liyun Lao  
Associate Supervisor: Dr Patrick Verdin

August 2022

CRANFIELD UNIVERSITY

School of Water, Energy and Environment (SWEE)  
Energy and Power

PhD  
Academic Year: 2019 – 2022

Mehmet Akarcay

An Experimental Study on Oil-Water Slug Flow in Export  
Pipelines with Shallow Inclined Elevations

Supervisor: Dr Liyun Lao  
Associate Supervisor: Dr Patrick Verdin  
August 2022

This thesis is submitted in partial fulfilment of the requirements  
for the degree of PhD in Energy and Power

© Cranfield University 2022. All rights reserved. No part of this  
publication may be reproduced without the written permission of  
the copyright owner.

---

# ABSTRACT

The present study aims to better understand liquid-liquid intermittent flow regimes under different operational and flow conditions, such as flowrates of fluids, pipe inclination and fluid properties, with a focus on the pipe inclination alternating between  $0^\circ$  and  $+5^\circ$ . A  $0.0254m$  diameter pipe loop multiphase flow rig was utilised to conduct the experimental study. The fluids used for tests were tap water ( $\rho_w = 997kg/m^3$  and  $\mu_w = 1mPa.s$  under the normal temperature and pressure (i.e. NTP,  $15^\circ C$  and  $1atm$ ) with an oil. Two different oils, EDM250 ( $\rho_o = 811kg/m^3$  and  $\mu_w = 7mPa.s$  under the NTP) and H100 ( $\rho_o = 878kg/m^3$  and  $\mu_w = 423mPa.s$  under the NTP) were used for tests to cover the variations in density and viscosity. It was found that less dense and viscous oils are less likely to develop intermittent flow regimes than heavier oils. In addition, regardless of the oil type present, intermittent flows are more likely to develop in a pipe with a higher degree of upwards inclination. This is particularly more effective for lighter oils because the inclination factor alters the angle between multiphase flow direction and gravity. This, in turn, aids the oil phases to intrude into the water phase region to have a greater prospect of developing and widening the relevant flow regimes envelopes such as slug and plug flows. Additionally, this thesis also proposes a modified liquid-liquid flow regime grouping method based on the modified Froude numbers. The proposed dimensionless parameter takes water hold-up variables into consideration by defining the hydraulic diameter to coincide with each phase's gravitational and inertial forces. Furthermore, correlations of pressure gradient and hold-up are also developed and presented. The developed models are then implemented with a dimensionless scale-up protocol to demonstrate scaling across laboratory experimental data generated from systems with different pipe diameter sizes. Overall, the models developed show improved performance for grouping flow patterns consistently, hence allowing for better prediction of liquid-liquid flow regimes that transition between intermittent flows. The significant outcomes of this project are the following: (1) evidence of intermittent flow regimes existing across a wide range of dual-incompressible multiphase flow conditions, (2) the development of design charts for pipelines that consider the prevention of intermittent flow regimes and (3) utilising the proposed hold-up and pressure gradient correlations with a scale-up protocol to predict larger pipeline behaviours.

## **Key Words:**

Oil-Water Flow; Dual Incompressible; Multiphase Flow; Liquid-liquid Flow; Slug Flow; Plug Flow; Intermittent Flow; Scale-up; Flow Regime Grouping; Pressure Correlation; Hold-up Correlation; Froude Number.

---

# ACKNOWLEDGEMENTS

This work has been undertaken within the Consortium on Transient and Complex Multiphase Flows and Flow Assurance (TMF). The author acknowledges the contributions made to this project by ASCOMP, BP Exploration; Cameron Technology & Development; CD adapco; Chevron; KBC (FEESA); FMC Technologies; INTECSEA; Granherne; Institutt for Energiteknikk (IFE); Kongsberg Oil & Gas Technologies; MSi Kenny; Petrobras; Schlumberger Information Solutions; Shell; SINTEF; Statoil and TOTAL. The author is particularly grateful to BP Exploration for sponsoring this project. A general thank you to all family, friends and university peers for supporting the author through this PhD journey for the past three years. All your love and support will neither go unrepaid nor forgotten.

## **Special Individual Acknowledgements:**

Liyun Lao:

To my initial supervisor for this project, you have guided me and helped me to become a better researcher and engineer. Your patience, enthusiasm and love for science have been an inspiration, which I will use as a foundation for my work in the future.

Patrick Verdin:

To my secondary supervisor for this project, it has been a pleasure knowing you, and I could not have asked for a better second supervisor. Your understanding and knowledge of multiphase flow have been invaluable and a significant aid in completing this project.

Stan Collins:

To the PSE laboratory manager, with your years of experience, you have supported the project's experimental set-up, data collection and analysis, which have been a fundamental boost for my development as a researcher.

Sudem Devecioğlu:

To my darling fiancé, your constant support over the last few years has been amazing. Your smile always gives me that extra bit of motivation to keep going. Please never stop smiling. I love you.

---

# TABLE OF CONTENTS

ABSTRACT.....	II
ACKNOWLEDGEMENTS .....	III
TABLE OF CONTENTS .....	IV
LIST OF FIGURES.....	VII
LIST OF TABLES .....	XV
NOMENCLATURE.....	XVII
ABBREVIATIONS.....	XXII
CHAPTER 1 – INTRODUCTION.....	1
1.1 Research Background .....	3
1.1.1 Key Studies of Liquid-Liquid Flow in Pipes.....	5
1.1.2 Previous Experimental Work from Cranfield University.....	7
1.2 Project Motivation and Objectives.....	8
1.3 Thesis Structure .....	9
CHAPTER 2 – LITERATURE REVIEW.....	11
2.1 Key Oil-Water Flow Parameters and Definitions in Pipes .....	13
2.1.1 Phase Hold-up and Phase Volume Fraction.....	14
2.1.2 Phase Velocity and Slip.....	16
2.1.3 Mixture Parameters .....	18
2.1.4 Forces Acting on Droplets.....	20
2.1.5 Physical Oil Properties .....	23
2.2 Multiphase Flow Measurements .....	25
2.2.1 Density Measurements .....	28
2.2.2 Velocity Measurements.....	30
2.2.3 Momentum Flux Measurements.....	32
2.2.4 Mass Flowrate Measurements.....	33
2.3 Flow Regimes .....	35
2.3.1 Oil-Water Stratification of Layers and Mixtures .....	39
2.3.2 Oil-Water Emulsions.....	40
2.4 Phase Inversion.....	41
2.5 Oil-Water Pressure Gradients and Frictional Losses .....	44
2.5.1 Empirical Correlations .....	44
2.5.2 Flow Pattern Based Correlations.....	47

---

2.5.3 Two Fluid Flow Model .....	48
2.6 Controllable Parameter Influences.....	51
2.7 Dimensionless Flow Regime Maps.....	53
2.8 Previous Experimental Work on Liquid-Liquid Flow .....	56
2.8.1 Liquid-liquid Slug Flow with Horizontal Pipe Configuration .....	56
2.8.2 Summary of Horizontal Liquid-Liquid Intermittent Flows.....	78
2.8.3 Liquid-liquid Slug Flow with Orientated Pipe Configuration.....	80
2.8.4 Summary of Orientated Liquid-Liquid Intermittent Flows .....	83
CHAPTER 3 – METHODOLOGY AND EXPERIMENTAL SET-UP .....	85
3.1 Experimental Set-Up for 1-Inch Pipe Loop.....	85
3.1.1 Oil System.....	86
3.1.2 Water System .....	87
3.1.3 Air System.....	87
3.1.4 Liquid Cooling and Heating.....	87
3.1.5 Fluid Separation .....	87
3.1.6 Multiphase Flow Test section and Inclination .....	88
3.1.7 Data Acquisition.....	88
3.2 Experimental Procedure and Runs.....	89
3.3 Experimental Checks and Validity .....	91
3.3.1 Fluid Properties .....	91
3.3.2 Data Signals and Calibration.....	94
3.3.3 Single-Phase Flow Testing.....	96
3.3.4 Uncertainties .....	97
3.3.5 Flow Regime Identification.....	98
CHAPTER 4 – EXPERIMENTAL RESULTS.....	99
4.1 Flow Regime Mapping .....	99
4.2 Hold-up Analysis .....	102
4.3 Pressure Gradient Analysis .....	107
4.4 Intermittent Flow Analysis .....	109
4.5 Superimposing Flow Regime Maps.....	116
4.6 Intermittent Frequency Analysis.....	119
4.7 Summary of Results.....	123
CHAPTER 5 – DEVELOPMENT OF CORRELATIONS.....	124
5.1 Pressure Gradient Correlation.....	124

---

5.1.1	Examples of Current Pressure Gradient Models .....	124
5.1.2	Mathematical Development of New Pressure Gradient Model.....	127
5.1.3	Dimensional Analysis of Pressure Gradient Model .....	129
5.1.4	Pressure Gradient Model Comparison in Literature.....	130
5.2	Hold-up Prediction.....	131
5.2.1	Example of Current Hold-up Model .....	131
5.2.2	Mathematical Development of New Hold-up Model.....	132
5.2.3	Hold-up Comparison in Literature .....	136
5.3	Correlation Limitations.....	137
CHAPTER 6 – DIMENSIONLESS GROUPING .....		138
6.1	Mathematical Development of Grouping Model.....	138
6.2	Grouping Experimental Data .....	141
6.3	Grouping Literature Data.....	143
6.4	Grouping Limitations.....	144
CHAPTER 7 – SCALE-UP ANALYSIS .....		145
7.1	Scale-Up Methodology .....	145
7.2	Prototype Scaling.....	148
7.2.1	2-Inch Pipe Scaling .....	149
7.2.2	Industrial Pipe Scaling .....	152
7.3	Literature Data Scaling .....	154
CHAPTER 8 – CONCLUSION.....		157
8.1	Main Conclusions .....	157
8.2	Contribution to Knowledge.....	159
8.3	Attainment Against Objectives .....	160
8.4	Key Limitations of Work.....	161
8.5	Future Work.....	162
REFERENCES.....		164
APPENDICES.....		174

---

# LIST OF FIGURES

<i>Figure 1-1: Thesis chapter structure outline in chronological order.</i> .....	9
<i>Figure 2-1: Depiction of oil-water co-current and counter-current flow from varying boundary conditions that cause the two behaviours to occur.</i> .....	12
<i>Figure 2-2: Typical co-current two-phase flow in a pipeline between a heavier and lighter fluid phase <math>\alpha</math> and/or <math>\beta</math> (depicted example as - oil-water flow).</i> .....	13
<i>Figure 2-3: Laminar and turbulent flow patterns with Reynolds number transition from laminar to turbulent fluid flow within pipes.</i> .....	19
<i>Figure 2-4: External forces acting upon a liquid droplet within a flow.</i> .....	20
<i>Figure 2-5: Internal forces acting in a liquid droplet within a flow.</i> .....	20
<i>Figure 2-6: The four routes to multiphase flow metering. Adapted from (Falcone, Hewitt and Alimonti, 2009).</i> .....	26
<i>Figure 2-7: (a) Route 1 example of multiphase flow metering, (b) route 2 examples of multiphase flow metering and (c) route 3 examples of multiphase flow metering. Adapted from (Falcone, Hewitt and Alimonti, 2009).</i> .....	27
<i>Figure 2-8: A schematic example of a broad-beam gamma densitometer being used to measure fluid density from a section of pipe. Adapted from (Falcone, Hewitt and Alimonti, 2009).</i> .....	28
<i>Figure 2-9: A schematic example of (a) Strip type electrodes and (b) Ring type electrodes are used to identify the impedance of flow to measure fluid density from a section of pipe. Adapted from (Falcone, Hewitt and Alimonti, 2009).</i> .....	29
<i>Figure 2-10: An example of a typical set-up for the radioactive tracking method to measure velocity. In the flow measuring system; <math>I</math>, <math>M_1</math> and <math>F_2</math>, the detectors <math>F_1</math> and <math>F_2</math> are fixed. In the set-up, <math>I</math>, <math>M_1</math> and <math>M_2</math>, <math>M_2</math> is fixed but <math>M_1</math> can have its position varied. <math>I</math>, <math>F_1</math> and <math>F_2</math> control the systems for <math>I</math>, <math>M_1</math> and <math>M_2</math>. The Adapted from (Clayton, Clarke and Ball, 1960).</i> .....	31
<i>Figure 2-11: Cross-sectional internal schematic of a TMFM circulatory pump. Adapted from (John, Reimann and Müller, 1984).</i> .....	33
<i>Figure 2-12: Set-up for gyroscopic/Coriolis system (Smith, 1978).</i> .....	34
<i>Figure 2-13: Liquid-liquid flow regime criteria.</i> .....	36
<i>Figure 2-14: Cross-sectional analysis on three extremes of the same flow pattern type between oil-water two-phase flows. Adapted from (Vedapuri, Bessette and Jepson, 1997).</i> .....	39
<i>Figure 2-15: Types of oil-water emulsions; oil-in-water (O/W), water-in-oil (W/O) and water-in-oil-in-water (W/O/W) found within the petroleum industry (Martínez-Palou et al., 2011).</i> .....	40



---

<i>Figure 2-16: Viscosity vs percentage of continuous phase for water emulsions within oil-water multiphase flow. Adapted from (Escojido, Urribarri and Gonzalez, 1991).</i> .....	41
<i>Figure 2-17: Inversion processes for oil-water dispersion flow (Arirachakaran et al., 1989)</i> ...	42
<i>Figure 2-18: Schematic description of forces acting on a smooth oil-water two-phase flow system in a stratified flow regime within a horizontal or inclined concentric pipe.</i> .....	50
<i>Figure 2-19: Parameter flow chart of variables grouped within three sections that effect multiphase flow regimes. Flow regimes are mainly influenced by variables that are grouped from pipeline design, fluid properties and operational inputs.</i> .....	52
<i>Figure 2-20: Drawings of experimental results that contain oil with a viscosity of <math>\mu_o = 16.8\text{mPa.s}</math> flowing simultaneously with water of equal density while under the influence of alterations of superficial oil velocity <math>v_{so}</math> as the water superficial velocity <math>v_{sw}</math> is maintained at (a) low fixed velocity of <math>v_{sw} = 0.0305\text{m/s}</math> (b) medium fixed velocity of <math>v_{sw} = 0.208\text{m/s}</math> and (c) high fixed velocity of <math>v_{sw} = 0.622\text{m/s}</math>. Adapted from (Charles, Govier and Hodgson, 1961).</i> .....	57
<i>Figure 2-21: Summary of flow regime transitions for oil-water flow in a 1-inch diameter pipe with equal density and oil viscosities of (a) <math>\mu_o = 6.29\text{mPa.s}</math> and <math>\mu_o = 16.8\text{mPa.s}</math>, and (b) <math>\mu_o = 65.0\text{mPa.s}</math>. Oil and water velocities are represented on a logarithmic plot and singular lines are drawn to represent the regions of the flow regimes. Adapted from both (Charles, Govier and Hodgson, 1961) and (Ibarra, 2017).</i> .....	58
<i>Figure 2-22: Flow regime and transition maps as a function of the oil and water volumetric flowrates under three different internal pipe wall conditions; (top section) freshly cleaned pipeline, (middle section) non-freshly cleaned pipeline and (bottom section) hydrophobic pipe. As maps on the left represent the flow conditions that are 0.02m from the pipe inlet and maps on the right represent the flow conditions 0.2m from the pipe inlet. Adapted from (Hasson, Mann and Nir, 1970)</i> .....	60
<i>Figure 2-23: Experimental results for a liquid-liquid system with oil properties of <math>\mu_o = 21.7\text{mPa.s}</math> and, <math>\rho_o = 896\text{kg/m}^3</math> in a <math>D = 0.0394\text{m}</math> pipe in the form of a flow regime map. Conducted by (Guzhov et al., 1973), revisited and adapted from (Oglesby, 1979).</i> .....	61
<i>Figure 2-24: Experimental results for a liquid-liquid system with oil properties of <math>\mu_o = 84\text{mPa.s}</math> in a <math>D = 0.041\text{m}</math> pipe. Adapted from (Oglesby, 1979).</i> .....	63
<i>Figure 2-25: Flow regime map for experimental results of a horizontal pipe of <math>D = 0.0381\text{m}</math> containing oil-water flow with <math>\mu_o = 84\text{mPa.s}</math>. Adapted from (Arirachakaran et al., 1989).</i> .....	65
<i>Figure 2-26: A schematic description of observed experimental flow regimes and how individual superficial phase velocities of kerosene and water cause the transition between each flow regime. The horizontal arrows signify an increase in the kerosene velocity as a vertical arrow represents an increase in the water velocity. The size of the boxes that contained each flow regime is an estimated representation of the range found from the experiment. Adapted from (Raj, Chakrabarti and Das, 2005).</i> .....	67

---

<i>Figure 2-27: Experimental results of kerosene (oil)-water flow within a 2.13m long acrylic pipe of an internal diameter of 0.0254m, where water is assumed to be of standard fluid properties and <math>\mu_o = 1.2\text{mPa.s}</math> and <math>\rho_o = 787\text{kg/m}^3</math> as the overall phase velocity range was between 0.03-1.6m/s. Adapted from (Raj, Chakrabarti and Das, 2005).</i>	67
<i>Figure 2-28: Multiple experimental results superimposed on a single velocity graph comparing the original flow regimes without DRP within the flow line and the effects of flow regimes when using DRP under 20ppm and 50ppm injection rates. Adapted from (Al-Wahaibi, Smith and Angeli, 2007).</i>	69
<i>Figure 2-29: Changes in slug behaviour, (a) before the introduction of DRP and after the introduction of DRP where (b) shows shorter slug developments and (c) demonstrates closely compacted slugs. Adapted from (Al-Wahaibi, Smith and Angeli, 2007).</i>	69
<i>Figure 2-30: Experimental results of kerosene (oil)-water flow with a kerosene density and viscosity of <math>787\text{kg/m}^3</math> and <math>1.2\text{mPa.s}</math>. The graphs represent the flow regime maps of two separate experimental studies of (a) 0.0254m diameter pipe and (b) 0.012m diameter pipe. Adapted from (Mandal, Chakrabarti and Das, 2007).</i>	71
<i>Figure 2-31: Photographic results of kerosene (oil)-water flow within a 0.012m diameter pipe loop where (a) is the oil slug flow development and (b) are the oil plugs that are further spaced within a continuous water phase. Adapted from (Mandal, Chakrabarti and Das, 2007).</i>	71
<i>Figure 2-32: experimental comparison of horizontal oil-water flow under 0.012m and 0.0254m internal diameter loops to observe slug flow behaviour. Adapted from (Mandal, Das and Das, 2010)</i>	72
<i>Figure 2-33: Experimental results of oil-water horizontal flow under a 0.0254m diameter Perspex pipeline with and <math>\mu_o = 107\text{mPa.s}</math> and <math>\rho_o = 889\text{kg/m}^3</math> as the velocity ranges between 0.015-1.25m/s. Adapted from (Dasari et al., 2013).</i>	73
<i>Figure 2-34: Photographic results of oil-water flow within a 0.0254m diameter pipe loop where (a) is the elongated oil slug flow development and (b) is the oil plugs that are further spaced within a continuous water phase. Adapted from (Dasari et al., 2013).</i>	74
<i>Figure 2-35: Experimental results of oil-water horizontal flow under a 0.019m diameter Perspex pipeline with <math>\mu_o = 107\text{mPa.s}</math> and <math>\rho_o = 889\text{kg/m}^3</math> represented from the symbols and compared with the same set-up from (Yusuf et al., 2012) using a 0.019m diameter pipeline, represented with black boundaries. Adapted from (Al-Wahaibi et al., 2014).</i>	75
<i>Figure 2-36: Photographic experimental results of oil-water horizontal flow within a 0.0146m diameter acrylic where (a) is bubble flow, (b) slug flow and (c) plug flow. Adapted from (Tan et al., 2018).</i>	76
<i>Figure 2-37: Comparative experimental results of oil-water horizontal flow within a 0.0146m diameter acrylic pipeline on the effects of oil viscosity between (20#) <math>\mu_o = 20\text{mPa.s}</math> (200#) <math>\mu_o = 237\text{mPa.s}</math> and (400#) <math>\mu_o = 456\text{mPa.s}</math>. Adapted from (Tan et al., 2018).</i>	77

---

<i>Figure 2-38: Comparative experimental results of oil-water horizontal flow (0°) and a +5° inclination within a 0.038m diameter steel pipeline with oil viscosity and density of and <math>\mu_o = 5.5\text{mPa}\cdot\text{s}</math> and <math>\rho_o = 828\text{kg}/\text{m}^3</math>. Adapted from (Lum, Al-Wahaibi and Angeli, 2006).</i> .....	80
<i>Figure 2-39: Experimental results of oil-water flow under (a) +5° inclination and (b) -5° decline within a 0.020m diameter acrylic glass pipeline with oil viscosity and density of and <math>\mu_o = 4.5\text{mPa}\cdot\text{s}</math> and <math>\rho_o = 840\text{kg}/\text{m}^3</math>. Adapted from (Hanafizadeh, Hojati and Karimi, 2015).</i> .....	82
<i>Figure 3-1: P&amp;ID schematic of multiphase flow test facility applicable for both 1-inch test loop containing gas a section (red), oil section (black), water section (blue), multiphase section (green) and heating/chilling region (yellow).</i> .....	86
<i>Figure 3-2: Schematic view of multiphase flow test section of the 1-inch air-oil-water rig with all dimensions. The ECT pipe sensor is located directly after the test section. (Not to scale).</i> .....	88
<i>Figure 3-3: UL adapter set-up for the Brookfield DV-I Prime viscometer for viscosity ranging between 1 – 2000mPa.s between temperatures of 10 °C – 40 °C in increments of 0.5 °C. Adapted from (Brookfield Engineering Laboratories Inc., 2020).</i> .....	92
<i>Figure 3-4: EDM250 oil data for changes in temperature to (a) viscosity and (b) density, data from Esther (2014).</i> .....	93
<i>Figure 3-5: H100 oil data for changes in temperature to (a) viscosity and (b) density.</i> .....	93
<i>Figure 3-6: Flowmeter calibration check of (a) water electromagnetic flowmeter and (b) oil Coriolis flowmeter.</i> .....	95
<i>Figure 3-7: DP1 DRUCK PMP 4170 pressure calibration.</i> .....	95
<i>Figure 3-8: Friction Factor comparison of horizontal single-phase flow of water in a 1-inch Perspex pipeline.</i> .....	97
<i>Figure 3-9: Pressure gradient comparison for horizontal single-phase flow of water in a 1-inch Perspex pipeline.</i> .....	97
<i>Figure 4-1: Superficial water velocity vs superficial water velocity flow regime map of (a) experiment with EDM250 oil at a pipe inclination of 0° from the horizontal and (b) experiment with H100 oil at a pipe inclination of 0° from the horizontal.</i> .....	100
<i>Figure 4-2: Superficial water velocity vs superficial water velocity flow regime map of a) experiment with EDM250 oil at a pipe inclination of 5° from the horizontal and (b) experiment with H100 oil at a pipe inclination of 5° from the horizontal.</i> .....	100
<i>Figure 4-3: (a) Water hold-up fluctuation (b) corresponding PDF grouping of all flow regime type examples from the experiment with EDM250 at a pipe inclination of 0°.</i> .....	103
<i>Figure 4-4: (a) Water hold-up fluctuation (b) corresponding PDF grouping of all flow regime type examples from the experiment with H100 at a pipe inclination of 0°.</i> .....	103

---

Figure 4-5: (a) Water hold-up fluctuation and (b) corresponding PDF grouping of all flow regime type examples from the experiment with EDM250 at a pipe inclination of  $0^\circ$ . ..... 104

Figure 4-6: (a) Water hold-up fluctuation and (b) corresponding PDF grouping of all flow regime type examples from the experiment with H100 at a pipe inclination of  $5^\circ$ . ..... 104

Figure 4-7: (a) Pressure drop fluctuation vs time (b) corresponding PDF pressure drop grouping of all flow regime type examples from the EDM250 experiment at  $0^\circ$  pipe inclination. .... 107

Figure 4-8: (a) Pressure drop fluctuation vs time (b) corresponding PDF pressure drop grouping of all flow regime type examples from the H100 experiment at  $0^\circ$  pipe inclination. .... 108

Figure 4-9: Pressure drop fluctuation vs time (b) corresponding PDF pressure drop grouping of all flow regime type examples from the EDM250 experiment at  $5^\circ$  a pipe inclination. .... 108

Figure 4-10: Pressure drop fluctuation vs time (b) corresponding PDF pressure drop grouping of all flow regime type examples from the H100 experiment at  $5^\circ$  a pipe inclination. .... 109

Figure 4-11: Intermittent flow analysis of EDM250 (light oil) of (a) hold-up vs time data, (b) PDF analysis of hold-up and the resulting 2D ECT plot of the measured permittivity between the two fluids under the conditions of; (c)  $v_{sw}=0.50\text{m/s}$   $v_{so}=0.10\text{m/s}$  at  $0^\circ$ , (d)  $v_{sw}=0.60\text{m/s}$   $v_{so}=0.10\text{m/s}$  at  $0^\circ$ , (e)  $v_{sw}=0.50\text{m/s}$   $v_{so}=0.15\text{m/s}$  at  $0^\circ$ , (f)  $v_{sw}=0.55\text{m/s}$   $v_{so}=0.15\text{m/s}$  at  $0^\circ$ , (g)  $v_{sw}=0.55\text{m/s}$   $v_{so}=0.10\text{m/s}$  at  $5^\circ$  and (h)  $v_{sw}=0.50\text{m/s}$   $v_{so}=0.15\text{m/s}$  at  $5^\circ$ . .... 110

Figure 4-12: Intermittent flow analysis of H100 (heavy oil) of (a) hold-up vs time data, (b) PDF analysis of hold-up and the resulting 2D ECT plot of the measured permittivity between the two fluids under the conditions of; (c)  $v_{sw}=0.50\text{m/s}$   $v_{so}=0.10\text{m/s}$  at  $0^\circ$ , (d)  $v_{sw}=0.34\text{m/s}$   $v_{so}=0.15\text{m/s}$  at  $0^\circ$ , (e)  $v_{sw}=0.40\text{m/s}$   $v_{so}=0.15\text{m/s}$  at  $0^\circ$ , (f)  $v_{sw}=0.45\text{m/s}$   $v_{so}=0.15\text{m/s}$  at  $0^\circ$ , (g)  $v_{sw}=0.40\text{m/s}$   $v_{so}=0.10\text{m/s}$  at  $5^\circ$  and (h)  $v_{sw}=0.35\text{m/s}$   $v_{so}=0.15\text{m/s}$  at  $5^\circ$ . .... 111

Figure 4-13: Superimposed flow regime map of (a) modified from (Mandal, Chakrabarti and Das, 2007) against the EDM250 experiment (light oil) both at pipe incline of  $0^\circ$  and (b) modified from (Dasari et al., 2013) against the H100 experiment (heavy oil) both at pipe incline of  $0^\circ$ . .... 117

Figure 4-14: Superimposed flow regime maps of (a) EDM250 (light oil) experiment at a pipe incline at  $0^\circ$  against EDM250 oil experiment at pipe incline at  $5^\circ$  and (b) H100 oil experiment at pipe incline at  $0^\circ$  against H100 oil experiment at pipe incline at  $5^\circ$ . .... 118

Figure 4-15: Intermittent flow frequency analysis of EDM250 (light oil) at experimental conditions of, (a)  $v_{sw}=0.50\text{m/s}$   $v_{so}=0.10\text{m/s}$  at  $0^\circ$ , (b)  $v_{sw}=0.60\text{m/s}$   $v_{so}=0.10\text{m/s}$  at  $0^\circ$ , (c)  $v_{sw}=0.50\text{m/s}$   $v_{so}=0.15\text{m/s}$  at  $0^\circ$ , (d)  $v_{sw}=0.55\text{m/s}$   $v_{so}=0.15\text{m/s}$  at  $0^\circ$ , (e)  $v_{sw}=0.55\text{m/s}$   $v_{so}=0.10\text{m/s}$  at  $5^\circ$  and (f)  $v_{sw}=0.45\text{m/s}$   $v_{so}=0.15\text{m/s}$  at  $5^\circ$ . .... 121

Figure 4-16: Intermittent flow analysis of H100 (heavy oil) at experimental conditions of (a)  $v_{sw}=0.50\text{m/s}$   $v_{so}=0.10\text{m/s}$  at  $0^\circ$ , (b)  $v_{sw}=0.34\text{m/s}$   $v_{so}=0.15\text{m/s}$  at  $0^\circ$ , (c)  $v_{sw}=0.40\text{m/s}$   $v_{so}=0.15\text{m/s}$  at  $0^\circ$ , (d)  $v_{sw}=0.45\text{m/s}$   $v_{so}=0.15\text{m/s}$  at  $0^\circ$ , (e)  $v_{sw}=0.40\text{m/s}$   $v_{so}=0.10\text{m/s}$  at  $5^\circ$  and (f)  $v_{sw}=0.35\text{m/s}$   $v_{so}=0.15\text{m/s}$  at  $5^\circ$ . .... 122

---

<i>Figure 5-1: Pressure gradient correlation prediction vs measured pressure examples from (a) (Elseth, 2001) and (b) (Shi, Jepson and Rhyne, 2003). Both utilising the experimental data from this study which the data is split between the experiment type of experimental oil and pipe inclination. ....</i>	<i>126</i>
<i>Figure 5-2: Pressure gradient correlation prediction vs measured pressure examples from (a) (Elseth, 2001) and (b) (Shi, Jepson and Rhyne, 2003). Both utilising the experimental data from this study which the data is split between flow regimes. ....</i>	<i>126</i>
<i>Figure 5-3: Newly proposed pressure gradient correlation vs measured pressure. Experimental data from this study which the data is combined across all experiments. ....</i>	<i>128</i>
<i>Figure 5-4: Newly proposed pressure gradient correlation vs measured pressure. Experimental data and measured pressure split between (Chakrabarti, Das and Ray, 2005; Vielma et al., 2008; Atmaca et al., 2009; Vuong et al., 2009). ....</i>	<i>130</i>
<i>Figure 5-5: (a) (Elseth, 2001) pressure gradient correlation and (b) (Shi, Jepson and Rhyne, 2003) pressure gradient correlation vs measured pressure. Experimental data and measured pressure split between (Chakrabarti, Das and Ray, 2005; Vielma et al., 2008; Atmaca et al., 2009; Vuong et al., 2009). ....</i>	<i>131</i>
<i>Figure 5-6: Water hold-up correlation from (Arney et al., 1996) vs measured water hold-up. All experimental data from this study is separated into flow regimes. ....</i>	<i>132</i>
<i>Figure 5-7: Water hold-up correlation from (Arney et al., 1996) vs measured ECT water hold-up. All experimental data from this study is combined. ....</i>	<i>133</i>
<i>Figure 5-8: Newly proposed hold-up correlation vs measured ECT hold-up. (a) Experimental data from this study are segregated based on flow regimes and (b) experimental data is combined while excluding the exception of the DOW data. ....</i>	<i>135</i>
<i>Figure 5-9: (a) Newly proposed hold-up correlation vs experimentally measured hold-up and (b) (Arney et al., 1996) hold-up correlation vs experimentally measured hold-up. Experimental data and measured hold-up arranged between (Vielma et al., 2008; Atmaca et al., 2009; Vuong et al., 2009). ....</i>	<i>136</i>
<i>Figure 6-1: Hydraulic diameter cross-section examples (a) the heavier fluid (water) occupies less than half of the pipe as the lighter fluid contains the rest of the remaining area (b) the heavier fluid (water) equals or more than half-filled in the pipe as the lighter fluid (oil) contains the rest of the area. ....</i>	<i>139</i>
<i>Figure 6-2: Modified Froude number grouping comparison between (a) only 0° inclined experimental data from this study and (b) all experimental data from this study. Intermittent flows are plugs (P) and Slugs (SLo). ....</i>	<i>142</i>
<i>Figure 6-3: Modified Froude number grouping comparison between experiments by (Mandal, Chakrabarti and Das, 2007; Hanafizadeh, Hojati and Karimi, 2015; Tan et al., 2018) and this study, focusing on pipe internal diameter sizes between 0.012m and 0.0254m. ....</i>	<i>143</i>

---

<i>Figure 7-1: 2-inch diameter pipeline prototype scale-up analysis of pressure between all the 1-inch experimental data from this work.....</i>	<i>149</i>
<i>Figure 7-2: 2-inch diameter pipeline prototype scale-up analysis of water hold-up between all the 1-inch experimental data from this work.....</i>	<i>149</i>
<i>Figure 7-3: 2-inch diameter pipeline prototype scale-up analysis of pressure between all the 1-inch experimental data from this work which have been separated between oil types with density ratios of EDM250 oil = 0.813 and H100 oil = 0.880. ....</i>	<i>150</i>
<i>Figure 7-4: 2-inch diameter pipeline prototype scale-up analysis of pressure between all the 1-inch experimental data from this work which have been separated between pipeline inclinations of 0° and 5° upwards from the horizontal. ....</i>	<i>150</i>
<i>Figure 7-5: 2-inch diameter pipeline prototype scale-up analysis of hold-up between all the 1-inch experimental data from this work which have been separated between oil types with density ratios of EDM250 oil = 0.813 and H100 oil = 0.880. ....</i>	<i>151</i>
<i>Figure 7-6: 2-inch diameter pipeline prototype scale-up analysis of hold-up between all the 1-inch experimental data from this work which have been separated between pipeline inclinations of 0° and 5° upwards from the horizontal. ....</i>	<i>151</i>
<i>Figure 7-7: 42-inch diameter pipeline prototype scale-up analysis of pressure between all the 1-inch experimental data from this work.....</i>	<i>152</i>
<i>Figure 7-8: 42-inch diameter pipeline prototype scale-up analysis of pressure between all the 1-inch experimental data from this work which have been separated between oil types with density ratios of EDM250 oil = 0.813 and H100 oil = 0.880. ....</i>	<i>152</i>
<i>Figure 7-9: 42-inch diameter pipeline prototype scale-up analysis of pressure between all the 1-inch experimental data from this work which have been separated between pipeline inclinations of 0° and 5° upwards from the horizontal. ....</i>	<i>153</i>
<i>Figure 7-10: Superimposed hold-up scale-up correlation vs measured hold-up. Experimental data and measured hold-up were split between multiple experiments from (Vielma et al., 2008; Atmaca et al., 2009; Vuong et al., 2009; Esther, 2014). ....</i>	<i>155</i>
<i>Figure 7-11: Superimposed pressure gradient scale-up correlation vs measured pressure gradient. Experimental data and measured pressure were split between multiple experiments from (Vielma et al., 2008; Atmaca et al., 2009; Vuong et al., 2009; Esther, 2014). ....</i>	<i>155</i>
<i>Figure 7-12: Superimposed scaled-up dimensionless Froude number grouping of flow regimes between multiple experiments from (Vielma et al., 2008; Vuong et al., 2009; Esther, 2014)...</i>	<i>156</i>
<i>Figure Apx B-1: (a) Water PCP-1 Calibration at 10l sequences for each flowrate test (b) oil PCP-2 Calibration at 10l sequences for each flowrate test and (c) voltage output for water PCP-1 calibration at 10l sequences for each flowrate. ....</i>	<i>182</i>
<i>Figure Apx B-2: Oil PCP-2 Calibration at 20l sequences for each flowrate test.....</i>	<i>182</i>

---

Figure Apx C-1: (a) P1 WIKA S-11 pressure transducer calibration, (b) P2 DRUCK PMP1400 pressure transducer calibration, (c) P3 WIKA S-11 pressure transducer calibration and (d) P5 DRUCK PMP1400 pressure transducer calibration. .... 183

Figure Apx D-1: Intermittent flow frequency analysis of EDM250 (light oil) at  $0^\circ$  pipe inclination at experimental conditions of, (a)  $v_{sw} = 0.45\text{m/s}$   $v_{so} = 0.10\text{m/s}$ , (b)  $v_{sw} = 0.50\text{m/s}$   $v_{so} = 0.10\text{m/s}$ , (c)  $v_{sw} = 0.55\text{m/s}$   $v_{so} = 0.10\text{m/s}$ , (d)  $v_{sw} = 0.60\text{m/s}$   $v_{so} = 0.10\text{m/s}$ , (e)  $v_{sw} = 0.50\text{m/s}$   $v_{so} = 0.15\text{m/s}$  and (f)  $v_{sw} = 0.55\text{m/s}$   $v_{so} = 0.15\text{m/s}$ ..... 184

Figure Apx D-2: Intermittent flow frequency analysis of EDM250 (light oil) at  $5^\circ$  pipe inclination at experimental conditions of, (a)  $v_{sw} = 0.40\text{m/s}$   $v_{so} = 0.10\text{m/s}$ , (b)  $v_{sw} = 0.45\text{m/s}$   $v_{so} = 0.10\text{m/s}$ , (c)  $v_{sw} = 0.50\text{m/s}$   $v_{so} = 0.10\text{m/s}$ , (d)  $v_{sw} = 0.55\text{m/s}$   $v_{so} = 0.10\text{m/s}$ , (e)  $v_{sw} = 0.60\text{m/s}$   $v_{so} = 0.10\text{m/s}$ , (f)  $v_{sw} = 0.65\text{m/s}$   $v_{so} = 0.10\text{m/s}$ , (g)  $v_{sw} = 0.45\text{m/s}$   $v_{so} = 0.15\text{m/s}$ , (h)  $v_{sw} = 0.50\text{m/s}$   $v_{so} = 0.15\text{m/s}$ , (i)  $v_{sw} = 0.55\text{m/s}$   $v_{so} = 0.15\text{m/s}$  and (j)  $v_{sw} = 0.60\text{m/s}$   $v_{so} = 0.15\text{m/s}$ . .... 186

Figure Apx D-3: Intermittent flow frequency analysis of H100 (heavy oil) at  $0^\circ$  pipe inclination at experimental conditions of, (a)  $v_{sw} = 0.30\text{m/s}$   $v_{so} = 0.10\text{m/s}$ , (b)  $v_{sw} = 0.34\text{m/s}$   $v_{so} = 0.10\text{m/s}$ , (c)  $v_{sw} = 0.40\text{m/s}$   $v_{so} = 0.10\text{m/s}$ , (d)  $v_{sw} = 0.45\text{m/s}$   $v_{so} = 0.10\text{m/s}$ , (e)  $v_{sw} = 0.50\text{m/s}$   $v_{so} = 0.10\text{m/s}$ , (f)  $v_{sw} = 0.34\text{m/s}$   $v_{so} = 0.15\text{m/s}$ , (g)  $v_{sw} = 0.40\text{m/s}$   $v_{so} = 0.15\text{m/s}$ , (h)  $v_{sw} = 0.45\text{m/s}$   $v_{so} = 0.15\text{m/s}$ , (i)  $v_{sw} = 0.51\text{m/s}$   $v_{so} = 0.15\text{m/s}$  and (j)  $v_{sw} = 0.55\text{m/s}$   $v_{so} = 0.15\text{m/s}$ . .... 188

Figure Apx D-4: Intermittent flow frequency analysis of H100 (heavy oil) at  $5^\circ$  pipe inclination at experimental conditions of, (a)  $v_{sw} = 0.25\text{m/s}$   $v_{so} = 0.10\text{m/s}$ , (b)  $v_{sw} = 0.30\text{m/s}$   $v_{so} = 0.10\text{m/s}$ , (c)  $v_{sw} = 0.35\text{m/s}$   $v_{so} = 0.10\text{m/s}$ , (d)  $v_{sw} = 0.40\text{m/s}$   $v_{so} = 0.10\text{m/s}$ , (e)  $v_{sw} = 0.45\text{m/s}$   $v_{so} = 0.10\text{m/s}$ , (f)  $v_{sw} = 0.50\text{m/s}$   $v_{so} = 0.10\text{m/s}$ , (g)  $v_{sw} = 0.30\text{m/s}$   $v_{so} = 0.15\text{m/s}$ , (h)  $v_{sw} = 0.35\text{m/s}$   $v_{so} = 0.15\text{m/s}$ , (i)  $v_{sw} = 0.40\text{m/s}$   $v_{so} = 0.15\text{m/s}$ , (j)  $v_{sw} = 0.45\text{m/s}$   $v_{so} = 0.15\text{m/s}$ , (k)  $v_{sw} = 0.50\text{m/s}$   $v_{so} = 0.15\text{m/s}$  and (l)  $v_{sw} = 0.55\text{m/s}$   $v_{so} = 0.15\text{m/s}$ ..... 190

---

# LIST OF TABLES

<i>Table 2-1: Classification of solid settling flow regimes.</i> .....	22
<i>Table 2-2: Categorised flow pattern results for an oil-water multiphase system with oil properties of <math>\mu_o = 21.7\text{mPa}\cdot\text{s}</math> and, <math>\rho_o = 896\text{kg}/\text{m}^3</math> in a <math>D = 0.0394\text{m}</math> pipe in the form of a flow regime map. Adapted from (Guzhov et al., 1973), revisited and adapted from (Oglesby, 1979).</i> .....	62
<i>Table 2-3: Comparison of set-up configurations of previous experimental studies that have observed intermittent flow regimes which are categorised as bubble, plug and slug flow regimes while under either horizontal or slightly deviated pipeline configurations.</i> .....	84
<i>Table 3-1: Key range of parameters that are incorporated across all four experiments. Uncertainties are not considered.</i> .....	90
<i>Table 3-2: Key experimental fluid properties of EDM250 oil, H100 oil and water at 15°C.</i> .....	92
<i>Table 3-3: Maximum uncertainty range of all key parameters from this study.</i> .....	98
<i>Table 4-1: All flow regime type examples from the experiment with EDM250 (light oil) at a pipe inclination of 0° from the horizontal. Flow travelling from left to right.</i> .....	101
<i>Table 4-2: All flow regime type examples from the experiment with H100 (heavy oil) at a pipe inclination of 0° from the horizontal. Flow travelling from left to right.</i> .....	101
<i>Table 4-3: Flow regime examples from the experiment with EDM250 (light oil) at a pipe inclination of 5° from the horizontal. Flow travelling from left to right.</i> .....	101
<i>Table 4-4: All flow regime type examples from the experiment with H100 (heavy oil) at a pipe inclination of 5° from the horizontal. Flow travelling from left to right.</i> .....	102
<i>Table 4-5: ECT images of cross-section examples and 2D frame image stacking of all flow regime type examples from the experiment with EDM250 at a pipe inclination of 0°.</i> .....	105
<i>Table 4-6: ECT images of cross-section examples and 2D frame image stacking of all flow regime type examples from the experiment with H100 at a pipe inclination of 0°.</i> .....	105
<i>Table 4-7: ECT images of cross-section examples and 2D frame image stacking of all flow regime type examples from the experiment with EDM250 at a pipe inclination of 5°.</i> .....	106
<i>Table 4-8: ECT images of cross-section examples and 2D frame image stacking of all flow regime type examples from the experiment with H100 at a pipe inclination of 5°.</i> .....	106
<i>Table 4-9: All intermittent flow regimes observed with all measured parameters from the experiment with EDM250 oil at a pipe inclination of 0°.</i> .....	112
<i>Table 4-10: All intermittent flow regimes observed with all measured parameters from the experiment with EDM250 oil at a pipe inclination of 5°.</i> .....	113



---

*Table 4-11: All intermittent flow regimes observed with all measured parameters from the experiment with H100 oil at a pipe inclination of 0°..... 114*

*Table 4-12: All intermittent flow regimes observed with all measured parameters from the experiment with H100 oil at a pipe inclination of 5°..... 115*

*Table 4-13: Intermittent flow frequency grouping matrix between oil and water superficial velocities at  $v_{sw} = 0.30 - 0.70\text{m/s}$  and  $v_{so} = 0.10 - 0.20\text{m/s}$  of all four experiment types. .... 120*

*Table 5-1: Pressure gradient correlation constant changes between flow condition thresholds. .... 128*

*Table 5-2: Key pipe variables and fluid properties from experiments of (Chakrabarti, Das and Ray, 2005; Vielma et al., 2008; Atmaca et al., 2009; Vuong et al., 2009)..... 130*

*Table 5-3: Water hold-up correlation constant changes between mixing conditions. .... 134*

*Table 7-1: List of selected Scale-up compatibilities between selected studies from literature and experimental data from the current work..... 154*

---

# NOMENCLATURE

- $A$  – Cross-sectional area of a pipe ( $m^2$ )  
 $A_o$  – Cross-sectional area of oil in a pipe ( $m^2$ )  
 $\tilde{A}_o$  – Dimensionless cross-sectional area for oil  
 $A_p$  – Projected (Surface) area of a droplet ( $m^2$ )  
 $A_w$  – Cross-sectional area of water in a pipe ( $m^2$ )  
 $\tilde{A}_w$  – Dimensionless cross-sectional area for water  
 $A'_w$  – Describes an expression for  $dA_w/dh_w$   
 $A_{\alpha\beta}$  – Cross-sectional area of one of the multiphase fluids in a pipe ( $m^2$ )  
 $A_1$  – Initial venturi throat area ( $m^2$ )  
 $A_2$  – Secondary venturi throat area ( $m^2$ )  
 $a$  – The total radioactivity of the injected solution (Bq)  
 $C$  – The concentration of the tracer at the injection point to the main flow line ( $mol/m^3$ )  
 $C_D$  – Drag coefficient  
 $C_L$  – Lift coefficient  
 $C_q$  – Constant of the geometric relationship for the dimensions of the respective venturi system  
 $C_v$  – A calibration constant for the venturi system  
 $C_w$  – Water cut  
 $C_1$  – The concentration of the tracer downstream by the external counter after mixing ( $mol/m^3$ )  
 $C_2$  – The background concentration of the tracer upstream of the injection point ( $mol/m^3$ )  
 $D$  – Internal diameter of a pipe (m)  
 $D_H$  – Hydraulic diameter (m)  
 $\tilde{D}_{Ho}$  – Dimensionless hydraulic diameter for oil (m)  
 $\tilde{D}_{Hw}$  – Dimensionless hydraulic diameter for water (m)  
 $D_p$  – Diameter of a particle/droplet (m)  
 $D_o$  – Hydraulic diameter of oil (m)  
 $D_w$  – Hydraulic diameter of water (m)  
 $E_o'$  or  $E_o$  – Eötvös number  
 $e$  – Arbitrary value based on the respective fluid densities and interactive pressure gradients  
 $F$  – A dummy variable for the steady-state solution  
 $F_B$  – Buoyancy force (N)  
 $F_D$  – Drag force (N)  
 $F_{Down}$  – Forces acting down upon a particle (N)  
 $F_G$  – Gravitational force ( $N^2$ )  
 $F_L$  – Lift force (N)  
 $F_{up}$  – Forces acting up upon a particle (N)  
 $Fr_o$  – Oil Froude Number  
 $Fr_{on}$  – Modified oil Froude Number  
 $Fr_w$  – Water Froude Number  
 $Fr_{wn}$  – Modified water Froude Number  
 $f$  – Moody frictional coefficient

---

$f_i$  – Frictional factor of the pipeline induced by the interface  
 $f_m$  – Mixture frictional factor of the pipeline induced by the mixture phase  
 $f_n$  – Individual frequency at one of many points (Hz)  
 $f_o$  – Frictional factor of the pipeline induced by the oil phase  
 $f_w$  – Frictional factor of the pipeline induced by the water phase  
 $f_\alpha$  – Frequency of sample rate (Hz)  
 $\frac{G}{V}$  – Ratio between gravitational and viscous forces  
 $g$  – Acceleration due to gravity (9.81 m/s<sup>2</sup>)  
 $g_c$  – A conversion factor, which in terms of SI (metric) units will be negligible as a value of 1  
 $H_D$  – Hydrostatic diameter (m)  
 $H_o$  – Water hold-up  
 $H_w$  – Water hold-up  
 $\bar{h}$  – Water hold-up ratio  
 $h_w$  – Height of the water phase between the furthest point of the pipe and the interface (m)  
 $h_{\alpha\beta}$  – Height of the reference phase between the furthest point of the pipe and the interface (m)  
 $j$  – Complex number  
 $K$  – Virtual diffusion coefficient  
 $K_{C_w}$  – Adjustable pressure gradient and hold-up correlation constant for the water cut term  
 $K_{H_w}$  – Adjustable hold-up correlation constant  
 $K_{f_m}$  – Adjustable pressure gradient correlation constant for the frequency term  
 $K_\theta$  – Adjustable pressure gradient and hold-up correlation constant for the inclination term  
 $K_\mu$  – Adjustable pressure gradient and hold-up correlation constant for the viscosity term  
 $K_\rho$  – Adjustable pressure gradient and hold-up correlation constant for the density term  
 $k_f$  – Individual signal points  
 $k_1$  – Wall/liquid contact perimeter in the form of an in-situ configuration (m)  
 $k_2$  – A reflection of the flow regime behaviour within each phase.  
 $L$  – Length of a pipeline at a given position (m)  
 $M_R$  – Torque subjected across the rotor (Nm)  
 $\dot{m}$  – Mass flowrate (kg/s)  
 $\dot{m}_m$  – Mixture mass flowrate (kg/s)  
 $\dot{m}_o$  – Oil mass flowrate (kg/s)  
 $\dot{m}_w$  – Water mass flowrate (kg/s)  
 $N$  – The total number of sample points  
 $\bar{N}$  – Random whole number  
 $n$  – Arbitrary value based on the respective fluid densities and interactive pressure gradients  
 $n_f$  – Frame number  
 $n_o$  – Advanced variable for oil parameter from the Blasius equation for the friction factor  
 $n_w$  – Advanced variable for water parameter from the Blasius equation for the friction factor  
 $n_1$  – Arbitrary value based on the respective fluid densities and interactive pressure gradients  
 $n_2$  – Arbitrary value based on the respective fluid densities and interactive pressure gradients  
 $P$  – Static fluid pressure (Pa or N/m<sup>2</sup>)  
 $\tilde{P}_i$  – Dimensionless pressures from the interface

---

$P_{i_o}$  – Dynamic fluid pressures within the oil phase bordered by the interface (Pa or N/m<sup>2</sup>)  
 $P_{i_w}$  – Dynamic fluid pressures within the water phase bordered by the interface (Pa or N/m<sup>2</sup>)  
 $P_l$  – Liquid continuum phase pressure (Pa or N/m<sup>2</sup>)  
 $P_p$  – Particle pressure (Pa or N/m<sup>2</sup>)  
 $\tilde{P}_o$  – Dimensionless pressures from the oil phase  
 $\tilde{P}_w$  – Dimensionless pressures from the water phase  
 $p_i$  – Pipe perimeter in contact with the interface (m)  
 $\tilde{p}_i$  – Dimensionless perimeter from the interface  
 $p_o$  – Pipe perimeter in contact with the oil phase (m)  
 $p_w$  – Pipe perimeter in contact with the water phase (m)  
 $p_{\alpha\beta}$  – Pipe perimeter of reference phase in contact with the pipe (m)  
 $Q_m$  – Mixture mass flux (kg/m<sup>2</sup>.s)  
 $\dot{q}$  – Volumetric flowrate (m<sup>3</sup>/s)  
 $\dot{q}_o$  – Volumetric flowrate of oil (m<sup>3</sup>/s)  
 $\dot{q}_t$  – Volumetric injection rate of the tracer (m<sup>3</sup>/s)  
 $\dot{q}_w$  – Volumetric flowrate of water (m<sup>3</sup>/s)  
 $\dot{q}_\alpha$  – Volumetric flowrate of the heavy continuous phase (m<sup>3</sup>/s)  
 $\dot{q}_\beta$  – Volumetric flowrate of the light phase (m<sup>3</sup>/s)  
 $R$  – Rotar radius (m)  
 $Re_m$  – Mixture Reynolds number  
 $Re_p$  – Particle Reynolds number  
 $Re_o$  – Oil Reynolds number  
 $Re_w$  – Water Reynolds number  
 $r$  – Pipe radius (m)  
 $r_p$  – Particle radius (m)  
 $r_\rho$  – Density Ratio  
 $r_{v_{sw_o}}$  – Superficial velocity ratio of oil and water  
 $s_x$  – Sample rate (frame/s)  
 $s_G$  – Specific gravity  
 $T$  – Temperature ( °C )  
 $t$  – Time (s)  
 $V$  – Pipe volume (m<sup>3</sup>)  
 $V_o$  – Oil volume (m<sup>3</sup>)  
 $V_w$  – Oil volume (m<sup>3</sup>)  
 $V_p$  – Particle volume (m<sup>3</sup>)  
 $v_a$  – Average velocity (m/s)  
 $v_f$  – Velocity at the venturi throat (m/s)  
 $v_m$  – Mixture velocity (m/s)  
 $v_o$  – In-situ average phase velocities of oil (m/s)  
 $\tilde{v}_o$  – Dimensionless oil velocity  
 $v_s$  – Slip velocity (m/s)  
 $v_{sm}$  – Superficial mixture velocity (m/s)

---

$v_{so}$  – Superficial oil velocity (m/s)  
 $v_{sw}$  – Superficial water velocity (m/s)  
 $v_{s\alpha\beta}$  – Superficial phase velocity (m/s)  
 $v_t$  – Terminal velocity (m/s)  
 $v_w$  – In-situ average phase velocities of oil (m/s)  
 $\tilde{v}_w$  – Dimensionless water velocity  
 $v_{\alpha\beta \text{ Real}}$  – Real phase velocity (m/s)  
 $We$  – Webber number  
 $X(k_f)$  – A set of  $N$  amplitudes for each of the individual signal points ( $k_f$ )  
 $x(n_f)$  – The data point at frame number ( $n_f$ )  
 $Z$  – A calibration factor which is unique to individual pumps  
 $z$  – An arbitrary value where Reynolds number exponents calculate the frictional coefficients  
 $\alpha$  – Representation of heavy continuous phase in liquid-liquid multiphase flow  
 $\alpha_{H_w}$  – Mixing ratio threshold between oil and water for the hold-up correlation  
 $\alpha_p$  – Pipe condition pressure threshold for the pressure gradient correlation (m/mPa.s)  
 $\beta$  – Representation of light phase in liquid-liquid multiphase flow  
 $\beta_\theta$  – Angle from the centre point of the pipe - forms between the endpoints of the interface ( $^\circ$ )  
 $\gamma$  – Gas phase  
 $\Delta L$  – Pipe length differential ( $\text{kg/m}^3$ )  
 $\Delta P$  – Differential Pressure (Pa or N/m)  
 $\Delta \rho$  – Density differential ( $\text{kg/m}^3$ )  
 $\varepsilon$  – Internal pipe roughness (m)  
 $\varepsilon_w^I$  – Critical water cut invasion point (PIP)  
 $\zeta_o$  – Advanced variable for oil parameter from the Blasius equation for the friction factor  
 $\zeta_w$  – Advanced variable for water parameter from the Blasius equation for the friction factor  
 $\theta$  – Angle of pipe inclination ( $^\circ$ )  
 $\lambda_o$  – Volume fraction of oil  
 $\lambda_w$  – volume fraction of water  
 $\lambda_{\alpha\beta}$  – volume fraction of a phase  
 $\mu_l$  – Liquid viscosity (mPa.s)  
 $\mu_m$  – Mixture velocity (mPa.s)  
 $\mu_o$  – Oil viscosity (mPa.s)  
 $\mu_r$  – A constant viscosity value maintained at 1mPa.s. (mPa.s)  
 $\mu_w$  – Water viscosity (mPa.s)  
 $\pi$  – Constant value of 3.14  
 $\rho_l$  – Liquid density ( $\text{kg/m}^3$ )  
 $\rho_m$  – Mixture density ( $\text{kg/m}^3$ )  
 $\rho_o$  – Oil density ( $\text{kg/m}^3$ )  
 $\rho_p$  – Particle density ( $\text{kg/m}^3$ )  
 $\rho_w$  – Water density ( $\text{kg/m}^3$ )  
 $\sigma$  – Surface tension or Interfacial tension (N/m)  
 $\tau$  – Pipe shear stress ( $\text{N/m}^2$ )

---

$\dot{\tau}$  – Pipe shear rate ( $s^{-1}$ )  
 $\tau_i$  – Pipe shear stress acting along the interface ( $N/m^2$ )  
 $\tau_o$  – Pipe shear stress acting along the oil phase ( $N/m^2$ )  
 $\tau_w$  – Pipe shear stress acting along the water phase ( $N/m^2$ )  
 $\tau_W$  – Wall shear stress ( $N/m^2$ )  
 $\tau_{W_o}$  – wall shear stress acting from the oil phase ( $N/m^2$ )  
 $\tau_{W_w}$  – wall shear stress acting from the water phase ( $N/m^2$ )  
 $\Phi$  – Pressure gradient ratio between the fluid mixture and one of the individual phases  
 $X$  – Pressure gradient ratio between two constituent fluids within the mixture  
 $\omega$  – Angular velocity (rad/s)

---

# ABBREVIATIONS

*AN – Core Annular Flow*  
*ANW – Core Annular Wavy Flow*  
*API – American Petroleum Institute (of Gravity)*  
*Bb, or B<sub>o</sub> – Bubble/bubbly Flow (also known as Plug flow)*  
*BV – Ball Valve*  
*BV2W – Two-Way Ball Valve*  
*CTD – Computational Fluid Dynamics*  
*DAS – Data Acquisition System*  
*DC – Dual Continuous Flow*  
*DOW – Dispersions of Oil in Water Flow*  
*DOW&W – Dispersion of Oil in Water Layer + Pure Water Layer Flow*  
*DOW&WO – Dispersions of Oil in Water Layer + Dispersions of Water in Oil Layer Flow*  
*DP – Differential Pressure*  
*DRP – Drag Reduction Polymer*  
*DWO – Dispersions of Water in Oil Flow*  
*ECT – Electrical Capacitance Tomogram*  
*HDD – High Definition Display*  
*ID – Internal Diameter*  
*IFT – Interfacial Tension*  
*LDA – Laser Doppler Anemometry*  
*MFM – Multiphase Flow Metering*  
*MMTC – Multi-Modality Tomography Configurator*  
*NI – National Instruments*  
*NTP – Normal Temperature and Pressure*  
*PCP – Progressive Cavity Pump*  
*PIP – Phase Inversion Point*  
*PIV – Particle Image Velocimetry*  
*PLIF – Planar Laser-Induced Fluorescence*  
*PMMA – Polymethyl-Methacrylate*  
*PSE – Process Systems Engineering*  
*PTV – Particle Tracking Velocimetry*  
*PVC – Polyvinyl Chloride*  
*PPE – Personal Protective Equipment*  
*P, P<sub>o</sub> or PL<sub>o</sub> – Oil Plug in Water Flow*  
*P<sub>w</sub> – Water Plugs in Oil Flow*  
*P&ID – Piping and Instrumentation Diagram*  
*SL, SL<sub>o</sub> or SG – Oil Slug Flow*  
*SL<sub>w</sub> – Water Slug Flow*  
*SS – Smooth Stratified Flow*  
*ST – Stratified Flow*  
*ST&MI – Stratified flow with mixing at the interface*

---

*SW- Stratified Wavy Flow*

*TMFM – True Mass Flowrate Meter*

*2D – Two-Dimensional*

*3D – Three-Dimensional*

*3L or SM – Three-Layered Flow/Stratified Mixed Flow*



# CHAPTER 1

## INTRODUCTION

The optimisation of transporting hydrocarbons through export pipelines over long distances has proven to become an increasingly important factor within the petroleum industry. Once hydrocarbons and aqueous liquids such as water have been extracted from production wells, the flow of two or more immiscible fluid phases would typically travel simultaneously within a shared pipeline, giving rise to the complex phenomena of multiphase flow. This results in a variety of different physical hydrodynamic configurations between the separate phases, known as flow regimes. Several possible flow regimes can develop during multiphase flow, one of which is classified as slug flow. Slug flow, which is categorised under a larger section known as intermittent flow, is a very undesirable flow regime in flow assurance engineering, as it can compromise the integrity of a pipeline through harsh vibrational effects due to its unstable nature. Vital operating and measuring equipment such as valves and gauges can be impaired, making the pipeline more difficult to control.

In extreme cases, this can cause production to stop or drastically lower efficiency by conditions such as; damages or leaks from pipes, acceleration of corrosion rates; compromise onsite personnel safety, a requirement for higher pumping capacity during significant pressure drops, sudden pressure build-up, diminishment of production time and requirement of slug-catcher units, resulting to the further expenditure of maintenance and repairs. However, this two-phase flow system has not been as commonly studied as its counterpart, gas-liquid flow and even further limited studies are found that incorporate slug flow developments. In addition, the interaction between two incompressible fluids cannot represent similar flow behaviours to that of gas-liquid mixtures. This is due to gas and liquid physical states of matter having significant dissimilarities between each other under compression and expansion conditions. In fact, gas-liquid flow systems have a much lower density and viscosity ratio in comparison to that of liquid-liquid systems.

---

Therefore, liquid-liquid studies must be conducted separately under various configurations of pipe design and oil properties (Russell and Charles, 1959; Charles, Govier and Hodgson, 1961).

Examples of oil-water flow within the petroleum industry can be seen from the following: (1) water-lubricated transport flow of heavy oil and (2) residual water content remaining after separation. With the further depletion of conventional light crude oil resources and the rapid increase of global energy demands, the petroleum industry has recently deviated its attention to the production and transportation of heavy crude oil. However, the mobility of heavy crude oil is very low and difficult to pump economically through pipelines at ambient pressure and temperature due to its high viscosity. One proposal for transporting heavy oil more efficiently across flow lines is to heat the respective oil to lower its viscosity by insulating the respective flow line that carries oil to decrease the oil viscosity in order to upsurge mobility. In addition, heating oil and insulating pipelines require significant capital investment and continuous operational expenses. One of the most effective methods of transporting heavy oil is to simultaneously implement an immiscible liquid of lower viscosity, such as water. This technique is known as a water-lubricated transport flow. The ideal condition of water-lubricated flow techniques is for injected water to take the form of a thin annular film across the walls of the pipeline while the oil is maintained in the core. This technique requires low volumes of water to be injected to sustain this oil-water multiphase flow process continuously. However, the ideal condition may not always be achieved due to the possible presence of a variety of different flow regimes (Ooms et al., 1984).

In remote and challenging areas to develop oil production sites such as subsea systems, limitations of separator size restrictions arise due to the shortage of space available on platforms or financial and technical challenges that take place when implementing subsea separators. The combination of oil and water production volumes may also exceed the volume capacity of separators. The residual water may not be fully separated from the oil phases, which can lead to oil-water flow in export pipelines to refineries for further separation to instigate. These issues usually arise when a field begins to mature. The excessive production of water towards the end of field life can increase, and water cuts may rise to as high as 95% due to multiple water sources that typically immerse over time throughout production (Morgan et al., 2012a). The source of accumulated water can be from (either one or a combination of) resident formation water that exists alongside the hydrocarbons in a reservoir, a natural aquifer that is contiguous to a reservoir and artificially injected water to provide further pressure support to increase overall recovery.

Flow regimes depend on combinations between physical fluid properties, flow geometry, orientation, the material of the pipe path and operational variables subjected across the relevant

---

flow line (Beretta et al., 1997). Variable arrangements need to be further studied in liquid-liquid formations to have a better understanding of how specific flow regimes such as slug flow develop in concentric flow paths. This can enable industries to optimise pipeline design by predicting which flow regime will arise over a series of different periods of field life production. Continuous necessary operational changes can also be implemented to prevent slug flow patterns in accordance with dynamic changes in multi-fluid volumes and properties such as water cut, dual liquid viscosity and pressure gradients. Resulting in a substantial increase in production capability and minimising costs through the prevention of damage, reducing the rate of wear and hence better preservation of export pipeline assets.

## **1.1 Research Background**

Multiphase flow is a complex phenomenon of the simultaneous flow between two or more distinct phases within a common flow line that forms a fluid mixture. This physical flow occurrence can be found through numerous types of media size extremes within the petroleum industry, such as; multiphase flow in porous media from sedimentary reservoir rock or pipelines that transport the extracted reservoir fluids. Typical phases that can be present are gas (e.g. CO<sub>2</sub>, air and hydrocarbon gas), liquid (e.g. oil and water), and/or solid (e.g. sand from the reservoir production face and metal from piping wear or debris). Among these three states of matter, numerous configurations of multiphase flow can exist. Examples within the petroleum industry typically find; two-phase flow (e.g. gas-liquid and liquid-liquid), three-phase flow (e.g. gas-liquid-liquid) and what is considered to be the most complex arrangement of multiphase flow, four-phase flow (e.g. gas-liquid-liquid-solid).

When a multiphase flow system is present in larger formations such as pipelines, the phase interactions can result in a variety of alternating hydrodynamic configurations known as flow regimes. Fluid properties, operational inputs and physical pipe characteristics result in the advances of different flow regimes through variations in forces acting upon the separate phases, such as; interfacial tension (IFT), gravitational effects, inertial forces and turbulence. The forces acting upon the phases have direct consequences on multiphase flow behaviour which includes individual phase velocities, in-situ phase fraction, pressure drop/build-up, interfacial shear stress and droplet breakup. Liquid-liquid two-phase flow has not been comprehensively studied to the same degree as gas-liquid flow. The small variations of density within two separate incompressible liquids, compared to that of gas-liquid flow, have higher complexity of flow configurations that make predicting, modelling and classifying individual flow behaviours more difficult. On the contrary, an increasing surge of liquid-liquid multiphase flow studies has been

---

conducted over the past two decades through the encouragement of optimising heavy-oil transportation using water-lubricated flow techniques and improving pumping requirements in mature oil fields that have increased water production rates. Despite this, most of the applicable literature is based around the earlier work of the construction of flow regime maps; however, inconsistencies in flow behaviour in various experimental arrangements between numerous authors have caused further confusion on the true behaviour of liquid-liquid flows. In addition, there is a very limited data set of oil-water flow regimes, particularly slug flow developments in both horizontal and slightly deviated pipelines throughout literature. Hence, the formation of dual liquid slug flow between transitions of other flow regimes is still unclear.

A majority of previous works are of great interest to this project because they can be used as a baseline to isolate regions of possible parameter configurations to pinpoint slug flow development within a concentric flow path. A variety of liquid-liquid flow regimes have been observed. The majority of the early studies identify the flow behaviours based on various conventional techniques such as monitoring abrupt fluctuations in the average flow line pressure drops, visual observations or standard photographic/video imaging (Brauner, 2003). Recent studies now use additional techniques in correspondence to conventional methods for data back-up and validation, such as measurements of conductivity from probes, local hold-up samples from Gamma measurements for density variants and average water hold-up measurements. Subsequently, during high flowrates, the flow regimes and transitions cannot be seen through standard imaging techniques nor with the capability of the naked human eye. Further developments have emerged in measuring and identifying different flow regime patterns in more complex and turbulent systems. A popular example can be seen in high-speed imaging tools that use shadowgraph techniques to capture high-velocity flow patterns with significant turbulence and the instantaneous closure of valves to measure in-situ phase flow fraction. In addition, experimental set-ups for multiphase flow investigations have advanced even further.

The use of in-pipe tools to measure flow has substantial limitations when collecting data, such as only being applicable to localised regions, physical interaction against the flow line can affect the flow behaviour, and the capability of velocity measurements in continuous changes of spatial distributions are not considered. Developments of Laser Doppler Anemometry (LDA) provide the ability to obtain flow velocity data at specific regions of a test section that intrusive probes cannot achieve. This laser-controlled experimental technique can allow for a better understanding of liquid-liquid flow characteristics through the use of Planar Laser-Induced Fluorescence (PLIF) and Particle Image Velocimetry (PIV) or Particle Tracking Velocimetry (PTV). Many previous studies have adopted this technique when observing liquid-liquid flow behaviour by identifying

---

in-situ phase fractions and instantaneous velocity parameters; (Kumara, Halvorsen and Melaaen, 2010; Morgan *et al.*, 2012a; Morgan *et al.*, 2012b; Morgan *et al.*, 2013; Ibarra, 2017). Understanding the fundamental behaviour of various configurations of multiphase flow is difficult to achieve. The application of thermodynamic and material balance principles through the conservation and momentum cannot reliably apply to multiphase flow in ways that more simplistic systems such as single-phase laminar flow can be applied. This is because introducing more than one phase component within a common flow line, typically in a turbulent form, results in both experimental and computational complications. Hence, alternative approaches must be considered. Proposals of superimposing closure relationships incorporating eddy-flow currents have been made where turbulent flow models can be developed, and experimental data can be instigated to enhance and validate new models of predicting flow behaviour. Nevertheless, the accuracy and reliability can vary depending on the experimental conditions a dataset was gathered from.

The human bias of judgement that decides on which categories of flow regimes are defined can also impact false data acquisition. These issues must be further checked, and a clear distinction of flow behaviour for individual flow types must be set in place. From early work, the identification of experimental and computational studies have resulted in empirical correlations for predicting pressure drops across in-situ phase fractions and flow regimes within pipes of various orientations. See examples by Hagedorn and Brown (1965) and Beggs and Brill (1973) that are still being used in current applications such as oil and gas pipelines and refineries. In addition, there have been proposals for solving the conservation and momentum equation when coupled with closure relationships that produce a mechanistic model to predict flow regime behaviour in gas-liquid flows under horizontal and slightly deviated pipelines with slug flow models from Taitel and Dukler (1976) and Taitel and Barnea (1990) respectably. Developments for liquid-liquid flow patterns still need to be made, as further understanding of the mechanism of multi-incompressible flow is required to be understood through consistent experimental investigations that are applicable to current industrial circumstances.

### **1.1.1 Key Studies of Liquid-Liquid Flow in Pipes**

Publications of liquid-liquid flow studies in pipes began between the late 1950s and early 1960s. The pioneering work of Russell and Charles (1959) steered the idea of multiphase flow to new perspectives, as three distinct physical observations of flow patterns had been made when instigating changes of operational variables upon a horizontal pipeline containing an oil-water mixture. The flow patterns that were observed were entitled by the authors as stratified flow,

---

bubble flow and mixed flow. It was also revealed that these flow behaviours have an impact on the ability to transfer liquids more efficiently across a pipeline and had therefore developed a friction factor based on the superficial water velocity. However, this was only applicable to specific experimental conditions. Hence, further studies followed, which led to one of the most significant developments in oil-water multiphase flow by Charles, Govier and Hodgson (1961). This was the first publication to discover a new flow regime known as slug flow and developed systematic descriptions of various flow regime types from 2D maps. Sinclair (1970) had shown that the transitions from laminar/turbulent flows between multiple phases could result in changes between stable/unstable flow regimes in oil-water flows through pipes. Therefore, adopting a similar approach to Russell and Charles (1959), by developing the Reynolds number-friction factor correlation, which was applied successfully to large diameter pipes. Later on, further studies started to arise that specifically looked at oil-water horizontal pipes; Hasson, Mann and Nir (1970); Oglesby (1979); Arirachakaran et al. (1989) and many more. Yet, these investigations are only limited to looking at directly horizontal orientated pipes.

Recent advancements in understanding multiphase flow have found that slight changes in the inclination of pipe orientation directly from the horizontal have a substantial effect on flow behaviour. Gravitational influences act depending on the direction of liquid-liquid flow regime transitions, which is contingent on the type of inclination the flow travels through. For instance, flow on upward inclinations requires greater pumping power (and hence a more significant pressure differential) to reach the same velocity under a horizontal condition. In contrast, downward inclinations have the opposite effect (Kumara, Halvorsen and Melaaen, 2009). There are merely a handful of studies that have investigated inclined flow behaviour; (Oddie et al., 2003; Lum, Al-Wahaibi and Angeli, 2006; Rodriguez and Oliemans, 2006; Atmaca et al., 2009; Strazza et al., 2011; Shi, 2015; Ibarra, 2017; Nossen et al., 2017). The majority of studies that investigate either or both horizontal and inclined flow typically use medium-heavy oil due to the current state of interest within the petroleum industry, where larger quantities of heavy oil are produced due to the substantial depletion of conventional light oil.

In recent publications, the use of technological advancements in multiphase flow pipeline measurements have also been developed to better characterise liquid-liquid flows. As previously explained, these advanced measuring techniques and apparatuses have been implemented in various studies from literature; (Morgan et al., 2012b; Morgan et al., 2013; Ibarra et al., 2018). These studies benefited from the use of highly accurate laser-based imaging tools such as a PLIF, PIV or PTV to provide more detailed flow information and allow to study various flow configurations to obtain information on droplet size distribution, phase distribution and in-situ

---

phase fraction on horizontal and slightly-inclined pipes. In-depth review papers on liquid-liquid experiments using horizontal and slightly-inclined pipe orientations can be found in literature; (Ghosh et al., 2009; Martínez-Palou et al., 2011; Ibarra, Matar and Zadrazil, 2015; Ismail et al., 2015a; Wong, Lim and Dol, 2015)

### **1.1.2 Previous Experimental Work from Cranfield University**

Numerous studies have investigated (to some degree) liquid-liquid flow behaviours in either or both horizontal and slightly inclined pipe configurations at Cranfield University - Oil and Gas Engineering Centre. All experimental data from each study (including the data obtained from this project) was gathered from a common/related lab arrangement. All previous focused work observed the characterization of high-viscosity oils using at least one of the two experimental test rigs, which were (1) the horizontal (inclinable) 1-inch (0.0254m) rig and (2) the 3-inch (0.0762m) internal diameter loop chronologically conducted by Al-Awadi (2011); Alagbe (2013); and Shi (2015).

Al-Awadi (2011) studied a heavy-oil-based experimental investigation between both two-phase (air-oil and water-oil) flows and three-phase (air-water-oil and oil-water-sand) fluid mixtures. The oil used was CYL1000 with a viscosity that experimentally varies between 3800-17000mPa.s. The principal objective of Al-Awadi (2011) was to examine the effects of water cut, variations in temperature and pressure drop on flow regime characteristics such as slug flow, then compare models from literature with the author's findings. Alagbe (2013) numerically and experimentally studies the behaviour of heavy oil flow mixtures. Using both CYL680 and CYL1000 oil with viscosities varying between 3700-7100mPa.s within a 1-inch internal diameter pipe of direct horizontal orientation in a continuously stabilised temperature of 25°C. Two-phase and three-phase flow behaviour was observed using water-sand, oil-water and oil-water-sand mixtures. Multiple flow regimes were identified within the experimental analysis, particularly from the oil-water set-up, where observations of intermittent plugs (smaller slug formations) were made in the forms of both water and oil phases. These intermittent formations were oil plugs in water ( $P_o$ ) and water plugs in oil ( $P_w$ ). Successful numerical comparisons were achieved by imposing a concentric inlet boundary condition of the modelled test pipe, coupled with a series of turbulent models enabled by user-defined functions.

Finally, the most recent study of relevance to this thesis was conducted by Shi (2015) by further studying the behaviour of highly-viscous oils in a horizontal 1-inch internal diameter pipe loop through an experimental investigation using CYL680 with a viscosity between 3300-5600mPa.s. Furthermore, the experimental data is compared through numerical and mechanistic

---

analytical comparisons using Computational Fluid Dynamics (CFD). It can be suggested that there is no real collaboration of data from literature; hence the work of Shi (2015) can be appreciated as a very valuable asset to liquid-liquid multiphase flow. This is because the study has collected and compared various data sets from previous experimental work, both internally and externally, from the University of Cranfield to collate a better understanding of how several proposed models behave against diverse experimental results.

## **1.2 Project Motivation and Objectives**

There is very little understanding of how slug flow patterns are formed within liquid-liquid formations. The simultaneous transportation of two or more incompressible fluids through a conventional pipeline (particularly oil-water flow) over long distances of varying terrain is becoming increasingly common within industrial applications. Hence, there is a great need to optimise pipe design and carefully consider tactical operational inputs to maximise flow efficiency by preventing unwanted hydrodynamic behaviour (slug flow in particular), which depends on the pipeline conditions that vary over time. Optimising pipe configurations is extremely advantageous, as this can prevent and/or mitigate; compromise of pipe integrity, a decline of fluid pumping performance/capacity, increases in operation and capital expenditure, environmental risks and risk of field safety. Hence, this study aims to demonstrate the existence of both terrain and hydrodynamic induced liquid-liquid intermittent flow regimes under steady-state (or pseudo steady-state) conditions and be able to predict and prevent the development of dual incompressible intermittent flow regimes such as oil-water slug flow.

To achieve this aim, the following objectives are considered: (1) Investigate the behaviour and conditions required for intermittent flow to develop by means of setting up and conducting a series of experimental investigations on oil-water multiphase flow. This is achieved by using a 1-inch pipe multiphase flow loop test system under horizontal and slightly-inclined orientations. The study will primarily examine how flow hydrodynamics such as flow regimes/flow transitions, pressure gradients and water hold-up are affected through changes of (i) multiple fluid properties such as oil density and viscosity, (ii) pipeline design attributes such as the scale-up effect through changes in pipe diameter sizes (by experimenting on 1-inch multiphase pipeline test loops and comparing the results from large pipe diameters from literature) and gravitational effects by changing the angular orientation of the pipeline (horizontal and slightly-inclined angles from  $0^\circ$  to  $5^\circ$ ), (iii) operational constraints of controlling the liquid flow through alterations of flow velocity by accordingly adjusting the pumping power and (iv) analyse the physical behaviour of intermittent flow by utilising frequency analysis of the changes in hold-up attributions. (2)



---

Predicting the development of intermittent flow. The resulting experimental data will provide a detailed insight of the possible combinations of fluid properties, pipe design and operational variables that can cause slug flow within liquid-liquid pipes. When sufficient data for slug flow is attained, this study will look to produce dimensionless 2D maps that predict the advances of liquid-liquid slugs and the respective transitioning flow regimes. In addition, new categories of flow regimes will be suggested to fit better for the behaviour of various hydrodynamic changes for liquid-liquid flow. (3) Predict the behaviour of larger oil-water pipelines by means of scale-up analysis. The experimental data and corresponding maps will then be validated against other experimental data collected from previous literature work and superimposed all data to compare/contrast the findings. The resulting information from this work will aim to expand the fundamental understanding of liquid-liquid multiphase flow behaviour by developing better correlations of hold-up and pressure gradient, which in turn will allow to predict the flow when scaling. The experimental data and maps will also aim to aid pipelines to be designed and continuously operated effectively over a range of alternating conditions that continues to alter over time based on the conditions of the pipeline and potential fluid source.

### 1.3 Thesis Structure

The structure of this thesis is sectioned into eight separate chapters in chronological order based on how the information and data were attained throughout the project time period. This is systematically shown in *Figure 1-1*.

<b>CHAP-1</b>	<b>INTRODUCTION</b>
<b>CHAP-2</b>	<b>LITRITURE REVIEW</b>
<b>CHAP-3</b>	<b>EXPERIMENTAL SET-UP AND METHODOLOGY</b>
<b>CHAP-4</b>	<b>EXPERIMENTAL RESULTS</b>
<b>CHAP-5</b>	<b>DEVELOPMENT OF KEY CORRELATIONS</b>
<b>CHAP-6</b>	<b>DIMENSIONLESS GROUPING</b>
<b>CHAP-7</b>	<b>SCALE-UP ANALYSIS</b>
<b>CHAP-8</b>	<b>FUTURE WORK, RECOMMENDATIONS AND</b>

*Figure 1-1: Thesis chapter structure outline in chronological order.*

---

Excluding the introduction, the structure of this thesis begins in chapter 2, where an in-depth literature review is discussed on liquid-liquid flows in pipes, particularly when looking into oil-water multiphase flow systems. The topics mentioned are; current theoretical models of key variables, typically seen behaviour of liquid-liquid multiphase flow, flow regimes and corresponding results from literature along with a summary of all the experimental results and set-up configurations. Chapter 3 is based on the experimental analysis of this study and the detailed layout of how the experiment is set up, executed and controlled. Calibration procedures of both fluid phases and system equipment are also considered. Chapter 4 demonstrates the processed findings from the experiment in such that flow regime maps, high-speed images of all observed flow regimes, along with the processed pressure and hold-up data are presented. Additionally, frequency analysis was also conducted on intermittent flows. Chapter 5 uses the experiment's measured pressure and hold-up data to develop the respective correlations. The correlations are then compared to other data from literature to validate the applicable range of system variables and condition combinations. Additionally, other well-known and used correlations in both industry and literature are also compared against the same data to assess the contrasting models. Chapter 6 uses the results from chapter 4 to see how the attained data can be used to develop a new approach to mapping flow regimes using 2D dimensionless mapping analysis by means of modifying the Froude number via the hydraulic diameter of the individual phases. Furthermore, other similar works from literature are also subjected to the newly proposed dimensionless Froude number. Chapter 7 is an analysis of the scale-up protocol from the 1-inch data based on dimensionless methods. There are two parts to this section: a prototype is developed based on the correlations of pressure and hold-up, and experimental and industrial-sized pipes are scaled. The other is real experimental work from literature with real data and has undergone the same scale-up procedure. Finally, chapter 8 is split between industrial recommendations to prevent and mitigate the development of oil-water intermittent flows and the future work that would complement the results of this work. Finally, a concluding section that answers this thesis's research question is presented, summarising the work that has been done as a contributing factor to knowledge.

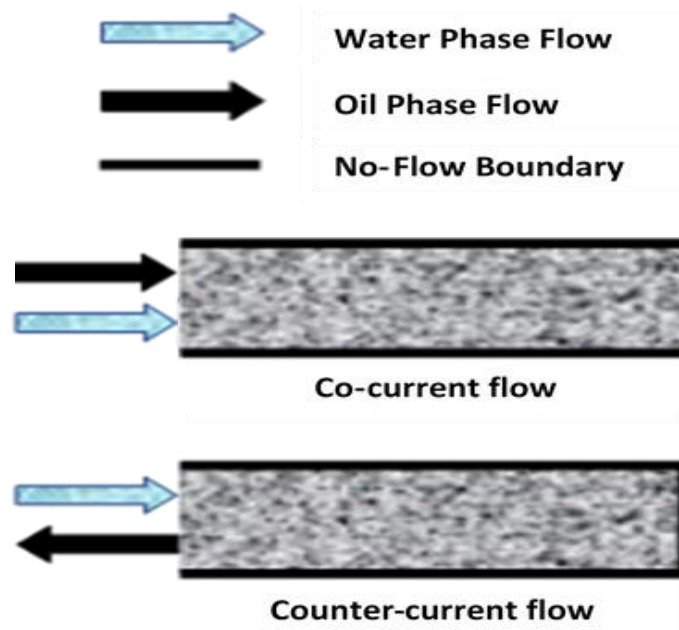
## CHAPTER 2

# LITERATURE REVIEW

Fluid motion through channels and pipes of various dimensions and size extremes can be found in both nature and industrial applications under numerous mixtures of different immiscible phases that simultaneously travel through a common flow path. This phenomenon is known as multiphase flow and has been studied extensively to predict flow behaviour under various combinations of parameter configurations that affect individual flow characteristics in order to optimise the transportation of fluids. Parameters that are known for contributing to changes in flow behaviour are geometric configurations/gravitational orientations of the relevant flow line, fluid properties and operational/volumetric quantities. The simplest form of flow is considered to be single-phase. The equation for conservation and momentum can accurately describe single-phase flow using the Navier-Stokes equations in terms of pressure, volume and temperature under laminar flow conditions. However, the introduction of additional phases and unstable (turbulent) behaviour further complicates the analysis and prediction of flow behaviour due to the presence of additional parameters that need to be considered in multiphase systems.

There are many mixtures of multiphase flow under the conditions of either counter-current or co-current flow directions. Co-current flow is the displacement of two or more separate phases that simultaneously flow in the same direction. As counter-current flow institutes at least one of the phases to undergo a fluid displacement in the opposite direction of injecting, which usually results from an injected fluid from the inlet to displace the residing fluid out from the same inlet due to the presence of no-flow boundaries of the medium. An example of co-current and counter-current flow can be found in *Figure 2-1*. Whether a multiphase flow system is under co-current or counter-current conditions is dependent on no-flow boundaries that contain the fluids and force flow in the geometrical form of the medium that contains the fluids. However, counter-current conditions are usually found in porous formations of sedimentary rock that contain faults and/or

cementations, condemning the fluid to have no other flow path option, resulting in this flow displacement. Pipes, ducts or any other tubular medium which carries fluids usually do not undergo counter-current conditions as the flow paths are designed to transport multiple phases through a single direction.



*Figure 2-1: Depiction of oil-water co-current and counter-current flow from varying boundary conditions that cause the two behaviours to occur.*

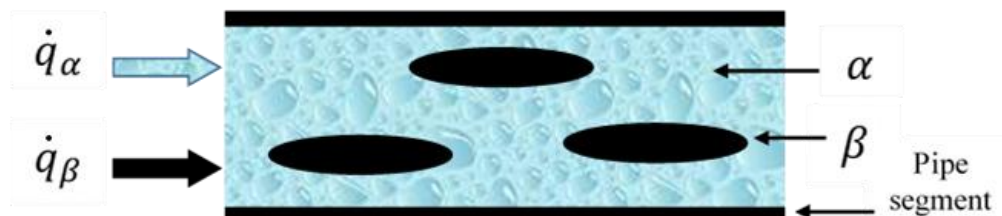
Typical multiphase flow types are usually in the form of two-phase flow gas-liquid, liquid-liquid and solid-liquid mixtures. Three-phase flows typically incorporate mixtures of gas-liquid-liquid and gas-liquid-solid. Finally, a four-phase flow would typically see all phases of state and matter to commingle in the form of gas-liquid-liquid-solid. The description of each flow must integrate the interactions between different phases in a physical form, such as the momentum of inertia, mass transfer, phase distribution and interfacial forces that form a representative governing equation. Closure relationships of governing equations for individual multiphase flow mixtures have been used to produce predictive models. These models are usually generated from simplifications by incorporating assumptions and correlations that are gathered from experimental datasets. However, there is very little understanding of how the physics of multiphase flow is mechanised, and a great ordeal of inconsistent experimental results have been found across literature. In addition, the interactions and spatial configurations between different phases that flow together through pipes known as flow regimes can have significant changes in physical

characteristics based on various parameter changes and configurations. In fact, the behaviour of one type of multiphase flow mixture cannot be represented in the same way as other mixtures due to individual phases having their own unique properties that interact in accordance when paired with different phases. For instance, liquid-liquid flows cannot be characterised in the same way as gas-liquid flows. Hence, individual characteristics must be identified to distinguish different multiphase flow mixtures.

Oil-water two-phase flow is the displacement of two incompressible and immiscible liquids that interact with each other in the form of an aqueous phase (water) and a non-aqueous, organic phase (oil). Investigations of oil-water two-phase flows have not been as extensively explored compared to other multiphase flow mixtures. They are becoming a greater concern within the petroleum industry with the increase and decrease in water and oil production, respectively. This thesis will mainly focus on the industrial applications found within the petroleum industry and the issues that arise when dealing with the transportation of only two-phase liquid-liquid flows of oil-water emulsions in export pipes of horizontal and slightly inclined orientations. In the present study, liquid-liquid flow is considered to have some degree of phase separation between the different components of a given mixture at scales much greater than the molecular level. However, this still leaves a great ordeal of diverse multiphase flow fields that have also been investigated and not yet fully understood. This thesis acknowledges the great extent to which different multiphase studies exist and currently still need to be explored.

## 2.1 Key Oil-Water Flow Parameters and Definitions in Pipes

This section will discuss the typical flow parameters and definitions used to describe the most basic form of multiphase flow behaviour of two-phase oil-water flow under co-current flow. Where one of the two phases is considered to be either a heavier phase ( $\alpha$ ) and lighter phase ( $\beta$ ) in terms of density while flowing with their own respective volumetric flowrates  $\dot{q}_\alpha$  and  $\dot{q}_\beta$ , depicted in *Figure 2-2*.



*Figure 2-2: Typical co-current two-phase flow in a pipeline between a heavier and lighter fluid phase  $\alpha$  and/or  $\beta$  (depicted example as - oil-water flow).*

---

### 2.1.1 Phase Hold-up and Phase Volume Fraction

Phase hold-up  $H_{\alpha\beta}$  is the volumetric measurement of the quantity of some localised individual phase  $\alpha\beta$ , that flows through a controlled volume with additional phases. In multiphase flow, during the simultaneous displacement of two fluid phases in a controlled volume (e.g. pipeline), individual phase behaviours are observed quantitatively in the form of volumetric analysis to study both individual and combined flow parameters and performance, such as velocities and the presence of slips. Phase hold-up can vary depending on operational inputs and pipe geometry; in fact, the hold-up of water and oil  $H_w$  and  $H_o$ , respectively, have a direct relationship with the medium geometry as this controls the fluid interface height within the pipe. This defines the vertical length from the lowest region of the pipe to alternated regions less than the diameter of the pipe  $D$ . There are two forms of describing individual phase hold-up. One is obtained in the form of a volume ratio, the in-situ phase hold-up of water and oil is described by:

$$H_w = \frac{V_w}{V} = 1 - H_o \quad (2-1)$$

$$H_o = \frac{V_o}{V} = 1 - H_w \quad (2-2)$$

The individual volume of water and oil phases found within a common flow line,  $V_w$  and  $V_o$ , respectively, that is occupied over the total volume of the respective pipeline  $V$  represents the phase hold-up. The second approach is to look at phase hold-up in terms of cross-sectional analysis, and hence Eqs. (2-1) and (2-2) can also be written in the form of:

$$H_w = \frac{A_w}{A} = \frac{A_w}{\frac{\pi}{4}D^2} = 1 - H_o \quad (2-3)$$

$$H_o = \frac{A_o}{A} = \frac{A_o}{\frac{\pi}{4}D^2} = 1 - H_w \quad (2-4)$$

where,  $A_w$  and  $A_o$  is the phase areas occupied by water and oil from a given pipe cross-section  $A$ , respectively. Irrespective of whether volumetric or cross-sectional dimensions are considered, the ratios between the heavier and lighter fluids are indirectly proportional to each other as:

$$H_w + H_o = 1 \quad (2-5)$$

Hence, the pipe volume and cross-sectional area can be defined from the sum of individual phases:

---


$$V_w + V_o = V \quad (2-6)$$

$$A_w + A_o = A \quad (2-7)$$

The phase volume fraction is also a vital multiphase flow parameter as this identifies the inlet water fraction, which acts as an individual phase hold-up for water. In terms of the water phase, water cut (phase fraction for water) and water hold-up differ depending on discrete fluid properties such as density and viscosity. Water cut and oil cut utilises volumetric flowrates to develop volume in terms of fractions of the respective phase  $\lambda_{\alpha\beta}$ . The non-slip homogeneous phase volume fractions for water and oil are described as follows:

$$\lambda_w = \frac{\dot{q}_w}{\dot{q}_w + \dot{q}_o} = 1 - \lambda_o \quad (2-8)$$

$$\lambda_o = \frac{\dot{q}_o}{\dot{q}_w + \dot{q}_o} = 1 - \lambda_w \quad (2-9)$$

$$\lambda_o + \lambda_w = 1 \quad (2-10)$$

where  $\lambda_w$  and  $\lambda_o$  is the phase volume fraction of water and oil, respectively while  $\dot{q}_w$  and  $\dot{q}_o$  is the individual phase volumetric flowrate of water and oil, respectively. Similarly to in-situ phase hold-up, phase volume fractions can also be expressed in terms of cross-section:

$$\lambda_w = \frac{A_w}{A_w + A_o} = 1 - \lambda_o \quad (2-11)$$

$$\lambda_o = \frac{A_o}{A_w + A_o} = 1 - \lambda_w \quad (2-12)$$

When in-situ phase hold-up and inlet phase fraction are attained, the phase hold-up ratio  $\bar{h}$  is:

$$\bar{h} = \frac{H_w \lambda_o}{H_o \lambda_w} \quad (2-13)$$

---

The hold-up can be used as a means of a parameter that describes the phenomenon that combines inlet and local phase hold-up for individual phases to form a unity between different scenarios and phase interactions of the pipe flow. In two-phase flow, the use of a hold-up ratio can reveal the slip conditions with respect to the co-existing phases that interact with each other within the pipeline and is greatly dependent on phase velocity.

### 2.1.2 Phase Velocity and Slip

The flow velocity of a given phase and/or the combined mixture of phases throughout the entire multiphase system is described in diverse ways. The definition of the superficial velocity of a given phase is the fluid's average velocity over the entire cross-sectional area of the pipe in such a way that individual phases are treated to be flowing through the pipeline isolated, without the presence of the other partnering fluids. Superficial velocity can be written as:

$$v_{sw} = \frac{\dot{q}_w}{A} = \frac{\dot{m}_w}{\rho_w A} = \frac{\dot{m}_w}{\rho_w \frac{\pi}{4} D^2} \quad (2-14)$$

$$v_{so} = \frac{\dot{q}_o}{A} = \frac{\dot{m}_o}{\rho_o A} = \frac{\dot{m}_o}{\rho_o \frac{\pi}{4} D^2} \quad (2-15)$$

$$v_m = v_{sw} + v_{so} \quad (2-16)$$

where,  $v_{sw}$  and  $v_{so}$  are the superficial velocities of the water and oil phases, respectively. The volumetric flowrate can also be written in terms of mass flow, the low rate of water and oil,  $\dot{m}_w$  and  $\dot{m}_o$  over the density of the phase  $\rho_w$  and  $\rho_o$  in respective order. It is also indicative that the superficial velocities can be expressed based on the geometric area of the pipe in terms of diameter when using the same approach as Eqs. (2-3) and (2-4). The mixture velocity  $v_m$ , throughout the entire pipe foundation can be conveyed through the sum of the individual superficial phase velocities as shown in Eq. (2-16). Similar to that of phase hold-up, the measurement of phase velocity along the pipe inlet cross-section can also be different from measurements along the entire scale of the pipeline system. This type of velocity is known as the in-situ average phase velocity:

$$v_w = \frac{\dot{q}_w}{A_w} = \frac{\dot{m}_w}{\rho_w A_w} = \frac{v_{sw} A}{A_w} = \frac{v_{sw}}{H_w} = \frac{v_{sw}}{1 - H_o} \quad (2-17)$$



---


$$v_o = \frac{\dot{q}_o}{A_o} = \frac{v_{so}A}{A_o} = \frac{v_{so}}{H_o} = \frac{v_{so}}{1 - H_w} \quad (2-18)$$

The in-situ average phase velocities of water and oil,  $v_o$  and  $v_w$ , respectively, can be expressed in terms of the relevant inlet pipeline velocity over the cross-sectional hold-up. However, it must be noted that these velocities do not construct the true velocity for distinct fluid phases of the varying hold-up. This is because the true velocity is actually expressed in terms of the volumetric flowrate of the respective phase going through a pipe cross-section at a point in time divided by the portion the phase occupies from the respective cross-section. The real velocity of some given phase  $\alpha\beta$  is as follows:

$$v_{\alpha\beta \text{ real}} = \frac{\dot{q}_{\alpha\beta}}{A_{\alpha\beta}} \quad (2-19)$$

where the real flow velocity of a phase is given as,  $v_{\alpha\beta \text{ real}}$ ,  $\dot{q}_{\alpha\beta}$  is the volumetric flowrate of the same phase while  $A_{\alpha\beta}$  is the area occupied by the phase against the pipe cross-section. Consequently, it is difficult to calculate the true portion of the area a phase occupies due to issues that arise when measuring these areas, which continuously change throughout the entire multiphase flow process. Hence, superficial velocities are commonly acquired by measuring the fluid rate and using the known internal diameter of the manufactured pipeline that transports the fluid. The superficial velocity of a phase  $v_{s\alpha\beta}$  is typically much smaller than the real velocity value because the areas that institute the equations are not the same ( $A_{\alpha\beta} < A \rightarrow v_{s\alpha\beta} < v_{\alpha\beta \text{ real}}$ ). Nevertheless, superficial and in-situ velocities are widely used throughout multiphase flow analysis. Other phenomena of velocity interactions between multiple phases are slip velocities  $v_s$ . Slip velocity is defined as the difference of in-situ average phase velocities between two or more fluids that form a multiphase mixture.

$$v_s = \frac{v_{sw}}{H_w} - \frac{v_{so}}{H_o} = \frac{1}{A} \left( \frac{\dot{q}_w}{1 - H_o} - \frac{\dot{q}_o}{H_o} \right) \quad (2-20)$$

This occurs when one fluid travels faster than its corresponding pair, resulting in overtaking the slower fluid within the pipeline. Slower fluids typically depend on combinations between their constituent fluid properties of high density and high viscosity bounds and vice versa for faster fluids. Changes can be seen from slip velocities when studied under different geometric views.

---

For example, observing slip velocity from a pipe diameter segment would differ from when observed under a volumetric geometry. However, when the presence of slip is negligible, the volume hold-up is equal to the phase cross-sectional hold-up. Slips are expressed in terms of flowrates and hold-ups (usually in terms of cross-sectional geometry) and correlate these two parameters to find the system slip velocity, as shown in Eq. (2-20).

### 2.1.3 Mixture Parameters

Mixture parameters are similar to that of typical individual fluid variables such as density, velocity and viscosity from distinct phases. The mixture mass flux  $Q_m$  can be mathematically written as:

$$Q_m = \frac{\dot{m}_m}{A} = \frac{\dot{m}_m}{\frac{\pi}{4} D^2} \quad (2-21)$$

The mixture mass flux is defined as the ratio between the mass flowrate of the mixture  $\dot{m}_m$  over the cross-sectional area of the inner pipeline diameter. It behaves similarly to that of the mixture velocity, where the reduction of pipe internal diameter that incorporates a continuous flowrate will result in an increase in flux. However, this, in turn, can reduce the flux capacity of the respective pipeline. This can cause significant turbulent flows, resulting in the increase in pipe wear and corrosion rates as flow speeds intensify. Key mixture variables such as density, viscosity and velocity are difficult to directly measure in mixtures because fluid flows continuously change in terms of quantity and flow pattern as it travels across various distances over a pipeline. Identifying key mixture variables is classically premeditated through a combined formula that incorporates individual measurements of each constituent phase within the mixture:

$$\rho_m = H_w(\rho_w - \rho_o) + \rho_o \quad (2-22)$$

$$\mu_m = H_w(\mu_w - \mu_o) + \mu_o \quad (2-23)$$

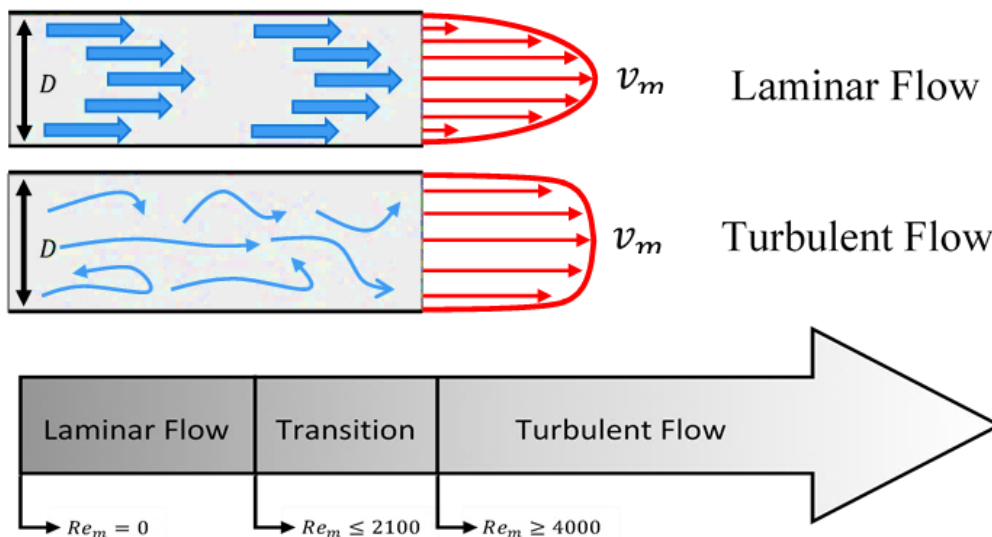
$$v_{sm} = \frac{H_w \rho_w v_{sw} + (1 - H_w) \rho_o v_{so}}{\rho_m} \quad (2-24)$$

Eqs. (2-22) - (2-24) represent the mixture variables of density  $\rho_m$ , viscosity  $\mu_m$  and superficial velocity  $v_{sm}$ . These predictions are mainly based on the hold-up of the phases derived from a pipe's cross-section. When dealing with oil-water two-phase flows, water phase hold-up is used

as a reference point to describe the capacity of each phase. The final parameter that describes a mixture's flow behaviour is the Reynolds number  $Re_m$ . The Reynolds number is a dimensionless form of measurement which describes the fluid flow behaviour and determines whether a system is under laminar or turbulent conditions. It is important to predict these flow behaviours because turbulence condemns fluids to progressively mix and cause shear between the fluids and the pipe walls. Consequently, this results in amplified viscous losses, which lowers pumping efficiency.

$$Re_m = \frac{\rho_m v_{sm} D}{\mu_m} \quad (2-25)$$

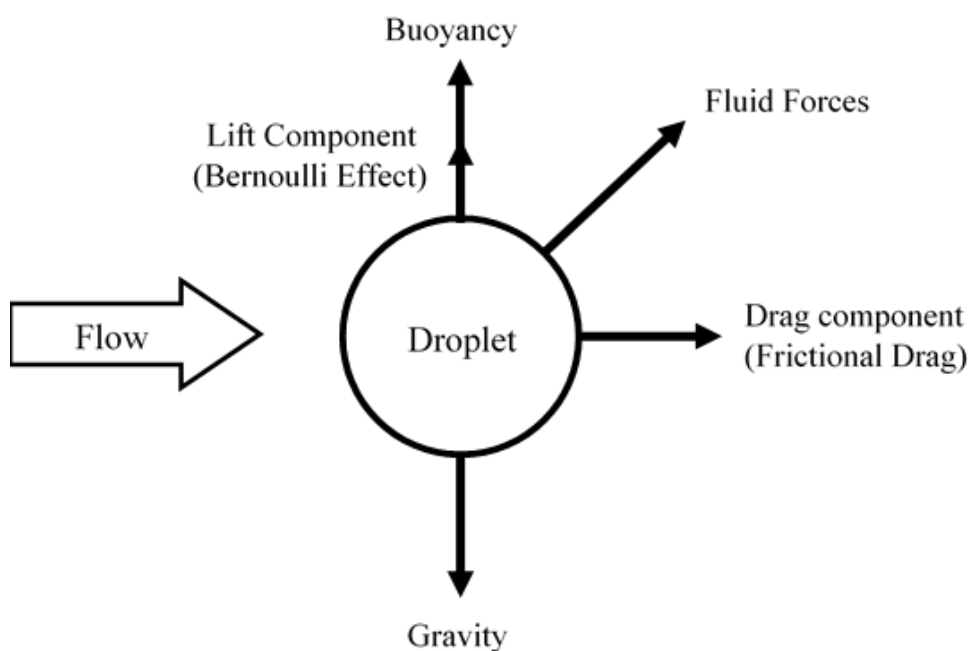
As shown in Eq. (2-25), the Reynolds number is directly proportional to the product of the mixture density, velocity and representative pipe internal diameter, while the mixture viscosity is indirectly proportional to the Reynolds number. Fluid flow within pipes has the Reynolds number to represent laminar flow as  $Re_m \leq 2100$  whereas turbulent flow is represented as  $Re_m \geq 4000$ . When  $2100 \leq Re_m \leq 4000$ , this is known as the flow to be in a state of transition between laminar and turbulent flow, as shown in *Figure 2-3*. It can either be classified as a laminar or turbulent regime which requires additional models to verify which flow types the transition favours to become. However, this is not fully necessary when dealing with fluid pipeline transportation. Designing pipelines for fluid export usually integrate systems with true turbulent or laminar characteristics depending on the applications.



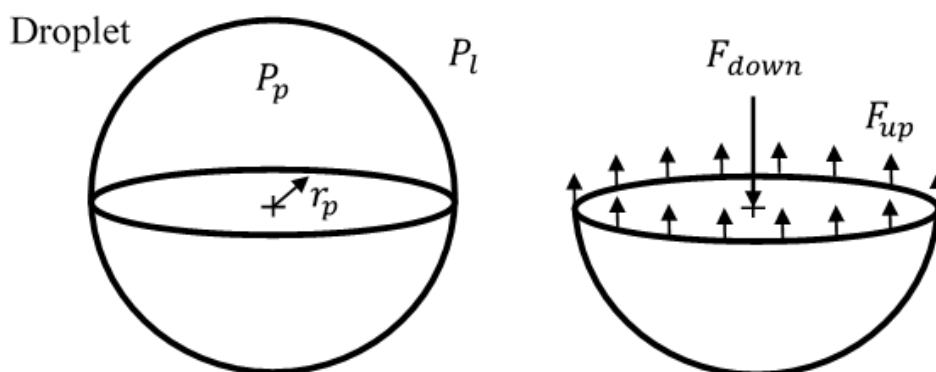
*Figure 2-3: Laminar and turbulent flow patterns with Reynolds number transition from laminar to turbulent fluid flow within pipes.*

## 2.1.4 Forces Acting on Droplets

The forces a spherical liquid droplet (particle) is subject to can be divided into two parts. The first one covering the surrounding forces acting upon the droplet phase, and the second one covering the internal forces found within droplets, which are predominantly driven by their surface tension and differential pressure. *Figure 2-4* and *Figure 2-5* show the key forces that typically act upon a droplet within another fluid, externally and internally, respectively.



*Figure 2-4: External forces acting upon a liquid droplet within a flow.*



*Figure 2-5: Internal forces acting in a liquid droplet within a flow.*

---

When considering spherical droplets within a fluid flow, these droplets experience external forces from the surrounding flow. Especially, the force balance on the vertical axis can determine which direction the droplets will be moving towards. There are four common forces which act on a droplet on the vertical axis: (1) forces due to gravity, (2) forces due to buoyancy, (3) forces due to viscous drag subjected from the external fluid and (4) lifting force which is a result from a pressure differential around the droplet (Bernoulli effect). Gravitational forces are among the most dominating forces when a flow stream is under a laminar state. This is because the movement of individual phase droplets is not dynamic enough to overcome the gravitational and buoyancy forces acting upon each phase. The rate of separation is far greater than the opposing disturbances that occur, such as drag and inertial forces that can cause lift and mixing to initiate. When under a liquid-liquid state, gravitational forces are not as prominent as gas-liquid flow because of the noticeable density differences between each two-phase condition (Taitel and Dukler, 1976; Morgan et al., 2017); the two forces can be respectively expressed as:

$$F_G = \rho_p g V_p \quad (2-26)$$

$$F_B = \rho_l g V_p \quad (2-27)$$

where  $F_G$  and  $F_B$  are the forces due to gravity and buoyancy, respectively,  $\rho_p$  and  $\rho_l$  are the density of the droplet and surrounding continuous liquid, respectively,  $g$  is the acceleration due to gravity and  $V_p$  is the particle volume. In the case of conventional oil-water flow, water tends to be in a denser phase, while oil is in a lighter phase. The heavier the droplet, the more gravitational forces are favoured over the buoyancy forces and vice versa for less dense fluids (Raj, Chakrabarti and Das, 2005). Hence, gravitational forces are one of the key factors that prevent intermittent flows from developing when acting as the dominant force, as segregated flows prevent intermittent characteristics from forming in the direction of the flow (Tan et al., 2018). Drag  $F_D$  and lift  $F_L$  forces exerted on a droplet can be written as:

$$F_D = \frac{1}{2} \rho_l C_D v_t^2 A_p \quad (2-28)$$

$$F_L = \frac{1}{2} \rho_l C_L v_t^2 A_p \quad (2-29)$$

where  $C_D$  and  $C_L$  are the drag and lift coefficients, respectively,  $v_t$  is the terminal velocity and  $A_p$  is the projected area of the droplet. These forces are mainly driven by the inertial forces in the direction of the flow. For droplets of different sizes, their settling/rising behaviour can be

categorised into three criteria for distinguishing major liquid-liquid flow regimes, based on the particle Reynolds number  $Re_p$ :

$$Re_p = \frac{D_p \rho_l v_t}{\mu_l} \quad (2-30)$$

where  $\mu_l$  is the viscosity of the continuous phase and  $D_p$  is the droplet diameter. The classification of the three flow regime criteria is summarised in *Table 2-1*. Furthermore, when numerous droplets are in concentrated suspensions, they tend to collide with each other, slowing down their terminal velocity as the velocity gradients around each droplet are affected by the presence of nearby droplets. This is referred to as a hindered movement. Inertial forces imply to be the forces due to the momentum of a fluid and can be treated as key driving forces within multiphase flow systems. The main stability of a flow stream is heavily dominated by the product of phase velocity, the length of the flow span perpendicular to the direction of the flow, and the mass (density) of the respective phase(s) that flow through a coherent medium (Joseph, Bannwart and Liu, 1996). The cause of unstable flow patterns, such as intermittent flows, is mainly instigated by the momentum of each phase flow, such that the hydrodynamic conditions are suitable to sustain large accumulations of droplets without causing a breakup. Turbulent flow conditions are where a majority of cases of liquid-liquid intermittent flow arise on a macro scale. Assuming constant fluid viscosity, if a fluid system's inertial force is great enough to initiate turbulent flow, it may be able to form instabilities between the two fluid phases. In some cases, this can cause Eddy current-like formations to form between the two phases creating intermittent segregation. Hence, inertial forces are a vital factor in initiating flow instabilities leading to intermittent flow patterns in macro-scale pipes. However, inertial forces are not the only cause of intermittent characteristics to develop, as other mechanisms are needed to prevent droplet breakup.

<i>Settling Law</i>	<i>Criteria</i>	<i>Terminal Velocity</i>
<i>Stokes Law</i>	$Re_p < 1$	$v_t = \frac{g D_p^2 (\rho_p - \rho_l)}{\mu_l}$
<i>Intermediate Law</i>	$1 < Re_p < 1000$	$v_t = \left[ \frac{2g}{27} \left( \frac{\rho_p - \rho_l}{\rho_l} \right) \right]^{5/7} \left( \frac{D_p^{8/7}}{\mu_l^{3/7}} \right)$
<i>Newton's Law</i>	$Re_p > 1$	$v_t = \sqrt{3 D_p g \left( \frac{\rho_p - \rho_l}{\rho_l} \right)}$

*Table 2-1: Classification of solid settling flow regimes.*

---

Droplets also contain forces within and around their surface. Surface tension is the combination of the cohesive and adhesive forces between a liquid phase and a corresponding adjacent phase or surface (Mandal, Chakrabarti and Das, 2007). In more confined spaces such as a tubular medium, the contact between two adjacent immiscible fluids creates a communal phase boundary layer between each phase and is defined as the interface. When considering two immiscible liquids, such as an oil-water system, the molecular structures of each type of fluid would naturally be equally attracted to their neighbouring constituent droplets in all directions, as close to each other as possible, through certain internal energy (Rodriguez and Castro, 2014). However, the presence of a phase boundary neglects any further neighbouring droplets to be attracted beyond the constituent flow layer. Hence, the molecules of the boundaries develop the greatest amount of cohesive force, causing a tendency in liquids to resist separation through their surface tension, creating an upward/outer force against the surrounding liquid.

Adhesion and cohesion forces are key to the interaction of distinct fluid phases at the interface. Typical intermittent patterns, such as large elongated plugs in a microscale, typically depend on the surface tension. The larger the surface tension, the more difficult it is to breakdown the plug's contouring formation. However, in a macro-scale context, intermittent patterns are rarely seen as spherical forms because of their dynamic nature, which has yet to reach equilibrium (Ramey, 1973). Therefore, intermittent flows attain their unstable characteristics from the shape made from the accumulation of many droplets that are continuously progressing into larger and higher pressured clusters within a lower pressured phase continuum. Intermittent flows generally travel along the edge of a pipeline due to the additional surface tensions found between the liquid and the solid surface of the inner pipe.

$$F_{down} = \pi r_p^2 (P_p - P_l) \quad (2-31)$$

$$F_{up} = 2\pi r_p \sigma \quad (2-32)$$

Eqs. (2-31) and (2-32) show the forces acting within a droplet, where  $F_{up}$  and  $F_{down}$  are the forces acting due to the pressure difference between the droplet  $P_p$  and the continuous liquid phase  $P_l$ ; and surface tension or interfacial tension (IFT)  $\sigma$  respectively, while  $r_p$  is the droplet radius.

### 2.1.5 Physical Properties of Oil

The two essential properties of liquid oil are density and viscosity. This allows a wide range of engineering disciplines to understand the type of oil that will be transported across a flow line.

---

Oil is normally categorised in terms of weight through the oil's own density. Examples such as light oil and heavy oil are found throughout industry. The petroleum industry tends to characterise the type of oil by using the American Petroleum Institute Gravity (*API*) standard to measure how heavier or lighter the oil is in comparison to standard water properties. *API* is associated with the specific gravity  $S_G$  which is defined by the density ratio between the analysed oil fluid and standard water reference density at  $1000 \text{ kg/m}^3$  where,  $S_G = \rho_o / \rho_w$  at  $60^\circ F$  ( $15.56^\circ C$ ) as shown:

$$^\circ API = \frac{141.5}{S_{G \text{ at } 60^\circ F}} - 131.5 \quad (2-33)$$

If water was to be the analysed fluid instead of oil, while still maintaining the water to be the reference fluid,  $^\circ API = 10$  as  $S_G$  would correlate to a one-to-one ratio. The value of  $10^\circ API$  is the standard weight of water within the petroleum industry and is used as a reference point to compare the weight of oil and categorise them. The lower the *API* gravity rating is, the heavier the fluid is reflected to be. There are five categories of oil types when using the *API* system. Any oil compound that has an *API* lower than the water reference at  $10^\circ API$ , is classified as Extra-heavy crude oil, a difficult oil type to extract and transport when using conventional methods. This is because this oil type is much heavier and less mobile in comparison to water. In addition, since injected water is conventionally used to shift the oil through porous rock and pipelines, the dominance of the density and viscosity of heavy oil to water makes production for this oil type challenging. Crude oil is also classified as heavy oil, similar to that of extra heavy oil; however, its density and viscosity is far less than its heavier counterpart and, above all, less than the water reference. Heavy crude oil is defined between  $10 < ^\circ API \leq 23.3$ . Moving onto lighter fluids, intermediate (medium-heavy) oils have an *API* classification between  $23.3 \leq ^\circ API \leq 31.1$ , while very light crude oils have a value of  $^\circ API > 31.1$  (Alboudwarej et al., 2006; Al-Otaibi and Habib, 2015).

It is important to mention that the terms heavy and light oils are references to the degree of load each category compares against based on a fluid's density. However, when considering the transportation of fluids within pipes, it is, in fact, the viscosity that is mainly focused upon during fluid transportation as this controls the fluid mobility and hence productivity throughout a pipeline. There is no definite relationship that uses the viscosity with the *API* system in such a way the density is exploited, but these parameters can be considered compatible with one another because oils that are considered heavier are generally denser and more viscous and vice versa. Nevertheless, viscosity parameters that define the categories of oil types are unclear as multiple



---

authors, institutes and etc., define crude oil groups under different ranges of viscosities (Veil, Quinn and Garcia, 2009). Light and intermediate oils tend to behave similarly to Newtonian fluids under laminar conditions, which are fluids that follow a linear relationship of Newton's law based on the shear stress  $\tau$  against the rate of shear  $\dot{\tau}$ , which is the shear stress over the fluid viscosity. Heavier fluids such as heavy oil-water emulsions tend to not follow the linear relationship of shear stress, and shear rate and hence are classified as non-Newtonian fluids. The density dominance in comparison to the viscosity causes heavier fluids to act in non-linear behaviours between shear stress and respective shear rate across other media such as pipe walls and even against other constituent phases within the flow line.

## 2.2 Multiphase Flow Measurements

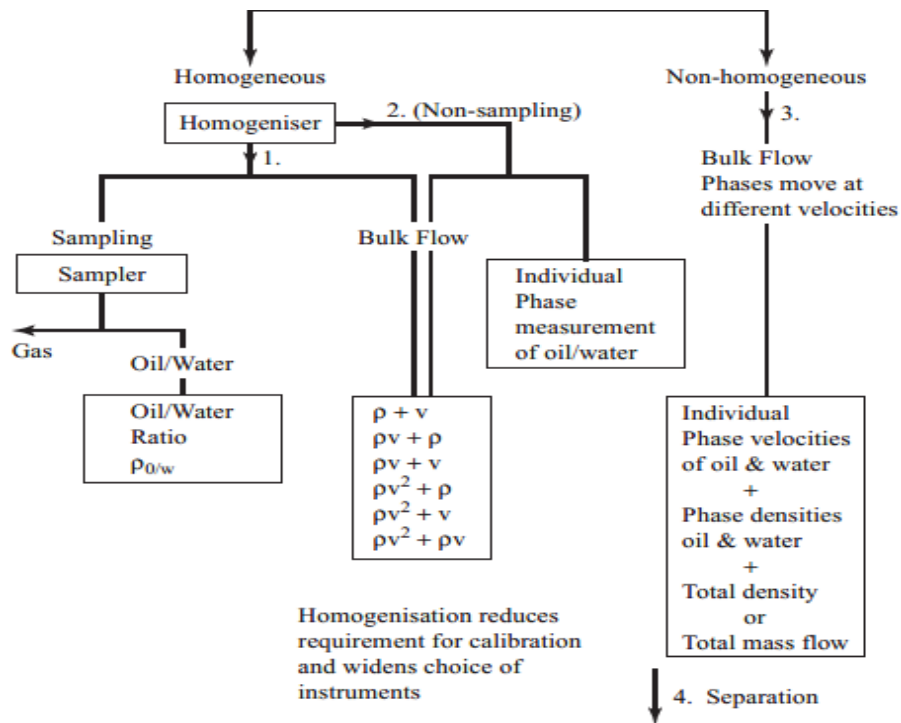
Measuring techniques for fluid mixtures within pipes is a fundamental discipline within both experimental and industrial applications; this is known as multiphase flow metering (MFM). The scope of different MFM techniques and/or tools is vast throughout the petroleum industry and academic research. This section will briefly discuss some enhanced conventional techniques and tools that will be mainly used for the experimental investigation of this work to measure the flow and key parameters of an oil-water multiphase system. The extensive work of Falcone, Hewitt and Alimonti (2009) describes four different routes that lead to MFM when dealing with different types of multiphase systems that contain either or a combination of gas, oil and water phases, as shown in *Figure 2-6*. The first route to MFM is a sampled homogenised system which incorporates three measuring instruments and a separator unit depicted in *Figure 2-7(a)*. Once the main flow system passes through the homogeniser, a sample is extracted from the homogenous flow line and separated between its constituent matters of the state of gas and liquid (if there is any presence of gas phases). When the main flow passes downstream of the homogeniser towards meters 1 and 2, the assumption is made that meters 1 and 2 measure the mean streamline velocity and density mixtures. Meter 3 determines the density of the individual oil-water segments of the flow line by segregating the fluids and identifying their individual volumetric proportions such that the density ratios are obtained to calculate the overall mixture density from the following principle:

$$\rho_m = \alpha\rho_w + \beta\rho_o + \gamma\rho_g = (1 - \beta - \gamma)\rho_g + \beta\rho_o + \alpha\rho_w \quad (2-34)$$

where  $\gamma$  is the gas phase ratio and is incorporated to account for any propagation of small amounts of gas content within the mixture developed from the oil phase and included within the

calculation. As meter 3 establishes the density of the oil and water ratio of the mixture and hence provides a measurement for the gas density ratio, Eq. (2-34) can be used to solve individual phase proportions of all constituent fluids involved ( $\alpha$ ,  $\beta$  and  $\gamma$ ). However, the model assumes the phase densities are already known or measured separately. When sampling is not included with a homogenous flow line, it leads to the encounter of route 2 of MFM, depicted in *Figure 2-7(b)*.

Similar to route 1, route 2 requires three instruments in series with the homogeniser where two of the meters measure the average velocity and density. Meter 3 is used to measure the individual phase data of one of the two liquid contents. Conversely, both systems (route 1 and 2) require three instruments because all the relevant phase components are assumed to be travelling at equal velocities. Route 3 can be described as the measurement of non-homogeneous flow of a multiphase system, where all fluid phases of the respective mixture are travelling across a pipeline with different velocities. In cases such as this, five distinct measurements will be required. More refined techniques are needed to measure independent phase component velocities and hold-up through volumetric analysis, as shown in *Figure 2-7(c)*. Hence three individual component velocities need to be measured, along with a volumetric comparison in terms of mixture composition. Route 4 employs only individual stream measurements of each phase. Finally, the fifth measurement is the overall density of the mixture.



*Figure 2-6: The four routes to multiphase flow metering. Adapted from (Falcone, Hewitt and Alimonti, 2009).*

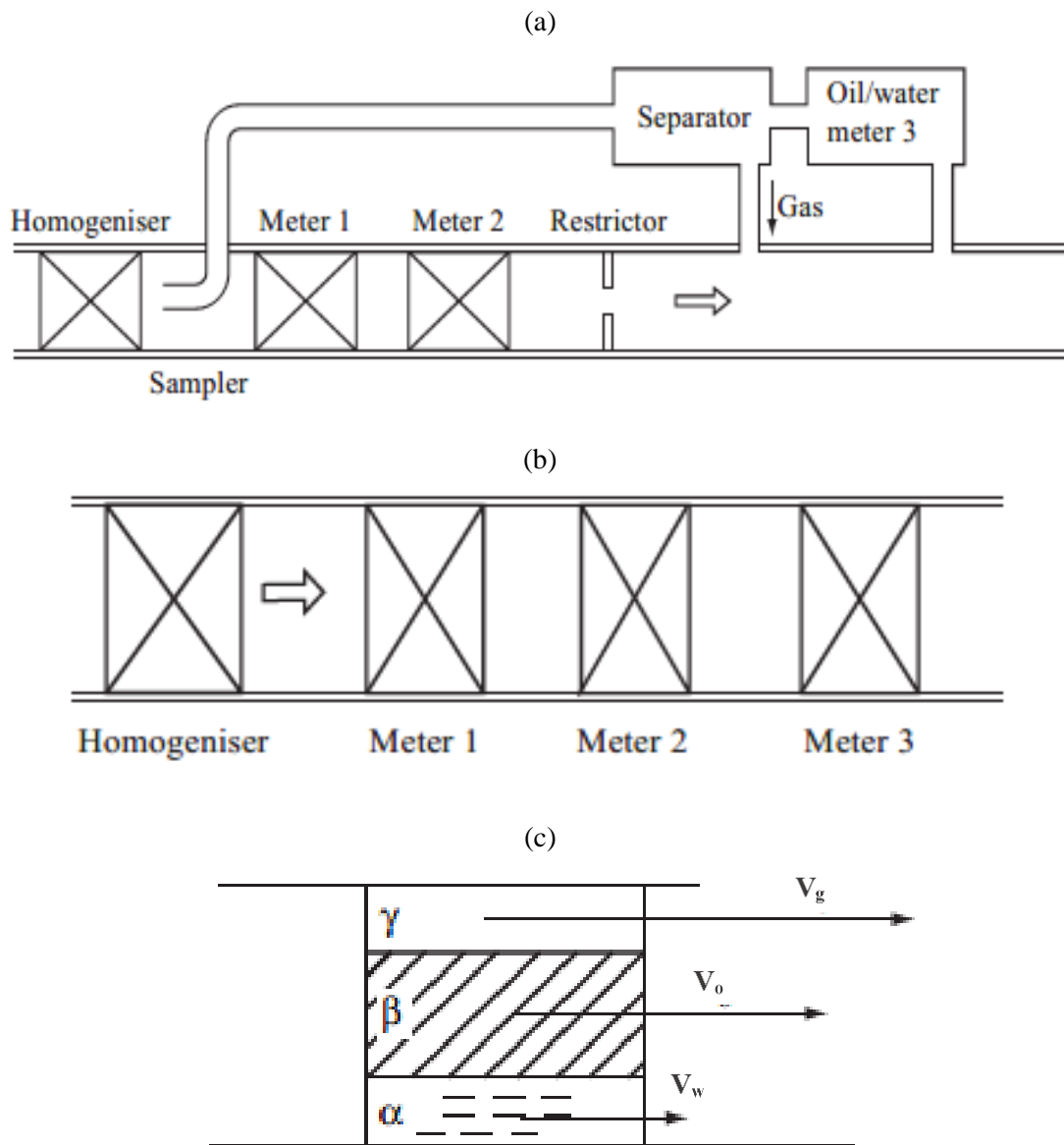


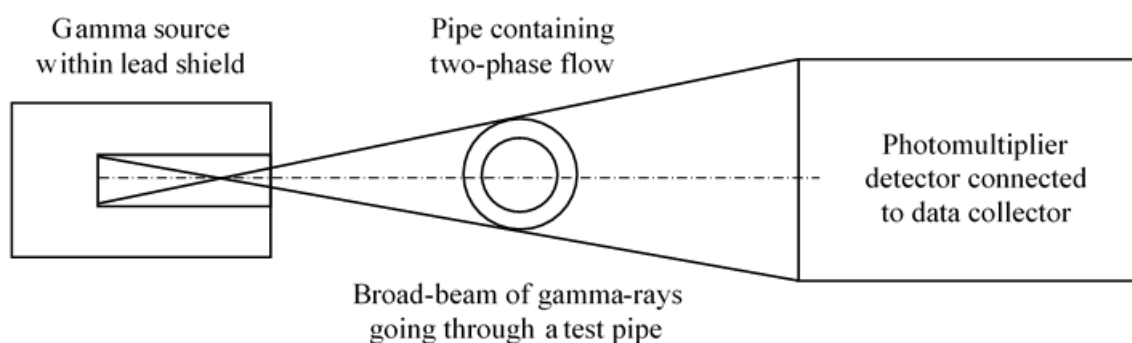
Figure 2-7: (a) Route 1 example of multiphase flow metering, (b) route 2 examples of multiphase flow metering and (c) route 3 examples of multiphase flow metering. Adapted from (Falcone, Hewitt and Alimonti, 2009).

Unfortunately, there is not a single type of device which can measure all multiphase flow parameters. Hence, combinations between a diverse range of techniques and tools must be incorporated upon pipeline formations, both internally and/or externally, from the flow path to measure multiple parameters and achieve reliable data. The following sub-sections are a brief acknowledgement of the types of measuring techniques that are available throughout industry and research.

---

### 2.2.1 Density Measurements

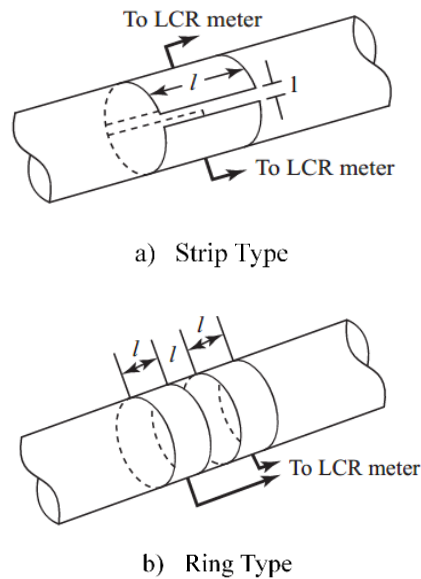
Instruments that measure density through a section of pipeline containing the relevant fluids are either directly measured or indirectly calculated by measuring another parameter related to the density and using some correlated equation to find the fluids' density theoretically. There are many methods of measuring density: weighing of pipes through pipe deflection, vibrations from spring mounts, acoustic attenuation, microwave attenuation and neutron scattering/absorption. However, the most commonly used systems are either the gamma-ray absorption or electrical impedance. There are multiple methods of measuring density when using gamma-ray technology, but the easiest, most common and relatively accurate set-up is the broad-beam gamma densitometer, otherwise known as the “one-shot” gamma densitometer, depicted in *Figure 2-8*. The gamma photons are beamed across a pipe section at slightly divergent angles, covering the entire diameter of the tube, and attenuation occurs from both the pipe walls and fluids that are contained within. The average void fraction is attained very easily as this only requires a single measurement to acquire the information. However, there are limitations with this process as data averaging distortion can arise. The sections of the beam which invade the near outer edges of the pipe walls have to pass through a greater amount of tubular material compared to the photons located towards the centre of the beam and tube (Ferrell and McGee, 1965). Hence the combinations of variable chord length and additional absorption will provide distortions of the average fluid data in contact with the pipe wall.



*Figure 2-8: A schematic example of a broad-beam gamma densitometer being used to measure fluid density from a section of pipe. Adapted from (Falcone, Hewitt and Alimonti, 2009).*

The second common method of measuring density is the use of electrical impedance systems. Impedance within multiphase flow varies with the dispersion and scales of individual phases as they flow through a pipeline. Electrical impedance methods are a very valuable and popular form of pipeline analysis because this method instantaneously provides a response at a specific point

in time as fluids continuously flow. Electrodes can be either implemented upon the channel walls or within the actual flow line. Depending on which type of electrical configuration is instigated, the impedance is governed by conductance, capacitance, or a combination of the two. When operating with impedance systems with both capacitance and conductance, it would normally have one of the functions be the dominant factor across the circuit than the other. Additionally, it can be suggested that the optimum way to operate these systems is to maintain a balance of sampling frequency and external noise reduction. The sampling frequency must be great enough to capture the alternating dielectric changes within the different phases that flow within a respective pipe but low enough to prevent the capture of external vibrations which can distort the sampled data. Furthermore, the testing environment must be considered, such that vibrations and large continuous changes in temperature must be taken into account when calibrating in individual phases for sampling. There are two types of widely used impedance systems, (1) a strip-type system and (2) a ring-type system, as shown in *Figure 2-9* (Shu, Weinberger and Lee, 1982; Green and Cunliffe, 1983).



*Figure 2-9: A schematic example of (a) Strip type electrodes and (b) Ring type electrodes are used to identify the impedance of flow to measure fluid density from a section of pipe. Adapted from (Falcone, Hewitt and Alimonti, 2009).*

Combining both the broad-beam gamma densitometer and the electrical impedance measuring technologies can be used to quantify the transition of fluid mass from a constant pipe at some sampling frequency. However, these devices do not have the correspondence to measure flow attributes such as velocity.

---

## 2.2.2 Velocity Measurements

Velocity measurements can be made either directly by cross-correlations or found indirectly through volumetric analysis. During homogenous flows, the measurement of the entire flow line represents each phase component. Therefore, individual phase velocities can be measured to represent the velocity of the entire mixture. However, when dealing with non-homogenous flows, the analysis of velocity between the entire mixture and individual phases is more difficult to measure during multiphase flow. Individual phases do not flow at the same velocity as each other, resulting in further complications such as the effect of slips which distort the information. There are many different types of devices that range from conventional to highly sophisticated equipment that can measure fluid velocity in terms of either a homogeneous mixture or via the individual phase velocities that coincide together within the multiphase flow system. Examples of technology that measures velocity are; optical particle-tracking, pulsed photon/neutron activation, acoustic analysis and mechanical turbine flowmeters. However, one of the most used apparatuses for measuring velocity is the radioactive tracking method, the set-up shown in *Figure 2-10*. A tracer of radioactive solute is implemented directly in the flow line via a pulse or continuous injection while moving downstream, the tracer concentration is examined. Other solutes can be used for this process, but radioactive material tends to be the best possible source of flow tracking as they can be easily detected in very minute quantities. This in turn prevents the injected foreign material from considerably affecting the flow behaviour, eliminating the need for sampling.

There are two types of tracer techniques to measure flow velocity: (1) The isotope distribution method or (2) the isotope velocity method. The distribution method starts by implementing a radioactive substance within a compound such as sodium-24 combined with sodium chloride, which dissolves within a specific volume of one of the pipeline fluids. The tracer is implemented within the main streamline of the pipe at a controlled rate and mixes with the respective fluids. Ultimately, the change in concentration of the tracer downstream from the injection point is used to measure the flowrate at a constant position (Clayton, Clarke and Ball, 1960). This is measured by interpreting the continuous change in radioactive concentration by using a count rate detector attached outside of the pipe. The following equations are used to calculate the mean mixture velocity  $v_{m\ mean}$ .

$$\dot{q} = \dot{q}_t \frac{C}{C_1 - C_2} \quad (2-35)$$

$$C = at^{-1/2} e^{\left[\frac{-(L-v_{m\ mean}t)^2}{4Kt}\right]} \quad (2-36)$$

The individual volumetric flowrate  $\dot{q}$  of the phase that contains the tracer can be found from Eq. (2-35); where  $a$  is the total radioactivity of the injected solution,  $\dot{q}_t$  is the volumetric injection rate of the tracer,  $C$  is the concentration of the tracer at the injection point to the main flow line,  $C_1$  is the concentration of the tracer measured downstream by the external counter after being completely mixed and  $C_2$  is the background concentration upstream of the injection point ( $C_2$  is occasionally negligible when slips are not present). If significant turbulence is subjected within the flow line, the turbulent diffusion causes axial dispersion of the tracer, then Eq. (2-36) can be used (Taylor, 1954). The relationship for  $C$  is a function of the distance the tracer has travelled across the pipe  $L$ , at time  $t$ , after injection. Additionally,  $a$  represents the radioactivity of the injected fluid and  $K$  is the virtual diffusion coefficient. Moving on to the isotope velocity method, the set-up of the second method is identical to that of the first. However, the count rates are measured and implemented on a rate count vs time plot, which typically shows ripples of data sequences. The velocity peaks of the rippled data are directly related to the mixture flow velocity. Hence the velocity can be determined by implemented successive detectors downstream of where the highest peaks are found.

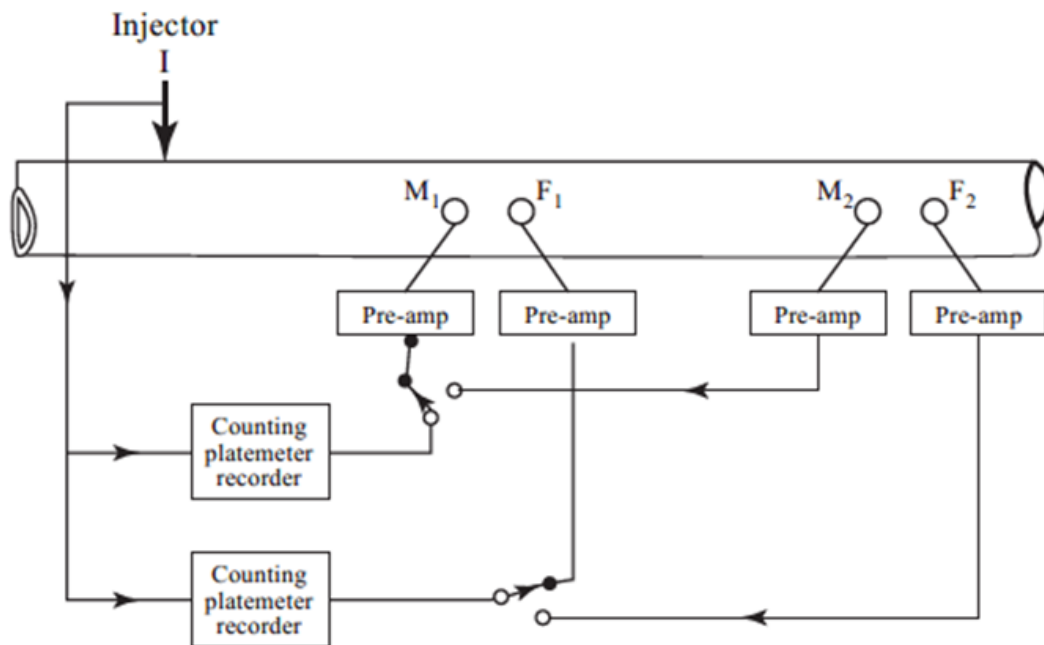


Figure 2-10: An example of a typical set-up for the radioactive tracking method to measure velocity. There are two separate systems which count the isotope tracer between two points across the pipe as it is being injected into the flow line. The first is the flow measuring system for  $I$ ,  $F_1$  and  $F_2$ , where the detectors  $F_1$  and  $F_2$  are fixed. The second set-up is  $I$ ,  $M_1$  and  $M_2$ , where the  $M_2$  detector is fixed but  $M_1$  can have its position varied.  $I$ ,  $F_1$  and  $F_2$  is a calibration (control) system for  $I$ ,  $M_1$  and  $M_2$  in the case of any sudden slip between multiple fluids. Adapted from (Clayton, Clarke and Ball, 1960).

---

### 2.2.3 Momentum Flux Measurements

Momentum flux is the change in fluid momentum that acts in the direction perpendicular to the fluid velocity flow. This is mathematically defined as the product between the mass flux and fluid velocity, which is equivalent to the fluid active stress for a force per unit acting in the plain of the respective fluids. During laminar flow, the momentum flux is dominated by the viscous properties of the respective fluids as molecular diffusion between the fluids occurs. In the case of turbulent flow, eddy currents enforce the momentum flux as inertial forces will be the dominant force within the flow system. Measurements for momentum flux are typically conducted using pressure drop apparatus such as Pitot tubes and Orifice meters. However, these devices have limitations when dealing with non-homogenous multiphase flows. Hence a variety of models have been deduced from literature and may need continuous extensive calibrations when using these devices. The venturi meter is one of the most popular and accurate systems to measure momentum flux. Under two-phase flow conditions, the fluids can travel at different velocities. If the flow is homogenised, then Bernoulli's equation for frictionless flow can apply:

$$constant = P \frac{\rho_m v_m^2}{2} \quad (2-37)$$

where  $P$  is the static pressure. The velocity at the venturi throat  $v_f$  is defined as:

$$v_f = C_q \sqrt{\frac{2\Delta P}{\rho_m}} \quad (2-38)$$

$$C_q = \frac{C_v}{\sqrt{1 - (A_2^2/A_1^2)}} \quad (2-39)$$

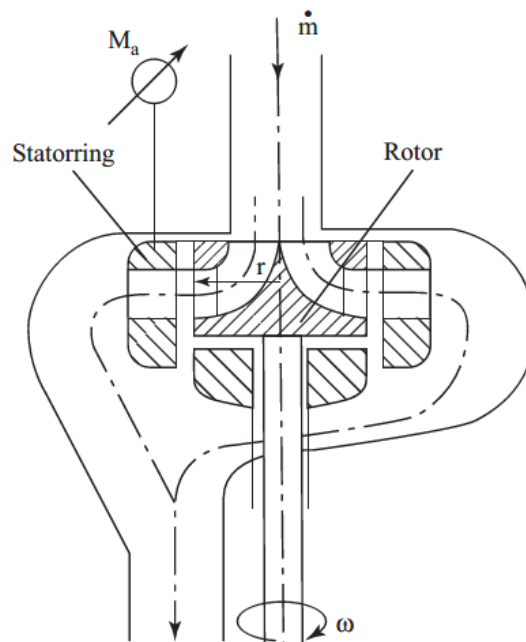
Based on Eqs. (2-38) and (2-39)  $\Delta P$  is the pressure difference between the flow line before and at the initial and secondary venturi throat areas against the flow path  $A_1$  and  $A_2$  respectively.  $C_q$  is the inclusion of the geometric relationship for the dimensions of the respective venturi system, which also includes a calibration constant  $C_v$ . The volumetric flowrate can then be deduced by multiplying  $v_f$  against the secondary throat area  $A_2$ . Under non-homogenous flow, slip ratios are implemented within the analysis to incorporate the relative velocity of two-phase flow, which may involve calibration.



---

## 2.2.4 Mass Flowrate Measurements

Unfortunately, there is no measuring device that directly identifies the individual components of the mass flowrate within a multiphase flow system. However, the total mass flowrate can be found using instruments such as the True Mass Flowrate Meter (TMFM) and the gyroscopic/Coriolis system. The TMFM system is a circulatory pump that comprises of a rotor system that has an axial inlet, radial outlet and a radial stator. The multiphase fluids exit the rotor from a constant angular velocity. The stator is used to fully contain the angular flow to zero value, resulting in a torque force against the swirling flow, which is related to the mass flowrate. An internal cross-sectional schematic of the TMFM can be found in *Figure 2-11*.

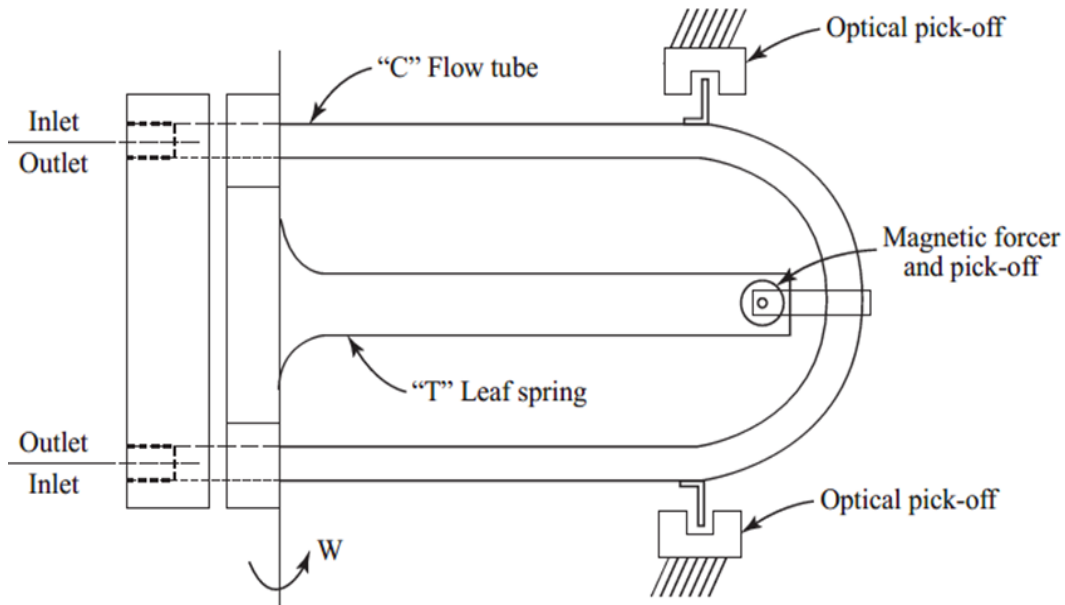


*Figure 2-11: Cross-sectional internal schematic of a TMFM circulatory pump. Adapted from (John, Reimann and Müller, 1984).*

Three bending springs placed in equally distanced axial formations, which also have strain gauges attached, are used to suspend the stator. Low levels of the elastic deformation of the spring are measured via the attached strain gauges. The deformation is proportional to the torque subjected to the stator. The vibrational aspects of the pump can result in the high resonant frequency of the pump system, which also consists of the stator and spring. The stator also contains mercury that is filled within the spring's annular channels to dampen any rotational oscillations and is adjustable (John, Reimann and Müller, 1984). The following equation directly solves the mass flowrate:

$$\dot{m} = \frac{ZM_R}{R^2\omega} \quad (2-40)$$

Eq. (2-40) is the modification of the Euler's pump formula where,  $\dot{m}$  is the mass flowrate,  $M_R$  is the torque subjected across the rotor,  $R$  as the rotor radius,  $\omega$  is the angular velocity and  $Z$  is a calibration factor which is unique to individual pumps. Another means of measuring the overall mass flowrate of a multiphase flow system is to use a gyroscopic/Coriolis instrument. It comes in the form of a C-shaped pipe with a T-shaped leaf spring, as shown in *Figure 2-12*. The T-shape leaf spring oscillates the pipeline through the use of an electromagnetic induced force which subjects each individual particle with the C-shaped pipeline under a Coriolis acceleration. This leads to a series of forces deflecting the pipeline at an angle inversely proportional to the pipe deformation initialisation (stiffness). The angular deflection of the test pipe is optically analysed multiple times during each cycle under oscillation, represented by signals corresponding to deflection and hence proportional to the mass flowrate. In addition, the natural frequency of the leaf spring is related to the density of the fluid within the C-shaped pipe. Therefore, it can be deduced that the known geometric and mass variables of pipe and fluid, respectively, can determine the average density of the fluid when using the gyroscopic/Coriolis system (Smith, 1978).



*Figure 2-12: Set-up for gyroscopic/Coriolis system (Smith, 1978).*

---

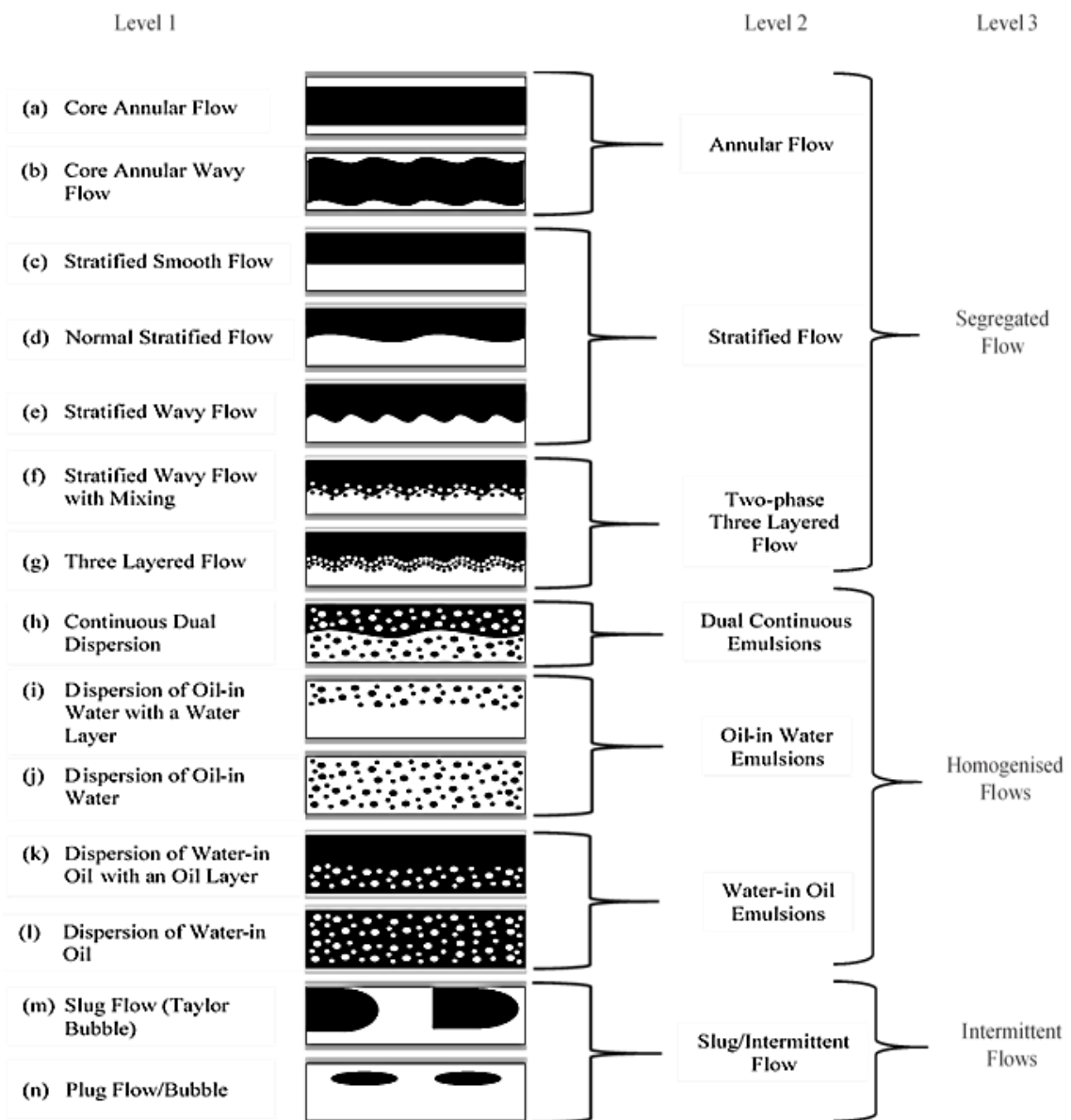
## 2.3 Flow Regimes

Flow regimes are physical formations of fluid phases augmented in a series of categorised patterns, which have been discovered and grouped through published experimental investigations. Flow regimes are formed between the interactions of two or more fluid phases and their environmental state on which several forces act upon, changing the physical dimensions of the multiphase system. Flow pattern analysis is a key focus to dictate the behaviour of multiphase flow within pipelines and optimise fluid transportation from a perspective of both pumping efficiencies and pipeline preservation (Nädler and Mewes, 1997). These two aspects of fluid transportation optimisation are two of the industry's many key issues. The particular case of slug flow is a destructive and unstable pattern of intermittent fluctuations of contrasting densities across a common pipeline. Nonetheless, no other flow regime acts in the same manner as slug flow does, nor do many take as much caution to prevent it from developing or at least mitigate its effects (Joseph, Bannwart and Liu, 1996; Barrett and King, 1998; Mandal, Das and Das, 2010).

Consequently, in comparison to gas-liquid slug flow, there is very little focus on liquid-liquid slug flow and the mechanism at which it develops. Flow regime classifications must be set to compare flow pattern transitions that occur between slug flow and other flow regimes. There is very little consistency within literature regarding the type of pattern which is classified, particularly for liquid-liquid flows. For instance, the conventional idea of slug flow is heavily related to gas-liquid flows, where the formation of the classic bullet-shaped Taylor bubble is considered to be only a slug flow formation. Nevertheless, liquid-liquid flows behave very differently to gas-liquid flows, where the presence of different arrangements and dominance of various force exertions act separately between both distinct two-phase systems. Hence, the altered combinations of fluid properties and states of matter will define how a system will physically react toward a range of diverse pipeline set-ups and operations.

There is a great challenge to form a universal liquid-liquid flow classification, as it has been recently noticed through the inconsistencies found in literature. There are many possible reasons for this issue, but one key aspect which has hardly been considered is the discrepancies in the variation of flow regime criteria. Previous research seems to have only used gas-liquid-based criteria in dual-incompressible flows, leading to different interpretations from different authors (Trallero, 1995; Trallero, Sarica and Brill, 1997; Xu, 2007; Nossen et al., 2017). Therefore unified, concise and consistent liquid-liquid flow regime criteria must be instigated and followed consistently throughout literature. This work has identified the groupings of each flow regime type based on relevance and most frequently encountered transitions of liquid-liquid slug flow, based on similar criteria proposed by (Dasari et al., 2013; Ibarra, Matar and Zadrazil, 2015). A

refined criterion specifically for liquid-liquid multiphase flow in horizontal and slightly deviated pipe orientations is set, as shown in *Figure 2-13*. Flow regimes can be grouped under three levels. Level 1 is the most detailed specification, where specific flow regimes are considered diverse from each other, based on small differences in flow characteristics and are never grouped. Level 2 grouping allows for flow regime grouping key characteristics of a flow pattern. Finally, Level 3 grouping allows for Level 2 characteristics to be further grouped based on three base representative flow behaviours which are segregated, homogenised and intermittent flow regimes.



*Figure 2-13: Liquid-liquid flow regime criteria.*

---

**Annular Flow:** Annular flow is the distinct flow of one fluid phase to develop a thin film across the entire inner section of a pipe, while the remaining void within the pipe is a core (centre) occupied by another fluid. This is typically known as core annular flow (AN) when under a stabilised, laminar flow condition. Core annular wavy flow (ANW) is a more turbulent system which causes waves at the interface between the two fluids. When under its turbulent state, there is the risk of breaking the film boundary and developing into other less stable flow regimes, such as slug flow classifications. In cases of oil-water flow, this flow regime is typically seen in equal density systems or extra-heavy or heavy oil transportation to shift the highly viscous, low-mobility oil types more proficiently; this process is also known as lubricating flow. Core annular flows can transition to intermittent (slug) characteristics when under high to medium flowrates for both respective fluids (Joseph et al., 1997). When there is a phase velocity difference, instabilities between the film and the core occur, resulting in the rupture of the film, leading to intermittent flows (Bai, Chen and Joseph, 1992).

**Stratified Flow:** Two fluid phases of contrasting density are segregated through a gravitational effect, causing a distinct layered configuration. In cases of conventional oil-water flow, the heavier/denser fluid (water) would naturally sink to the bottom of the pipe as the lighter fluid (oil) is suspended above the heavier fluid. Stratified flow (ST) also consists of further sub-categories that incorporate the degree of interfacial stability of the flow pattern. For instance, smooth stratified flows (SS) and wavy stratified flows (SW) are two extremes of what stratified flow can become when under a significant laminar or turbulent state (Kurban, 1997; Brauner, Moalem Maron and Rovinsky, 1998; Fairuzov et al., 2000). When the water phase velocities increase, the amplitude of water waves occurs and begins to enlarge as the velocity difference (also known as slip) between the two phases enlarges, eventually causing intermittent flow.

**Two-phase Three-Layered Flow:** A more complex and unstable form of stratified wavy flow is stratified flow with droplets at the interface. When significant enough turbulence occurs, mixing between the two segregated phases is initiated through droplets forming across the interface. Each phase droplet can even move within the opposite phase layer. It can be suggested that this flow type is a transition between the stratified flows and further turbulent dispersions such as slug flow patterns (Vedapuri, 1999). The higher the intensity of the turbulent flow regime, the more droplets begin to become clustered at the interface, making a distinct third central layer. This flow regime is also known as three-layered flow (3L).

---

**Continuous Dual Dispersion:** This flow regime rarely occurs within pipelines, but it is a unique and unstable configuration of stratified flow. It incorporates a combination of two types of flow regimes, such that stratified flow is present through the gravitational forces and acts as the continuum phase. Within both layers, the constituent phase in the form of droplets is also located within each other through viscous forces that coexist to form this distinctive arrangement. As oil droplets are found in the water layer, and water droplets develop in the oil layer. There are no documented concepts of slugs to transition from continuous dual dispersions (DOW&WO) concerning the top section of the pipeline. Oil-water droplets can accumulate to develop water slugs in a partial oil continuum (Arirachakaran et al., 1989; Yeo et al., 2002).

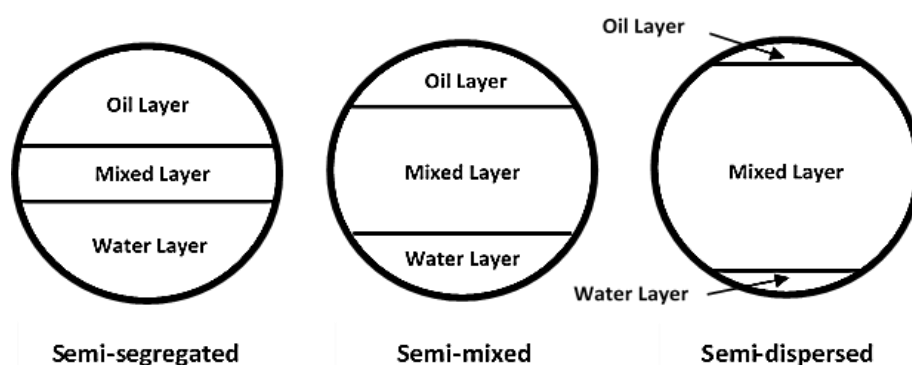
**Dispersion of Oil-in-Water/Water-in-Oil:** Dispersion of oil-in-water (DOW) are emulsions of oil droplets within a water-dominated continuum present throughout the entire section of the pipeline. These oil droplets are located in the entire flow formation, both longitudinal and latitudinal special distributions. A more complex form of oil-water dispersions is the dispersion of oil-in-water with a water layer (DOW&W). Oil droplet emulsions only develop at the top of the pipeline when a smaller volume of oil is present under a heavily dominated water production. Hence gravitational forces are still playing a role in the lighter fluid. This flow pattern is generally remnants of intermittent flow breakup when oil flowrates have increased enough to not support larger droplet sizes (Brauner and Ullmann, 2002). Dispersion of water-in-oil (DWO) is essentially the equivalent of the DOW flow, however, the two regimes are a reversal of each other between the oil and water patterns of this phenomenon. Hence, gravitational forces still play a role upon the heavier fluid, dragging this phase towards the gravitational direction.

**Intermittent Flow:** Classified as slug flow (SL), this unstable, undesirable flow regime is very problematic within the industry and general flow line applications. Concentrated forms of mass from an accumulation of droplets of one pure phase develop large, extended ovular shape plugs, surrounded by a separate dominating liquid continuum. From the perspective of oil-water flows, oil slugs (SLo) and water slugs (SLw) are typically seen within these flow regimes depending on the hold-up/water cut resulting in phase inversion shifts. They can be encountered in any orientated pipeline and fluid properties. Plug flow (P), or bubble flow (Bb), is also similar to that of slug flow and is more frequently seen in liquid-liquid flows. In addition, the size of plugs is not as large or elongated as a conventional slug flow regime found in gas-liquid flows (Joseph, Bannwart and Liu, 1996; Barrett and King, 1998; McKibben, Gillies and Shook, 2000a; Al-Wahaibi *et al.*, 2014). Nevertheless, the terms slug and plug flow are used interchangeably in the context of dual-liquid systems in this work and are grouped under a single intermittent category.

### 2.3.1 Oil-Water Stratification of Layers and Mixtures

When producing and transporting oil-water two-phase flow, it is important to understand that the mixtures of oil and water are rarely ever under fully miscible conditions, nor are they ever under a pure emulsified state unless under stringently controlled conditions. In fact, both circumstances are regularly present amongst each other and travel simultaneously through pipelines, causing varied flow patterns. However, the degree of which is more dominant within the flow does vary, as shown in *Figure 2-14*. In the case of an oil-water system, the density difference between oil and water will result in a pure oil layer being found above all phase-type layers and the respective pure water composition being below the same respective phase-type layers. Hence, a density average between both liquid forms would advance the mixed layer between the pure phases. The work of (Vedapuri, Bessette and Jepson, 1997) experimentally found that there are typically three different flow pattern mixtures from oil-water flow.

The set-up of the experiments was a pipe loop test rig with a  $0.1m$  diameter under both horizontal ( $0^\circ$ ) and slightly inclined ( $\pm 2^\circ$ ) orientations. Alterations of oil viscosity were conducted between  $2 - 90mPa.s$  and varying mixture velocity and water cuts from  $0.1 - 2m/s$  and  $20 - 80\%$ , respectively. The authors have categorised these physical flow behaviours as semi-flow patterns (or three-layered flow) and have given them the title of; semi-segregated, semi-mixed and semi-dispersed. These flow types are however conventionally classified under the flow regime stratified flow with mixing at the interface (ST&MI). Severe mixing was not present in this experimental investigation. This is evident from Eq. (2-25), where the Reynolds number is proportional to the pipe diameter and the mixture velocity. With the size of these variables being small, this suggests that significant turbulent flows were not present within the experiment, preserving the contrast of the multi-layer segregation between the two-phase components.



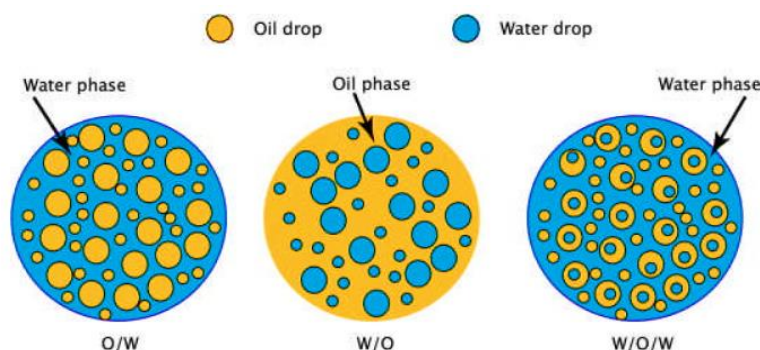
*Figure 2-14: Cross-sectional analysis on three extremes of the same flow pattern type between oil-water two-phase flows. Adapted from (Vedapuri, Bessette and Jepson, 1997).*

---

### 2.3.2 Oil-Water Emulsions

When oil and water phases are immiscible, the emulsions can generate bubbled/droplet forms within each respective phase to create flow regimes, as shown in *Figure 2-15*. For the purpose of this study, water-in-oil-in-water will be excluded as a representative flow regime as the pattern is far more complex than its constituent forms and is very rarely encountered. Depending on whether the fluid is dominant in oil or water, the phase bubbles/droplets and the surrounding phase will vary. When emulsions are unstable, they can be unfavourable for fluid transportation as this can lead to decreased production efficiency through a lower pressure drop and is more challenging to conduct dehydration and separation of the constituent fluids during refining. However, stable emulsions can be another technique of using flow regimes to transport heavy oil as this can reduce the oil viscosity to enhance the hydrocarbon's mobility. These flow types are stabilised by implementing chemical additives within the streamline (Pilehvari et al., 1988).

Implementing chemicals have to be carefully considered to maintain stability throughout the pipe. Instability is typically caused by irregular pumping rates, operating instruments (flow valves) and intruding measurement instruments (gauges). The viscosity has an inverted exponential proportionality to the water cut of an oil-water system and is graphically depicted in *Figure 2-16*. When larger water contents are present in the flow line (40 – 60% of water content), the viscosity effects begin to be less effective within the system. This allows pipeline operations to be designed in the most optimal form during the early stages of field life. In fact, when formation water and/or artificially injected water production begins to increase, direct water injections within pipelines can be reduced to minimise pumping costs. This technique was mainly used during the 1980s in Venezuelan oil fields to emulsify bitumen-water fluids (Martínez-Palou et al., 2011). However, this process was replaced with more efficient methods to produce heavy oils in larger quantities, such as the use of annular flow.



*Figure 2-15: Types of oil-water emulsions; oil-in-water (O/W), water-in-oil (W/O) and water-in-oil-in-water (W/O/W) found within the petroleum industry (Martínez-Palou et al., 2011).*



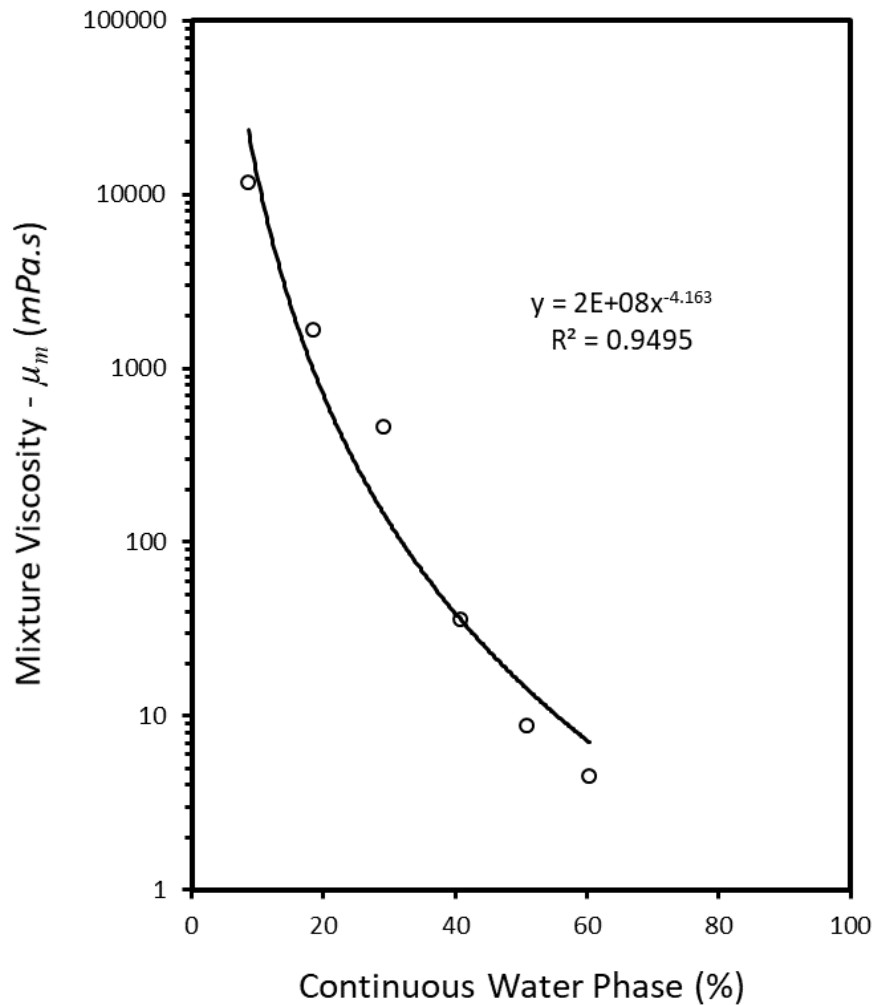


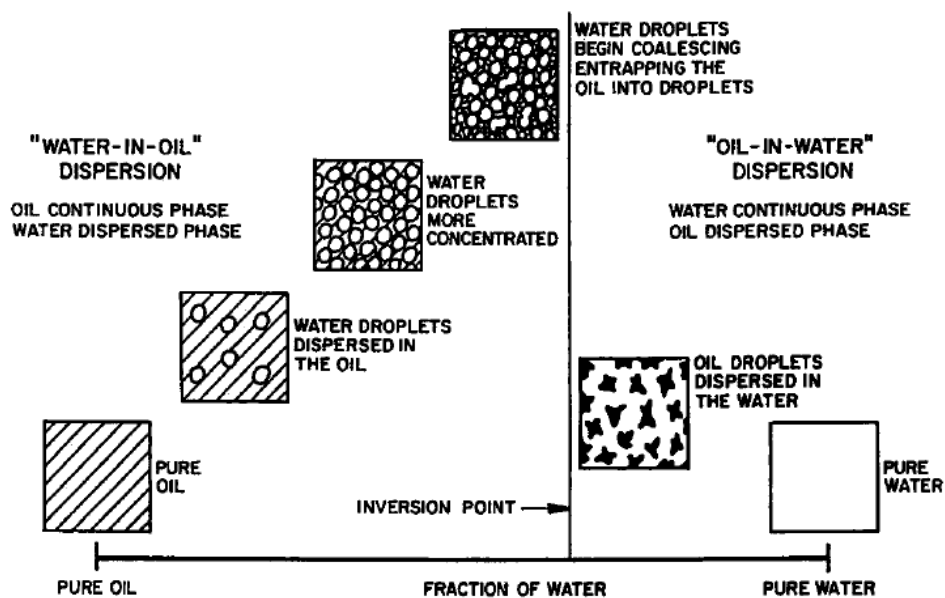
Figure 2-16: Viscosity vs percentage of continuous phase for water emulsions within oil-water multiphase flow. Adapted from (Escojido, Urribarri and Gonzalez, 1991).

## 2.4 Phase Inversion

Phase inversion is the change of fluid flow dispersions in two-phase flow through small alterations of operational variables (Brauner and Ullmann, 2002). Examples in oil-water systems can be seen from oil-in-water dispersions to transforming to water-in-oil, where the continuous and bubble/droplet phases have altered. Selker and Sleicher (1965) defined the known (ambivalent) regions and conditions at which phase inversion can occur as the phase inversion point (PIP). They describe it as an unknown variation of a phase volume fraction where if that phase is above the PIP, it will be considered a continuous state and below will be classified as a dispersed state. Within the unknown range, one of the two phases will be subject to a dispersed form. Hence, the PIP is a valuable tool for pipeline designs and operational analysis because the rheological characteristics of the associated fluids under dispersion can also indicate sudden pressure drops

throughout the flow line as the volume fraction defines whether the phase is dominant enough to become the continuous phase. A depiction describing phase invasion and PIP is shown in *Figure 2-17*.

Many applications, such as industrial mixers, are affected by phase invasion when incorporating multiphase fluid flows. Conversely, the most widely used medium is pipe flow which has been explored for the effects of phase invasion studies throughout literature (Arirachakaran et al., 1989; Nädler and Mewes, 1997; Wang and Gong, 2009). When characterising the effects of critical volume fractions, a series of parameters as a function of the volume and fluid behaviour of the stream path must be considered, such as the operational conditions, pipeline geometry and fluid source predictively. Consequently, most pipeline studies have focused on phase invasions when using medium-low oil viscosities. Generally, studies show the intuitive approach of increasing both the viscosity (density) and occupancy of a dispersed oil formation within a respective flow line will result in the oil phase turning continuous. Increasing the oil viscosity will strengthen the liquid's ability to maintain a larger mass and eventually transition to a continuous phase when enough volume and mass are sustained. However, this does not fully depend on the entire system as the water phase also must be considered in terms of its volumetric dominance. Studies by Norato, Tavlarides and Tsouris (1998) discovered by increasing the viscosity ratio, the unknown dispersion-continuous phase transition will expand, leaving the system more sensitive to parameter variations.



*Figure 2-17: Inversion processes for oil-water dispersion flow (Arirachakaran et al., 1989).*

---

Research within phase inversion has generally seen compelling correlations of other factors manipulating the ambivalent range. These additional influences have been reported to be from variables such as the system initial conditions, flow/mixing speed, fluid surface tension and medium material containing the fluids. All listed variables have an individual role that can be collectively used to determine the exact condition for phase inversion (Yeo et al., 2002). Furthermore, pressure drops are highly important to be used as a strong indication of the manifestation of phase invasion within a flow system. Studies have shown that at the PIP, the pipeline pressure drops occur substantial changes. At the same time, concentrations of water droplets start to conglomerate until the water has fully established a continuous form at the maximum apparent viscosity through increased water content. However, once the system has exceeded the PIP, the apparent viscosity and pressure drop restabilise after a transition is achieved (Angeli and Hewitt, 2000). There have been many proposed models for predicting phase invasion based on the viscosity of both fluids and even incorporating density. One of the most well-established empirical correlations for phase invasion is from (Arirachakaran et al., 1989):

$$\varepsilon_w^I = \left( \frac{v_{sw}}{v_{so}} \right)_I = 0.5 - 0.1108 \log_{10} \left( \frac{\mu_o}{\mu_r} \right); \quad \mu_r = 1 \text{ mPas} \quad (2-41)$$

where,  $\varepsilon_w^I$  is the critical water cut invasion point (PIP) and  $\mu_r$  is a constant viscosity value maintained at  $1 \text{ m.Pa.s}$ . This technique is based on the correlation of the ratios between the superficial velocities of oil and water and the respective phase viscosities. Studies from (Nädler and Mewes (1997) have also proposed more progressive correlations, which also incorporate factors such as fluid density, mixture velocity, pipe obstructions and geometry for phase invasion, as shown:

$$\varepsilon_w^I = \frac{1}{1 + k_1 \left[ \frac{\zeta_o \rho_o^{1-n_o} \mu_o^{n_o}}{\zeta_w \rho_w^{1-n_w} \mu_w^{n_w}} (Dv_m)^{n_w-n_o} \right]^{1/k_2}} \quad (2-42)$$

Eq. (2-42) integrates more advanced variables where  $\zeta_o$ ,  $\zeta_w$ ,  $n_o$  and  $n_w$  are oil and water parameters from the Blasius equation for the friction factor,  $k_1$  and  $k_2$  are empirical parameters. The authors have set  $k_1$  to represent the wall/liquid contact perimeter in the form of an in-situ configuration and  $k_2$  reflects the flow regime behaviour within each phase.

---

## 2.5 Oil-Water Pressure Gradients and Frictional Losses

Pressure gradients of oil-water pipe flow have been extensively studied since the 1950s. The alterations of flow regime characteristics due to changes in influential parameters result in fluctuations of pressure drops across the entire pipeline. Hence, there are two methods of developing models for predicting pressure gradients. (1) Using pure empirical correlations and (2) incorporating different flow regime types (Angeli and Hewitt, 1998). Many authors have proposed different predictive models throughout literature. The following are examples of one of many popular approaches from each method used extensively in both research and industry. Broad reviews and comparisons of other models can be found throughout literature (Arney et al., 1993; McKibben, Gillies and Shook, 2000b; Brauner, 2003; Liu et al., 2008; Edomwonyi-Otu and Angeli, 2015; Luo et al., 2017; Prieto et al., 2018).

### 2.5.1 Empirical Correlations

Starting from the empirical correlation, Charles and Lilleleht (1966) used the empirical parameters of  $X$  and  $\Phi$  from Lockhart and Martinelli (1949) for gas-liquid flow within horizontal pipes. This can also be used to represent liquid-liquid flows where the parameters of  $X$  and  $\Phi$  are mathematically represented as:

$$X^2 = \frac{(dP/dL)_w}{(dP/dL)_o} \quad (2-43)$$

$$\Phi^2 = \frac{(dP/dL)_m}{(dP/dL)_o} \quad (2-44)$$

where  $(dP/dL)_o$  and  $(dP/dL)_w$  is the individual pressure gradients of oil and water when its constituent phase is not present within the pipe channel, respectively, as  $(dp/dL)_m$  is the combined pressure gradient of the oil-water mixture. This implies that the empirical parameters of  $X$  represent the pressure gradient ratio between the two constituent fluids within the mixture, as  $\Phi$  signifies the pressure gradient ratio between the fluid mixture and one of the individual phases (in this case, the oil phase). Furthermore, the experimental data developed from Eqs. (2-43) and (2-44) found the resulting curves for liquid-liquid flow to merely shift from the Lockhart-Martinelli-based curves of gas-liquid flow with very similar trends. Based on the two results, Theissing (1980) accredited this curve shift to be established on the density ratio difference that exists between gas-liquid and liquid-liquid flows. Theissing (1980) had therefore developed a

correlation for two-phase flow that can be equipped for both types of phase mixture configuration and is described as:

$$\left(\frac{dP}{dL}\right)_m = \left[ \left(\frac{dP}{dL}\right)_{om.\dot{m}}^{\frac{1}{ne}} \left(\frac{\dot{m}_o}{\dot{m}_m}\right)^{\frac{1}{e}} + \left(\frac{dP}{dL}\right)_{wm.\dot{m}}^{\frac{1}{ne}} \left(\frac{\dot{m}_w}{\dot{m}_m}\right)^{\frac{1}{e}} \right]^{ne} \quad (2-45)$$

$$e = 3 - 2 \left( \frac{2\sqrt{\rho_o/\rho_w}}{1 + \rho_o/\rho_w} \right)^{\frac{0.7}{n}} \quad (2-46)$$

$$n = \frac{n_1 + (1/X)^{0.2} n_2}{1 + (1/X)^{0.2}} \quad (2-47)$$

$$n_1 = \frac{\ln[(dP/dL)_{om}/(dP/dL)_{om.\dot{m}}]}{\ln(\dot{m}_o/\dot{m}_m)} ; \quad n_2 = \frac{\ln[(dP/dL)_{wm}/(dP/dL)_{wm.\dot{m}}]}{\ln(\dot{m}_w/\dot{m}_m)} \quad (2-48)$$

The pressure gradients presented are denoted by  $(dP/dL)_{om}$  and  $(dP/dL)_{wm}$  which represent the individual oil and water flows within a pipe at their respective mass flowrates  $\dot{m}_o$  and  $\dot{m}_w$ . As  $(dP/dL)_{om.\dot{m}}$  and  $(dP/dL)_{wm.\dot{m}}$  is the pressure gradients of oil or water when under a single-phase flow at the total mixture mass flowrate,  $\dot{m}_m$ . The parameters of  $e, n, n_1$  and  $n_2$  are arbitrary values based on the respective fluid densities and interactive pressure gradients between individual fluids and the entire multiphase system from the sum of the separate phase mass flowrates ( $\dot{m}_o + \dot{m}_w$ ). This model incorporates the combined factors of different interactions of pressure gradient with the entire system and in individual phases, along with the fluid density contributions. When considering the pipe flow orientation, gravitational influences would affect pressure gradients. The principles of conservation and momentum for fluid mass within an inclined continuous concentric cross-section are used. The model only incorporates the pressure gradient due to the hydrostatic head while neglecting acceleration. From the use of force balance, the wall shear stress is considered to result in frictional losses (otherwise known as viscous shear) to signify a pipe differential element. Viscous shear stress occurs most ominously from the internal walls of the pipe, which are in contact with the respective fluids; hence energy losses are present, which are defined by the friction factor. The equation for the pressure gradient for oil-water flow through an inclined pipe would therefore become:

---


$$\frac{dP}{dL} = \frac{g}{g_c} [\rho_m \sin(\theta)] + \frac{f \rho_m v_m^2}{2g_c D} \quad (2-49)$$

where,  $g_c$  is a conversion factor, which in terms of SI (metric) units will be negligible as a value of 1,  $\theta$  is the angle of the pipeline inclination from the horizontal, and  $f$  is the frictional coefficient based on the moody frictional factor (which is four times larger than the Fanning friction factor). The friction factor for laminar flow is as follows:

$$f = \frac{8\tau_w g_c}{\rho_m v_m^2} = \frac{64}{Re_m} \quad (2-50)$$

where,  $\tau_w$  is the wall shear stress and is defined as:

$$\tau_w = \frac{D}{4} \left( \frac{dP}{dL} \right)_f \quad (2-51)$$

where,  $(dP/dL)_f$  is the pressure gradient due to viscous shear, which is still under the moody frictional correlation and is also defined as:

$$\left( \frac{dP}{dL} \right)_f = \frac{f \rho_m v_m^2}{2g_c D} \quad (2-52)$$

The mixture velocities for the individual phase, the Reynolds number and the mixture fluid parameters are previously defined in section 2.1. In addition, for cases of turbulent flow regimes, the frictional coefficient would change to the Blasius equation:

$$f = \frac{(0.316)}{(Re_m)^{0.25}} \quad (2-53)$$

As this is valid for  $3 \times 10^3 \leq Re_m \leq 10^5$ . From this, the use of the Reynolds number can be applied to calculate the frictional factors when under low-end turbulent conditions, which is generally applicable to export pipelines (Mukherjee, Brill and Beggs, 1981). Hence, the pressure drop due to frictional losses can be obtained from Eq. (2-52).

---

## 2.5.2 Flow Pattern Based Correlations

There are many proposals of a variety of different models based on individual flow patterns, such as dispersed flow, core annular flow, and the simplest and most common correlation that will be demonstrated within this thesis is stratified flow. Nevertheless, there has not yet been a breakthrough in literature in developing an analytical model for slug/intermittent flows. Hence, one suggestion for a possible approach to which other correlations can be applied is to observe the limits of individual flow patterns towards the region at which slug flows develop and converge. Stapelberg and Mewes (1994) also used the liquid-liquid Lockhart-Martinelli correlations to represent their experimental pressure gradients which were extracted from two different pipe diameters. Interestingly, their data was of a similar trend to Charles and Lilleleht (1966) but found to have scale-up effects from the pipe size alterations. In addition, single models may not always suffice to integrate pressure gradients into all types of incompressible multiphase flow systems. Hence, models for individual flow regimes have been developed, and in the following case, the simplest and most industrially applicable is stratified flow because the flow regimes are mainly restricted to laminar flow conditions.

There are two methods of development. (1) To solve the solution analytically using the Navier-Stokes equations, which incorporate the full flow field that considers the multiphase interfaces (Brauner, Moalem Maron and Rovinsky, 1998); and (2) is based on an approach similar to that of the empirical correlations, where the theoretical analysis of Taitel and Dukler (1976) for gas-liquid flows can be used. In terms of a liquid-liquid system, oil and water phases are treated as separate entities of discrete regions. Hence, the empirical correlations are then used based on the wall, and interfacial shear stresses along with the gravitational effects that occur during alterations of pipe inclination. Considering smooth stratified flow, the equilibrium equation for water and oil is shown in Eqs. (2-54) and (2-55).

$$\text{Water Phase:} \quad -A_w \left( \frac{dP}{dL} \right) - \tau_{W_w} p_w - \tau_i p_i + \rho_w A_w g \sin(\theta) = 0 \quad (2-54)$$

$$\text{Oil Phase:} \quad -A_o \left( \frac{dP}{dL} \right) - \tau_{W_o} p_o - \tau_i p_i + \rho_o A_o g \sin(\theta) = 0 \quad (2-55)$$

where,  $\tau_{W_o}$  and  $\tau_{W_w}$  are the wall shear stress acting from the individual phases of oil and water, respectively as  $\tau_i$  is the interfacial shear stress between the oil-water interface. The variables  $p_o$  and  $p_w$  are the oil-wetted and water-wetted wall perimeters respectably, while  $p_i$  is the interfacial

---

perimeter throughout the region where interfacial shear stress acts upon. The model has been adapted for liquid-liquid flows; see Brauner (2003) for an in-depth review and derivation of the model. In light of this, the model provides the ability to include the effects of relative velocities to determine the equivalent hydrodynamic diameter and the respective interfacial shear stress. The one-dimensional model assumes a fully developed flow pattern under steady-state conditions, which is applied to a smooth and flat interface. In contrast to intermittent conditions, the transition of steady stratified conditions in comparison to that of intermittent flows such as slugs or plugs may not necessarily apply to the two-fluid model but can reveal the estimated limitations of stability loss leading towards intermittent conditions, which is generally in conjunction to the hydraulic diameters between the two phases.

$$D_w = \frac{4A_w}{p_w + p_i}; D_o = \frac{4A_o}{p_o} \quad \text{and} \quad f_i = f_w \quad \text{for} \quad v_w > v_o \quad (2-56)$$

$$D_w = \frac{4A_w}{p_w}; D_o = \frac{4A_o}{p_o + p_i} \quad \text{and} \quad f_i = f_o \quad \text{for} \quad v_o > v_w \quad (2-57)$$

$$D_w = \frac{4A_w}{p_w}; D_o = \frac{4A_o}{p_o} \quad \text{and} \quad f_i \cong 0 \quad \text{for} \quad v_o \approx v_w \quad (2-58)$$

Eqs. (2-56) to (2-58) demonstrate the determination of the hydraulic diameter. As  $D_o$  and  $D_w$  is the hydraulic diameter for oil and water respectively, and  $f_o$ ,  $f_w$  and  $f_i$  are the frictional factor of the pipeline induced by the oil phase, water phase and the small abundance found at the interface between the two phases.

### 2.5.3 Two Fluid Flow Model

The two-fluid flow is one of the most popular models used to analyse liquid-liquid flows. It allows for the segregation of the individual phases to be considered and is also able to look into instabilities that are typically characterised in flows transitioning to intermittent regimes. In addition, single models may not always suffice to integrate pressure gradients into all types of incompressible multiphase flow systems. The simplest method is to assume the system to be in stratified flow because it is the most segregated flow regime between the two constituent phases. The main method is based on an approach similar to that of the empirical correlations, where the theoretical analysis of Taitel and Dukler (1976) for gas-liquid flows can be used. In terms of a liquid-liquid system, oil and water phases are treated as separate entities of discrete regions.



Hence, empirical correlations can be applied based on the wall and interfacial shear stresses and the gravitational effects that occur during alterations of pipe inclination. Starting from the continuity equation of oil and water:

$$\frac{\partial}{\partial t}(\rho_w A_w) + \frac{\partial}{\partial L}(\rho_w A_w v_w) = 0 \quad (2-59)$$

$$\frac{\partial}{\partial t}(\rho_o A_o) + \frac{\partial}{\partial L}(\rho_o A_o v_o) = 0 \quad (2-60)$$

The Momentum equation is expressed as:

$$\frac{\partial}{\partial t}(\rho_w A_w v_w) + \frac{\partial}{\partial L}(\rho_w A_w v_w^2) = \tau_w p_w + \tau_i p_i - A_w \frac{\partial P_{iw}}{\partial L} - \rho_w A_w g \cos(\theta) \frac{\partial h_w}{\partial L} - \rho_w A_w g \sin(\theta) \quad (2-61)$$

$$\frac{\partial}{\partial t}(\rho_o A_o v_o) + \frac{\partial}{\partial L}(\rho_o A_o v_o^2) = \tau_o p_o + \tau_i p_i - A_o \frac{\partial P_{io}}{\partial L} - \rho_o A_o g \cos(\theta) \frac{\partial h_w}{\partial L} - \rho_o A_o g \sin(\theta) \quad (2-62)$$

where,  $h_w$  is the height of the heavier reference fluid (water) from the bottom of the pipe to the interface,  $\tau_o$  and  $\tau_w$  are the individual wall shear stresses acting on the perimeter region where the pipe is in contact with the water and oil, respectively.  $P_{iw}$  and  $P_{io}$  are the dynamic fluid pressures within the water and oil phases bordered by the interface, respectively. Assuming the flow to be incompressible, the two momentum equations can be combined by eliminating the pressure terms using the approximate relation. As oil and water fluids are considered incompressible, the pressure terms can be eliminated in Eqs. (2-61) and (2-62) using the relationship:

$$P_{io} - P_{iw} = \sigma \frac{\partial^2 h_w}{\partial L^2} \quad (2-63)$$

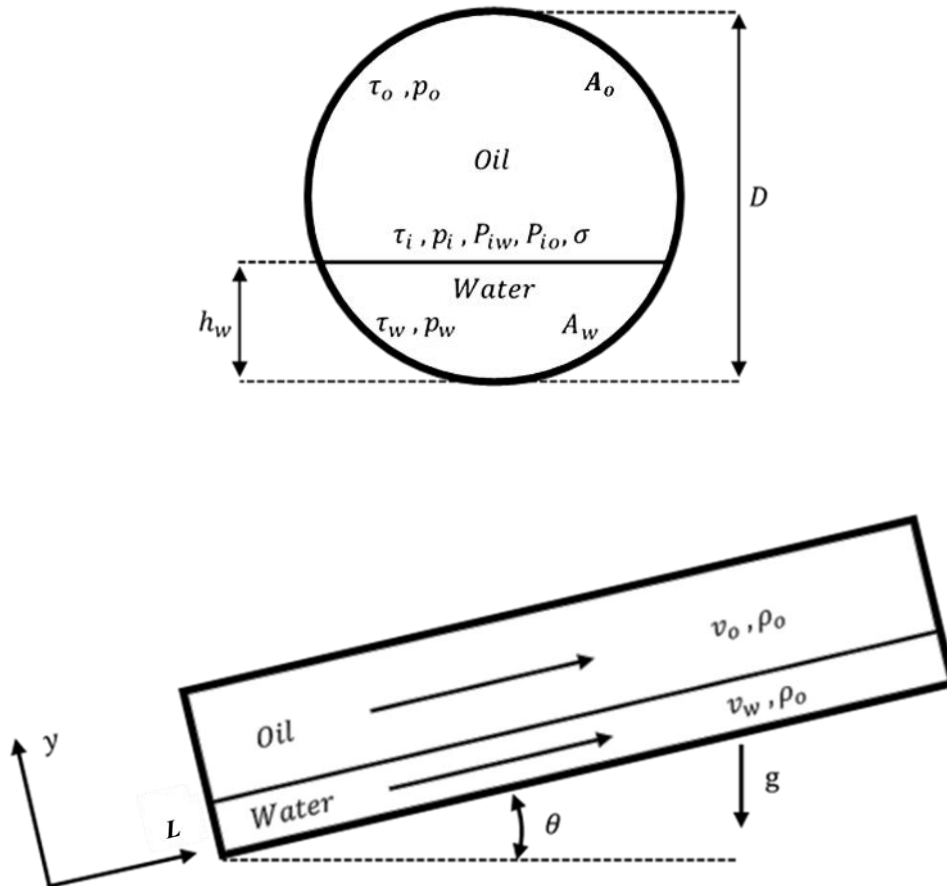
$$\frac{\partial h_w}{\partial t} + \frac{A_w}{A'_w} \frac{\partial v_w}{\partial L} + v_w \frac{\partial h_w}{\partial L} = 0 \quad (2-64)$$

$$\frac{\partial h_w}{\partial t} - \frac{A_o}{A'_w} \frac{\partial v_o}{\partial L} + v_o \frac{\partial h_w}{\partial L} = 0 \quad (2-65)$$

$$\rho_w \frac{\partial v_w}{\partial t} - \rho_o \frac{\partial v_o}{\partial t} + \rho_o v_w \frac{\partial v_w}{\partial L} + (\rho_w - \rho_o)g \sin(\theta) \frac{\partial h_w}{\partial L} - \sigma \frac{\partial^3 h_w}{\partial L^3} = F \quad (2-66)$$

$$F = -\frac{\tau_w p_w}{A_w} + \frac{\tau_o p_o}{A_o} + \tau_i p_i \left( \frac{1}{A_w} + \frac{1}{A_o} \right) - (\rho_w - \rho_o)g \sin(\theta) \quad (2-67)$$

In Eqs. (2-64) and (2-65),  $A'_w$  describes an expression for  $dA_w/dh_w$ , and  $F$  is an expression given to equate Eqs. (2-66) and (2-67). Hence, when  $F = 0$ , this reveals the steady-state solution (Barnea and Taitel, 1994). This configuration is mainly applicable for stratified groups as shown in *Figure 2-18*, but can also be used to analyse boundaries through instabilities, which can transition to intermittent conditions.



*Figure 2-18: Schematic description of forces acting on a smooth oil-water two-phase flow system in a stratified flow regime within a horizontal or inclined concentric pipe.*

---

The shear stress is obtained through the use of the Lockhart-Martinelli empirical correlations of friction factor against the phase interactions between constituent phases and the pipe wall. Non-dimensional parameters are used when reverting the interfacial shear stress to be equal to the wall shear stress (in this case water bounded surfaces  $\tau_{w_w}$ ). From Eqs. (2-54) and (2-55) the following is derived:

$$X^2 \left( \frac{\tilde{D}_{H_o} \tilde{v}_o}{\tilde{D}_{H_w} \tilde{v}_w} \right)^{-z} \left( \frac{\tilde{v}_o}{\tilde{v}_w} \right)^2 \frac{\tilde{P}_o}{\tilde{A}_o} - \frac{\tilde{P}_w}{\tilde{A}_w} - \tilde{p}_i \left( \frac{1}{\tilde{A}_o} + \frac{1}{\tilde{A}_w} \right) + (\rho_w - \rho_o)g \sin(\theta) = 0 \quad (2-68)$$

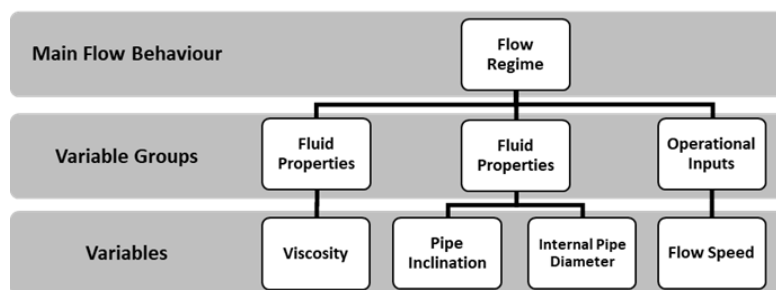
$$\Phi^2 = \frac{1}{4\tilde{A}_w X^2} (\tilde{D}_{H_w} \tilde{v}_w)^{-z} \tilde{v}_w^2 (\tilde{P}_o + \tilde{P}_w) \quad (2-69)$$

as,  $\tilde{v}_o$  and  $\tilde{v}_w$  are the dimensionless quantities of the average oil and water velocity, respectively,  $z$  is some arbitrary value defined from the Reynolds number exponents for the calculation of the frictional coefficients,  $\tilde{P}_i$ ,  $\tilde{P}_o$  and  $\tilde{P}_w$  are dimensionless pressures for the individual phases for the interface, oil and water, respectively,  $\tilde{p}_i$  is the dimensionless perimeter of the interface in contact with the wall,  $\tilde{A}_o$  and  $\tilde{A}_w$  are dimensionless cross-sectional areas for the individual phases of oil and water within a pipe, respectively and  $\tilde{D}_{H_o}$  and  $\tilde{D}_{H_w}$  are the dimensionless hydraulic diameters for oil and water flow, respectively. The height of the interface  $h_w$  (otherwise, the high of the water from the bottom of the pipe to the interface with the oil layer) defines the dimensionless parameters as this is a key factor within the geometric boundaries between individual phase interactions against the pipe and resulting shear stress for Eqs. (2-68) and (2-69). In fact, the high of the interface (water phase) can be derived from Eq. (2-69). by estimating the pressure gradient ratio between the fluid mixture and water phase (Angeli and Hewitt, 1998).

## 2.6 Controllable Parameter Influences

Understanding the combined alterations of various variables of multiphase flow systems within pipes is a key aspect of how different flow behaviours are developed. Each unique configuration may allow a multiphase system to develop a specific flow regime or reach a transition between two or more strongly defined regimes as the physical characterisations deviate from each other in the spatial distribution from the interface between the separate phases (Torres et al., 2015). For the purpose of this study, controllable system parameters are categorised into three separate groups based on the direct influences they have upon individual system characteristics. These categories are (1) fluid properties, which are variables that directly govern flow behaviour, (2)

pipeline geometry of physical design characteristics of the flow stream channel and (3) operational variables, which are used to control the flow line without affecting the physical pipeline characteristics and fluid properties. The fluid properties group will typically incorporate variables of only oil as water is regularly standardised, while oil has many complex molecular compositions which can cause significant changes in fluid properties such as viscosity and density through the smallest temperature changes. These variables affect fluid mobility, which will significantly affect a fluid's ease of transport and ability to be broken down and transition to a neighbouring flow regime. Pipeline design also plays a key role in a fluids ability to travel through a pipeline based on variables such as pipeline inclinations that act with or against gravitational forces and pipe internal diameters, which result in scaling-up principles that affect velocity profiles throughout the streamline and the respective material the pipeline is made from which may alter frictional losses between the internal pipe surface and respective fluids that flow within the pipeline. Finally, pipeline operations are generally controlled variables that can be used to sustain desired characteristics within a multiphase system. Inputs that control the flow regime are limited to only one variable, which is flow speed manipulation through chokes and valves. This in turn, can also alter the pressure distribution across the pipeline, yet this cannot be considered a direct operational input as pressure variables are not precisely controllable. All possible variables that are categorised in one of these three groups are systematically shown in *Figure 2-19*.



*Figure 2-19: Parameter flow chart of variables grouped within three sections that effect multiphase flow regimes. Flow regimes are mainly influenced by variables that are grouped from pipeline design, fluid properties and operational inputs.*

There are many other variables that can be incorporated within each group, but based on the current experimental work, the stated variables are the few that can be best controlled in laboratory conditions. In fact, there are even fewer manageable variables when under industrial conditions and must also be considered to ensure the experimental analysis of this work applies to industrial-scaled applications as field operations are more challenging to control. Examples such as viscosity and density cannot be fully controlled at an industrial scale without considering the large cost implications.

---

## 2.7 Dimensionless Flow Regime Maps

Flow regime maps are conventionally constructed under dimensional variables such as superficial velocities of oil and water or normalized ratios such as water cut or phase fraction identified through a single value varying from zero to one. These flow maps mainly depend on dimensional quantities when incorporating or examining other variables affecting flow regimes for a two-phase system. These variables can be seen under the three categories for experimental/field variables as previously discussed in section 2.6, (1) geometrical alteration, where examples can be seen through the alterations of pipeline design such as pipe diameter and inclination, (2) fluid properties such as density, viscosity and surface tension and (3) operational variables through phase flow and timing at which the operation was conducted. All specified pipeline attributes depend on the dimensional form and are also known to be valid for a particular flow configuration; hence the applicability of these maps is limited (Brennen, 2005). There have been a number of attempts to develop a universal flow regime map under both dimensional and dimensionless construction in literature, such as; (1) implementing fluid property correction factors; (Govier and Aziz, 1972; Weisman and Kang, 1981), (2) velocity ratios between the individual superficial phase and superficial mixture velocity ( $v_{s\alpha\beta}/v_{sm}$ ) and (3) incorporating dimensionless values to correlate the forces that are attributed to a flow system.

Correction factors and velocity ratios have been established to be only dependable for a limited range of system set-ups due to these maps being constructed from experimental data. Hence, dimensionless analysis is more commonly used for better multiphase flow classification by analysing the combined effects of fluid properties, pipeline design and individual phase flowrates relative to the corresponding phases. The key dimensionless groups that govern liquid-liquid flow are ratios of forces acting in conjunction with the flow line. These forces are classified as inertial, viscous, gravitational, and interfacial tension (through capillary effects). All have some degree of influence within the system, some greater than others depending on the conditions the system is subjected under. Furthermore, the dimensional variable groups that hinder or enhance a multiphase system, such as fluid properties, pipe design and operational inputs can all be integrated to develop a dimensionless number. One of the most commonly used dimensionless parameters for liquid-liquid flow is the Eötvös number,  $E_o'$ . It is described as the ratio of the gravitational forces against the surface or interfacial tension. This was proposed by Brauner (2003) to characterise oil-water flow behaviours in horizontal pipes. The Eötvös number is incorporated with a factor of 8,

---

generated from the Young-Laplace equation when predicting the interface shape under stratified conditions and is represented as:

$$E_o' = \frac{\Delta\rho g D^2}{8\sigma} \quad (2-70)$$

where the Eötvös number is a function of the change in fluid densities,  $\Delta\rho$  gravity, internal pipe diameter, and IFT. The main classification for oil-water systems depending whether this value is  $E_o' > 1$  or  $E_o' < 1$ . Under the conditions which result to  $E_o' > 1$  represents the two-phase flow system to be dominated by gravitational forces, which typically correlate to stratified flow conditions when the density difference and pipe diameter are considerably large enough to suppress interfacial forces, which can be considered flat. When  $E_o' < 1$  is a good indication of a dual liquid system to be dominated under interfacial tension forces and is associated naturally with the core annular flow and to some degree with other intermittent flow regimes (Shi and Yeung, 2017). Another dimensionless quantity is the Weber number,  $We$  is the ratio of inertial forces to interfacial forces. The Weber number is typically combined with the Eötvös number as  $We/E_o$  which expresses the ratio of inertia forces against the gravity influences. A larger  $We/E_o$  ratio is an indication of dominant inertial forces that have the tendency to cause some form of unstable conditions at the interface, leading to possible intermittent flow regimes such as slug flow, plug flows and even dispersed flows. At low  $We/E_o$ , gravity forces prevail, causing full segregation of oil-water to occur, developing stratified flow patterns.

$$\frac{We}{E_o} = \frac{\rho_m v_m^2 D}{\Delta\rho g D^2} \quad (2-71)$$

The ratio between gravitational and viscous forces  $G/V$ , which incorporate the effects of the mixture viscosity relative to the mixture velocity under liquid-liquid configurations, can be expressed as:

$$\frac{G}{V} = \frac{\Delta\rho g D^2}{\mu_m v_m} \quad (2-72)$$

---

When the  $G/V$  is considered high under oil-water flows, gravitational forces are the dominant driving mechanism for the flow line as viscous forces would be considerably lower and vice versa. The fluid mixture at the interface can easily segregate when high enough kinetic energy is present, developing flow structures such as stratified flow and dispersed flow of one continuum phase within the other. In contrast, at low oil-water  $G/V$ , stratified conditions are less probable to form as gravitational forces are reduced. This is mainly due to the lack of differential density between the two phases, but pipe diameter also has some degree of influence. In general, oil phases that are too viscous to be segregated or dispersed into fine droplets but broken apart into lumps of various sizes and shapes, will typically lead to flow regimes such as core annular flow or intermittent flow regimes (mainly slug and plug flows) at which the shear stress is minimised.

The Reynolds number in terms of the fluid mixture is also used as a dimensionless quantity to conduct comparisons of oil-water flow systems. This dimensionless form is classified as the ratio of the inertia force to viscous force in a flow system, as previously demonstrated in Eq. (2-25). The mixture Reynolds number is calculated through the use of the homogeneous flow model, as also previously shown by the use of Eqs. (2-22)-(2-24), where mixture density, viscosity and velocity, respectively. These are assumed to be functions of the phase hold-up either in terms of volumetric or cross-sectional analysis or mass fractions which assumes a no-slip system. However, in the perspective of flow regime mapping, the Reynolds number is customarily accompanied by the Eötvös number as  $Re/E_o$ . When this dimensionless entity is related to the water cut, a series of flow patterns can be observed. When water cut is fixed and the  $Re/E_o$  ratio is increased, this may lead to the transition between distinctly segregated flows to dispersed flows. At lower water cuts ( $C_w < 0.1$ ), it has been witnessed in previous studies that stratified flow occurs with droplets at the interface. In addition to these conditions, an increase in the dimensionless quantity can also prevail in dual continuous transition from stratified flow (Ibarra, Markides and Matar, 2015). The Froude number is a not-so-common dimensionless quantity which assesses the individual phases relative to the system dynamics of differential density and pipe diameter in terms of their superficial velocity developed by Zapke and Kröger (2000) for phase analysis of oil and water  $Fr_o$  and  $Fr_w$  respectively.

$$Fr_o = \frac{v_{so}\sqrt{\rho_o}}{\sqrt{\Delta\rho gD}} \quad (2-73)$$

$$Fr_w = \frac{v_{sw}\sqrt{\rho_w}}{\sqrt{\Delta\rho gD}} \quad (2-74)$$

---

## 2.8 Previous Experimental Work on Liquid-Liquid Flow

There has been a recent upsurge in experimental work with liquid-liquid multiphase flow analysis using looped test pipe systems under various pipeline design configurations within the last 20 years. However, a very limited amount of experiments have been dedicated to understanding or have come across the behaviour of intermittent flow regimes within oil-water systems since the early 1960s. This thesis will mainly look at experimental work that contains results of flow regimes that are associated with the intermittent flow pattern group, as discussed in section 2.3. Hence, the desired flow regimes of this experiment will predominantly consider intermittent flows to be achieved through the presence of further detailed subcategorised patterns of slug, plug and bubble flow regimes. For the purpose of clarity, this thesis will refer to all the intermittent flows as either slug or plug flow. In addition to the presence of slug patterns, analysis of other studies that have also observed these flow behaviours under the influence of pipe inclinations will also be reflected on where this study will focus on slight-inclined pipe orientations, which will be considered to be no more than  $\pm 5^\circ$  from the horizontal.

### 2.8.1 Liquid-liquid Slug Flow with Horizontal Pipe Configuration

(1) (Charles, Govier and Hodgson, 1961)

Slug flow was not discovered until the resulting work of Charles, Govier and Hodgson (1961), as this pioneering work was the first to ascertain the effects of slug flow and its developments across concentric channels based on superficial oil and water velocity by merely adjusting the oil viscosity. This work was not only the first to discover slug flow patterns but also core annular flow under incompressible two-phase flow. The study experimentally investigated oil-water flow of equal densities within a horizontal 1-inch (0.0254m) pipeline diameter of a 7.315m long test pipe made from a transparent plastic material to conduct visual observations of physical flow regime behaviours. Carbon tetrachloride was implemented within the oil phase to induce the oil to increase in density to develop an almost equal density configuration against the corresponding water phase ( $\rho_w = \rho_o = 988\text{kg/m}^3$ ). Oil and water phases were introduced to the test pipeline simultaneously as the two phases were combined via a nozzle in which the oil was guided into the water. Three different oils with veering viscosity ratios of 6.29, 16.8, and 65.0mPa.s were used in the experiment. The results showed that the experiment had found five different types of flow regimes: (1) water drops in oil, (2) oil in water concentric (core annular flow), (3) oil slugs in water, (4) oil bubbles in water, and (5) oil drops in water. Each oil viscosity showed relatively similar hydrodynamic behaviours, as shown in the author's sketches of the flow regime photographs from the experiment in *Figure 2-20*.



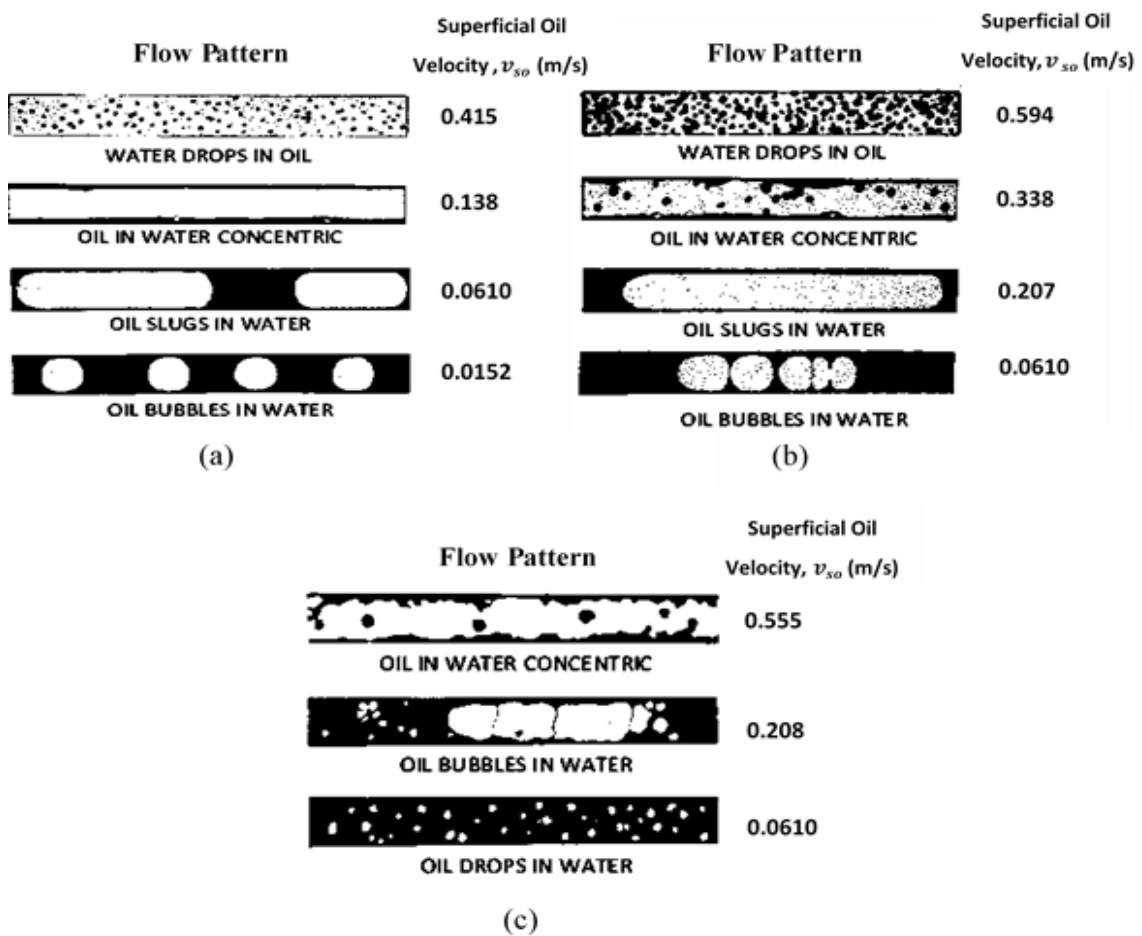


Figure 2-20: Drawings of experimental results that contain oil with a viscosity of  $\mu_o = 16.8\text{mPa}\cdot\text{s}$  flowing simultaneously with water of equal density while under the influence of alterations of superficial oil velocity  $v_{so}$  as the water superficial velocity  $v_{sw}$  is maintained at (a) low fixed velocity of  $v_{sw} = 0.0305\text{m/s}$  (b) medium fixed velocity of  $v_{sw} = 0.208\text{m/s}$  and (c) high fixed velocity of  $v_{sw} = 0.622\text{m/s}$ . Adapted from (Charles, Govier and Hodgson, 1961).

The study concluded that despite the significant range of oil viscosity used, the alteration of flow regime patterns was minutely affected by the oil viscosity in concurrence with the relationship between oil and water flowrates. Despite the greatest viscosity to show the most dissimilar behaviour under a high oil-water input ratio. The authors believed this to be merely the oil-water interfacial interactions to cause further modification to the flow behaviour. The transition between the flow regimes can be characterised in order of highest to lowest oil superficial velocity while maintaining a constant superficial water velocity. From highest to lowest oil flowrate under laminar conditions, the following flow regimes will develop: first water drops in oil, then core annular flow, oil slugs in water and oil bubbles in water in respective order for two immiscible liquids in a pipe. This can be seen in *Figure 2-21* graphically demonstrates these flow conditions as a function of the superficial velocities of the respective multiphase compositions.

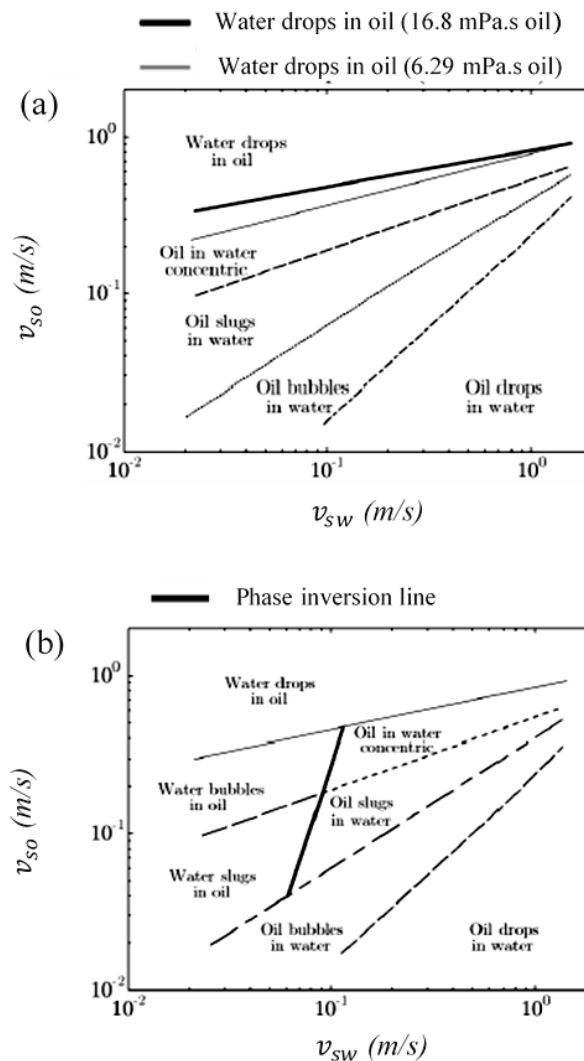


Figure 2-21: Summary of flow regime transitions for oil-water flow in a 1-inch diameter pipe with equal density and oil viscosities of (a)  $\mu_o = 6.29\text{mPa.s}$  and  $\mu_o = 16.8\text{mPa.s}$ , and (b)  $\mu_o = 65.0\text{mPa.s}$ . Oil and water velocities are represented on a logarithmic plot and singular lines are drawn to represent the regions of the flow regimes. Adapted from both (Charles, Govier and Hodgson, 1961) and (Ibarra, 2017).

During the experiment, the investigators noted that the circulation of oil, when taking the form of slugs and bubbles in continuous water, is provoked by the flowrates that are relative to the average flow velocity. This is because the direction of rotation of the slug form is suggested to be dependent on the density differential vector between oil and water. In addition, a circulatory movement was observed within the continuous water phase between each slug patch. Indicating that although the flow was under a laminar state, the slugs and bubbles are induced by miniscule eddy currents, which designate signs of segregated turbulent and laminar flow developments that are shared within a common flow, which represent the transitional stages of stable/unstable flow.

---

(2) (Hasson, Mann and Nir, 1970)

A combination of empirical observations and phenomenological approaches were conducted in the studies developed by Hasson, Mann and Nir (1970). Slug flow characteristics were found within this study when demonstrating the changes in flow regime conditions over variations of  $0.02m$  and  $0.2m$  distances from the pipe inlet. Observations were mainly focused on core annular flow and respective liquid film breakups when injecting water within this flow regime through a T-junction inlet nozzle. This led to the development of other dynamic flow patterns such as slugs and also demonstrated the effects of flow pattern behaviours in altered degrees of contamination or cleanliness of the internal pipe wall that the fluids come to contact with. A glass pipeline  $2.7m$  long with an internal diameter of  $0.0126m$  was used in the experiment. Distilled water and kerosene-perchloroethylene solution were the fluids used in the experiment of almost equal density mixtures as both combined compositions developed a mixture density of  $1020kg/m^3$  and viscosities of  $0.8mPa.s$  and  $1.0mPa.s$  in respective order. The fluids were maintained at a constant temperature of  $30^\circ C$  while superficial velocities of oil and water ranged from  $0-3.33m^3/s$  and  $0-6.67m^3/s$ , respectively. The combinations of these fluids had initially developed a concentric flow in a rather unconventional manner. The water phase was initiated within the core of the annular flow regime as the oil fluid would take the form of the annulus region.

The resulting breakup for this particular configuration was observed, and other stable flow patterns later followed as two distinct types of breakups were noticed; (1) a wall film rupture which is a phenomenon present at low flow speed intervals where the internal forces are not great enough to sustain the annulus or (2) a collapse of the core from the progression of the interfacial wave strengthening which in contrast to film ruptures occurs under higher flowrates. The breakdown of the liquid films is largely associated with the wall wetting properties as the water phase favours the wall wetting condition on the internal glass pipe surface. In this circumstance, the water phase is the core of annular flow, and it employs a disorderly impact on the oil film due to the water's tendency to be in contact with the inner pipe wall. Evidence of this behaviour is shown from the alterations of wall wetting properties of the glass pipe test section by silicon solution treatment. This made the internal pipe walls hydrophobic and provided the ability to sustain stable core-annular flows under the same previous conditions where film breakup developed near the fluid entrance. In contrast to core deterioration, the mechanism was described as influenced by waves and ripples by the interface between the two fluids in their respective form of an annulus and core structure. The waveforms were based on the phenomena of the Rayleigh-type waves, which originate from studies that had observed low-speed jet fragmentation. Wall wettability comparisons have developed further with the contrast of a recently cleaned glass

(hydrophilic) pipe wall. The experimental work demonstrated a series of other flow regimes after the breakup of annular flow. The flow patterns observed in the study are water slugs in continuous oil, oil slugs in continuous water, stratified flow, dispersions of oil in water and dispersions of water in oil.

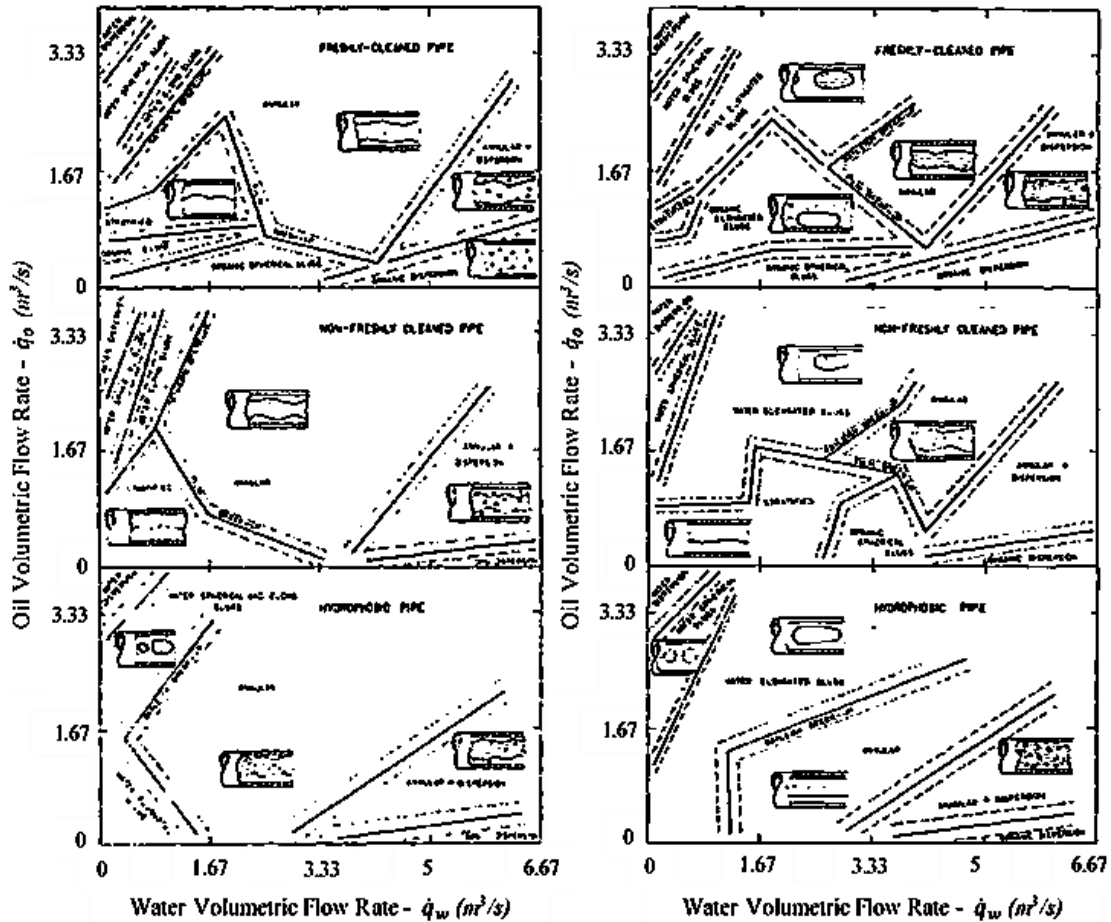


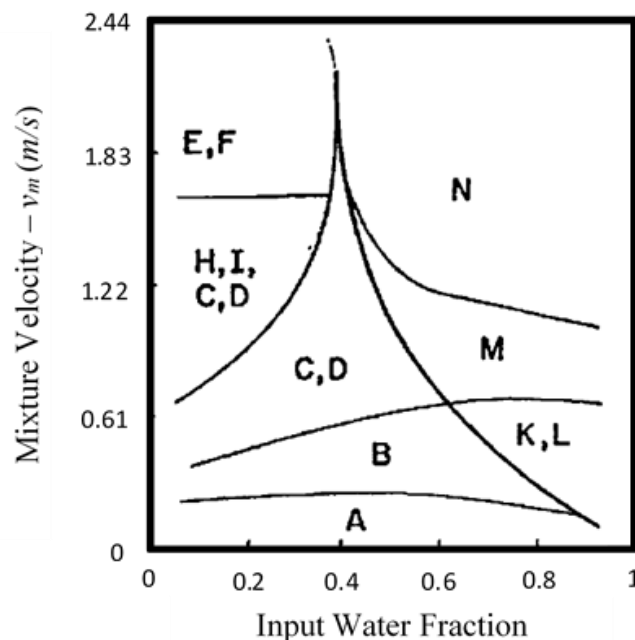
Figure 2-22: Flow regime and transition maps as a function of the oil and water volumetric flowrates under three different internal pipe wall conditions; (top section) freshly cleaned pipeline, (middle section) non-freshly cleaned pipeline and (bottom section) hydrophobic pipe. As maps on the left represent the flow conditions that are 0.02m from the pipe inlet and maps on the right represent the flow conditions 0.2m from the pipe inlet. Adapted from (Hasson, Mann and Nir, 1970)

The resulting flow regime maps for the experiment expressed in terms of superficial fluid velocity are shown in Figure 2-22. The study concluded that flow regimes depend on not only the individual fluid flowrates but also the breakup mechanism of a fully stable concentric flow system from internal pipe wettability. When pipes are under hydrophobic or hydrophilic from acid or non-acid cleaning, the wall wetting conditions differ, resulting in a diverse flow regime to

develop. Pipes under hydrophobic conditions maintain core annular flow patterns by preserving the water films, whereas hydrophilic pipes induce the breakup of the annulus to form a continuous water phase while the dispersed oil core flows in the form of slugs, dispersions or a stratified layer. In contrast, when the breakup is characterised by increases in oil to water flowrates, the oil becomes the continuous phase, and the water takes the form of slugs or a dispersion, regardless of the internal pipe wall conditions. With regards to oil slug, these flow developments are generally associated with the combination of low water flowrates and high oil flowrates when wave amplitude reaches the core centre causing unstable disruptions.

(3) (Guzhov et al., 1973)

The Russian-based work of Guzhov et al. (1973) also found developments in slug flow behaviour when attempting to determine the pressure drops and respective flow regimes of an oil-water multiphase system. The oil properties were defined with a viscosity of  $21.7\text{mPa}\cdot\text{s}$  and a density of  $896\text{kg}/\text{m}^3$ , indicating that the oil is medium-heavy, while the temperature was maintained at a continuous value of  $20^\circ\text{C}$  when all fluids were contained in a  $0.0394\text{m}$  diameter pipeline. The resulting flow patterns are as shown in *Figure 2-23*, where flow regimes were observed as functions of the water fraction contained within the entire multiphase system and the mixture velocity.



*Figure 2-23: Experimental results for a liquid-liquid system with oil properties of  $\mu_o = 21.7\text{mPa}\cdot\text{s}$  and  $\rho_o = 896\text{kg}/\text{m}^3$  in a  $D = 0.0394\text{m}$  pipe in the form of a flow regime map. Conducted by (Guzhov et al., 1973), revisited and adapted from (Oglesby, 1979).*

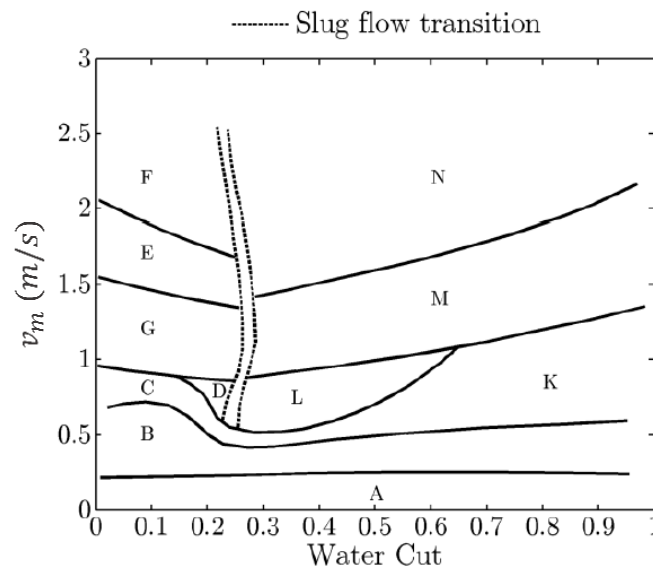
The results from Guzhov et al. (1973) became the basis for the incompressible flow models for slug flow, developed by Oglesby (1979). Flow regime categories are described in *Table 2-2*.

Category	Flow Regime
Segregated	(A) <b>Stratified flow:</b> No mixing at the interface
Semi-Segregated	(B) <b>Stratified flow with droplets at the interface:</b> Some mixing at the interface
Oil Dominant	(C) <b>Dispersion-oil-in-water:</b> Pure oil layer at the top section of the pipeline and oil-in-water dispersion at the bottom section of the pipe. The dispersion layer occupies <b>less</b> than half of the pipe cross-sectional area (semi-mixed)  (D) <b>Dispersion-oil-in-water:</b> Pure oil layer at the top section of the pipeline and oil-in-water dispersion at the bottom section of the pipe. The dispersion layer occupies <b>more</b> than half of the pipe cross-sectional area (mixed)  (E) <b>Non-homogeneous:</b> Water-in-oil-dispersion  (F) <b>Homogeneous:</b> Water-in-oil-dispersion  (G) <b>Annular flow:</b> Water in the core and oil in the annulus  (H) <b>Slug flow:</b> Water slugs in oil
Water Dominant	(I) <b>Slug flow:</b> Oil slugs in water  (J) <b>Annular flow:</b> Oil in the core and water- in the annulus  (K) <b>Dispersion-water-in-oil:</b> Pure water layer at the bottom section of the pipeline and water-in-oil dispersion at the top section of the pipe. The dispersion layer occupies <b>less</b> than half of the pipe cross-sectional area (semi-mixed)  (L) <b>Dispersion-oil-in-water:</b> Pure oil layer at the top section of the pipeline and oil-in-water dispersion at the bottom section of the pipe. The dispersion layer occupies <b>more</b> than half of the pipe cross-sectional area (mixed)  (M) <b>Non-homogeneous:</b> Oil-in-water-dispersion  (N) <b>Homogeneous:</b> oil-in-water-dispersion

*Table 2-2: Categorised flow pattern results for an oil-water multiphase system with oil properties of  $\mu_o = 21.7\text{mPa}\cdot\text{s}$  and,  $\rho_o = 896\text{kg}/\text{m}^3$  in a  $D = 0.0394\text{m}$  pipe in the form of a flow regime map. Adapted from (Guzhov et al., 1973), revisited and adapted from (Oglesby, 1979).*

(4) (Oglesby, 1979)

The work of Oglesby (1979) conducted experimental studies of incompressible two-phase flow when using oil and water. Similarly to all previously discussed studies, the water properties are assumed to be standardised, whereas the oil properties are investigated under a considerable amount of variations, with three varying oil viscosities of 32, 84 and 115 mPa.s within a 0.041 m diameter steel pipeline, while the fluids are sustained at a continuous temperature of 21°C. Flow maps were independently produced from each oil condition, and a resulting 442 data points were generated from this work. Flow regimes initially from the predeceasing work had also been found within this study, where; stratified, intermittent (slugs), and dispersed flow regimes were observed. However, Oglesby's experimental investigation was also reported to witness an additional flow pattern in the form of annular flow but with a water core and an oil annulus interface. An example of the flow pattern map is shown in *Figure 2-24*, where the 84 mPa.s viscosity of the oil is represented. *Table 2-2* applies to the lettering sequence for *Figure 2-24*, which is defined in the same manner as *Figure 2-23*. In the interest of slug flow formations, the regional area for this is found under large variations in mixture velocity but constrained under low and localised water cuts. Hence, this indicates that slug flow is, to a certain extent, independent of the mixture velocity but strongly dependent on specific water volumes to coexist in pipes. Slug characteristics are said to be conjectured by a relation with the system phase inversion point at which continuous phases are shifted from oil dominated to water dominated streams or vice-versa.



*Figure 2-24: Experimental results for a liquid-liquid system with oil properties of  $\mu_o = 84$  mPa.s in a  $D = 0.041$  m pipe. Adapted from (Oglesby, 1979).*

---

(5) (Arirachakaran et al., 1989)

Arirachakaran et al. (1989) initially conducted experimental investigations based on pressure drops and alterations of continuous phase invasion points and the effects this has on liquid-liquid emulsion patterned behaviours. The study utilised two horizontal pipe test sections, which contained water and oil multiphase mixtures. The two test conditions are; (1) with an internal diameter of  $0.0381m$  as the oil phase properties were altered in terms of the viscosity of 4.7, 58, 84 and  $115mPa.s$  while maintaining the streamline temperature at  $21^{\circ}C$  and (2)  $0.0410m$  pipeline was used with much greater oil viscosities in comparison to the first condition to replicated heavier as of 237 and  $2116mPa.s$ . The studied mixture velocities varied between  $0.46 - 3.66m/s$ , while applicable water cuts were tested from  $0.05 - 0.9$ . The experimental set-up can be deemed to provide a strongly representative variation of different industrial oil production conditions and shows the variation of scaling effects of small changes in pipe diameter sizes. The results of the experiments revealed seven distinct flow regimes, as shown in *Figure 2-25* and are classified by the author (with some adjustments from the present study) as follows:

- Stratified (S): The presence of two distinct phase layers, where gravitational effects segregate the lighter phase (top layer) and heavier phase (bottom layer) due to the density difference between the two phases. This category also incorporates the possibility of mixing at the interface.
- Annular (AO): water core with an oil annulus.
- Dispersed: A homogeneous mixture in two types of configurations:
  - i. Oil dispersion in water (DO)
  - ii. Water dispersion in oil (DW)
    - Dispersed mixed: A dispersion phase that can be in two types of configurations as one phase is distributed within another other with a possible pure layer:
      - i. Water dispersion with a pure oil layer (MO)
      - ii. Oil dispersion with water layer (MW)
        - Intermittent: Slugs of a continuous phase or an accumulation of droplets/bubbles.
- i. Oil slugs in water (IO)
- ii. Water slugs in oil (IW)



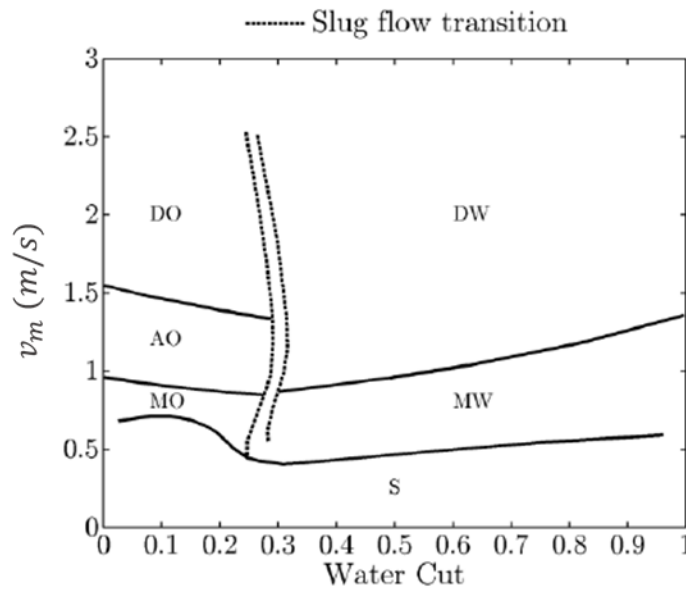


Figure 2-25: Flow regime map for experimental results of a horizontal pipe of  $D = 0.0381\text{m}$  containing oil-water flow with  $\mu_o = 84\text{mPa.s}$ . Adapted from (Arirachakaran et al., 1989)

The findings of this experimental investigation are noticeably similar to that of Oglesby (1979), which was conducted a decade earlier than Arirachakaran et al. (1989). From the flow regime maps of identical axial scaling factors as shown in Figure 2-24 and Figure 2-25. Centred on intermittent slugs, this flow regime seems to be strongly dependent on a localised water cut quantity between 20 – 30% while being able to exist across a large frequency of combined mixture velocities. In fact, Arirachakaran et al. (1989) found the oil viscosity to have inconsequential effects on flow regime behaviours in general water continuous formations. However, in terms of phase invasion to shift the fluid dominance from a continuous phase to a dispersed phase and vice-versa, oil viscosity and input water fraction in the well-defined laminar region were found to instigate a key role in these interchangeable coexisting shifts of individual phase behaviours. This implies that the viscosity may have an indirect influence on flow regimes despite not having a direct influence. It is important to note that this correlation was developed from the inclusion of data from previous studies by Charles, Govier and Hodgson (1961); Guzhov et al. (1973); and Oglesby (1979).

(6) (Raj, Chakrabarti and Das, 2005)

When exploring similarities and differences between gas-liquid and liquid-liquid phenomena, Raj, Chakrabarti and Das (2005) primarily set out to conduct experimental studies on dual-incompressible flow mixtures using kerosene (oil) and water. Water was assumed to be under standard conditions, and the experimental kerosene maintained at a constant temperature of  $25^\circ\text{C}$

---

has consistent fluid properties with a density of  $787\text{kg/m}^3$  and viscosity of  $1.2\text{mPa}\cdot\text{s}$ , which these properties indicate that the oil used can be considered a light and mobile oil type. The test section that contained these fluids was a  $2.13\text{m}$  long transparent polymethyl-methacrylate (PMMA) pipe with an internal diameter of  $0.0254\text{m}$  which was aligned directly to the horizontal. PMMA was set as the choice of pipe material to conduct visual and photographic observations on flow regime patterns through the test section. In addition to the pipeline acrylic, the separator system where the passing kerosene-water resolve is also made from acrylic and has the inclusion of baffles to enable maximum separation of the high-density contrasting fluids to be later redirected by separated pumps in individual phase tanks to be reused within the experiment. The acrylic design was implemented to be used as an additional measure to ensure the mixing of the two fluids is avoided. Different combinations of individual fluid velocities were explored in distributions ranging from  $0.03 - 1.6\text{m/s}$  as the investigators initially intended to search for stratified flow regimes. The experiment initially found stable, smooth stratified flow under low flowrate conditions from both phases, where kerosene had a flow velocity of  $0.003 - 0.15\text{m/s}$  and a water velocity flow at similar speeds between  $0.03 - 0.2\text{m/s}$ . During these combinations of slow flow conditions, the two phases can fulfil complete separation and create two-distinct layers. However, the increase of one of the fluids will initiate a disturbance in this flow regime, causing waves at the interface.

The stratified wave flow was observed under conditions where the superficial kerosene velocity ranged from  $0.03 - 0.3\text{m/s}$ , while the superficial water velocity ranged from  $0.2 - 1.0\text{m/s}$ . Further advancements in increasing the superficial velocity of kerosene cause increasing amplitudes of water waves which will substance the breakup of the aqueous phase to form dispersed droplets in a continuous kerosene phase at the bottom of the pipe and a pure oil layer found in the top section of the pipeline. Additional unstable behaviours occur when further increases the superficial kerosene velocity above  $2.0\text{m/s}$  while maintaining a slow water superficial velocity. The resulting flow regime behaviour is an inverted mixture of a large quantity of the water phases to be found at the top of the pipe and more oil to be found at the bottom, indicating that the kerosene velocity increase overcomes the system's gravitational influences. In contrast, low kerosene velocities between  $0.003 - 0.14\text{m/s}$  will manipulate the wavy stratified flow to come in contact with the upper internal pipe wall to develop deformed plugs/slugs flow patterns similarly observed in gas-liquid flow but are better defined. The existence of this flow regime is restricted to superficial water velocities less than  $0.2\text{m/s}$ . The flow regimes and transitions are developed when changing the superficial velocity of kerosene and water shown in *Figure 2-26*, as *Figure 2-27* is the resulting experimental flow regime map.

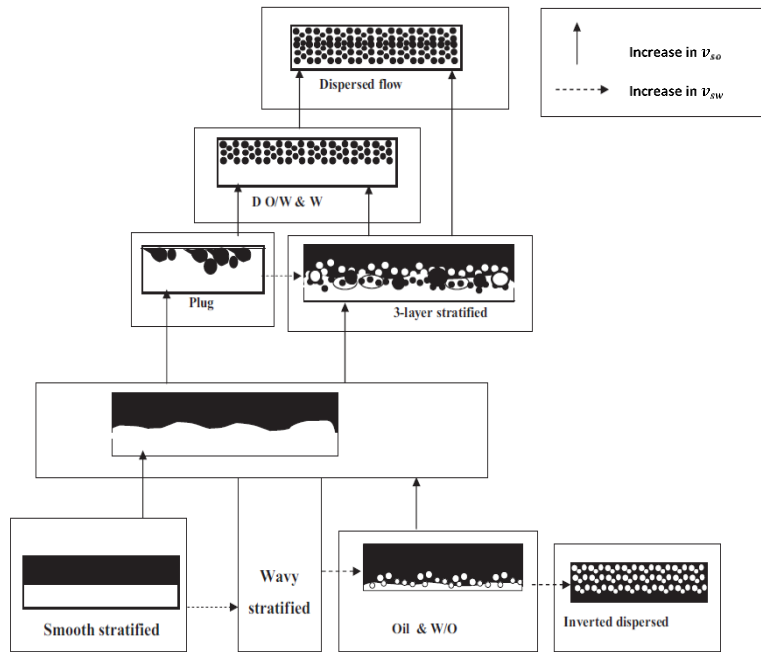


Figure 2-26: A schematic description of observed experimental flow regimes and how individual superficial phase velocities of kerosene and water cause the transition between each flow regime. The horizontal arrows signify an increase in the kerosene velocity shown as a vertical arrow represents an increase in the water velocity. The size of the boxes that contained each flow regime is an estimated representation of the range found from the experiment. Adapted from (Raj, Chakrabarti and Das, 2005).

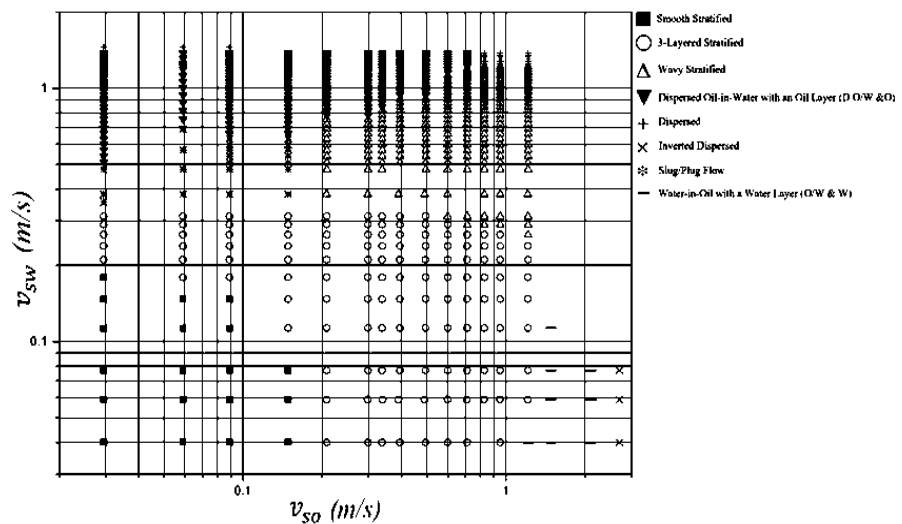


Figure 2-27: Experimental results of kerosene (oil)-water flow within a 2.13m long acrylic pipe of an internal diameter of 0.0254m, where water is assumed to be of standard fluid properties and  $\mu_o = 1.2\text{mPa}\cdot\text{s}$  and  $\rho_o = 787\text{kg}/\text{m}^3$  as the overall phase velocity range was between 0.03-1.6m/s. Adapted from (Raj, Chakrabarti and Das, 2005).

---

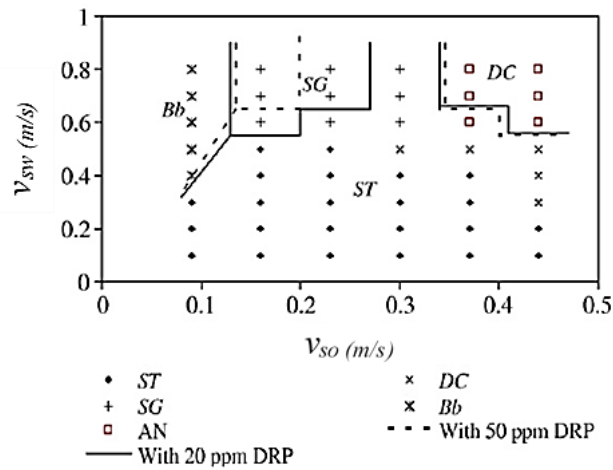
(7) (Al-Wahaibi, Smith and Angeli, 2007)

Moving on to studies that are more based on flow assurance and the implementation of chemical additives that are used to optimise flow behaviours, Al-Wahaibi, Smith and Angeli (2007) experimentally investigated the effects of drag-reducing polymer (DRP) that are subjected to the water phase during horizontal two-phase, oil-water flow. The flow set-up was mainly comprised of a 3.5m long test pipe section with a 0.014m diameter made from acrylic. The entire flow system temperature conditions were maintained at 25°C, as the experimental oil had a viscosity and density of 5.5mPa.s and 828kg/m<sup>3</sup>, respectively, while under test conditions that were set for two distinct types of drag reduction polymer solutions made from copolymer (Magnafloc 1011) of polyacrylamide and sodium acrylate. The two drag reduction additives were tested at the same varying injection conditions of 20ppm and 50ppm. The results revealed that there is a significant dependency on DRP in altering liquid-liquid flow patterns, as shown in *Figure 2-28*.

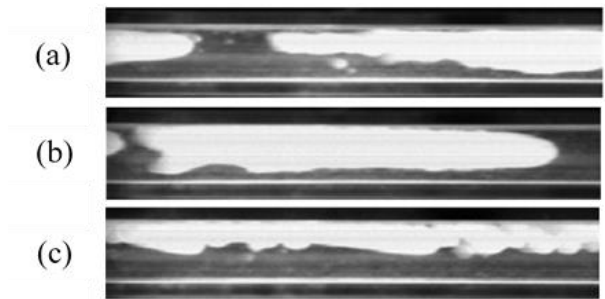
In the context of these effects against intermittent patterns, slug flow is occasionally altered to stratified flow conditions. In addition, in conditions where DRP was present, and the streamline was still maintained, the intermittent formations have also observed that the individual slugs/bubbles flow closer together compared to flow conditions without the injection of DRP. The reduction in pressure gradients that occurs across the pipeline due to the presence of the DRP solutions has also exploited the optimisation of the drag reduction by 50%, while both the water hold-up and phase interface height increased after implementing DRP. Observations of the combinations of superficial oil velocity show that the decrease of this operational variable within the region of 0.16 – 0.30m/s as the general water velocity also increases it will lead to the development of oil slug forms in favour of other more stable flow regimes.

The experiments had clearly shown that the addition of the DRP will either prevent slug flow developments and maintain stratified flow conditions at higher oil velocities between 0.23 – 0.30m/s or induce size reduction upon the intermittent flows while being closely packed together at much lower oil velocities at around 0.16m/s. It is believed that slug flow is attributed to the disturbance of the oil layer stability, leading to a thickness reduction of the oil layer during an upsurge of water velocity. Furthermore, the oil wetting conditions against the surface of the acrylic pipeline are more favourable to that of water and will conceal a larger cross-sectional area relative to the total mixture volume. As a result, the reduction of the oil-water ratio will substantially diminish the oil layer as the organic phase has a tendency to wet a larger section of the pipe's surface. Enhancements of turbulent flows from the increase of the water velocity will cause further instabilities within the flow line and hence the probabilistic mechanism of slugs to develop through the interface waves to come in contact with the upper pipe segment, consequently

breaking the oil layer into sections of slugs or elongated bubbles (plugs). This may be because the polymer solution causes a damping effect on the wave amplitudes of the interface as the turbulent flows are suppressed, which hinders the ability of the water phase to break up the oil layer. Slug lengths are also affected by polymer additives. Regular slugs can extend between 3 – 15 times the pipe diameters, but when DRP are present, the slug length decreases. The slug lengths are further decreased in tangent with the reduction of both constituent fluid velocities. The physical reason for this behaviour is the increase in the shedding rate of the water phase between individual slugs, as the polymer solution is initiated within the water, causing earlier oil breakups and shorter lengths and higher slug frequencies to form (Soleimani, Al-Sarkhi and Hanratty, 2002). Examples of observed slug pattern change from DRP implementation can be seen in *Figure 2-31*.



*Figure 2-28: Multiple experimental results superimposed on a single velocity graph comparing the original flow regimes without DRP within the flow line and the effects of flow regimes when using DRP under 20ppm and 50ppm injection rates. Adapted from (Al-Wahaibi, Smith and Angeli, 2007).*



*Figure 2-29: Changes in slug behaviour, (a) before the introduction of DRP and after the introduction of DRP where (b) shows shorter slug developments and (c) demonstrates closely compacted slugs. Adapted from (Al-Wahaibi, Smith and Angeli, 2007).*

---

(8) (Mandal, Chakrabarti and Das, 2007)

Experimental analysis of flow pattern behaviours in alterations of conduit sizes has been investigated by Mandal, Chakrabarti and Das (2007). Water and light kerosene with density and viscosity of  $787\text{kg/m}^3$  and  $1.2\text{mPa}\cdot\text{s}$  were used within a single flow loop rig containing two test pipe sections for scaling analysis on pipe diameter designs of  $0.0254\text{m}$  and  $0.012\text{m}$ . Both conditions exhibited intermittent patterns. In the  $0.0254\text{m}$  diameter pipeline, during the presence of low flowrates for kerosene, had led to the corresponding water waves to attain sufficient amplitudes to come to direct contact with the top of the internal pipe wall and develop plug flow conditions in irregular clusters between the water continuums. As flow within the  $0.012\text{m}$  diameter pipe showed larger regions of intermittent flows developing. The graphical data can be shown in *Figure 2-30*, where plug flow characteristics are again shown under high water velocity and low kerosene velocities. The advancement of water velocity has resulted in the conjuring of plugs to be shaped in the form of Taylor bubbles. In later stages, this pattern would take the appearance of slug flow, which also contains consecutive water slugs. The slug pattern had extended in a large range of velocity regions from the experiment of  $0.5 - 0.8\text{m/s}$  for water velocity and  $0.075 - 0.68\text{m/s}$  for kerosene velocities.

In normal circumstances, increasing phase velocities develop the breakup of the interface waves to form a three-layered flow through the progressive concentration of droplet accumulation at the same interface. However, in some cases observed in the experiment, slug developments occur under the same conditions within a smaller pipe. This is understood to be from surface tension that yields the additional surge to spread any interfacial waveforms against the top of the pipe wall and form slugs. Experimental photographic evidence of slug flow developments is shown in *Figure 2-31*. Further observations were made when comparing the reduction of pipe diameter as this influence becomes a critical factor within flow regime behaviour. The scaling-down effect has been quantified by the factor of the contact angles between the fluid interfaces and the corresponding pipe wall in contact with the fluids (Barajas and Panton, 1993). However, it must be noted that measurements of contact angle against a flat surface (plate) cannot be directly applicable to the same material in the form of a tubular section, but it can be assumed that the contact angle can be a generic characteristic of the material in its tubular form and respective fluids. Hence, diameter size can be attributed to the contact angles. In addition, it has been found that mixer initiation design, downstream of both fluid inlets of the test pipe during the distribution of the two liquids also plays a crucial role in flow behaviour. It was found that this phenomenon can also change the results of the flow regime map by only altering the order in which each individual fluid is introduced within the pipe test section.

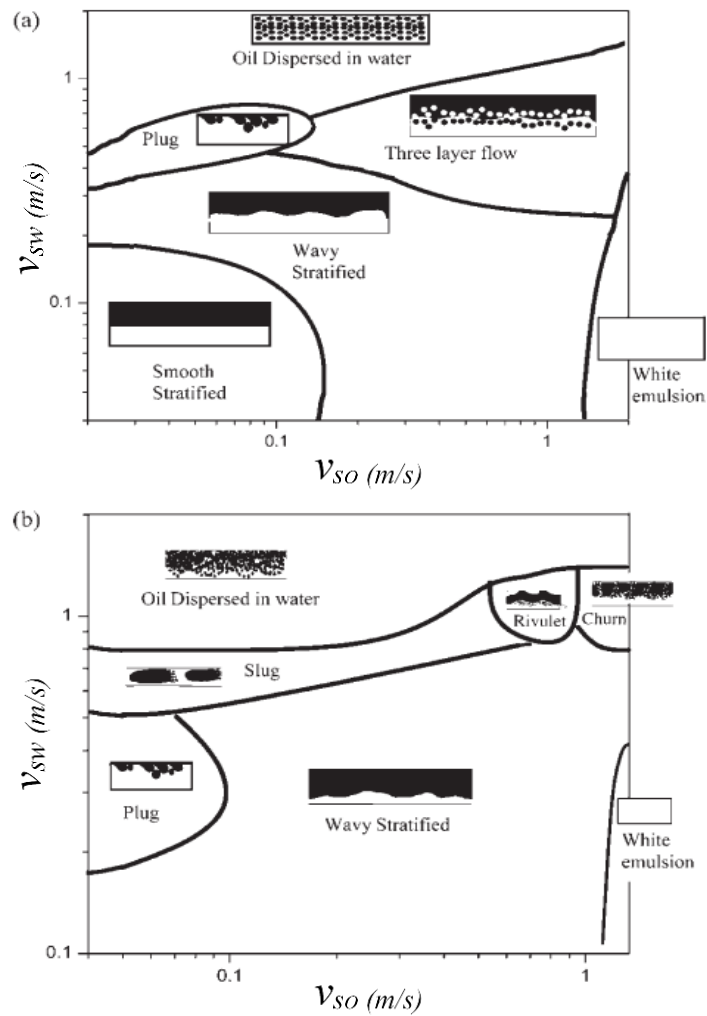


Figure 2-30: Experimental results of kerosene (oil)-water flow with a kerosene density and viscosity of  $787\text{kg/m}^3$  and  $1.2\text{mPa}\cdot\text{s}$ . The graphs represent the flow regime maps of two separate experimental studies of (a)  $0.0254\text{m}$  diameter pipe and (b)  $0.012\text{m}$  diameter pipe. Adapted from (Mandal, Chakrabarti and Das, 2007).

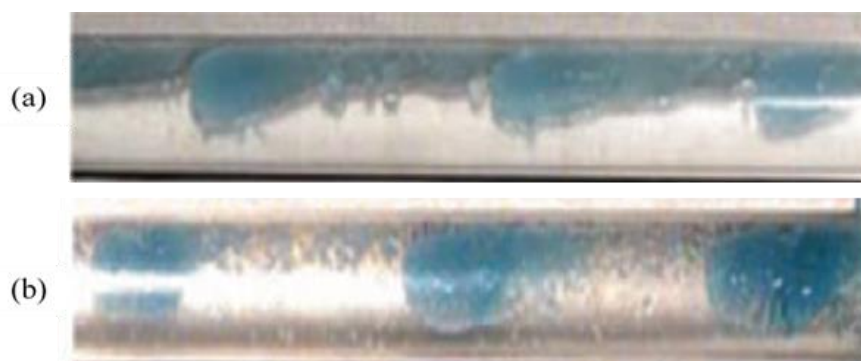
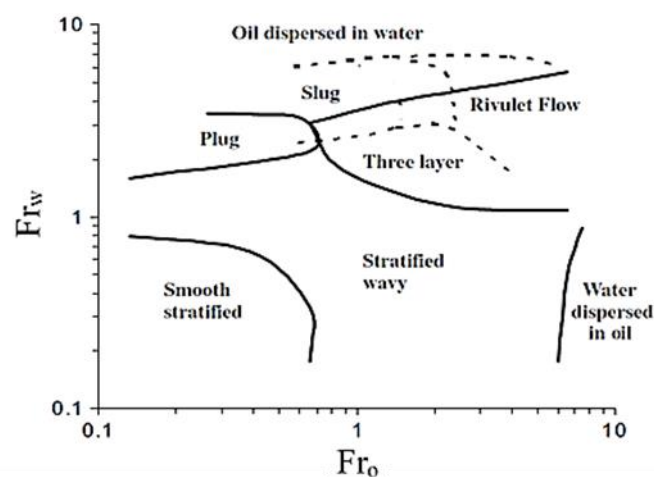


Figure 2-31: Photographic results of kerosene (oil)-water flow within a  $0.012\text{m}$  diameter pipe loop where (a) is the oil slug flow development and (b) are the oil plugs that are further spaced within a continuous water phase. Adapted from (Mandal, Chakrabarti and Das, 2007).

(9) (Mandal, Das and Das, 2010)

One of a very limited number of studies that mainly focuses on slug flow developments in liquid-liquid flow within pipes, Mandal, Das and Das (2010) investigated the developments of slug flow under numerous pipe orientations such as vertical, horizontal, and undulate (first inclined flow, then a sudden decline before levelling off again to horizontal) geometries. The authors noticed from previous literature that the range of slug flow and general intermittent characteristic developments are greater under narrow pipes, which are classified as pipes with internal diameters under  $0.0254m$ . Hence this experiment was conducted using a  $0.012m$  pipe loop and compared against a  $0.0254m$  pipeline, which shears the same rig. All horizontal and vertical pipes are made from PMMA,  $5m$  long, while the undulated (terrain-like) section was made from Perspex. Focusing on horizontal flow for this section of the present work, kerosene and water were selected as the experimental liquid-liquid phases.

Both visual operations and optical probe techniques were used to enhance the visual and photographic identification of flow regimes when under higher phase/mixture flowrates. In addition, visual observations are augmented by using visual laser signals. The study compared the scaling effect of internal pipe diameter changes by plotting the flow pattern maps to represent the Froude number of each corresponding phase which are functions of the respective phase superficial velocity, as shown in *Figure 2-32*. It was found that the narrow pipelines induce a greater range of slug flow under horizontal conditions as the interfacial are under more exposed conditions against the smaller pipe wall to transition between stable flow regimes to unstable intermittent flows. The study concluded that the information available for larger tubes cannot be extended to predict the flow distribution for smaller tubes where surface forces dominate.

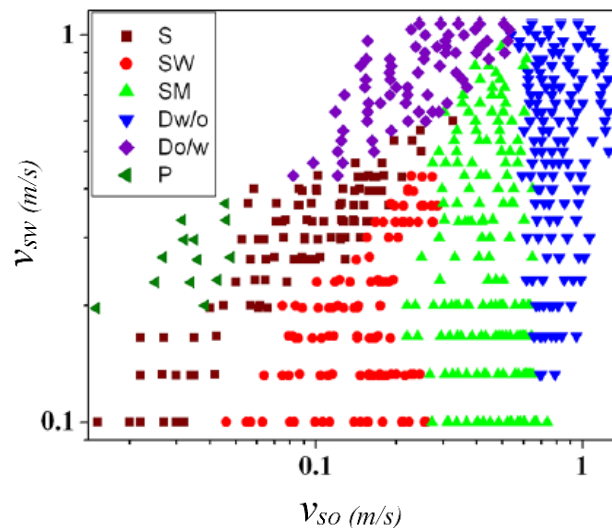


*Figure 2-32: experimental comparison of horizontal oil-water flow under  $0.012m$  and  $0.0254m$  internal diameter loops to observe slug flow behaviour. Adapted from (Mandal, Das and Das, 2010).*



(10) (Dasari et al., 2013)

Moderately viscous oil has been incorporated within an investigation to understand the hydrodynamic behaviour of oil-water multiphase flow within horizontal pipes of an internal diameter of  $0.0245m$  made from Perspex. The tested oil had a density of  $88kg/m^3$  and a viscosity of  $107mPa.s$  and was maintained under a constant temperature of  $25^\circ C$ . From this conventional horizontal oil-water experimental set-up, through the use of visual and photographic imaging techniques have observed the following flow regimes; plug/slug flow, stratified wavy flow, stratified mixed flow, dispersion of oil in water, and dispersion of water in oil flow while water was assumed at standard properties as shown in *Figure 2-33*. The superficial water velocity ranges between  $0.1 - 1.1m/s$ , and the superficial oil velocity ranges between  $0.015 - 1.25m/s$ .



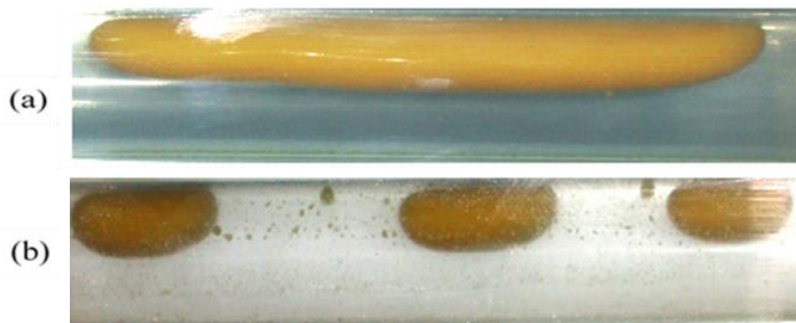
*Figure 2-33: Experimental results of oil-water horizontal flow under a  $0.0254m$  diameter Perspex pipeline with and  $\mu_o = 107mPa.s$  and  $\rho_o = 889kg/m^3$  as the velocity ranges between  $0.015-1.25m/s$ . Adapted from (Dasari et al., 2013).*

Slug flow was one of the flow regimes that were present in the experiment conducted in the respective study. Its presence is mainly dominated when both fluid phases of oil and water are under low velocities. The data indicated in *Figure 2-33* reveals the presence of slug flow begins at oil velocities of  $0.015m/s$  while the water velocity is initiated at  $0.6m/s$ . Slugs were seen to exist as far as oil velocity increasing to  $0.035m/s$  while corresponding to the change in water velocity up to  $0.6m/s$ . In addition to slug flow, further intermittent flow patterns were present under low flow conditions, such as plug flow. However, plug flow seems to present under more localised velocity conditions covering the small region of all flow regime developments. This is also evident from other studies in literature that have encountered plug flow. Slug flow behaviours change with the change of superficial velocity of each phase in accordance with the effects that

---

occur. When increasing both the oil and water superficial velocities to the same speed, the length of the slugs deteriorates.

As suggested from the data of Dasari et al. (2013) and similarly against previous studies, plug flow is found between superficial oil velocities from  $0.031 - 0.4\text{m/s}$  as the water velocity sustains plugs under superficial velocities of  $0.038 - 0.2\text{m/s}$ . When the phase velocity of oil is closer to that of water, usually by increasing the oil velocity, the water bridges that separate each oil slug/plug decrease in length, causing the slugs to further cluster against each other, eventually forming stratified wavy flow developments. This occurs after slug flow as the streamline becomes a further gravity-dominated system; hence, the flow configuration is further separated. The amplitude waves are suppressed at higher flowrates because the wave frequency between the two phases are more similar and hence are in almost harmonic states. This prevents the faster water phase from pushing the oil phase against the top of the pipeline to generate slugs or plugs. Photographic images of oil slugs and plugs observed in the experiment are seen in *Figure 2-34*.



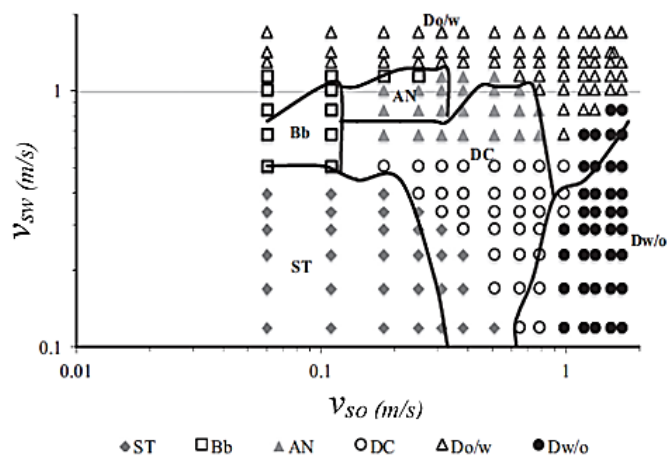
*Figure 2-34: Photographic results of oil-water flow within a 0.0254m diameter pipe loop where (a) is the elongated oil slug flow development and (b) is the oil plugs that are further spaced within a continuous water phase. Adapted from (Dasari et al., 2013).*

It should also be noted that core annular flow was not observed throughout the study, and the authors acknowledge this to be a consequence of the set-up of the experimental facility in terms of the coaxial arrangement relative to the direction of flow and the order at which fluids are implemented within the pipeline may have caused the absence of specific flow regimes in experimental work. In cases of intermittent flow behaviours, this is a critical aspect of experimental design as many other works from literature show inconsistent results against each other where intermittent behaviours are not reported; (Trallero, 1995; Lovick and Angeli, 2004; Sotgia, Tartarini and Stalio, 2008; Van Duin, Henkes and Ooms, 2018). Hence great care must be taken when implementing fluids within a test pipe in a specific order to generate the desired flow regime for further analysis.

(11) (Al-Wahaibi et al., 2014) via (Yusuf et al., 2012)

This paper investigated the behavioural changes of oil-water multiphase flow within an 8m long 0.019m diameter acrylic pipeline loop to better understand flow patterns and pressure gradients under an experimental study and compare the results under a 0.0254m pipe loop conducted by Yusuf et al. (2012) with the identical experimental set-up. The test fluids used were moderately viscous oil with a density of  $0.875\text{kg/m}^3$  and viscosity of  $12\text{mPa}\cdot\text{s}$  as water is standardised to its conventional properties. To reduce the effects of mixing, the fluids were implemented within the test pipe using a Y-junction directly  $45^\circ$  against the perpendicular of the flow line, where water (the heavier phase) was implemented at the bottom as oil (the lighter fluid) was introduced from the top section of the flow line. The experiments were conducted under superficial oil and water velocities that ranged from  $0.1 - 1.1\text{m/s}$  and  $0.1 - 1.1\text{m/s}$ , respectively, as the resulting flow regime map is shown in *Figure 2-35*.

In all experimental practices, it was strictly important to pre-wet the pipeline with oil before the two-phase mixture was initiated. In fact, many studies have shown that pre-wetting is a vital part of experimental set-up and design as this can affect the behaviour of a multiphase flow system and maintain consistent results. With regards to intermittent patterns, bubbly flow (plug/slug flow) was observed in both studies. This flow regime was found to be present in low superficial oil velocities of  $0.06 - 0.1\text{m/s}$  and moderately high water velocities of slightly above  $1.0\text{m/s}$ . However, the regime at which bubble flow exits slightly extends higher in terms of water velocity, and bubble lengths reduce when the diameter decreases, which is believed to be attributed to interfacial forces (Grassi, Strazza and Poesio, 2008).

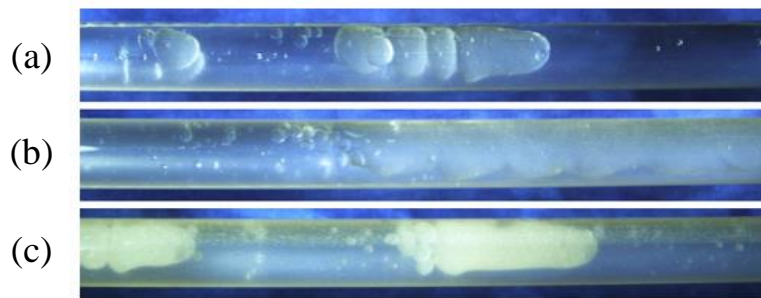


*Figure 2-35: Experimental results of oil-water horizontal flow under a 0.019m diameter Perspex pipeline with  $\mu_o = 107\text{mPa}\cdot\text{s}$  and  $\rho_o = 889\text{kg/m}^3$  represented from the symbols and compared with the same set-up from (Yusuf et al., 2012) using a 0.019m diameter pipeline, represented with black boundaries. Adapted from (Al-Wahaibi et al., 2014).*

---

(12) (Tan *et al.*, 2018)

One of the most recent studies used a 7.5m horizontal acrylic pipe loop with an internal diameter of 0.0146m conducted by (Tan *et al.*, 2018) with an experimental investigation on oil-water flow. This study aimed to identify the degree of effect each individual type of oil has on the behaviour of this specific two-phase flow system. The variables that are associated with the oil types are through their changes in density, viscosity and interfacial forces. Three different types of mineral oil were used as the testing fluid named as 20#, 200# and 400#, with viscosities varying from 20, 237 and 456mPa.s and density variations of 888, 869 and 896kg/m<sup>3</sup>, respectively. A high-speed camera system, pressure gradients and visual observations were used to conduct the analysis of the flow pattern presence under each experimental condition. Both water and oil phases were implemented within the test pipe using an individual T-junction for each fluid. However, before every new test condition is initiated, the pipeline is always flushed with water before introducing the multiphase simultaneously to remove pipe fouling to ensure viscous oils have been fully removed if adhered to the surface of the pipe. This precaution is performed to both maintain a clear visualisation of the internals of the pipeline and prevent fluid behaviour to change under surface alterations while maintaining controlled temperatures at 25°C. All intermittent flows were observed in the study, including plug, slug, and bubble flows, where superficial velocities were recorded between 0.1 – 2.4m/s between all three oil types. Photographs of all three intermittent flows seen within the experiment are shown in *Figure 2-36*.

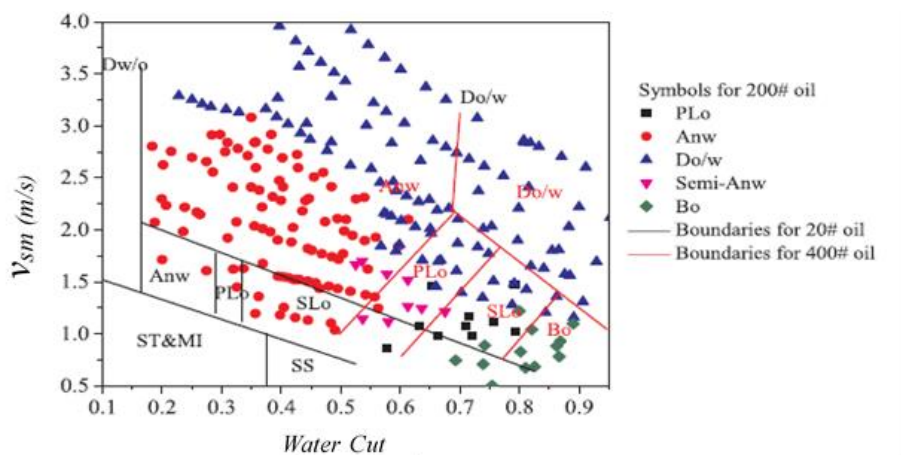


*Figure 2-36: Photographic experimental results of oil-water horizontal flow within a 0.0146m diameter acrylic where (a) is bubble flow, (b) slug flow and (c) plug flow. Adapted from (Tan *et al.*, 2018).*

At low viscous oil types, increasing the water velocity under stratified conditions that comprise of a high-density difference between the respective fluids allowing for a dominant gravity system, will lead to the oil-water interface to increase in wave amplitude until breakup is initiated within the upper oil layer which transitions into the intermittent flow. This occurs due to the inertia effects of the two fluids. By further increasing the water velocity, slug flow will develop due to

the balance of the water velocity being high enough to deteriorate the oil layer but not strong enough to maintain a continuous water film or layer within the top section of the pipeline. However, plug flow may occur when water inertia forces are great enough to sustain a water film on the top of the pipe. Otherwise, the plug can also be transitioned when oil flowrates are too low to counter the higher water flowrates to preserve the oil layer. Moderately high oils at low flowrates show similar behaviours to that of low viscous oils. Increasing the superficial velocity of both oil and water phases between  $0.1 - 2.28\text{m/s}$  and  $0.1 - 1.0\text{m/s}$ , respectively, will increase the stratified interface wave amplitude resulting from the peaks of the water phase in blocking the oil flow at the top of the pipeline resulting in intermittent flow patterns.

The shape and size of the individual intermittent oil patterns are found to be controlled by the oil flowrate, where high to low oil velocities will progressively narrow the slug/plug sizing causing more of a spherical formation and leading to bubble flow through the intermittent distribution. Finally, oils with higher viscosities show to generate bubble flow with the presence of high contrast between oil and water phase velocity due to the dominance of interfacial tensions instead of gravitational influences. As the velocity of oil increases, the bubble formation elongates to form plug flow and further increasing this phase velocity induces the plug tail coalesces to develop slug flow distributions. During these intermittent conditions, the increase in water velocity will cause a disturbance to the uniform distribution at the oil-water interface, which causes the mixing of multiphase droplets at the boundary between the two phases. In addition, increased oil viscosity causes the intermittent boundaries to be greater in terms of the total superficial velocity of the mixture against the water content range. A graphical comparison of viscous effects can be shown in *Figure 2-37*.



*Figure 2-37: Comparative experimental results of oil-water horizontal flow within a 0.0146m diameter acrylic pipeline on the effects of oil viscosity between (20#)  $\mu_o = 20\text{mPa.s}$  (200#)  $\mu_o = 237\text{mPa.s}$  and (400#)  $\mu_o = 456\text{mPa.s}$ . Adapted from (Tan et al., 2018).*

---

## 2.8.2 Summary of Horizontal Liquid-Liquid Intermittent Flows

After a brief review of the previously stated studies that incorporated a range of intermittent flow behaviours, which are categorised as elongated slug flow, plug flow and bubble flow under purely horizontal conditions, the following can be stated about oil-water two-phase flow developments of intermittent (slug) behaviours:

- Slug flow developments are normally attributed to the change of individual phase velocities of oil and water. Intermittent patterns are normally found under conditions of low oil velocity and moderate to high water velocity.
- The physical attribution of intermittent flow developments is stemmed from the interface transition behaviour between the two fluid phases before the breakup. The transition of intermittent flow has been typically attributed from stratified wavy conditions to be the easiest form of development, particularly for plug and slug flow. During an increasing water velocity surge, wave amplitudes escalate towards the top of the pipe segment. Until the water phases begin to come in contact with the upper section of the pipeline, the peaks of the water phase will cause a blockage for the upper oil streamline to flow and hence cause deteriorations within the oil layer to progress intermittent flow regimes.
- Intermittent flow regime developments are found more frequently under narrow pipelines. This concordance may be attributed due to the shorter distance between the top segment of the inner pipe walls and the interface between the two fluid phases. Hence, it would require less amount of water velocity surge for the water amplitude to ascend to the top of the pipeline, which will initiate slug flow.
- The shape and size of the individual intermittent oil patterns are found to be controlled by the oil flowrate. Where high to low oil velocities will progressively narrow the slug/plug sizing causing more of a spherical formation leading to bubble flow through the intermittent distribution.
- Oil phases with higher viscosities demonstrate a wider range of variable alterations to generate bubble flow. This occurs under the presence of a high contrast between the oil and water phase velocities due to the dominance of interfacial tensions instead of gravitational influences. As the velocity of oil further increases, the bubble formation slightly elongates to form plug flow and further increasing the oil phase velocity prompts the plug tail coalesces to develop into slug flow distributions.

- 
- Comparisons of pipe materials shows that flow regimes are also affected by this pipe design variable as the range of a variety of flow regimes in the steel pipes is smaller than that in the acrylic or Perspex pipes.
  - The condition of the internal pipe wall of the flow line also affects the range at which intermittent flow is present. When pipes are under hydrophobic or hydrophilic conditions from acid or non-acid cleaning, the wall wetting conditions differ and flow regime fluctuations occur. Pipes under hydrophobic conditions maintain core annular flow patterns by preserving the water films, whereas hydrophilic pipes induce the breakup of the annulus to form a continuous water phase while the dispersed oil core flows in the form of slugs, dispersions or a stratified layer. In contrast, when the breakup is characterised by increases in oil to water flowrates, the oil becomes the continuous phase, and the water takes the form of slugs or as a dispersion, regardless of the internal pipe wall conditions.
  - Mixer initiation design, downstream of both fluid inlets of the test pipe during the distribution of the two liquids also plays a crucial role in flow behaviour. It was found that this phenomenon can also change the results of the flow regime map by only altering the order in which each individual fluid is introduced within the pipe test section.
  - Plug and bubble flow regimes generally develop more localised regions compared to slug flow which can develop a wider range of oil velocity configurations with water. This is because of plug/bubble sensitivity behaviour across a small region.
  - Enhancements of turbulent flows from the increase of the water velocity will cause further instabilities within the flow line and hence the probabilistic mechanism of slugs to develop through the interface waves to come to contact with the upper pipe segment and consequently break the oil layer into sections of slugs or elongated bubbles. This may be because the polymer solution causes a damping effect on the wave amplitudes of the interface as the turbulent flows are suppressed, which hinders the ability of the water phase to break up the oil layer. Slug lengths are also affected by polymer additives.

These statements will serve as guidelines to better understand the behaviour of intermittent flow regimes, particularly for slug flow to produce slug flow within the experimental investigation of this present work. A comparison of all previous studies is shown in *Table 2-3*.

### 2.8.3 Liquid-liquid Slug Flow with Orientated Pipe Configuration

Even further limited amounts of experimental studies incorporate both intermittent flow conditions while attempting to understand the hydrodynamic mechanisms of pipeline inclination effects on oil-water flow regimes. For the purpose of comparison of previous work with the present study, slightly-deviated pipeline inclinations will be considered to be no more than  $\pm 5^\circ$  from the horizontal.

(1) (Lum, Al-Wahaibi and Angeli, 2006)

The effects of pipe inclinations were observed at  $\pm 5^\circ$  and  $+10^\circ$  under a  $0.038m$  internal diameter steel test pipe which incorporated mixture velocities between  $0.7 - 2.5m/s$  while using water phase fractions between  $0.1$  and  $0.9$ . The test oil had a density and viscosity of  $828kg/m^3$  and  $5.5mPa.s$ , respectively. Plug flow was the only intermittent flow that was observed throughout the experiment. However, compelling evidence has shown that increasing the pipe inclination from a downward to an inclined slop will induce a greater presence of slug flow. As no plug flow was observed at  $-5^\circ$ , increasing the inclination from  $0^\circ$ ,  $+5^\circ$  and  $+10^\circ$  saw a greater likelihood of an intermittent condition developing within the flow line.

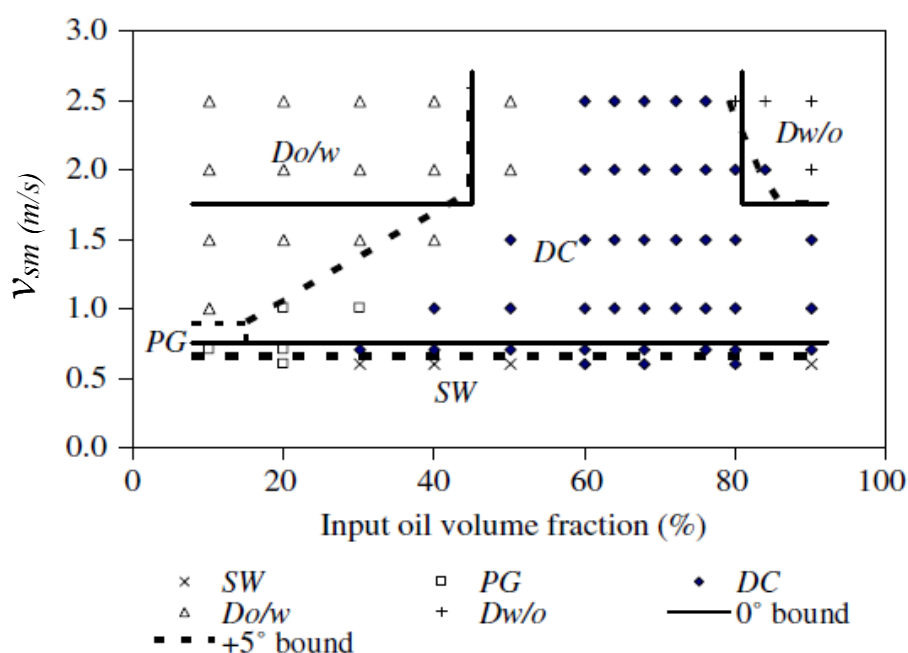


Figure 2-38: Comparative experimental results of oil-water horizontal flow ( $0^\circ$ ) and a  $+5^\circ$  inclination within a  $0.038m$  diameter steel pipeline with oil viscosity and density of  $\mu_o = 5.5mPa.s$  and  $\rho_o = 828kg/m^3$ . Adapted from (Lum, Al-Wahaibi and Angeli, 2006).



---

(2) (Hanafizadeh, Hojati and Karimi, 2015)

In the work conducted by Hanafizadeh, Hojati and Karimi (2015), flow patterns and representative transition boundaries were extensively investigated under alterations of pipeline inclinations between a range of  $\pm 45^\circ$  altering between each experimental extreme with increments of  $5^\circ$ . The experiment was conducted using an acrylic glass pipeline with an internal diameter of  $0.020m$  and  $6m$  in length. A high-speed camera was implemented within the experimental set-up for a visual aid of the flow regimes and further external review after image capturing to categorise the respective patterns better. Superficial velocities for the oil phase varied from  $0.085 - 0.65m/s$ , while the superficial water velocity was altered between  $0.16 - 1.0m/s$ . The oil density and viscosity used through the experimental investigation of a medium oil were  $840kg/m^3$  and  $4.5mPa.s$ , respectively. Numerous flow patterns were observed by the author of this study, such as bubble (plug), slug, smooth stratified, wavy stratified, churn, annular and dual continuous flow. In particular, the intermittent categories of bubble and slug flows were seen to be the most dominant non-stratified flow conditions during upward inclinations. However, stratified flows were seen to be the most dominant overall flow regimes when the direction of flow was ascending in downward inclinations pipes.

For the purpose of future comparison with slightly deviated pipe inclinations, this paper will only focus on the analysis of both the  $\pm 5^\circ$  results and how intermittent behaviours are associated with pipe orientations. The reason why slightly inclined pipes are considered to be between  $\pm 5^\circ$  from the horizontal in this work is due to maximizing the effect of inclination toward the respective multiphase flow system. Hence, the effects of inclination can be better analysed by overshadowing potential uncertainties when repeating experiments. Depicted in *Figure 2-39(a)*, this flow regime map demonstrates the effects of increasing the inclination of a pipeline by  $+5^\circ$ . It is superimposed with the data of the horizontal ( $0^\circ$ ) reference data conducted on the same rig.

The transition boundaries between the two intermittent flow conditions of slug and bubble flow have slightly expanded towards the right-hand side of the flow regime map. This implied that slug flow could occur at higher superficial oil velocities while also resulting in the transition of the annular flow to develop under a slightly smaller region of presence. The minute occurrence of transition fluctuation between the three flow regimes with respect to the superficial oil velocity is due to the gravitational (and buoyancy) forces that act against the direction of flow, requiring a higher phase velocity to overcome the inclination angle. This is particularly for the case of the oil phase, as this is the lighter phase above the heavier water. In contrast, as demonstrated in *Figure 2-39(b)*, downward inclinations of  $-5^\circ$  have the opposite effect on flow regimes when mapped. As the transition boundaries shift to the left-hand side of the mapping sequence,

indicating that the multiphase flow system required less flowrate input to overcome flow instability between two separate phases when under a downward inclination. In addition, the drive mechanism of the transition boundary shift is the gravitational effects between the stratified and non-stratified patterns because of gravity forces which act with the flow direction. Furthermore, for system stability, stratified flow is more likely to form under declined orientated flows while suppressing the region at which slug flow exists when comparing the two oppositely orientated conditioned results.

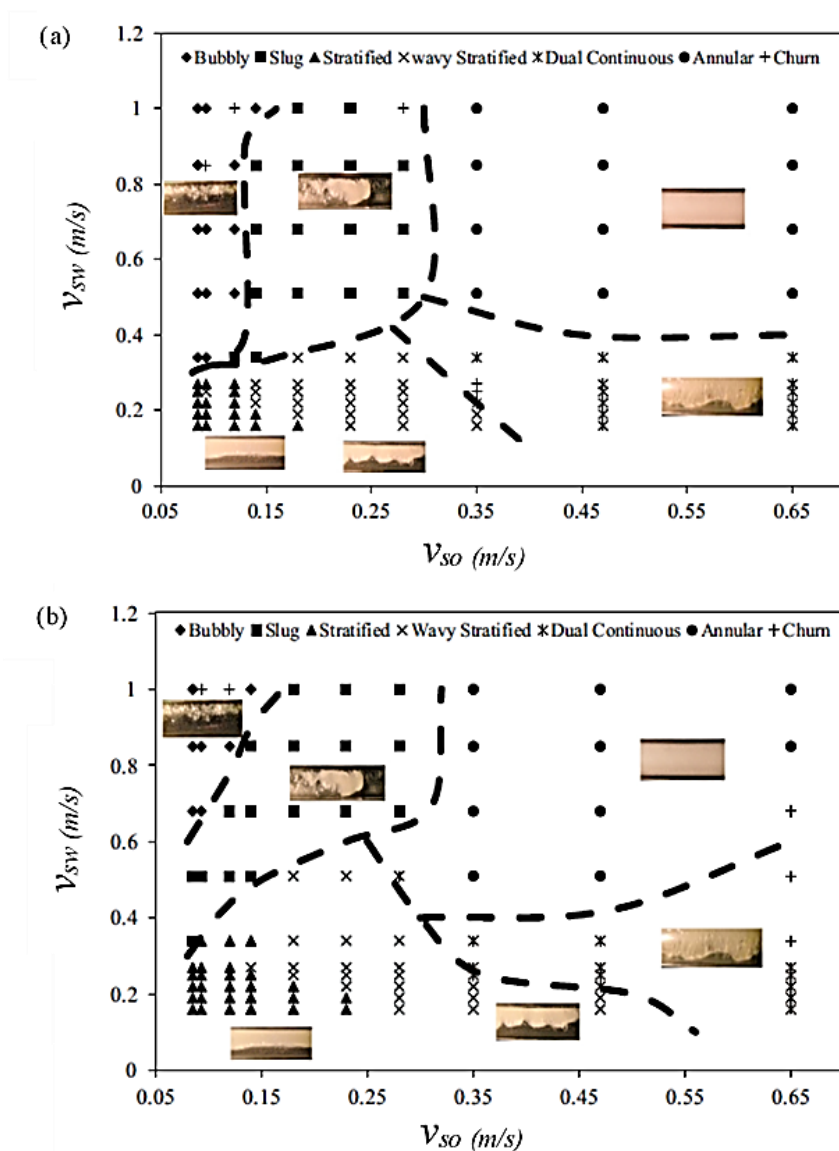


Figure 2-39: Experimental results of oil-water flow under (a) +5° inclination and (b) -5° decline within a 0.020m diameter acrylic glass pipeline with oil viscosity and density of and  $\mu_o = 4.5\text{mPa}\cdot\text{s}$  and  $\rho_o = 840\text{kg}/\text{m}^3$ . Adapted from (Hanafizadeh, Hojati and Karimi, 2015).

---

## 2.8.4 Summary of Orientated Liquid-Liquid Intermittent Flows

There is an infrequency in previous experimental studies throughout literature that have investigated or found intermittent flow characteristics and effects of respective transition boundaries from liquid-liquid multiphase flow systems within pipes when subjected to various slightly deviated orientations from the horizontal. However, there have been consistencies with the limited dataset and reasons based on physical explanations derived from understanding intermittent flow behaviours under horizontal flows, which can also reveal why there is a limited number of slug flow regimes within literature when exploring slightly inclined experimental conditions. Many experimental studies that have conducted slightly angled pipeline orientations under oil-water flow conditions have used large diameter pipes. From the previous summary of horizontal flow behaviours discussed for intermittent patterns in section 2.8.2, these types of unstable flow regimes are more likely to occur when travelling through smaller pipe diameters. As the various apparatus used to orientate the pipeline into multiple angles can only incorporate larger pipelines for easier handling, viewing and fitting. Some well-established studies, such as Rodriguez and Oliemans (2006), Atmaca et al. (2009), and Rodriguez and Castro (2014), all have used internal pipe diameters that are at least  $0.050m$  or greater. This may indicate the reason as to why these studies did not observe any form of intermittent flow characteristics.

When pipelines are orientated upwards in the direction of flow, the transition boundary for intermittent flows such as slug flow expands and other categories of flow patterns develop at higher phase velocities to initiate, such as core annular flow, which is particularly most dependent on the oil phase. While on the contrary, for downward angled pipelines, this configuration suppresses all intermittent flow regimes and revitalises the transition boundary at much smaller oil and water phase velocities, allowing for stable flow regimes such as stratified flow to dominate. In essence, flows travelling upwards are more unstable than downward flows. This phenomenon occurs due to gravitational forces acting against the denser fluid (water), while the same forces act for the less dense fluid (oil) as both phases flow together in an inclined system and vice versa. Overcoming the slope to maintain a specific condition requires a greater input of phase velocity and vice versa for fluids travelling downwards. Similar to the summary from the horizontal cases, this will still serve as a guideline for better understanding and predicting the behaviour of intermittent flow regimes. This will serve as a reference to produce intermittent flows, particularly slug flow, within the experimental investigation of this present work. The two explored works in this section are also presented with all previous horizontal studies in *Table 2-3*.

<i>Author(s)</i>	<i>Pipe ID Pipe Length (m)</i>	$\theta$ (°)	<i>Pipe Material</i>	$v_m$ (m/s)	$\frac{\mu_o}{\mu_w}$	$\frac{\rho_o}{\rho_w}$	$\sigma$ (mN/m)	<i>Intermittent Flow Regimes Observed</i>
<b>Charles et al. (1961)</b>	0.0254 7.315	0	Cellulose Acetate-Butyrate	0.05-2.09	6.29, 16.80, 65.00	1.00, 1.00, 1.00	44.0, 45.0, 30.0	Oil bubbles, Oil slugs
<b>Hasson et al. (1970)</b>	0.0126 2.700	0	Glass	-	1.20	1.02	17.0-17.5	Water slugs, Oil slugs
<b>Guzhov et al. (1973)</b>	0.0394 -	0	Steel	0.00-3.00	21.80	0.90	44.8	Water slugs, Oil slugs
<b>Oglesby (1979)</b>	0.0410 -	0	Steel	$v_{sw} = 0.03-3.19$ $v_{so} = 0.07-2.71$	32.00, 61.00, 167.00	0.86, 0.86, 0.87	30.1, 29.4, 35.4	Water slugs, Oil slugs
<b>Arirachakaran et al. (1989)</b>	0.0381, 0.0410 12.8	0	Steel	0.46-3.66	0.23, 0.019, 0.013, 0.0092	0.84	29.0-31.0	Water slugs, Oil slugs
<b>Raj et al. (2005)</b>	0.0254 2.13	0	PMMA	$v_{sw} = 0.03-1.10$ $v_{so} = 0.03-1.6$	1.43	0.79	45.0	Oil Plugs
<b>Al-Wahaibi et al. (2007)</b>	0.0140 3.5	0	Acrylic	$v_{sw} = 0.10-1.00$ $v_{so} = 0.09-0.50$	5.50	0.83	39.6	Oil Plugs, Oil Slugs
<b>Mandal et al. (2007)</b>	0.0120, 0.0254 5.00	0	PMMA	$v_{sw} = 0.20-1.10$ $v_{so} = 0.06-1.10$	1.20	0.79	31.5	Oil Plugs, Oil Slugs
<b>Mandal et al. (2010)</b>	0.0120, 0.0254 5.00	0	PMMA	$v_{sw} = 0.04-0.80$ $v_{so} = 0.02-0.93$	1.20	0.79	31.5	Oil Plugs, Oil Slugs
<b>Desari et al. (2013)</b>	0.0254 -	0	Perspex	$v_{sw} = 0.01-1.10$ $v_{so} = 0.02-1.25$	107.00	0.89	24.0	Oil Plugs, Oil Slugs
<b>Al-Wahaibi et al. (2014)</b>	0.0190, 0.0254 8.00	0	Acrylic	$v_{sw} = 0.10-2.25$ $v_{so} = 0.06-1.25$	12.00	0.88	21.0	Oil Bubbles
<b>Tan et al. (2018)</b>	0.0146 7.50	0	Acrylic	$v_{sw} = 0.10-2.40$ $v_{so} = 0.10-2.25$	20.00, 237.00, 456.00	0.89, 0.87, 0.9	19.0, 45.8, 51.5	Oil Bubbles, Oil Plugs, Oil Slugs
<b>Lum et al. (2006)</b>	0.0380 7.00	-5, 0, +5, +10	Steel	0.70 – 2.50	6.10	0.83	40	Oil Plugs
<b>Hanafizadeh et al. (2015)</b>	0.0200 6.00	-45 - +45	Acrylic	$v_{sw} = 0.10-0.65$ $v_{so} = 0.16-1.00$	4.50	0.84	-	Oil Bubbles, Oil Slugs

Table 2-3: Comparison of set-up configurations of previous experimental studies that have observed intermittent flow regimes which are categorised as bubble, plug and slug flow regimes while under either horizontal or slightly deviated pipeline configurations.

# CHAPTER 3

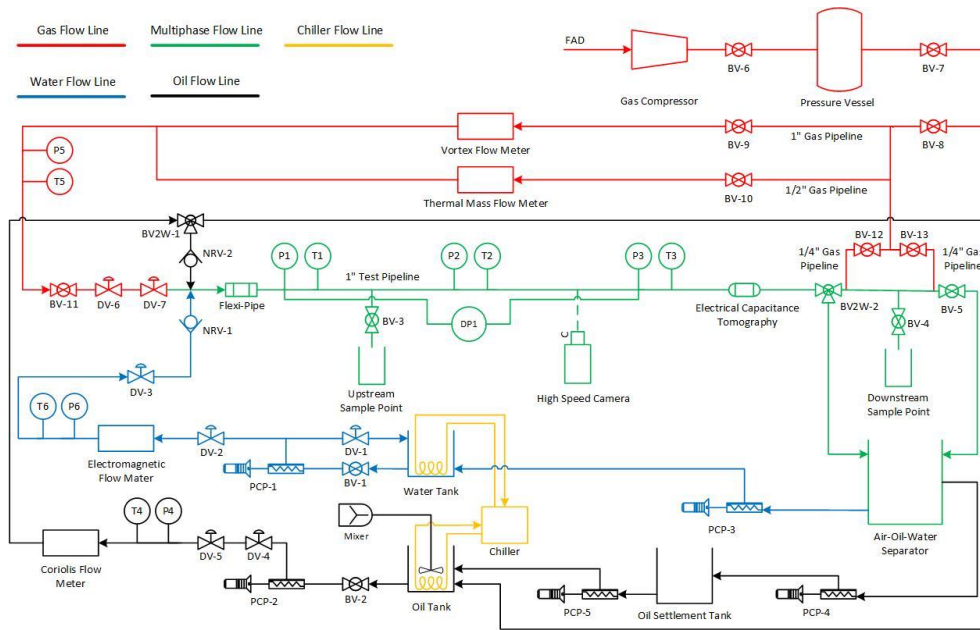
## METHODOLOGY AND EXPERIMENTAL SET-UP

The developed experimental set-up and procedure aim to produce experimental data suitable for conditions that induce oil-water intermittent flow regimes. Furthermore, the assessment of these flow regimes will be determined through changes in experimental parameters such as pipe inclination and individual phase velocity, along with changes in the relevant oil properties such as density and viscosity. All experiments from this study were conducted within the Process Systems and Engineering (PSE) lab of Cranfield University. Where the 1-inch (0.0254m) internal diameter multiphase flow rig was used to conduct numerous experiments to study the developments of liquid-liquid slug flow in horizontal and slightly-inclined pipes. This section will present the set-up of the experiments conducted and the corresponding operational procedures and methodologies, providing insight into correctly using and maintaining this unique facility while complying with global best practices.

### **3.1 Experimental Set-Up for 1-Inch Pipe Loop**

The 1-inch multiphase flow test facility operates under various multiphase flow combinations: air-oil, air-water, oil-water and air-oil-water. The facility consists of a slightly inclinable test section with angles ranging from  $0^\circ$  to  $5^\circ$  through the use of screwed struts that suspend the entire test section and are hinged from a stainless steel flexi-pipe found between the inlet and test sections. The main test section of the 1-inch test facility is fabricated from two Perspex pipes of 1m and the other 2.5m in length. An observation section, measuring instruments and sample points are placed at a distance of at least 10 pipe diameters from the last injection point to ensure stability and full development of the relevant flow regime. Injection points are installed upstream of the

test section for air, oil and water. Positions of the injection points of each phase are interchangeable between inlets. In the case of this set-up, the gas is located on the far end upstream of the test section, while the oil and water are directly vertical between each other. The test facility also comprises of an observation section, a data acquisition system (DAS) and a separation system. A Piping and Instrumentation Diagram (P&ID) of the common set-up of the 1-inch flow loop can be found in *Figure 3-1*.



*Figure 3-1: P&ID schematic of multiphase flow test facility applicable for both 1-inch test loop containing a gas (air) section (red), oil section (black), water section (blue), multiphase section (green) and heating/chilling region (yellow).*

### 3.1.1 Oil System

For the 1-inch rig, oil is stored in a  $0.15\text{m}^3$  tank capacity manufactured from plastic material and insulated with fibres on the periphery. A variable speed progressive cavity pump (PCP) with a maximum capacity,  $0.72\text{m}^3/\text{h}$ , is used in pumping oil through an Endress+Hausser's Promass 83I DN 50 Coriolis flowmeter with a range of  $0 - 180\text{m}^3/\text{h}$ , is used in oil metering. The flowmeter has three outputs: mass flowrate, density and viscosity, with a measurement accuracy of 0.1%,  $0.5\text{g}/\text{m}^3$  and 0.5%, respectively. The HART output from the meter is  $4 - 20\text{mA}$  and is connected to a DAS for data gathering. A variable speed, directly driven, portable "C" clamp adjustable GP-18 mixer is stationed above the oil tank. It allows the chiller unit to operate more efficiently in maintaining or changing the temperature across the entire fluid as it stirs the fluid within its corresponding tank. The GP-18 mixer is ranged to effectively stir between  $0.1 - 0.5\text{m}^3$  of fluid with maximum viscosities ranging from  $250 - 500\text{mPa}\cdot\text{s}$ , respectively.

---

### 3.1.2 Water System

Water is stored in a  $0.15m^3$  tank capacity made from plastic material and insulated with fibres on the periphery within the 1-inch test facility. A variable speed PCP with a maximum capacity of  $2.18m^3/h$  and maximum discharge pressure of  $10barg$  is used to pump water into the 1-inch test loop. Water flow is metered using an electromagnetic meter manufactured by Endress+Hauser Promag 50P50 D50, with a range of  $0 - 2.18m^3/hr$ . A  $4 - 20mA$  HART output is connected from the meter to the DAS.

### 3.1.3 Air System

A screw compressor manufactured by Anglian Compressors with set maximum discharge pressure of  $7.5barg$  and a maximum capacity of  $400m^3/h$  receives free air and compresses the fluid before supplying the air to the flow loop. To prevent any pulsating air supply to the test facility, the air from the compressor is discharged into a  $2.5m^3$  air tank before delivery to the test line, which is regulated to about  $7barg$ . To ensure that supplied air is moisture and debris free for easy and accurate metering, dryer and filters are installed in the compressor supply lines. Located near the test section, there are two gas flowmeters, a  $0.0127m$  diameter thermal mass flowmeter ranging between  $0 - 2m^3/h$  and a  $0.0254m$  diameter vortex flowmeter ranging from  $3 - 100m^3/h$ . Both gas flow meters are manufactured by Endress+Hauser and are used for air metering. Air is injected into the mainline via a  $0.0254m$  diameter flexible steel hose at  $0^\circ$  fully horizontal to the test line, more than 80 pipe diameters from the observation sections.

### 3.1.4 Liquid Cooling and Heating

A liquid heating/cooling system is installed to control the temperature of oil and water. It is a refrigerated bath circulator produced by Thermal Fisher. Copper coils submerged in the oil and water tank are connected to the circulator by running cold or hot glycol in the coils at specific time intervals, the temperature (and hence viscosity) of oil and water in the tank can be controlled based on heat transfer. The circulator temperature ranges from  $0$  to  $50^\circ C$ , with an accuracy of  $\pm 0.01^\circ C$ .

### 3.1.5 Fluid Separation

A bulk flow of multiphase fluids are collected in a separator of  $0.5m^3$  capacity. The separator is a rectangular-shaped tank with viewing windows to allow for liquid levels and separation process monitoring and an internal partition having a weir for overflow. After the separation of the phases

in the separator, oil and water are pumped back into the initial storage tank for reuse. The oil return pump is adjustable in inlet height to compensate for any oil-water interface height changes and to ensure full separation is achieved.

### 3.1.6 Multiphase Flow Test section and Inclination

The 1-inch test section is made up of three components: (1) polyvinyl chloride (PVC) inlet, (2) stainless steel flexi-pipe and (3) Perspex test view section. The inclination must be conducted by a trained technician and/or a contractor by adjusting the screw heights that suspend the test section pipeline accordingly to obtain any desired angle of up to  $+5^\circ$  from the horizontal. The inclination must be initiated from the centre point of the flexi-pipe to sustain minimal stress to the other parts of the fragile connecting pipework. The entire structure is  $5m$  long, with the main test section being  $3.5m$  long.

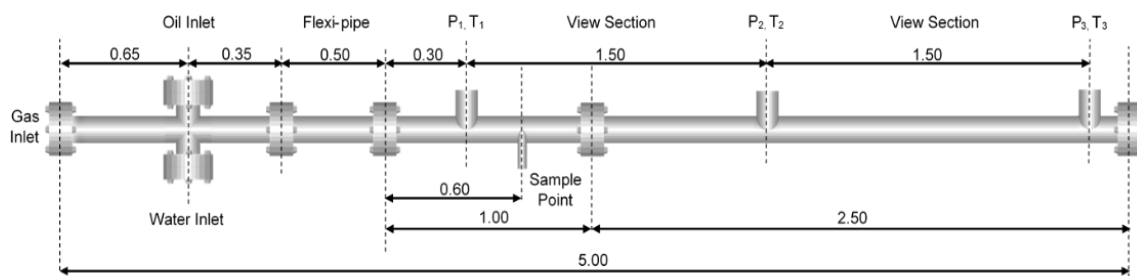


Figure 3-2: Schematic view of multiphase flow test section of the 1-inch air-oil-water rig with all dimensions. The ECT pipe sensor is located directly after the test section. (Not to scale).

### 3.1.7 Data Acquisition

Three separate single pressure transducers are found on the 1-inch test section of the rig, positioned at  $1.15m$ ,  $2.65m$  and  $4.15m$  from the water injection junction point. Two of the three pressure transducers used are WIKA pressure transmitter model S-11, with gauge pressure range  $0 - 6bar$ , overpressure limits of  $35bar$ , accuracy  $\leq \pm 0.25\%$  of span, and time response  $\leq 10ms$ . A further optional pressure sensor which can be used in this set-up is a differential pressure transducer, Honeywell STD120, with minimum pressure drop measurements of  $100Pa$  and an accuracy of  $\pm 0.05\%$ . The temperature of the test fluids on the test section is measured using J-type thermal couples with an accuracy of  $\pm 0.1^\circ C$  placed at different locations across the facility. Data acquired from the flowmeters, differential pressure transducer, pressure transducers and temperature sensors are saved to a Desktop Computer using a Labview® version 8.6.1 based system. The system consists of a National Instruments (NI) USB-6210 connector board interface that outputs signals from the instrumentation using BNC coaxial cables and the desktop computer.



---

One high-speed Sony DSCH9 camcorder, with 16 megapixels and a 60GB High Definition Display (HDD), is used for high-speed video recording and image capturing during the test to aid visual observations and analysis. In addition to imaging, behind the main test section is a white background that can be eliminated to maximise image clarity. A section for the measurement of in-situ liquid contents follows the pressure drop measurement & flow pattern observation section in the main multiphase flow line, which utilises the ITS M3000 Electrical Capacitance Tomography (ECT). The ECT set-up is separate from the entire DAS, as it requires the software Multi-Modality Tomography Configurator (MMTC) and Toolsuit to record and read the data, respectively.

### **3.2 Experimental Procedure and Runs**

After correct rig initiation (valves set-up, safety checks and ECT calibration) has been successful (see *Appendix A* for details); the following experimental procedures are conducted:

- i. There are two oil types used as the test fluid through the entire experimental process within the 1-inch rig. The first is EDM250 oil which is considered the light oil, and H100 oil which is considered to be the heavier oil. The initial tests ran EDM250 oil in the 1-inch rig under  $0^\circ$  from the horizontal inclination. All fluids are initially stored within their respective storage containers before any of the experiments begin or restart.
- ii. Oil and water temperatures are maintained at  $15^\circ\text{C}$  using the chiller/heater system. By starting the PCPs for water and oil, water is initially passed through the test section then the oil is later subjected to the test section with the water. The initial pumping speed is set based on the test section superficial velocity starting from  $0.1\text{m/s}$  for both fluids.
- iii. Begin recording the data for pressure, temperature, oil property parameters, individual phase flowrates/velocity, and high-speed video/image camera view of the test section for at least 60 seconds.
- iv. Conduct a hold-up test through the use of the ECT unit by recording at least 60 real-time seconds of the resulting flow regime using the MMTC software and later review the data in the Toolsuit software.
- v. The superficial water and oil velocities are altered in increments of  $0.05\text{m/s}$  between  $0.1 - 1\text{m/s}$  for water and  $0.1 - 0.5\text{m/s}$  (or as far as possible if not able to reach  $0.5\text{m/s}$ ) for oil. First, altering the superficial water velocity throughout the entire range while maintaining

a constant oil superficial velocity and incrementally increasing the oil superficial and repeating the altering process until both phases have undergone all possible combinations of individual superficial phase velocity to obtain the full mapping range between the oil and water phases. Repeating steps ii-iv for every increment to record all data.

- vi. Once the experiments are complete, the air system is used to flush any remaining fluids/droplets or debris.
- vii. Change the oil type of the system from EDM250 to H100 and repeat steps ii-vi.
- viii. After all the tests for both oils have been completed, incline the test section of the 1-inch rig to 5° from the horizontal and repeat steps i-vii.

The data is gathered and processed through three separate sources: (1) The DAQ system that contains the pressure, temperature and individual phase flowrates per second the data is recorded. (2) The high-speed camera is used to capture the high frame rate images of the flow regime and (3) the ECT data series is separately acquired per each experimental test run and utilises separate software to record and extrapolate data. All data is time-stamped accordingly in order to easily compare each data run from each of the three data sources to be further individually analysed and processed into flow regime maps. *Table 3-1* shows the key parameters and their respective range extremes that have been incorporated within all four of the experimental studies.

Parameter	Lower Limit	Upper Limit	Unit	Description
$v_{so}$	0.1	0.5	<i>m/s</i>	0.05 increments
$v_{sw}$	0.1	1	<i>m/s</i>	0.05 increments
$\mu_o$	7	421	<i>mPa.s</i>	Two oil types
$\mu_w$	998	998	<i>mPa.s</i>	Constant
$\rho_o$	811	878	<i>kg/m<sup>3</sup></i>	Two oil types
$\rho_w$	998	998	<i>kg/m</i>	Constant
$H_o$	0	1	-	Normalised
$H_w$	0	1	-	Normalised
$\theta$	0	+5	°	Two positions
$T$	15	15	°C	15 °C ± 0.1
$\Delta P$	0	1500	<i>Pa</i>	DP sensor

*Table 3-1: Key range of parameters that are incorporated across all four experiments. Uncertainties are not considered.*

---

### 3.3 Experimental Checks and Validity

A series of additional experiments were conducted before carrying out the main procedure of the multiphase flow analysis of the two rigs. The first was to check viscosity data to ensure the correct temperature and hence a consistent viscosity and density are maintained throughout each phase of the main experimentation. The second was signal and data calibrations from the pressure sensors and individual flowmeters of the water and oil to be implemented within the DAS for accurate results. Finally, testing the entire test facility in relation to the calibrated apparatus of flow metering and pressure analysis.

#### 3.3.1 Fluid Properties

Changes in oil viscosity through verifications in fluid temperature were measured using the Brookfield DV-I Prime viscometer set-up, as shown in *Figure 3-3*. To ensure the low viscosity ranges of the test fluids are able to be accurately measured, a closed tube system is used. A water jacket is mounted upon the viscometer, which contains both a large cylindrical spindle (YULA-15E) close to the sample chamber walls and immersed within 16ml of the test fluid. The large surface area of the spindle along with its close proximity to the sample chamber wall allows for accurate readings for low viscosity materials. A small submersible pump is placed within the bath to circulate the temperature-controlled water within the water jacket to reach a desired test oil temperature. The bath was initially filled with a combination of ice and water and maintained at 10°C followed by incrementally increasing the water temperature by half a degree within the bath until 30°C was reached. A digital thermometer probe placed within the test fluid was used to ensure the desired temperature was attained before data recording. *Figure 3-4(a)* and *Figure 3-4(b)* shows the viscosity and density data of the EDM250 oil respectively.

Both EDM250 and H100 test fluids were used in the exact same set-up and process for data collection of the viscosity data. *Figure 3-5(a)* and *Figure 3-5(b)* show the viscosity and density data of the H100 oil respectively. The EDM250 density data was gathered from previous work by using the same oil content as Esther (2014), which was conducted at Cranfield University and was predetermined using a dielectric method against changes in temperature. However, the H100 oil density analysis has not been previously conducted within the confinements of the PSE lab archives. Hence, it was assumed that as density has very small changes across a wide temperature variation, the temperature gradient of the EDM250 will be used as a baseline to predict the oil density. Combining the manufacturer data specifications of the H100 at 25°C with the EDM250 density gradient allowed to create a predictive density model against temperature variation. Additionally, EDM250 oil is colourless, which has similar transparency to water; therefore, a

specialised red dye caster was used to alter the colour of the EDM250 while having no effect on the water phase during multiphase flow testing. Additionally, the dye casting has no effect on the fluid properties such as density and viscosity because a very small amount of two grams (2g), which is the equivalent of half a small teaspoon, and was implemented for the entire  $0.15m^3$  (150l) EDM250 test oil. The H100 oil did not require dye casting because of its brown natural colouration.

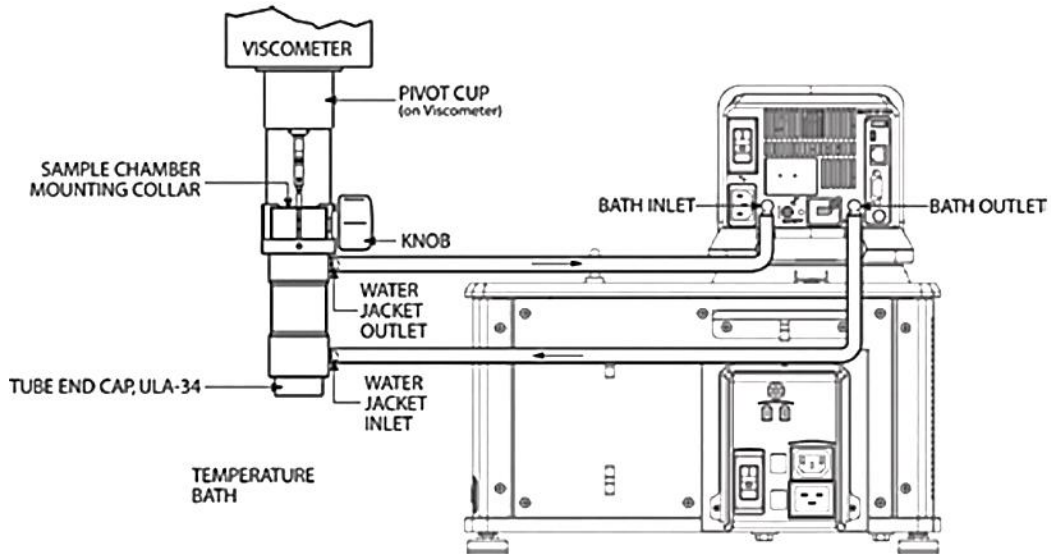


Figure 3-3: UL adapter set-up for the Brookfield DV-I Prime viscometer for viscosity ranging between 1 – 2000mPa.s between temperatures of 10°C – 40°C in increments of 0.5°C. Adapted from (Brookfield Engineering Laboratories Inc., 2020).

A total of three different test fluids were employed within this study, two oil phase types and standard tap water. The oil phases were chosen to characterise the changes in viscosity and density, EDM250 was utilised to represent the light oil phase and H100 as the heavier oil phase. Each oil phase is interchanged within the multiphase flow loop system to study the effects of fluid properties. The test fluid properties are presented in Table 3-2.

	Density ( $kg/m^3$ )	Viscosity ( $mPa.s$ )	Surface Tension ( $mN/m$ )
<b>EDM250</b>	811	7	28
<b>H100</b>	878	423	35
<b>WATER</b>	997	1	73.26

Table 3-2: Key experimental fluid properties of EDM250 oil, H100 oil and water at 15°C.

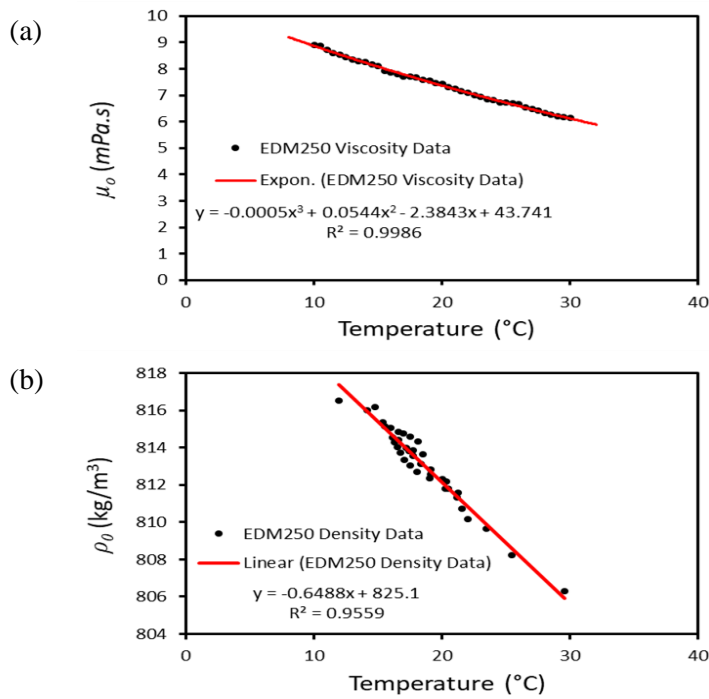


Figure 3-4: EDM250 oil data of changes in temperature against (a) viscosity gathered from the viscometer experiment and (b) density data gathered from a dielectric experiment. Density data utilised and adapted from Esther (2014).

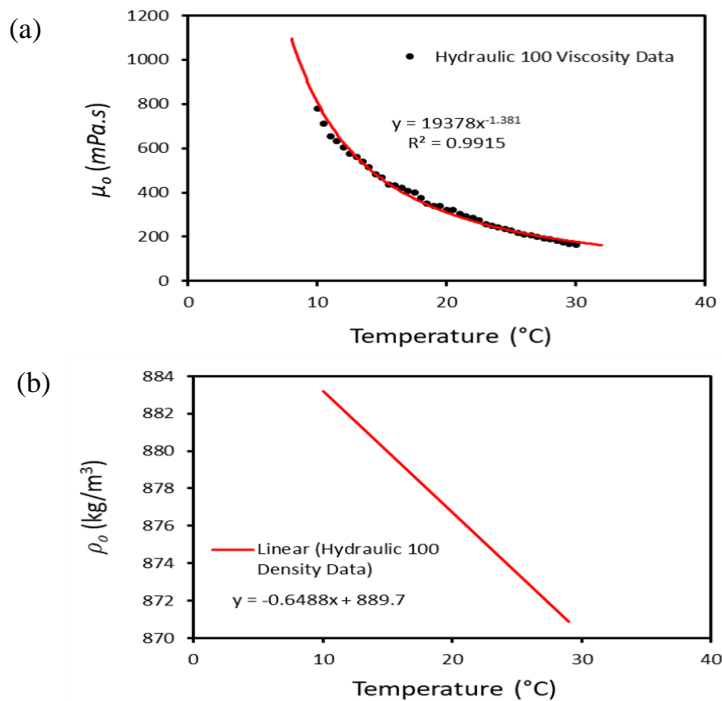


Figure 3-5: H100 oil data of changes in temperature against (a) viscosity, which was gained from the viscometer experiment and (b) density model, which was developed by combining the EDM250 data trend and H100 manufacturer density specifications at 25 $^{\circ}$ C.

---

### 3.3.2 Data Signals and Calibration

All apparatus that are connected to the DAS are represented by voltage output feeds to be converted into measurable data during experimentation, such as pressure signals and flowmeter outputs. Regular calibration is essential to ensure the data provided is maintained to be accurate and consistent. All pressure transducers and flowmeters were individually tested to ensure each measuring device was reading correctly and any linear offsets to be calibrated accordingly with relation to the DAS. The initial test was conducted for the oil and water flowmeter calibrations. To determine the off-set (if any) of each flowmeter, the rig separator was utilised as a fluid volume measuring set-up with precise volumes marked on the transparent walls of the separator in 20l increments with a total volume of 100l marked. Multiple test points of various flow speeds that ranged from the upper and lower pumping capacity limits of the rig with respect to the experiment were used to ensure a full range was analysed. To define the real flowrate, a stopwatch is used to determine the time it takes for the flow going into the separator to reach each set volume marked at 20l. To mitigate as much human error as possible, each passing of the 20l volume mark within the separator is time lapped until the maximum volume is reached, leaving a total of five time-laps averaged to a single time per 20l for each set flowrate.

The reading from both the flowmeter and DAS were also compared to see if specialist calibrations are needed for the flowmeter. A  $\pm 5\%$  error from the real flowrate is used to assess the readings provided by both the DAS and flowmeter, which can be found in *Appendix B*. The calibration for the water and oil flowmeters are shown in *Figure 3-6(a)* and *Figure 3-6(b)*, respectively, where both flowmeter errors were found within the  $\pm 5\%$  tolerance for only conducting offset adjustments on the DAS. The final calibration process was the pressure transducer offset, which in total are five, located across the experimental rig and that can be attached to the outer sections of the pipe test section, which are only indirectly linked to other equipment on the system. Each transducer was attached to a verified WIKA pressure sensor calibrator. The channels at which each individual pressure transducer was connected were set to receive voltage signals rather than the pressure unit measurement while attached to the calibrator. The high and low limits of each pressure sensor were calibrated from ascending to descending increments of 1barg. For the WIKA pressure transducers, the pressure was set from 0barg – 6barg, whereas the DRUCK had to be considered for atmospheric pressure as well while ascending and descending at the same range and increment. The main pressure transducer in the system is the DRUCK PMP 4170 differential pressure sensor which will identify the small pressure differences found between the test sections. This transducer is calibrated in a similar ascending and descending approach, but smaller pressure ranges were utilised from -160 –

200mbar as the voltage signal for the pressure extremes is the equivalent of 0 – 5 volts from negative to positive. The offset is then set within the rig DAS with an uncertainty of up to 5% for all pressure transducers. The example offset found for the calibration is shown in *Figure 3-7*; all other pressure transducer calibration offsets and data can be found in *Appendix C*.

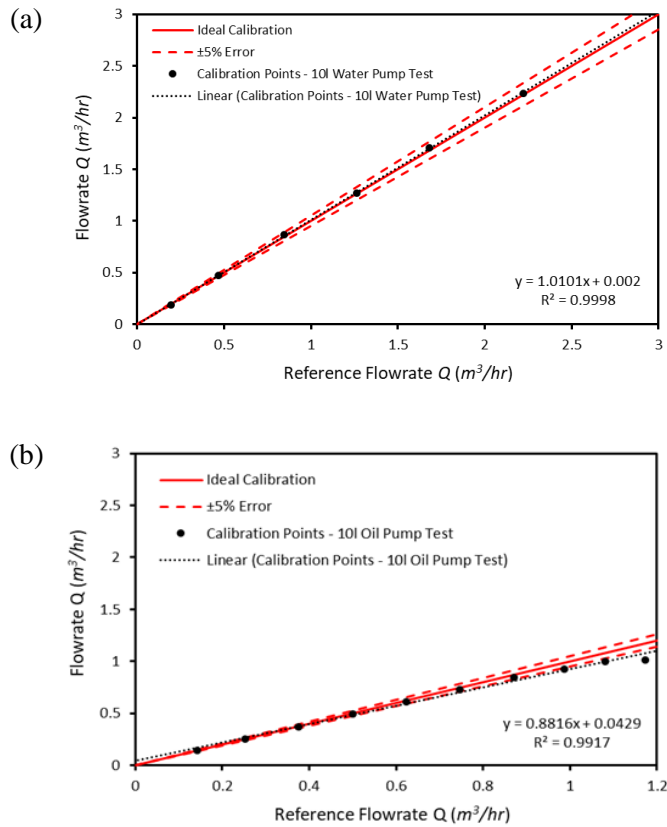


Figure 3-6: Flowmeter calibration check of (a) water electromagnetic flowmeter and (b) oil Coriolis flowmeter.

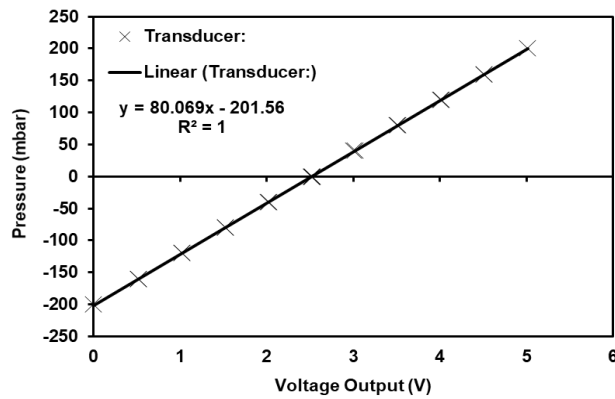


Figure 3-7: DP1 DRUCK PMP 4170 pressure calibration.

---

### 3.3.3 Single-Phase Flow Testing

To fully ensure the rig provides reliable and consistent data throughout the upper and lower setting limits, a rig experiment was conducted in relation to the newly calibrated set-up. A single-phase flow experimental pressure drop test was conducted based on water being looped around the rigs for recording the experimental friction factor in relation to the pressure sensors and flowmeters working correctly. The expression for the friction factor in a circular pipe can be expressed as:

$$f = \frac{2D\Delta P}{\rho_w v_a^2 \Delta L} \quad (3-1)$$

Derived from the conservation of mass and momentum, where  $\Delta L$  is the length between the pressure differential measurement taps,  $v_a$  is the average velocity defined as the volumetric flowrate over the cross-sectional area that the fluid travels through  $v_a = \dot{q}/A_p$  (Brill and Mukherjee, 1999).

$$\frac{1}{\sqrt{f}} = -2 \log \left\{ \frac{\epsilon}{3.7D} - \frac{5.02}{Re} \log \left[ \frac{\epsilon}{3.7D} - \frac{5.02}{Re} \log \left( \frac{\epsilon}{3.7D} + \frac{13}{Re} \right) \right] \right\} \quad (3-2)$$

Eq. (3-2) is the Zigrang and Sylvester (1982) friction factor correlation which applies to Newtonian fluids under a fully developed steady-state flow and is used to evaluate the experimental data. The reason why this particular correlation was selected is because it provides highly accurate friction factors under turbulent conditions ( $Re > 4000$ ). When exploring the upper limits of the rig, an accurate reflection of experimental data and the selected model would strongly indicate the rig is fit for experimental purpose. The surface roughness of the inner pipe  $\epsilon$ , made from Perspex, was deemed similar to that of acrylic and glass and was selected to be  $1.5 \times 10^{-6} m$ . *Figure 3-8* demonstrates the comparison between the experimental and friction factor and the Zigrang and Sylvester (1982) correlation which demonstrate a good agreement between the data Reynolds number and the respective friction model. Furthermore, Eq. (3-1) was used to compare the pressure gradient  $\Delta P/\Delta L$  developments from the experiment in comparison to the single-phase model, as shown in *Figure 3-9*, also demonstrating a near-perfect match against each other. Overall, the results suggest that the calibrations of the pressure transducers and flowmeters are acceptable to conduct the main experimental work of this study reliably.



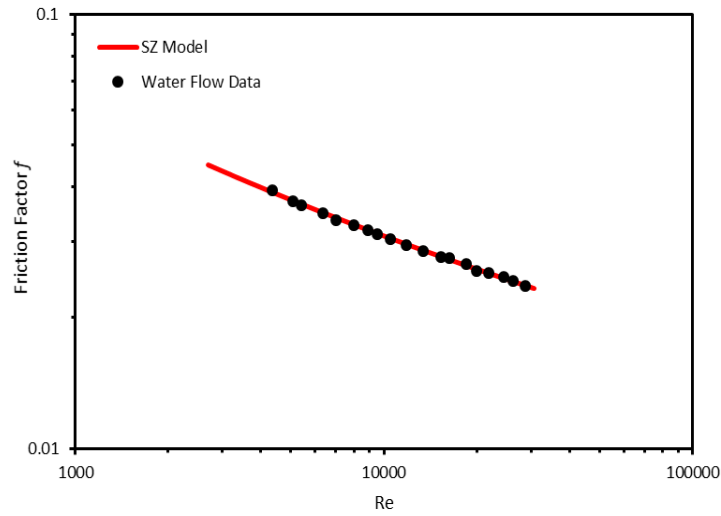


Figure 3-8: Friction Factor comparison of the horizontal single-phase flow of water in a 1-inch Perspex pipeline.

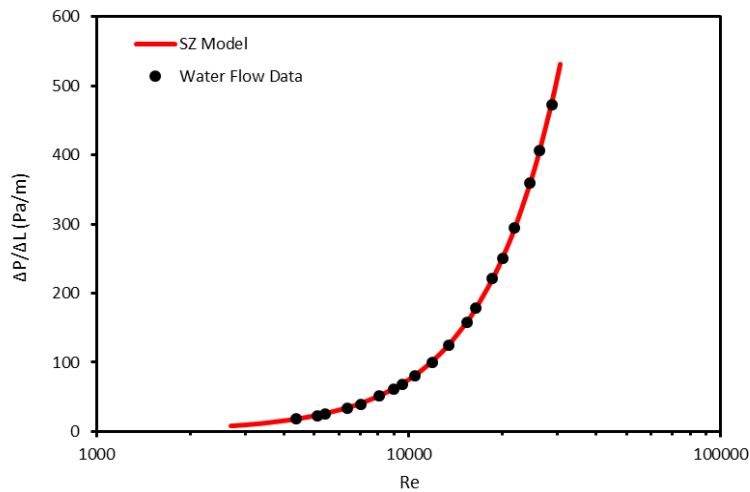


Figure 3-9: Pressure gradient comparison for the horizontal single-phase flow of water in a 1-inch Perspex pipeline.

### 3.3.4 Uncertainties

Uncertainty is a quantitative measurement of variability within a data series. Hence, uncertainty describes the idea that all variables of each data have a scale of expected values concerning the main measured value. Uncertainties play a key role in affecting the overall trend or final result of the data series due to a congregation of the multiple variables being combined to form a larger data offset. *Table 3-3* shows the key parameters and their respective maximum possible uncertainties that can impact the results of the experiment.

Parameter	Unit	Uncertainty Range
$v_{so}$	$m/s$	$\pm 0.02$
$v_{sw}$	$m/s$	$\pm 0.02$
$\mu_o$	$mPa.s$	$\pm 1$
$\mu_w$	$mPa.s$	$\pm 1$
$\rho_o$	$kg/m^3$	$\pm 1$
$\rho_w$	$kg/m$	$\pm 2$
$H_o$	-	$\pm 0.05$
$H_w$	-	$\pm 0.05$
$\theta$	$^\circ$	$\pm 0.1$
$T$	$^\circ C$	$\pm 0.1$
$\Delta P$	$Pa$	$\pm 10$

Table 3-3: Maximum uncertainty range of all key parameters from this study.

### 3.3.5 Flow Regime Identification

In general, the respective flow regime identification will be applied through visual interpretation based on the categories that best-fit level two flow regimes as previously explored in section 2.3. Identifying flow regimes across various combinations of experimental variables is both challenging and inconsistent due to the subjective nature of selecting the flow regime to be categorised, particularly near transition boundaries. Hence, a quantitative approach is also combined with visual interpretation, where the ECT data series will utilise the processed hold-up data series along with the time-stamped high-speed image recording to better categorise the flow regime such as intermittent flow. For example, smooth stratified flow is accepted when a clear waveless interfacial segregation is formed between the oil and water phases as the stratified wavey flow pattern is similar to that of smooth stratified flow with a wavey interface. However, the three-layered flow regime appears very similar to stratified wavey flow but the interface is much larger to the extent that a third layer between oil and water phases is developed. The ECT data is hence applied to tell the difference between pure oil, pure water and mixing layer through 2D imaging and data quantification through a probability density function (PDF) analysis of the hold-up of each run. PDF analysis is particularly important for this study as this will allow for better identification of intermittent flow regimes due to the continuous interchanging hold-up extremes which will typically demonstrate a bi-modal distribution attribute. This is further explored in the following chapter.

# CHAPTER 4

## EXPERIMENTAL RESULTS

### 4.1 *Flow Regime Mapping*

The resulting hydrodynamic flow regime maps of the superficial phase velocities of oil and water under a horizontal and 5° inclined test section, with the addition of both heavy and light oil tests are presented in *Figure 4-1* and *Figure 4-2* respectively. The following flow regimes that have been observed are smooth stratified flow (SS), stratified wavy flow (SW), plug flow (P), slug flow (SLo), three-layered flow (3L) and dispersed oil-in-water flow (DOW). Intermittent flow types were found across all experiments, where all light oil experiments developed plug flow and all heavy oil experiments developed slug flow. With the exception to smooth stratified flow, all non-intermittent flow regimes had similar neighbouring flow regimes transition boundaries between the relevant intermittent flow pattern for each experiment. Below the intermittent regions, stratified wavy flow is found, which is constituted by a lower superficial water velocity. Towards the right, an increase in the superficial oil velocity will result in a three-layered flow pattern to form. Finally, with a higher superficial water velocity, dispersed flow is developed. *Table 4-1* to *Table 4-4* demonstrates an example of each flow regime type around the intermittent flow regime envelope of each experiment type from the high-speed captured image. The results strongly suggest a consistent oil and water phase velocity combinations for intermittent flow envelopes to develop, which can be found within the regions of low superficial oil velocities ( $v_{so} > 0.3m/s$ ) and mid to high superficial water velocities ( $0.3 \ll v_{sw} \gg 0.8m/s$ ). Where oil-water multiphase flow with lighter oils has a better tendency to develop plug flow regimes whereas the heavier oil conditions favour slugging. This may be due to the change in density differential between the two systems, as lighter oils tend to remain suspended by the heavier water phase creating only partial plug formation, preventing the oil from engulfing the entire pipe diameter. In contrast, the heavier oil phases overcome these gravitational forces and can cover all or a majority of the pipe diameter.

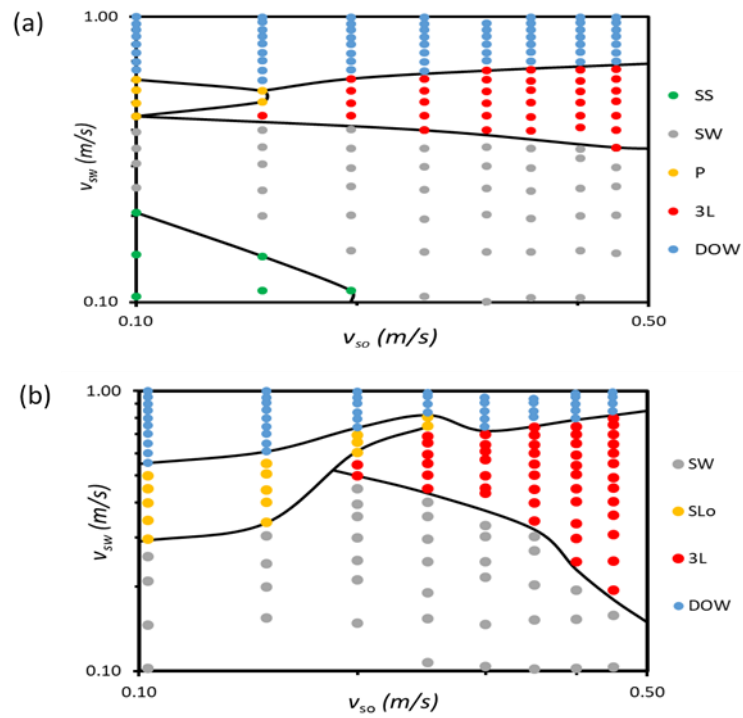


Figure 4-1: Superficial water velocity vs superficial water velocity flow regime map of (a) experiment with EDM250 oil at a pipe inclination of  $0^\circ$  from the horizontal and (b) experiment with H100 oil at a pipe inclination of  $0^\circ$  from the horizontal.

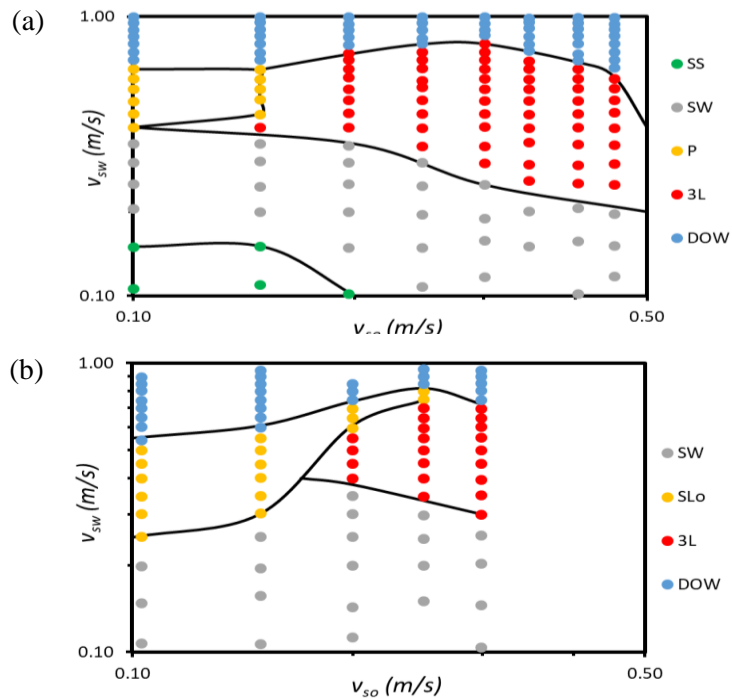


Figure 4-2: Superficial water velocity vs superficial water velocity flow regime map of (a) experiment with EDM250 oil at a pipe inclination of  $5^\circ$  from the horizontal and (b) experiment with H100 oil at a pipe inclination of  $5^\circ$  from the horizontal.




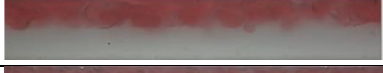

Flow Regime Type	Flow Conditions ( $m/s$ )	High-Speed Image Capture
Smooth Stratified (SS)	$v_{so} = 0.11$ $v_{sw} = 0.15$	
Stratified Wavy (SW)	$v_{so} = 0.10$ $v_{sw} = 0.39$	
Oil Plug (P)	$v_{so} = 0.10$ $v_{sw} = 0.45$	
Three-Layered (3L)	$v_{so} = 0.15$ $v_{sw} = 0.45$	
Dispersed (DOW)	$v_{so} = 0.10$ $v_{sw} = 0.65$	

Table 4-1: All flow regime type examples from the experiment with EDM250 (light oil) at a pipe inclination of  $0^\circ$  from the horizontal. Flow travelling from left to right.



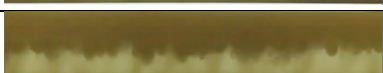
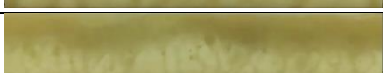
Flow Regime Type	Flow Conditions ( $m/s$ )	High-Speed Image Capture
Stratified Wavy (SW)	$v_{so} = 0.10$ $v_{sw} = 0.35$	
Oil Slug (SLo)	$v_{so} = 0.10$ $v_{sw} = 0.50$	
Three-Layered (3L)	$v_{so} = 0.25$ $v_{sw} = 0.50$	
Dispersed (DOW)	$v_{so} = 0.10$ $v_{sw} = 0.60$	

Table 4-2: All flow regime type examples from the experiment with H100 (heavy oil) at a pipe inclination of  $0^\circ$  from the horizontal. Flow travelling from left to right.






Flow Regime Type	Flow Conditions ( $m/s$ )	High-Speed Image Capture
Smooth Stratified (SS)	$v_{so} = 0.10$ $v_{sw} = 0.15$	
Stratified Wavy (SW)	$v_{so} = 0.10$ $v_{sw} = 0.35$	
Oil Plug (P)	$v_{so} = 0.10$ $v_{sw} = 0.40$	
Three-Layered (3L)	$v_{so} = 0.15$ $v_{sw} = 0.40$	
Dispersed (DOW)	$v_{so} = 0.10$ $v_{sw} = 0.70$	

Table 4-3: Flow regime examples from the experiment with EDM250 (light oil) at a pipe inclination of  $5^\circ$  from the horizontal. Flow travelling from left to right.





Flow Regime Type	Flow Conditions ( $m/s$ )	High-Speed Image Capture
Stratified Wavy (SW)	$v_{so} = 0.10$ $v_{sw} = 0.20$	
Oil Slug (SLo)	$v_{so} = 0.10$ $v_{sw} = 0.45$	
Three-Layered (3L)	$v_{so} = 0.25$ $v_{sw} = 0.50$	
Dispersed (DOW)	$v_{so} = 0.10$ $v_{sw} = 0.60$	

Table 4-4: All flow regime type examples from the experiment with H100 (heavy oil) at a pipe inclination of  $5^\circ$  from the horizontal. Flow travelling from left to right.

## 4.2 Hold-up Analysis

The ECT data is used to generate recorded hold-up data vs time, based on the sampling frame rate from the ECT. The sample rate for the ECT was between 5-7 frames per second and then applied to a PDF approach to assess the hold-up distribution and finalise the flow pattern grouping procedure. The physical meaning behind the hold-up data values is the average occupancy of the reference phase (water phase) at the pipe cross-sectional area. For example, a hold-up of 0.5 (50%), indicates that at a stable flow condition, an average of half the cross-sectional area contains the water phase. Examples of each flow regime from all four separate studies are presented between *Figure 4-3* and *Figure 4-6*. The analysis clearly shows that there is a distinct behaviour of phase hold-up distribution across different flow regimes. For example, stratified flows have a more localised distribution which typically have a greater PDF value. Whereas flow regimes, such as dispersed flow, are spread across a wider scope of the hold-up extremes but have a much smaller PDF value. Additionally, intermittent flow regimes have a very distinct characteristic with PDF formations since the interchanging phase shifts between oil and water continuously form a bi-modal distribution which consists of a dual peak formation that develops within the PDF.

The 2D image stacking generated from the ECT is also utilised to assess the regions where it is problematic to directly see from the high-speed imaging as only a single side of the pipeline is observed, and fluids may start to mix slightly, making it difficult to see the interacting flows, especially from the heavy oil conditions. Hence, when coupling the 2D stacked frames with individual cross-sections of the data, an almost 3D analysis of the flow regime can be better evaluated. *Table 4-5* to *Table 4-8* shows the resulting ECT imaging from each flow regime example from each of the four experiments. The top 2D ECT image represents the measured flow patterns from a side view, while the bottom image represents the flow as seen from a top view.

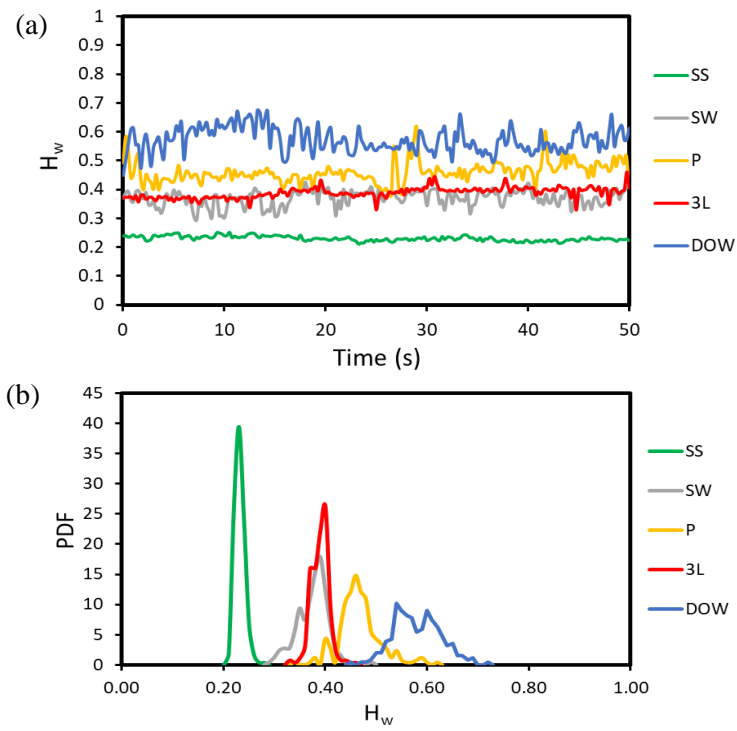


Figure 4-3: (a) Water hold-up fluctuation (b) corresponding PDF grouping of all flow regime type examples from the experiment with EDM250 oil at a pipe inclination of  $0^\circ$ .

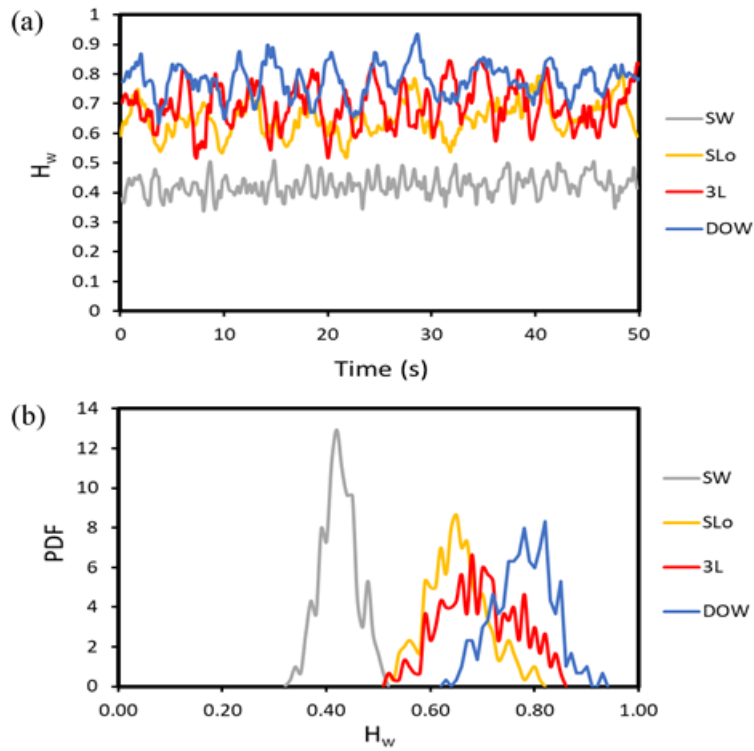


Figure 4-4: (a) Water hold-up fluctuation (b) corresponding PDF grouping of all flow regime type examples from the experiment with H100 oil at a pipe inclination of  $0^\circ$ .

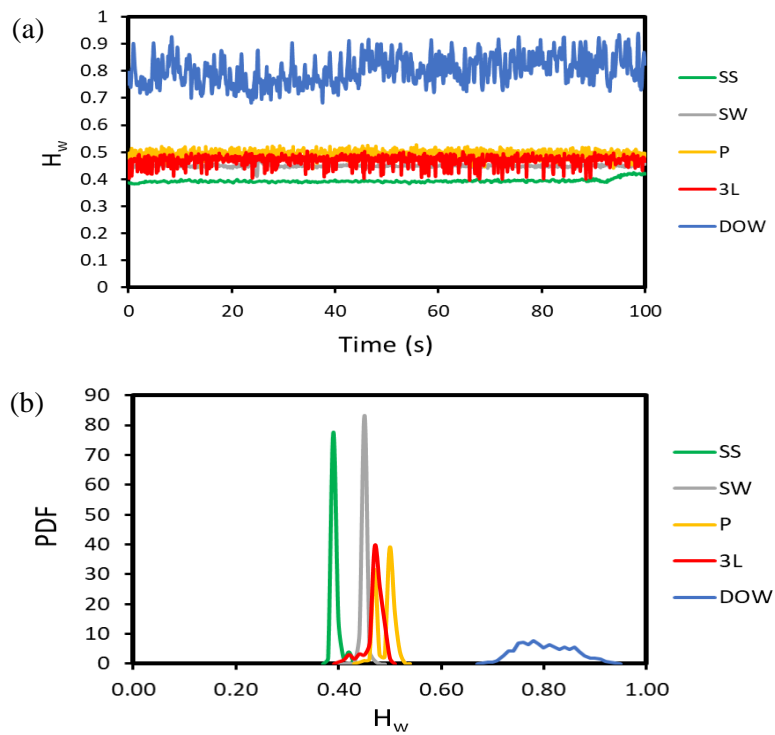


Figure 4-5: (a) Water hold-up fluctuation and (b) corresponding PDF grouping of all flow regime type examples from the experiment with EDM250 at a pipe inclination of  $0^\circ$ .

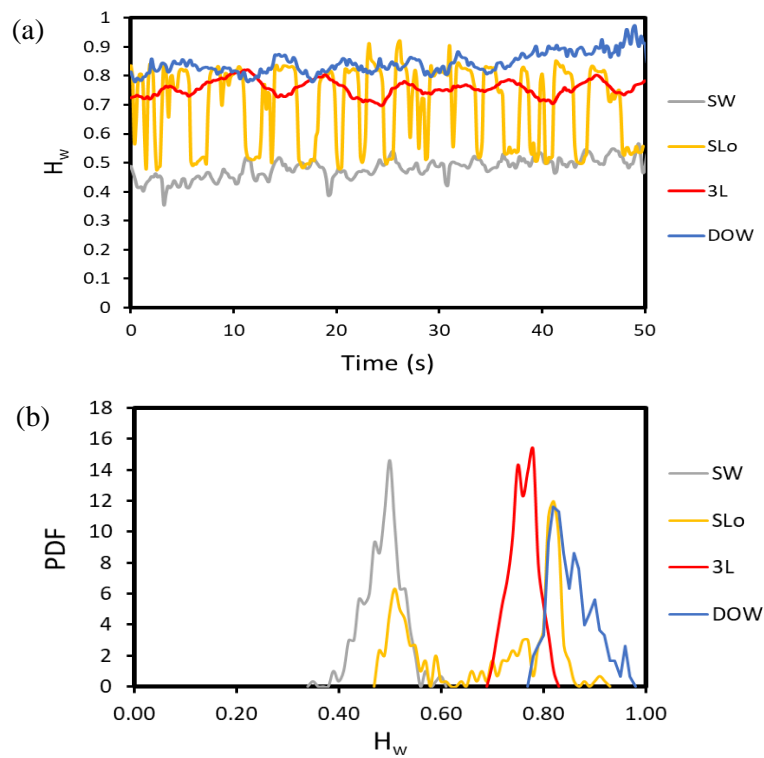


Figure 4-6: (a) Water hold-up fluctuation and (b) corresponding PDF grouping of all flow regime type examples from the experiment with H100 at a pipe inclination of  $5^\circ$ .



Flow Regime	Flow Conditions (m/s)	Average Hold-up	ECT Hold-Up and 2D Stacked Frame Images
Smooth Stratified (SS)	$v_{so} = 0.11$ $v_{sw} = 0.15$	0.26	
Stratified Wavy (SW)	$v_{so} = 0.10$ $v_{sw} = 0.39$	0.42	
Oil Plug (SLo)	$v_{so} = 0.10$ $v_{sw} = 0.45$	0.47	
Three-Layered (3L)	$v_{so} = 0.15$ $v_{sw} = 0.45$	0.39	
Dispersed (DOW)	$v_{so} = 0.10$ $v_{sw} = 0.65$	0.58	

Table 4-5: ECT images of cross-section examples and 2D frame image stacking of all flow regime type examples from the experiment with EDM250 at a pipe inclination of 0°.

Flow Regime	Flow Conditions (m/s)	Average Hold-up	ECT Hold-Up and 2D Stacked Frame Images
Stratified Wavy (SW)	$v_{so} = 0.10$ $v_{sw} = 0.35$	0.55	
Oil Slug (SLo)	$v_{so} = 0.10$ $v_{sw} = 0.50$	0.74	
Three-Layered (3L)	$v_{so} = 0.25$ $v_{sw} = 0.50$	0.70	
Dispersed (DOW)	$v_{so} = 0.10$ $v_{sw} = 0.60$	0.82	

Table 4-6: ECT images of cross-section examples and 2D frame image stacking of all flow regime type examples from the experiment with H100 at a pipe inclination of 0°.


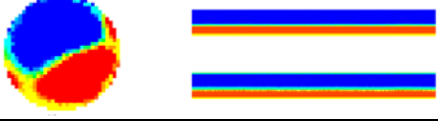
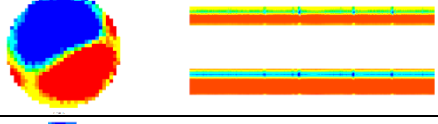
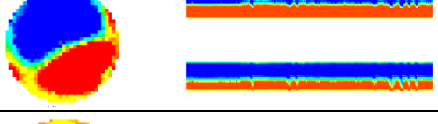
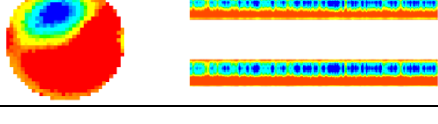
Flow Regime	Flow Conditions (m/s)	Average Hold-up	ECT Hold-Up and 2D Stacked Frame Images
Smooth Stratified (SS)	$v_{so} = 0.10$ $v_{sw} = 0.15$	0.39	
Stratified Wavy (SW)	$v_{so} = 0.10$ $v_{sw} = 0.35$	0.47	
Oil Slug (SLo)	$v_{so} = 0.10$ $v_{sw} = 0.40$	0.49	
Three-Layered (3L)	$v_{so} = 0.15$ $v_{sw} = 0.40$	0.47	
Dispersed (DOW)	$v_{so} = 0.10$ $v_{sw} = 0.70$	0.80	

Table 4-7: ECT images of cross-section examples and 2D frame image stacking of all flow regime type examples from the experiment with EDM250 at a pipe inclination of 5°.

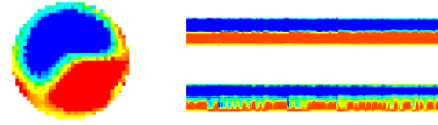
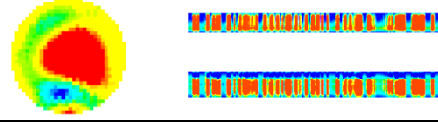
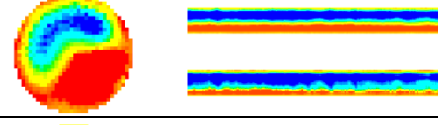
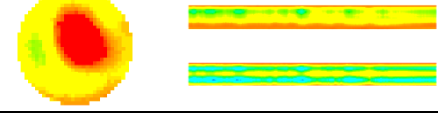
Flow Regime	Flow Conditions (m/s)	Average Hold-up	ECT Hold-Up and 2D Stacked Frame Images
Stratified Wavy (SW)	$v_{so} = 0.10$ $v_{sw} = 0.20$	0.49	
Oil Slug (SLo)	$v_{so} = 0.10$ $v_{sw} = 0.45$	0.70	
Three-Layered (3L)	$v_{so} = 0.25$ $v_{sw} = 0.50$	0.76	
Dispersed (DOW)	$v_{so} = 0.10$ $v_{sw} = 0.60$	0.86	

Table 4-8: ECT images of cross-section examples and 2D frame image stacking of all flow regime type examples from the experiment with H100 at a pipe inclination of 5°.

### 4.3 Pressure Gradient Analysis

Similarly, a PDF analysis was also applied to the pressure gradient where the DAS data set was utilised to take the measured differential pressure between P1 and P3, which are 3m apart from each other on the test section. The pressure gradient PDF analysis for each experimental example is shown between *Figure 4-7* and *Figure 4-10*, where the corresponding conditions are according to the data between *Table 4-5* and *Table 4-8*, respectively. In identical results, the stratified flows develop more stable localised pressure gradients, whereas dispersed flow has a greater range of different pressure gradients that are less frequent. Regarding intermittent flow, the results show that the pressure gradient PDF predominantly fluctuates more consistently due to a localised and dominant PDF value compared to other flow patterns, particularly dispersed flow regardless of oil type and pipeline inclination. This indicates that the change in alternating hold-up sequences has no significant effect on the corresponding pressure gradient. However, heavy oils develop less fluctuated pressure gradients across all flow regimes causing the peak PDF values to be similar to each regime type. This is due to possible mixing between the two immiscible fluids as the density difference between the oil and water phases is small enough to avoid instantaneous segregation, and the oil viscosity is large enough to avoid significant droplet breakup.

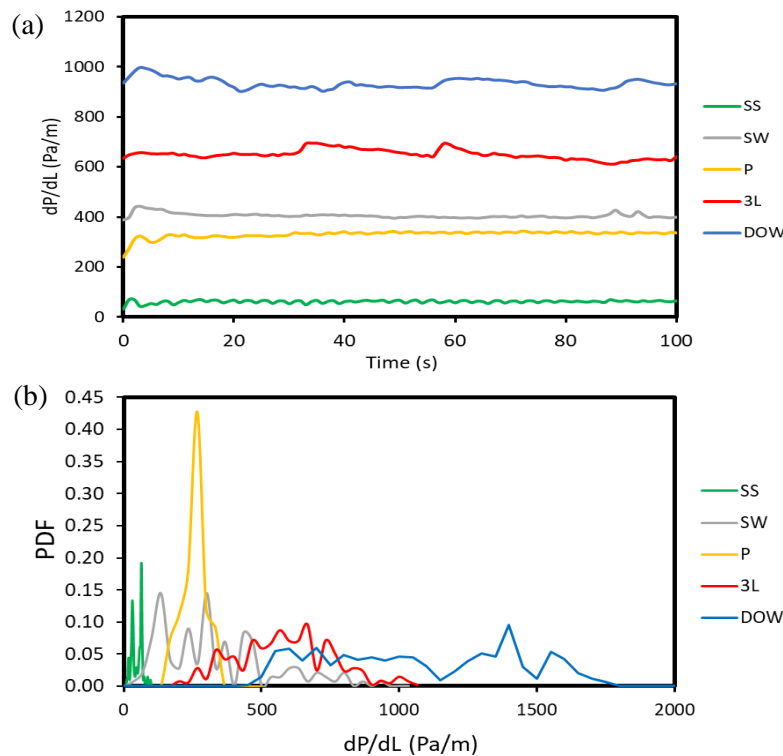


Figure 4-7: (a) Pressure drop fluctuation vs time (b) corresponding PDF pressure drop grouping of all flow regime type examples from the EDM250 experiment at  $0^\circ$  pipe inclination.

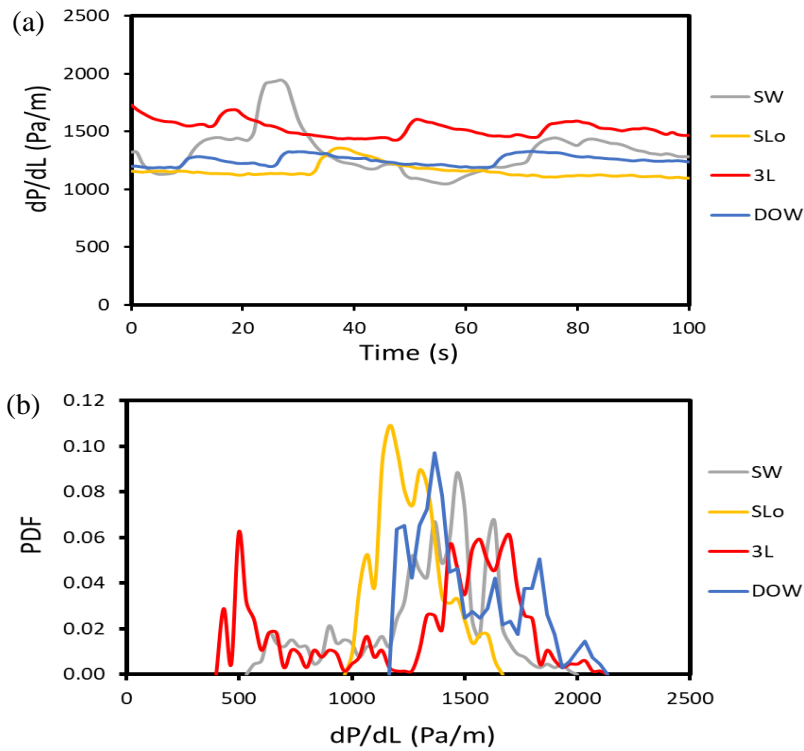


Figure 4-8: (a) Pressure drop fluctuation vs time (b) corresponding PDF pressure drop grouping of all flow regime type examples from the H100 experiment at  $0^\circ$  pipe inclination.

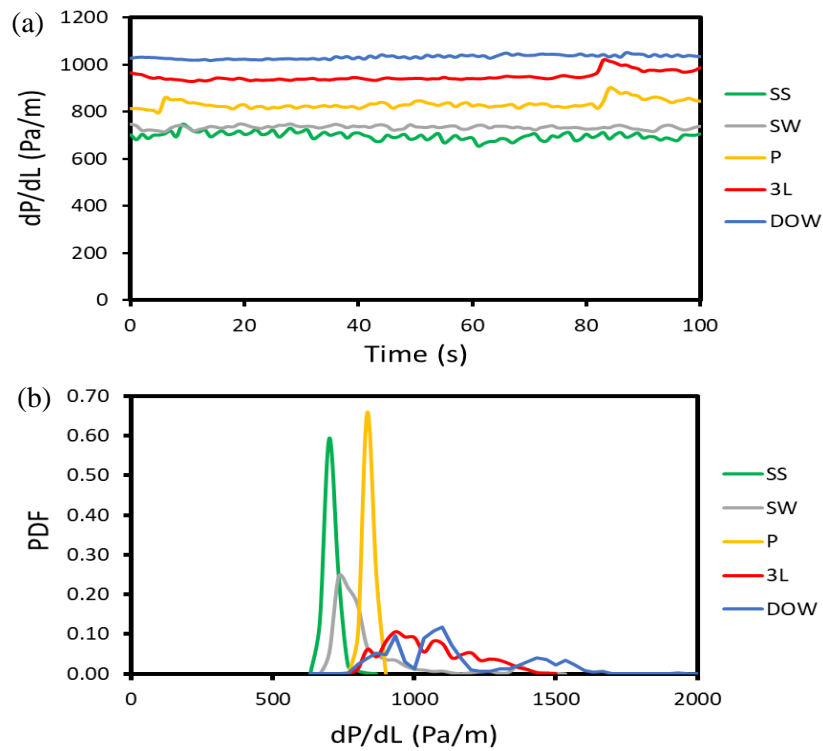


Figure 4-9: Pressure drop fluctuation vs time (b) corresponding PDF pressure drop grouping of all flow regime type examples from the EDM250 experiment at  $5^\circ$  a pipe inclination.

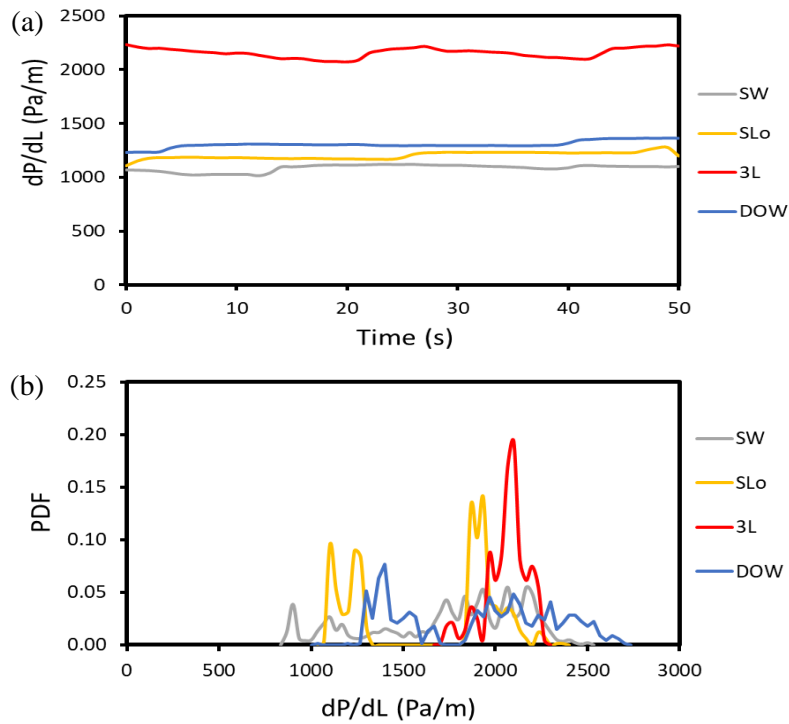


Figure 4-10: Pressure drop fluctuation vs time (b) corresponding PDF pressure drop grouping of all flow regime type examples from the H100 experiment at 5° a pipe inclination.

#### 4.4 Intermittent Flow Analysis

Focussing purely on intermittent flow (slug and plug flows), as shown in *Figure 4-11* and *Figure 4-12*, processed hold-up data coupled with the 2D stacked imaging shows compelling evidence of the existence of intermittent flows such as slug and plug flow regimes in liquid-liquid multiphase flow systems. The light oils that typically produce plug flow demonstrate smaller bimodal distributions across the hold-up extremes compared to that of slug flow due to the large change in hold-up fluctuations between the two alternating phase shifts. This indicates that plug flow is much more localised than its larger counterpart. However, through closer examination of each distribution crest, slug flow patterns generally have smaller peaks than that of plug flow distributions. Meaning that plug flow is a much more stable and consistent flow regime. This is because oil slug segments sustain themselves between the inner pipe walls when sandwiched between the water segments, whereas oil plug flows are stabilised by the gravitational effects of the surrounding water phase while in contact with the upper pipe wall. In addition, the phase density differential between oil and water is a stabilisation factor for intermittent flows. Therefore, slug formations are developed by the multiphase system to overcome the gravitational forces, and instabilities are hence formed in slugs which create turbulent conditions. Indicating that mixing is present between the fluids, which are located between the phase boundaries.

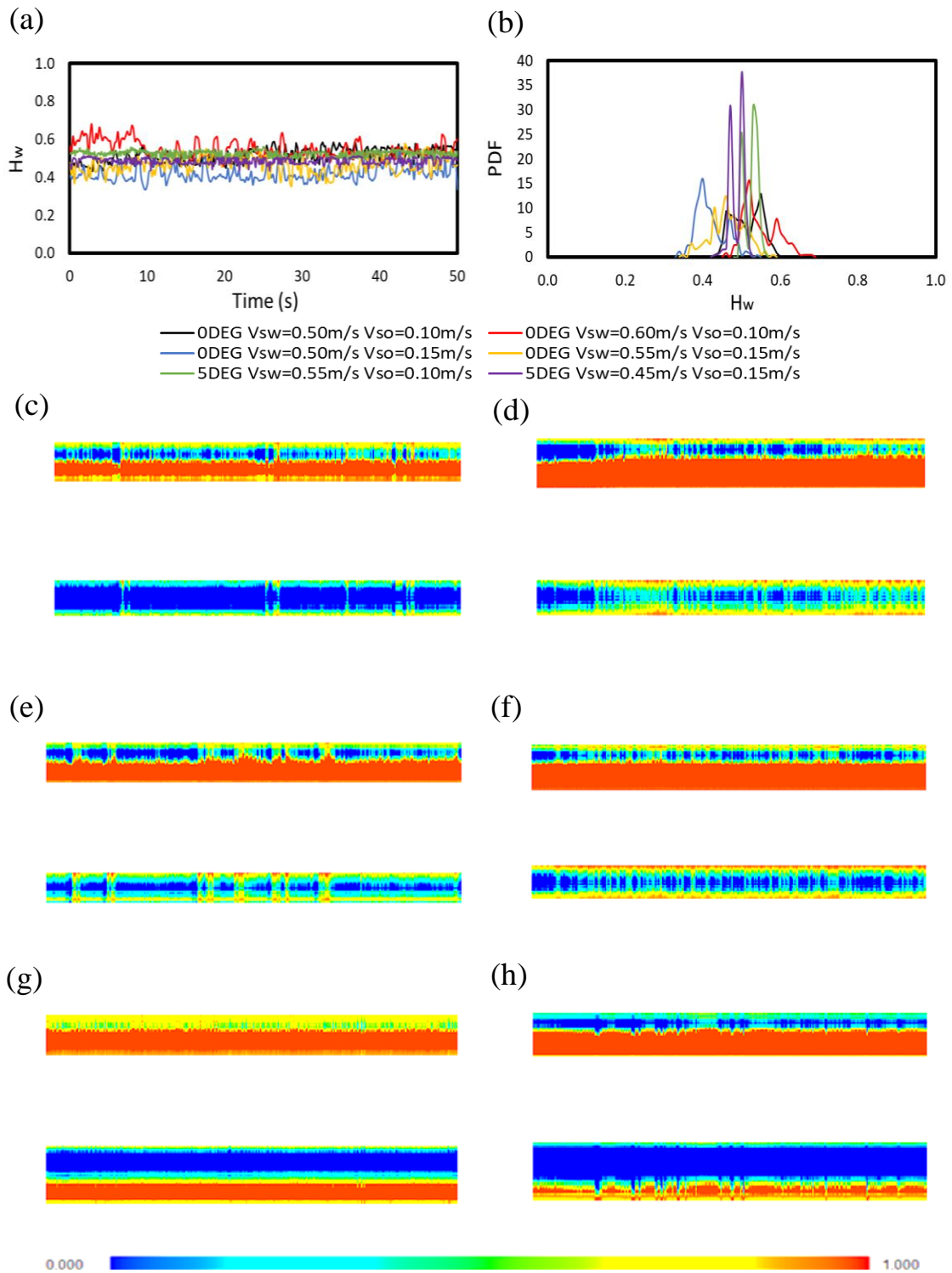


Figure 4-11: Intermittent flow analysis of EDM250 (light oil) of (a) hold-up vs time data, (b) PDF analysis of hold-up and the resulting 2D ECT plot of the measured permittivity between the two fluids under the conditions of; (c)  $v_{sw}=0.50\text{m/s}$   $v_{so}=0.10\text{m/s}$  at  $0^\circ$ , (d)  $v_{sw}=0.60\text{m/s}$   $v_{so}=0.10\text{m/s}$  at  $0^\circ$ , (e)  $v_{sw}=0.50\text{m/s}$   $v_{so}=0.15\text{m/s}$  at  $0^\circ$ , (f)  $v_{sw}=0.55\text{m/s}$   $v_{so}=0.15\text{m/s}$  at  $0^\circ$ , (g)  $v_{sw}=0.55\text{m/s}$   $v_{so}=0.10\text{m/s}$  at  $5^\circ$  and (h)  $v_{sw}=0.50\text{m/s}$   $v_{so}=0.15\text{m/s}$  at  $5^\circ$ .

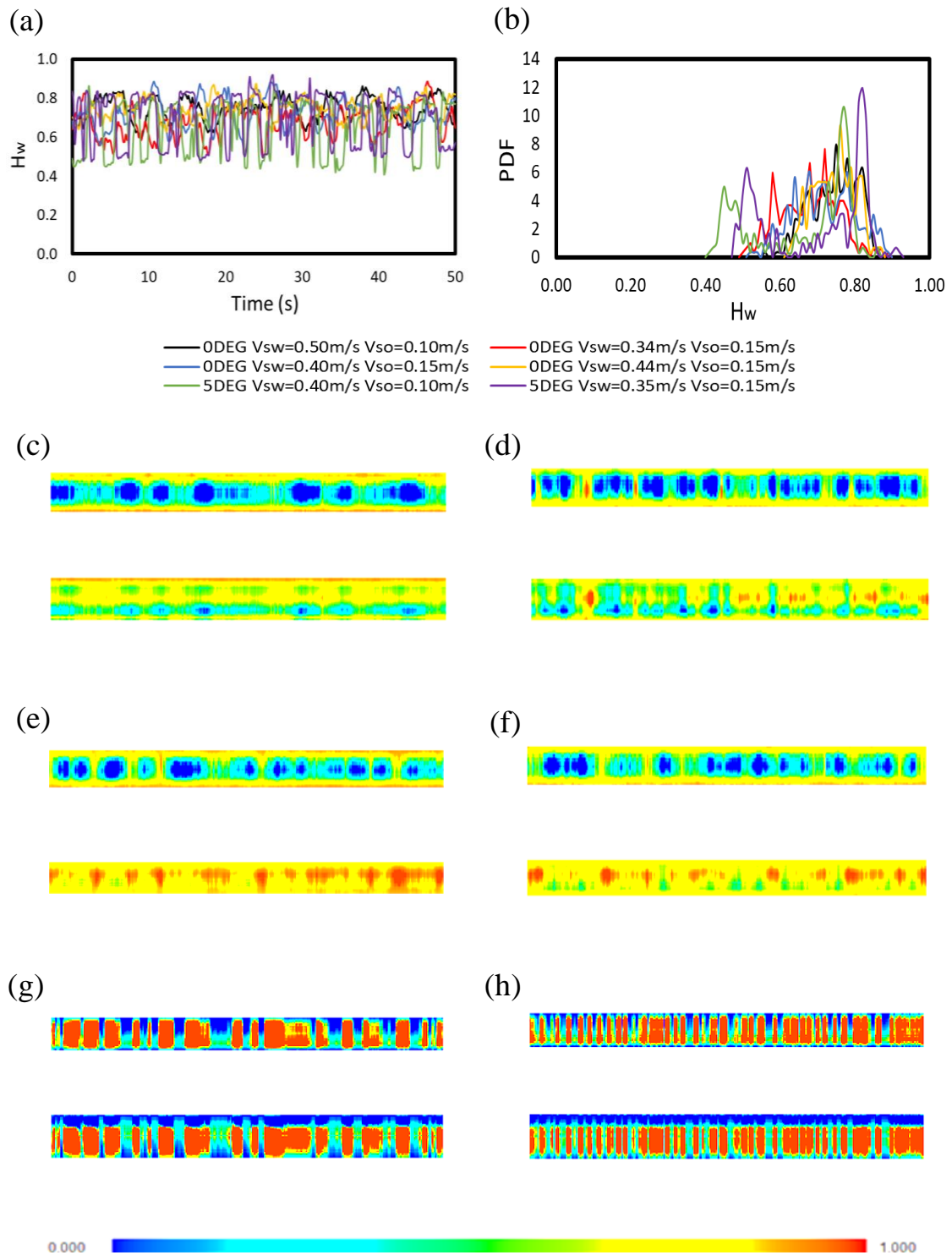


Figure 4-12: Intermittent flow analysis of H100 (heavy oil) of (a) hold-up vs time data, (b) PDF analysis of hold-up and the resulting 2D ECT plot of the measured permittivity between the two fluids under the conditions of; (c)  $v_{sw}=0.50\text{m/s}$   $v_{so}=0.10\text{m/s}$  at  $0^\circ$ , (d)  $v_{sw}=0.34\text{m/s}$   $v_{so}=0.15\text{m/s}$  at  $0^\circ$ , (e)  $v_{sw}=0.40\text{m/s}$   $v_{so}=0.15\text{m/s}$  at  $0^\circ$ , (f)  $v_{sw}=0.45\text{m/s}$   $v_{so}=0.15\text{m/s}$  at  $0^\circ$ , (g)  $v_{sw}=0.40\text{m/s}$   $v_{so}=0.10\text{m/s}$  at  $5^\circ$  and (h)  $v_{sw}=0.35\text{m/s}$   $v_{so}=0.15\text{m/s}$  at  $5^\circ$ .

Table 4-9 to Table 4-12 demonstrate a clearer development in the behavioural changes of the intermittent flow regimes as system conditions alter between all four experiment types. The lower the superficial water velocity is relative to a constant superficial oil velocity, the longer the slug/plug length will become. As the water flowrate increases, it begins to break apart the longer segments of the intermittent pattern, creating a higher frequency of smaller segments at more frequent intervals. Oil density and viscosity also have similar effects, and sustaining its form at high flowrates will limit higher intermittent frequencies to form. It is also important to note that despite having a clear image of some flow regime high-speed images, the ECT data may not be able to necessarily capture the fine details of each intermitted flow condition. This is because in cases such as the heavy oil flow, the water becomes contaminated from the oil phase causing the average water capacitance to be closer to the oil conductivity value. Hence, mixed colour coordinates can be interpreted as water if the phase inversion within the corresponding region is more water dominant (light blue to green) or oil if the phase inversion region is oil dominant (green-yellow).

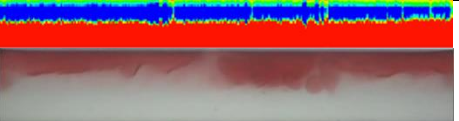
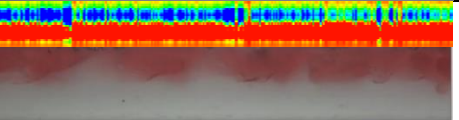
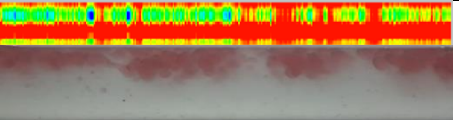

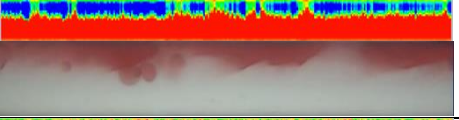
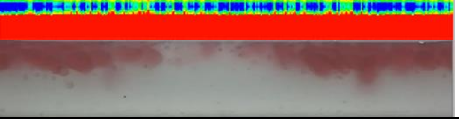
Flow Regime Test Point	Flow Condition ( $m/s$ )	Average Hold-up	Average Pressure Gradient ( $Pa/m$ )	High-Speed Image Capture and ECT 2D Stacked Imaging
P1	$v_{so} = 0.10$ $v_{sw} = 0.45$	0.47	230	
P2	$v_{so} = 0.10$ $v_{sw} = 0.50$	0.51	256	
P3	$v_{so} = 0.10$ $v_{sw} = 0.55$	0.52	267	
P4	$v_{so} = 0.10$ $v_{sw} = 0.60$	0.55	319	
P5	$v_{so} = 0.15$ $v_{sw} = 0.50$	0.42	263	
P6	$v_{so} = 0.15$ $v_{sw} = 0.55$	0.46	333	

Table 4-9: All intermittent flow regimes observed with all measured parameters from the experiment with EDM250 oil at a pipe inclination of  $0^\circ$ .



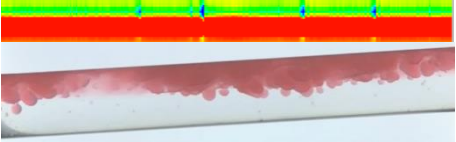
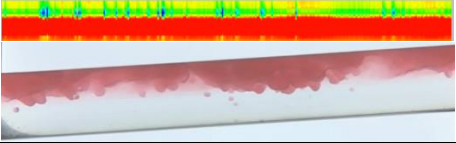
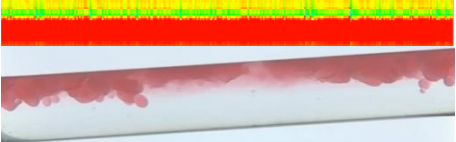

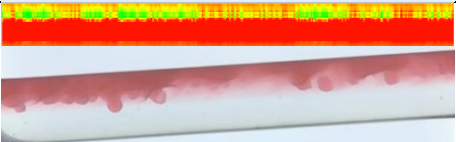
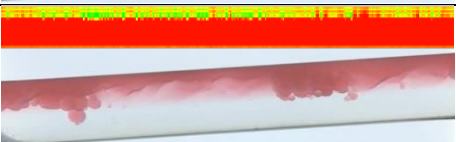
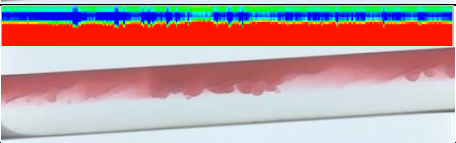
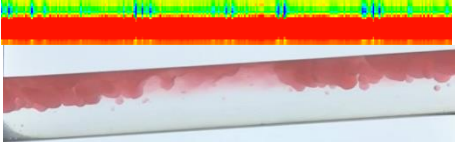
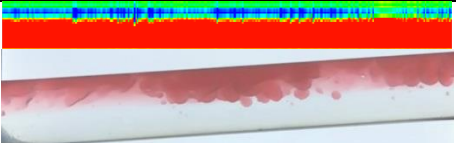
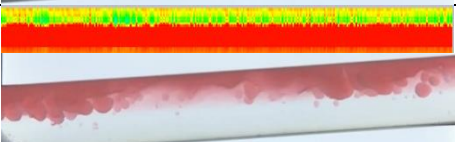
Flow Regime Test Point	Flow Condition (m/s)	Average Hold-up	Average Pressure Gradient (Pa/m)	High-Speed Image Capture and ECT 2D Stacked Imaging
P1	$v_{so} = 0.10$ $v_{sw} = 0.40$	0.49	813	
P2	$v_{so} = 0.10$ $v_{sw} = 0.45$	0.5	852	
P3	$v_{so} = 0.10$ $v_{sw} = 0.50$	0.51	885	
P4	$v_{so} = 0.10$ $v_{sw} = 0.55$	0.54	945	
P5	$v_{so} = 0.10$ $v_{sw} = 0.60$	0.57	991	
P6	$v_{so} = 0.10$ $v_{sw} = 0.65$	0.58	1047	
P7	$v_{so} = 0.15$ $v_{sw} = 0.45$	0.48	895	
P8	$v_{so} = 0.15$ $v_{sw} = 0.50$	0.5	886	
P9	$v_{so} = 0.15$ $v_{sw} = 0.55$	0.51	926	
P10	$v_{so} = 0.15$ $v_{sw} = 0.60$	0.55	813	

Table 4-10: All intermittent flow regimes observed with all measured parameters from the experiment with EDM250 oil at a pipe inclination of 5°.

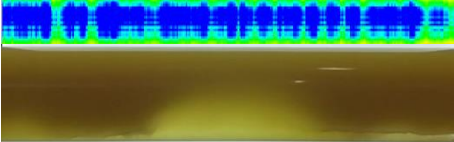
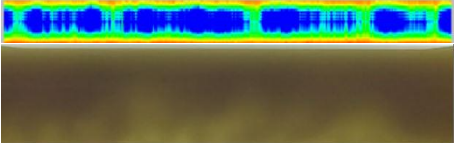
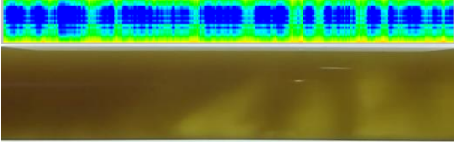
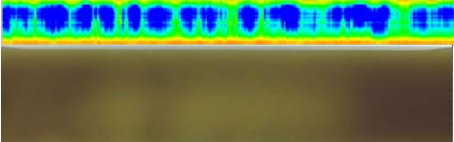
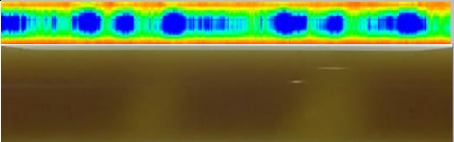
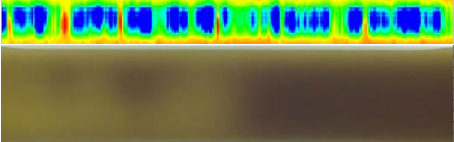
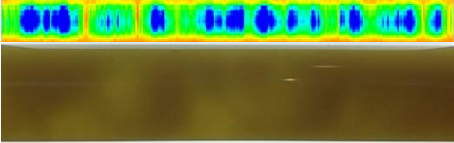
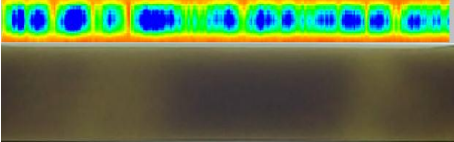

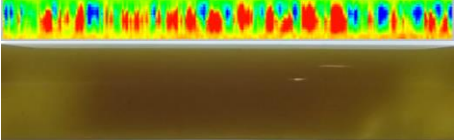
Flow Regime Test Point	Flow Condition (m/s)	Average Hold-up	Average Pressure Gradient (Pa/m)	High-Speed Image Capture and ECT 2D Stacked Imaging
SLo1	$v_{so} = 0.10$ $v_{sw} = 0.30$	0.49	1320	
SLo 2	$v_{so} = 0.10$ $v_{sw} = 0.35$	0.55	1350	
SLo 3	$v_{so} = 0.10$ $v_{sw} = 0.40$	0.58	1303	
SLo 4	$v_{so} = 0.10$ $v_{sw} = 0.45$	0.65	1051	
SLo 5	$v_{so} = 0.10$ $v_{sw} = 0.50$	0.74	1268	
SLo 6	$v_{so} = 0.15$ $v_{sw} = 0.34$	0.68	1495	
SLo 7	$v_{so} = 0.15$ $v_{sw} = 0.40$	0.72	1409	
SLo 8	$v_{so} = 0.15$ $v_{sw} = 0.44$	0.74	1370	
SLo 9	$v_{so} = 0.15$ $v_{sw} = 0.51$	0.76	1281	
SLo 10	$v_{so} = 0.15$ $v_{sw} = 0.55$	0.77	1357	

Table 4-11: All intermittent flow regimes observed with all measured parameters from the experiment with H100 oil at a pipe inclination of 0°.

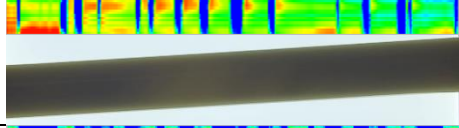
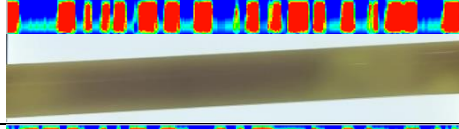
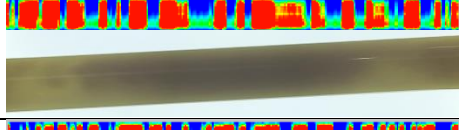
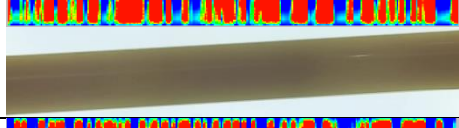
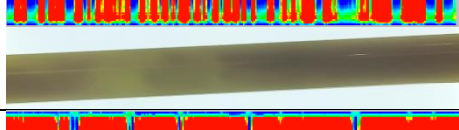
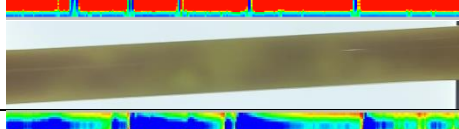
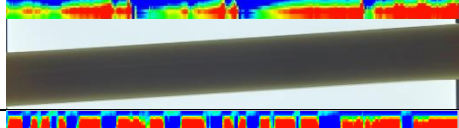
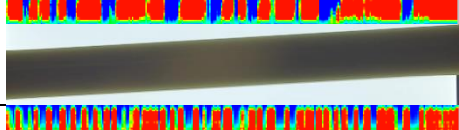
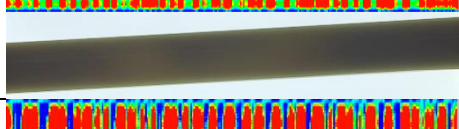
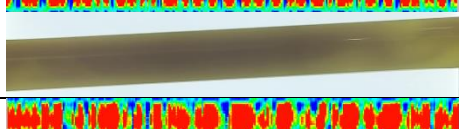
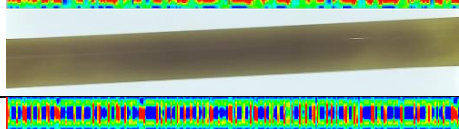

Flow Regime Test Point	Flow Condition (m/s)	Average Hold-up	Average Pressure Gradient (Pa/m)	High-Speed Image Capture and ECT 2D Stacked Imaging
SLo 1	$v_{so} = 0.10$ $v_{sw} = 0.25$	0.5	1098	
SLo 2	$v_{so} = 0.10$ $v_{sw} = 0.30$	0.55	1121	
SLo 3	$v_{so} = 0.10$ $v_{sw} = 0.35$	0.6	1178	
SLo 4	$v_{so} = 0.10$ $v_{sw} = 0.40$	0.66	1170	
SLo 5	$v_{so} = 0.10$ $v_{sw} = 0.45$	0.7	1273	
SLo 6	$v_{so} = 0.10$ $v_{sw} = 0.50$	0.78	1235	
SLo 7	$v_{so} = 0.15$ $v_{sw} = 0.30$	0.72	2096	
SLo 8	$v_{so} = 0.15$ $v_{sw} = 0.35$	0.74	2044	
SLo 9	$v_{so} = 0.15$ $v_{sw} = 0.40$	0.77	1991	
SLo 10	$v_{so} = 0.15$ $v_{sw} = 0.45$	0.8	1995	
SLo 11	$v_{so} = 0.15$ $v_{sw} = 0.50$	0.82	1997	
SLo 12	$v_{so} = 0.15$ $v_{sw} = 0.55$	0.84	1948	

Table 4-12: All intermittent flow regimes observed with all measured parameters from the experiment with H100 oil at a pipe inclination of 5°.

---

## 4.5 Superimposing Flow Regime Maps

The resulting flow regime grouping maps developed from this study have utilised two similar experimental works from literature for comparative analysis. The two studies have been specifically selected to compare the changes between the oil types to observe the consistency between the resulting mapping sequences of each flow regime. The mapping of all four experimental tests has been superimposed between their constituent oil types, as shown in *Figure 4-13*. The study that will be compared with the light oil experimental system is the work of Mandal, Das and Das (2010). Water and kerosene with density and viscosity of  $787\text{kg/m}^3$  and  $1.2\text{mPa}\cdot\text{s}$ , respectively, were used within a single flow loop rig that contained two test pipe sections to conduct scale analysis on pipe diameters of  $0.0254\text{m}$  and  $0.012\text{m}$ . In the  $0.0254\text{m}$  diameter pipeline, at very slow superficial kerosene velocities ( $v_{so} \leq 0.1\text{m/s}$ ), only plugs were observed.

It was noticed by the authors the flow regime envelope size for characteristic intermittent flow development is greater under narrow pipes, which the authors had classified to be pipelines with internal diameters under  $0.0254\text{m}$ . This is due to the greater dominance of the surface tension, which sustains the intermittent flow across the entire diameter of the pipe, which increases the likelihood for slugs to form even under light oil systems. The heavy oil experiment comparison will utilise the work of Dasari et al. (2013). High viscous oil has been incorporated within this experimental investigation to understand the hydrodynamic behaviour of oil-water multiphase flow within a horizontal pipeline loop of an internal diameter of  $0.0245\text{m}$  made from Perspex. The tested oil had a density of  $889\text{kg/m}^3$  and a viscosity of  $107\text{mPa}\cdot\text{s}$ , respectively, and the flow loop system was maintained under a constant temperature of  $25^\circ\text{C}$ . Visual and photographic imaging techniques have shown the following flow regimes: plug/slug flow, stratified wavy flow, three-layered flow, and dispersion. The water phase was set between  $0.1 - 1.1\text{m/s}$ , and the oil phase was varied at  $0.015 - 1.25\text{m/s}$ .

Slugs were seen to exist at oil velocity, which increased to  $0.35\text{m/s}$  while the respective water velocity would vary up to  $0.6\text{m/s}$ . Further intermittent flow patterns, such as plug flow, were present under low flow conditions. However, plug flow seemed to be present under more localised velocity conditions, covering the smallest region of all flow regime maps. When increasing both the oil and water superficial velocities to the same speed, the length of the slugs deteriorates. Plug flow is found between superficial oil velocities of  $0.031 - 0.4\text{m/s}$  as the water phase sustained plugs under superficial velocities of  $0.038 - 0.2\text{m/s}$ . When the phase velocity of oil is closer to that of water, the water bridges between each separate oil slug/plug and decreases in length, causing the slugs to cluster further against each other. Inevitably, the stratified wavy

flow will reform as the gravitational forces return to be the dominant force. Overall, both comparisons between the respective oil types show very similar flow regime envelope characteristics and are consistent with each other between the general shapes of the transition boundaries. The small shifts in the transition boundaries can be suggested to be due to a combination of a slight difference in fluid properties, experimental errors and differentiating flow regimes around the transition boundary when pre-grouping the visual results.

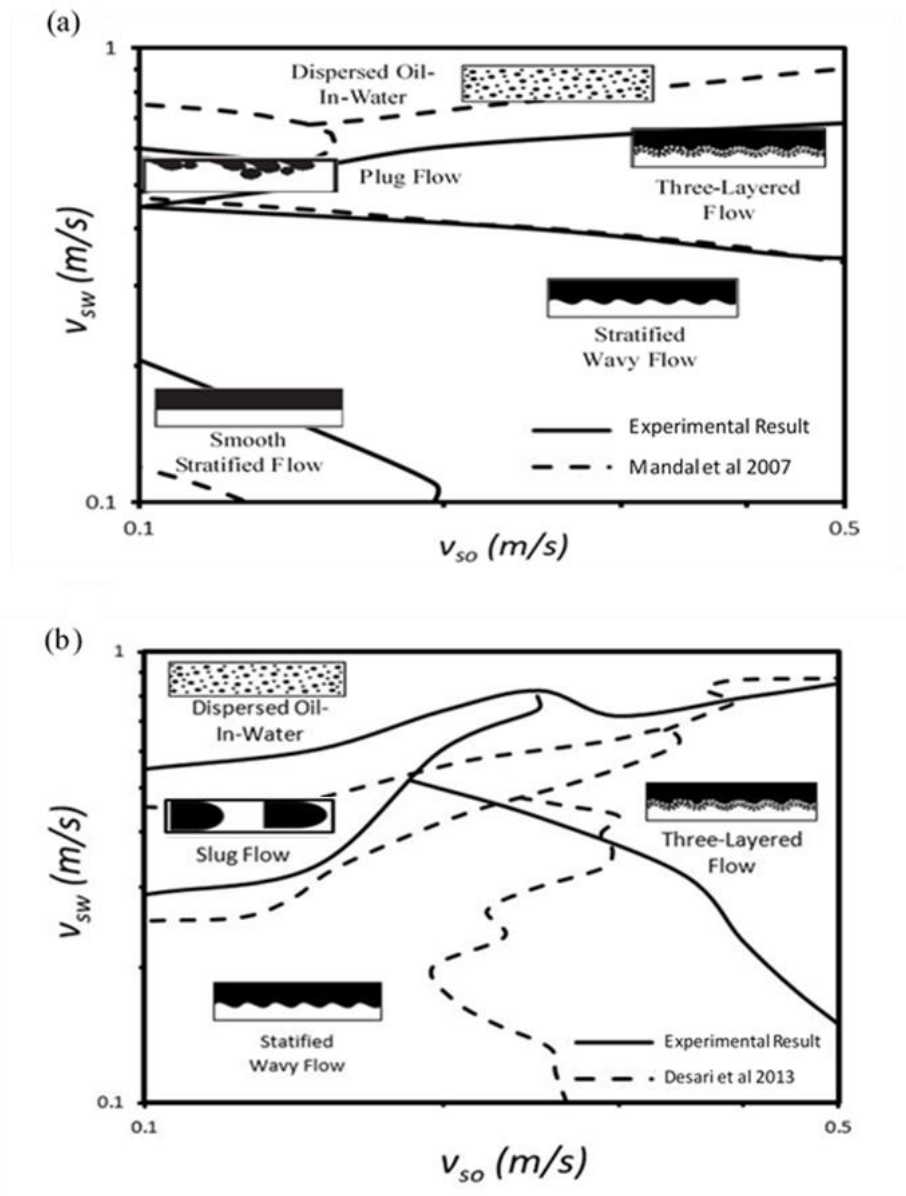
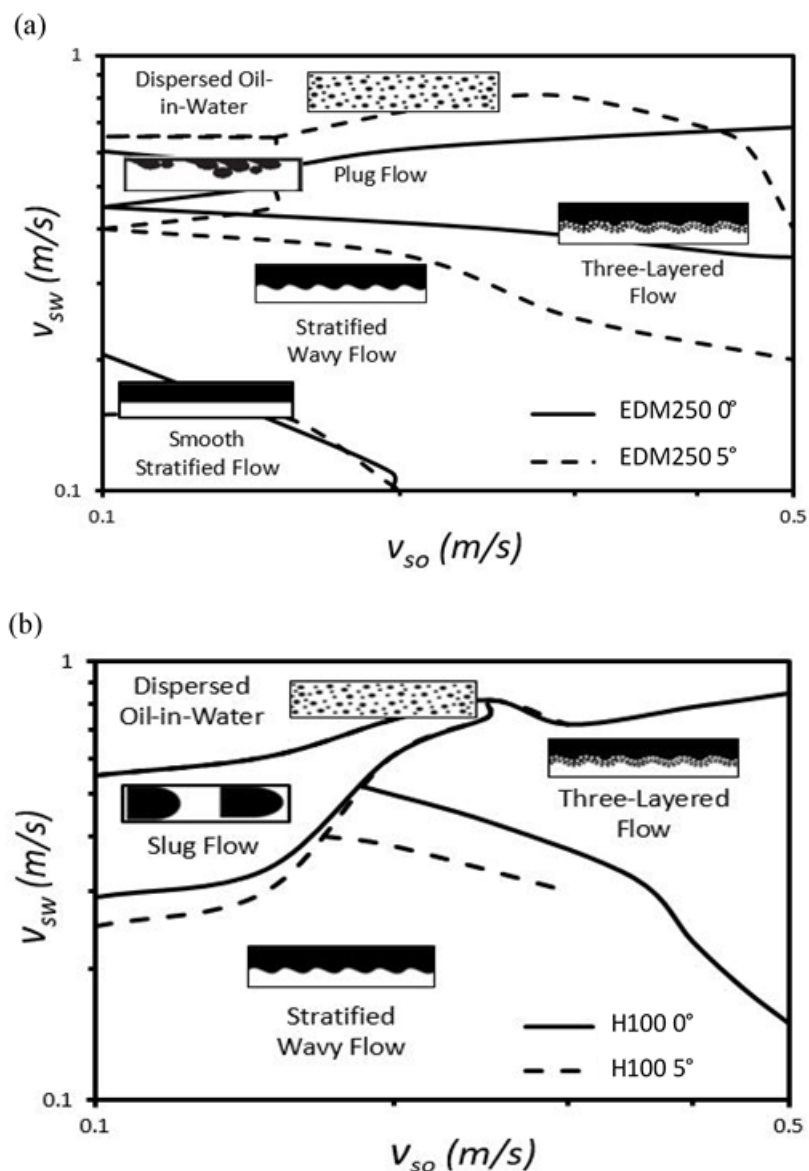


Figure 4-13: Superimposed flow regime map of (a) modified from (Mandal, Chakrabarti and Das, 2007) against the EDM250 experiment (light oil) both at pipe incline of  $0^\circ$  and (b) modified from (Dasari et al., 2013) against the H100 experiment (heavy oil) both at pipe incline of  $0^\circ$ .

Concerning the experiment of this study, a  $5^\circ$  incline was set on the test section to induce the highest possible effects on the flow regimes. As shown in *Figure 4-14*, the results present clear evidence for pipe orientation to have some effect on the flow regime mapping sequence, indicating that pipe inclination also plays a role in causing flow regime envelopes to change. Intermittent flow regimes are particularly affected by pipe inclination. The size of the Plug and Slug envelope between the two experiments has increased, indicating that pipe inclination in the direction of the respective flow induces intermittent flow.



*Figure 4-14: Superimposed flow regime maps of (a) EDM250 (light oil) experiment at a pipe incline at  $0^\circ$  against EDM250 oil experiment at a pipe incline at  $5^\circ$  and (b) H100 oil experiment at a pipe incline at  $0^\circ$  against H100 oil experiment at pipe incline at  $5^\circ$ .*

## 4.6 Intermittent Frequency Analysis

This section examines signal spectral analysis of the intermittent flow behaviours. The frequency analysis will again utilise the alternating hold-up data gathered from the ECT system. To subject the data to frequency analysis, a time scale between 40-50 seconds of each data set will utilise the Fast Frequency Transform (FFT) due to the analysis restricting the number of sample points to equal any whole value  $\bar{N}$ , to  $2^{\bar{N}}$  (e.g 2, 256), as the ECT frame rates varied between 5-7 frames per second. The FFT is an enhanced algorithm governed by the Discrete Fourier Transformation (DFT), as shown in Eqs. (4-1) and (4-2).

$$X(k_f) = \sum_{n_f=0}^{N-1} x(n_f) e^{\frac{-j2\pi n_f k_f}{N}} \quad (4-1)$$

$$f_\alpha = \frac{n_f}{s_x N} \quad (4-2)$$

for when;  $n_f = 0, 1, 2 \dots N - 1$

Where  $j$  is a complex number,  $N$  is the total number of sample points in the data signal,  $x(n_f)$  is the data point at frame number  $n_f$  and  $X(k_f)$  is a set of  $N$  amplitudes for each of the individual signal points  $k_f$ . The signal frequency  $f_\alpha$  is used to find the corresponding frequency for the given amplitude at each frame point  $n_f$ , while  $s_x$  is the sampling rate of the data. The data signal of the hold-up is sampled across the time spectrum and grouped into the frequency domain. The frequency amplitude will determine the dominant frequency within each test run; however, frequencies close to zero represent a stable system. Hence, when identifying the dominant frequency for intermittent flow in the 1" flow loop a criterion was used where the dominant frequency must be above 0.1Hz. This is then used to determine the change in frequential behaviour between the intermittent flows when other conditional variables are altered. An analysis of the unstable peak frequency for all intermittent flow conditions between superficial velocities and experiment types is presented in *Table 4-13*. Additionally, the hold-up frequency domain is presented between all the example test runs, as shown in *Figure 4-15* and *Figure 4-16*.

EDM250 0° Frequency (Hz)		$v_{sw}$ (m/s)								
		0.30	0.35	0.40	0.45	0.50	0.55	0.60	0.65	0.70
$v_{so}$ (m/s)	0.1	-	-	-	0.156	0.293	0.625	-	-	-
	0.15	-	-	-	0.410	0.410	0.371	-	-	-
	0.2	-	-	-	-	-	-	-	-	-



EDM250 5° Frequency (Hz)		$v_{sw}$ (m/s)								
		0.30	0.35	0.40	0.45	0.50	0.55	0.60	0.65	0.70
$v_{so}$ (m/s)	0.1	-	-	0.195	0.234	2.64	0.137	0.138	0.215	-
	0.15	-	-	-	0.176	0.215	0.176	0.117	0.137	-
	0.2	-	-	-	-	-	-	-	-	-

H100 0° Frequency (Hz)		$v_{sw}$ (m/s)								
		0.30	0.35	0.40	0.45	0.50	0.55	0.60	0.65	0.70
$v_{so}$ (m/s)	0.1	0.422	0.375	0.187	0.187	0.164	-	-	-	-
	0.15	-	0.141	0.117	0.328	0.234	0.234	0.281	0.234	0.258
	0.2	-	-	-	-	-	-	-	-	-

H100 5° Frequency (Hz)		$v_{sw}$ (m/s)								
		0.30	0.35	0.40	0.45	0.50	0.55	0.60	0.65	0.70
$v_{so}$ (m/s)	0.1	0.117	0.164	0.117	0.187	0.375	-	-	-	-
	0.15	0.141	0.328	0.258	0.375	0.422	2.16	-	-	-
	0.2	-	-	-	-	-	-	0.141	0.562	0.422

*Table 4-13: Intermittent flow frequency grouping matrix between oil and water superficial velocities at  $v_{sw} = 0.30 - 0.70$  m/s and  $v_{so} = 0.10 - 0.20$  m/s of all four experiment types.*

The frequency analysis suggests that the inclinations have a slight effect on the overall magnitude of the unstable frequencies, which is more effective for the lighter oil system. This, in turn, raises the point of light oils to act more sensitively towards changes in other multiphase flow system parameters such as operational input or pipe geometry. Furthermore, the alteration in superficial oil velocity significantly affects frequencies, which is dependent on the type of oils in use. As the superficial oil velocity is increased for lighter oils, the dominant frequency generally decreases, except for cases where the dominant frequency increases due to resonance with the water velocity. Conversely, for heavier oils, the superficial oil velocity is indirectly proportional to the dominant frequency. In contrast, the effect is reversed with lower superficial oil velocities as greater unstable dominant frequencies in light oils are formed and vice versa for heavier oils. This is more likely to be due to the difference in intermittent flow regimes where the light oil only produces plug flow regimes and the heavier oil only produces slug flow within this study. Moreover, it is clear that for plug flow, the overall dominant signal frequency is much closer to zero, which indicates a more stable system which typically represents stratified flow. This is because the form of plug flow is very close to that of stratified flow as the entire or at least a large majority of the pipeline cross-section is not engulfed by both phases during the intermittent process. Slug flow regimes, on the other hand, create a larger gap between hold-up extremes and will result in a higher dominant frequency because sudden large changes in hold-up will create instabilities. The remaining FFT analysis on the other intermittent flow data can be found in *Appendix D*.



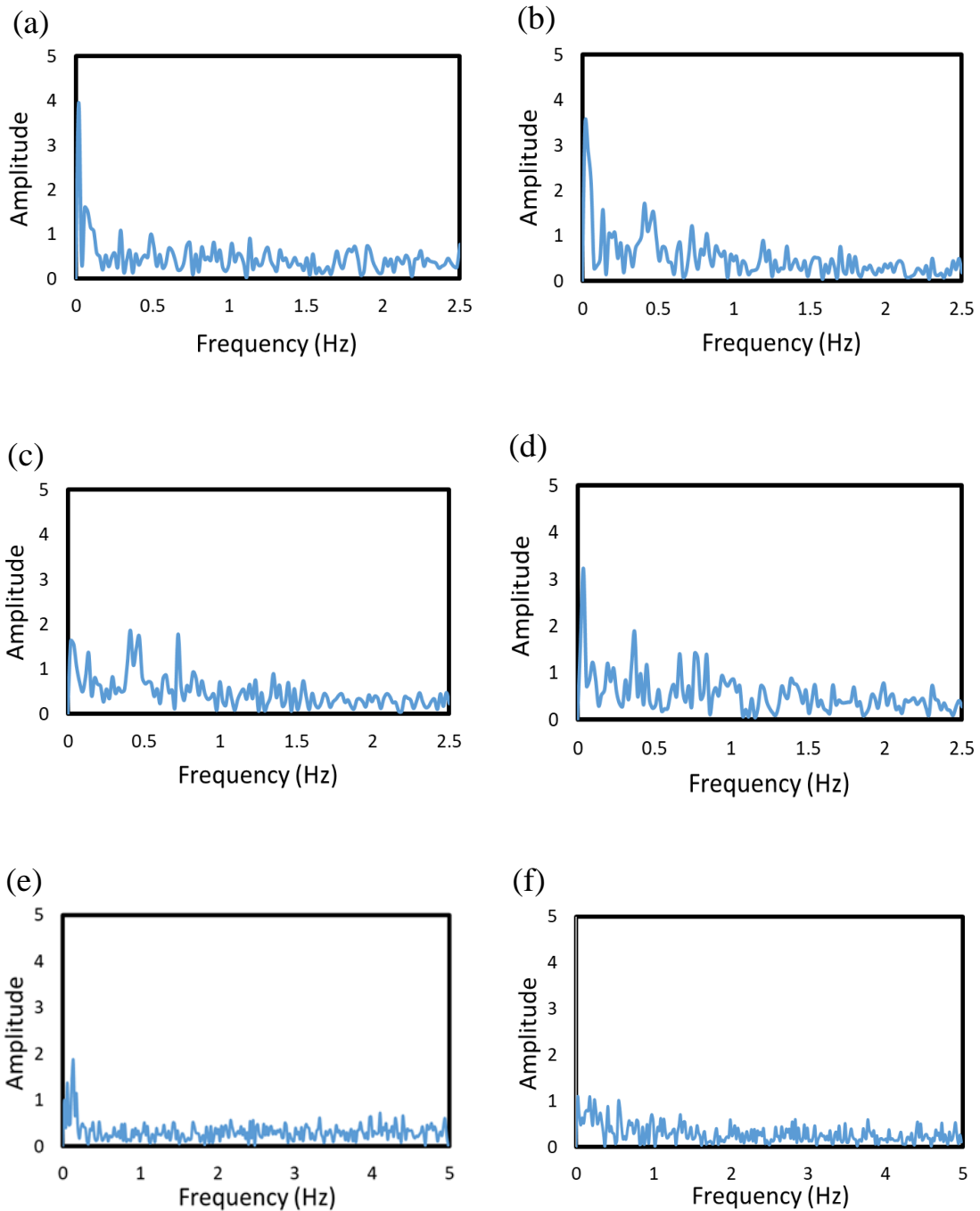


Figure 4-15: Intermittent flow frequency analysis of EDM250 (light oil) at experimental conditions of, (a)  $v_{sw} = 0.50\text{m/s}$   $v_{so} = 0.10\text{m/s}$  at  $0^\circ$ , (b)  $v_{sw} = 0.60\text{m/s}$   $v_{so} = 0.10\text{m/s}$  at  $0^\circ$ , (c)  $v_{sw} = 0.50\text{m/s}$   $v_{so} = 0.15\text{m/s}$  at  $0^\circ$ , (d)  $v_{sw} = 0.55\text{m/s}$   $v_{so} = 0.15\text{m/s}$  at  $0^\circ$ , (e)  $v_{sw} = 0.55\text{m/s}$   $v_{so} = 0.10\text{m/s}$  at  $5^\circ$  and (f)  $v_{sw} = 0.45\text{m/s}$   $v_{so} = 0.15\text{m/s}$  at  $5^\circ$ . The time domain of the ECT data of the eight experimental test examples of intermittent flow has been converted to the frequency domain. The highest amplitude point represents the dominant frequency of the fluctuation. Lighter oils in general have better stability and hence a lower dominant frequency in comparison to heavier oils.

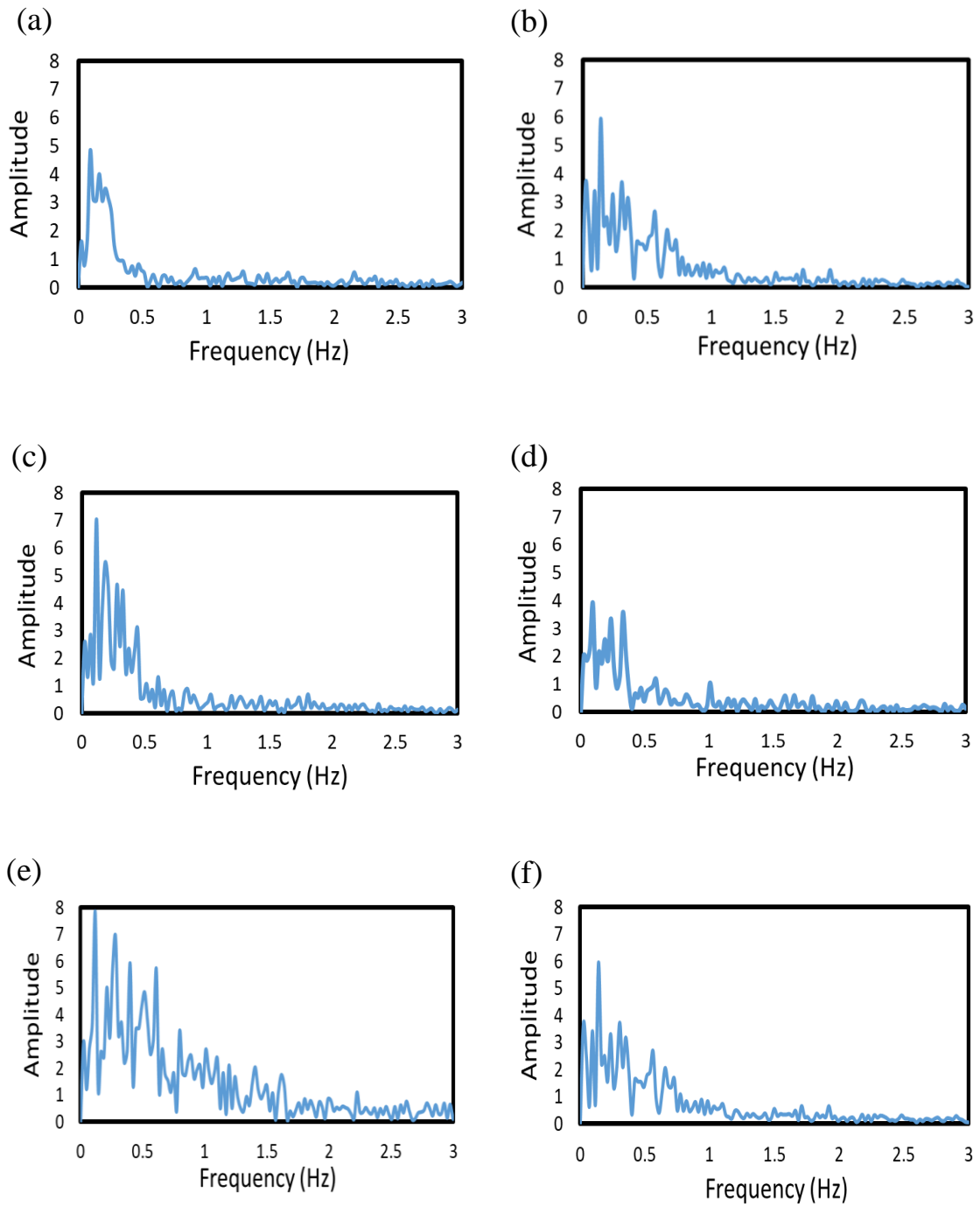


Figure 4-16: Intermittent flow analysis of H100 (heavy oil) at experimental conditions of (a)  $v_{sw} = 0.50\text{m/s}$   $v_{so} = 0.10\text{m/s}$  at  $0^\circ$ , (b)  $v_{sw} = 0.34\text{m/s}$   $v_{so} = 0.15\text{m/s}$  at  $0^\circ$ , (c)  $v_{sw} = 0.40\text{m/s}$   $v_{so} = 0.15\text{m/s}$  at  $0^\circ$ , (d)  $v_{sw} = 0.45\text{m/s}$   $v_{so} = 0.15\text{m/s}$  at  $0^\circ$ , (e)  $v_{sw} = 0.40\text{m/s}$   $v_{so} = 0.10\text{m/s}$  at  $5^\circ$  and (f)  $v_{sw} = 0.35\text{m/s}$   $v_{so} = 0.15\text{m/s}$  at  $5^\circ$ . The time domain of the ECT data of the eight experimental test examples of intermittent flow has been converted to the frequency domain. The highest amplitude point represents the dominant frequency of the fluctuation. Heavier oils in general have lower stability and hence a higher dominant frequency in comparison to lighter oils.

---

## 4.7 *Summary of Results*

The data presented in this chapter strongly suggests that intermittent flow is present across a wide range of oil-water flow conditions. Intermittent patterns generally show a tendency to develop under the conditions of low oil velocity in conjunction with a moderate rate of water velocity which would be the equivalent of a superficial phase velocity ratio of around 1:4 respectively. Heavier oils which have a greater density and viscosity have a greater tendency to develop intermittent flows and have a larger flow regime envelope due to the fluid properties countering buoyancy and inertial forces to stabilise oil slug/plug formations from backing into neighbouring flow regimes. The shape and size of the individual intermittent oil patterns are found to be mainly controlled by the oil flow rate, wherefrom higher to lower oil velocities will progressively narrow the slug/plug sizing, causing more of a spherical formation, leading to plug flow through the intermittent distribution, and vice versa for slug flow. Plug flow regimes generally develop in more localised conditions in comparison to slug flow, which can develop under a wider range of oil and water velocity configurations. Plug flow is typically developed with light oil types whereas slug flow develops with heavier oils.

When pipelines are slightly orientated upwards (up to +5°) in the direction of the flow, the transition boundary for intermittent flows such as slug flow expands, and other categories of flow patterns develop at higher phase velocities, hence the neighbouring flow regime envelopes become smaller such as stratified and dispersed flow regimes. Intermittent flow regimes can be identified by conducting a PDF analysis of the real-time hold-up data. If a bi-modal distribution is present, then the flow regime is typically identified as intermittent flow. For slug flow regimes, the hold-up bi-modal peaks are more spread-out across the extremes of the hold-up limits whereas plug flow regimes are more localised. When pipelines are slightly inclined, further instabilities are formed which create a further separation of the bi-modal distribution crests. Plug flow regimes show more stability similar to that of stratified flow due to a near-zero dominant frequency, whereas slug flow regimes are consistently unstable with dominant frequencies always exceeding the stability threshold of 0.1 Hz. Slightly inclined pipe orientations at +5° create further instabilities to intermittent flow regimes, particularly to plug flow causing this formation to exceed the 0.1 Hz stability threshold. In addition, the inclination process also averts mixing between oil and water which therefore creates a more pronounced intermittent flow regime structure to develop.

# CHAPTER 5

## DEVELOPMENT OF CORRELATIONS

In this section, the data gathered from the experimental work of this study will be utilised to develop a series of new correlations that can predict liquid-liquid multiphase flow pressure and hold-up parameters. The correlations will be based on the homogeneous model, which will implement a series of additional parameters for better performance and a wider range of applicability across different systems that vary in fluid properties and pipe geometry.

### 5.1 *Pressure Gradient Correlation*

#### 5.1.1 **Examples of Current Pressure Gradient Models**

The pressure gradient correlation is based on the improvement of the homogenous flow models for liquid-liquid multiphase flow explored by Elseth (2001) and Shi, Jepson and Rhyne (2003). Both correlations express similar frictional terms:

$$\left(\frac{dP}{dL}\right)_f = \frac{f_m \rho_m v_{sm}^2}{2D} \quad (5-1)$$

as  $f_m$  is the mixture friction factor between the two liquid phases. Furthermore, the mixture variables of density, viscosity and superficial velocity are also homogenised and represented as Eqs. (2-22) - (2-24). However, the mixture friction factor is different between the two focused studies based on the mixture Reynolds number parameters. Both studies utilise the case of turbulent flow regimes where the frictional coefficient would alter the Blasius equation, as shown in Eqs. (5-2) and (5-3) in respective chronological order. As the Elseth (2001) approach has a frictional coefficient valid for  $3 \times 10^3 \leq Re_m \leq 10^5$  and the Shi, Jepson and Rhyne (2003) approach is valid for mixture Reynolds number around  $1 \times 10^5$  (Kays and Crawford, 1993; Ismail et al., 2015).

---


$$f_m = 0.316Re_m^{-0.25} \quad (5-2)$$

$$f_m = 0.079Re_m^{-0.25} \quad (5-3)$$

Additionally, the mixture Reynolds number is also represented as a homogeneous term, as previously shown in Eq. (2-25). Finally, combining all aspects of the homogeneous models, the Elseth (2001) approach considers gravitational influences exerted from pipe inclination, while the Shi, Jepson and Rhyne (2003) approach does not consider gravitational influences, as shown in Eqs. (5-4) and (5-5), respectively:

$$\frac{dP}{dL} = \left( \frac{f_m \rho_m v_{sm}^2}{2D} \right) + \rho_m g \sin(\theta) \quad (5-4)$$

$$\frac{dP}{dL} = \left( \frac{2f_m \rho_m v_{sm}^2}{D} \right) \quad (5-5)$$

The correlations were tested against the experimental pressure measured in this study, and the data was split into two categories to examine the effects of pressure across various conditions. The categories are: (1) the experiment type was used to segregate the data where oil type and pipe inclination data points are found, and (2) flow regimes were also observed to identify any noticeable effects to and/or from pressure distributions of individual flow patterns. The comparison of the two correlations can be seen in *Figure 5-1* and *Figure 5-2*. The graphs demonstrate that the two examined correlations do not perform well with high viscous oil content, by generally underestimating the pressure gradient, due to the absence of the water cut as heavier oils further dominate pipe volume due to the lower density difference between the water phase. Furthermore, Eq. (5-4) performs better at predicting systems that contain less viscous oils under inclined pipe orientations than Eq. (5-5). Indicating that the gravitational term of the equation is an important performance factor in predicting the pressure gradient accurately. Additionally, flow regimes have no noticeable effect on the change in pressure gradient, nor does the pressure effect of the flow regime itself. This can be seen from finding all flow regime types across all various experimental conditions and pressure ranges. With respect to each graph examined, the pressure strongly depends on the oil type and fluid flow across both phases. Hence, when considering the model for pressure gradient prediction, individual phase behaviour must be separately considered as well as homogenising the friction and pipe inclination factors.

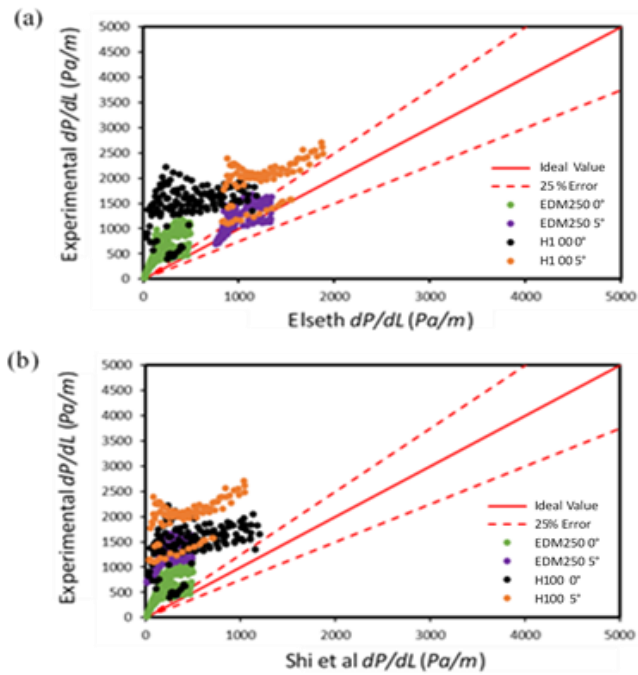


Figure 5-1: Pressure gradient correlation prediction vs measured pressure examples from (a) (Elseth, 2001) and (b) (Shi, Jepson and Rhyne, 2003). Both utilising the experimental data from this study which the data is split between the experiment type of experimental oil and pipe inclination.

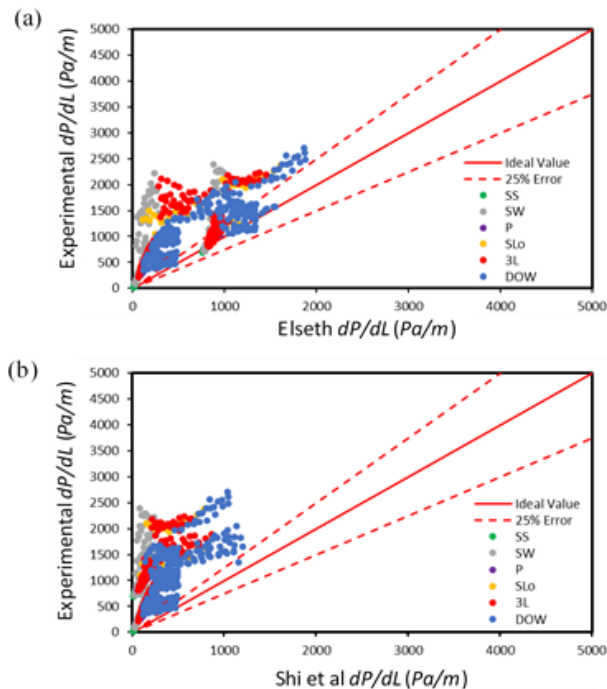


Figure 5-2: Pressure gradient correlation prediction vs measured pressure examples from (a) (Elseth, 2001) and (b) (Shi, Jepson and Rhyne, 2003). Both utilising the experimental data from this study which the data is split between flow regimes.

---

### 5.1.2 Mathematical Development of New Pressure Gradient Model

A newly proposed pressure gradient model for liquid-liquid multiphase flow will be displayed based on the Elseth (2001) correlation which will comprise of an identical formula with additional variables, which will increase the accuracy of the homogeneous model from aspects of the equation. First, the equation must satisfy the initial conditions such that as the mixture superficial velocity is equal to zero; hence the differential pressure must also be equal to zero, implying that;  $\frac{dP}{dL} = 0 \text{ Pa/m}$  for the flow condition when  $v_m = 0$ . However, Eq. (5-4) does not satisfy this condition as the effect of inclination will induce some pressure differential value. To resolve this, an additional constant and relevant fluid properties are required to be incorporated for the pipe inclination term, which will consider slip and the occupancy of each constituent phase. Along with homogenising the equation, individual oil properties will need to be incorporated without throwing the equation off balance and disrupting the homogeneous equation. In the proposed model shear stresses are considered using the single-phase friction factor equation, which in turn is developed using the average volume fraction and fluid physical properties such as viscosity and density. Hence, density and viscosity ratios are used in the equation to incorporate changes in oil properties to maintain its homogeneous aspect. Finally, a constant for each term must be implemented to widen the scope of the validity of the equation across different combinations of pipe geometry, fluid properties and fluid flow. Hence considering these three aspects, the following equation is proposed as an alternative pressure gradient correlation.

$$\frac{dP}{dL} = \left[ K_{f_m} \left( \frac{f_m \rho_m v_{sm}^2}{2D} \right) + C_w \rho_m g \sin(\theta) K_\theta \right] \left( \frac{\mu_o K_\mu}{\mu_w + \mu_o} \right) \left( \frac{\rho_o K_\rho}{\rho_w + \rho_o} \right) C_w K_{C_w} \quad (5-6)$$

$$C_w = \frac{v_{sw}}{v_{sw} + v_{so}} \quad (5-7)$$

Where;  $K_{f_m}$  is a constant for the mixture friction factor term,  $K_\theta$  is a constant for the gravitational term,  $K_\mu$  is a constant for the viscous term,  $K_\rho$  is a constant for the density term,  $C_w$  is the water cut and  $K_{C_w}$  is a constant for the water cut term. Moreover, the constants vary depending on the oil properties of a relevant system. However, the threshold between varying conditions is not dependent on a single fixed value but varies depending on the combination of flow conditions. Based on the current data that interchange between oil type and inclination, more viscous (heavy) oils develop a higher pressure gradient than that of less viscous (lighter) oils. The Reynolds number contains all mixture fluid properties and key fluid flow variables of the multiphase

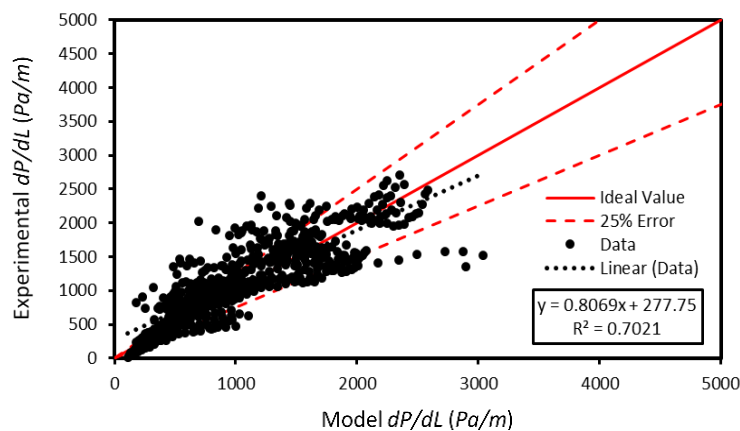
system. However, the main factor that causes pressure differences is the pipe diameter and oil viscosity; hence the following equation is developed to segregate the combined variables as:

$$\alpha_p = \frac{D}{\mu_m} \quad (5-8)$$

where,  $\alpha_p$  represents the pipe condition pressure threshold to determine if a system is under a high or low condition threshold point. When fluid properties such as viscosity and pipe geometry alter, the interactions between fluid and the pipeline would change and hence the behaviour of a respective multiphase system would also shift. As such, smaller diameter pipe systems would result in high pressure for a constant flow rate and vice versa. Additionally, fluid viscosity has a similar effect. Combining the two parameters would identify the degree to which fluid pressure is induced. With a trial and error approach and the incorporation of other work through literature, when  $\alpha_p < 1$  and  $\alpha_p > 1$  they are considered as the high and low end of the threshold pressure, respectively, and the correlation constants are as followed in *Table 5-1*. Finally, limits are implemented for the water cut towards Eq. (5-6) to maintain the conditions of multiphase flow and hence, the pressure correlation is applicable for when  $0.01 < C_w < 0.99$ . *Figure 5-3* shows the performance of the new pressure gradient correlation from the study of this work and demonstrates a strong improvement in predicting the pressure gradient at all conditions.

Pressure Type	$K_{f_m}$	$K_\theta$	$K_\mu$	$K_\rho$	$K_{C_w}$
$\alpha_p < 1$	0.04	0.8	16	20	15
$\alpha_p > 1$	3	1	10	2	20

*Table 5-1: Pressure gradient correlation constant changes between flow condition thresholds.*



*Figure 5-3: Newly proposed pressure gradient correlation vs measured pressure. All experimental data from this study is combined. Experimental uncertainty at  $\pm 10$  Pa/m.*



---

### 5.1.3 Dimensional Analysis of Pressure Gradient Model

To ensure the equation coincides with the correct mechanics and the utilised parameters are balanced to form the correct outcome of pressure gradient dimensional analysis is conducted on the proposed correlation. The analysis process first identified which parameters are dimensionless and removed from the equation. The following dimensionless terms are: (1) the constants of  $\alpha_p$  ( $K_{f_m}$ ,  $K_\theta$ ,  $K_\mu$ ,  $K_\rho$  and  $K_{C_w}$ ) (2)  $C_w$  is dimensionless by adopting superficial fluid velocity ratios between the water phase over the combined velocity between the oil and water phases and (3)  $\sin(\theta)$  (referring to a right-angle triangle) is defined as the length of the opposite length over the hypotenuse length resulting in a dimensionless term. The remaining dimensional parameters are then converted to their respective unit domains and simplified to derive the unit for pressure gradient:

$$\frac{dP}{dL} \rightarrow \left[ \left( \frac{f_m \rho_m v_{sm}^2}{2D} \right) + \rho_m g \right] \left( \frac{\mu_o}{\mu_w + \mu_o} \right) \left( \frac{\rho_o}{\rho_w + \rho_o} \right)$$

The remaining dimensional parameters are then converted to their respective unit domain:

$$\frac{dP}{dL} \rightarrow \left[ \left( \frac{(kg/m^3) \cdot (m^2/s^2)}{2m} \right) + (kg/m^3) \cdot (m^2/s^3) \right] \left( \frac{Pa \cdot s}{Pa \cdot s} \right) \left( \frac{kg/m^3}{kg/m^3} \right)$$

$$\frac{dP}{dL} \rightarrow \left( \frac{kg \cdot m^2}{2m^4 \cdot s^2} \right) + \left( \frac{kg \cdot m}{m^3 \cdot s^2} \right)$$

$$\frac{dP}{dL} \rightarrow \frac{kg \cdot m}{2s^2} \left( \frac{m}{m^4} + \frac{1}{m^3} \right)$$

$$\frac{dP}{dL} \rightarrow \frac{kg \cdot m}{m^3 s^2}$$

$$\frac{kg \cdot m}{s^2} \rightarrow N \quad \text{and} \quad N \rightarrow Pa/m^2$$

$$\therefore \frac{dP}{dL} \rightarrow Pa/m$$

Hence, the proposed correlation is valid for use and suitable to predict pressure gradients for multiphase flow systems at various pipe dimensions and flow conditions.

### 5.1.4 Pressure Gradient Model Comparison in Literature

The following liquid-liquid flow experiments from literature are used to compare the performance of the pressure gradient correlation. The following experiments all vary between oil properties, pipe inclination and pipe diameter to examine the accuracy range of the model across different experiments. The following experiments that have been used for comparison are; Chakrabarti, Das and Ray (2005); Vielma et al. (2008); Atmaca et al. (2009); and Vuong et al. (2009). Table 5-2 shows all the key pipe variables and fluid properties from each experiment.

Experiment	$\theta$ ( $^{\circ}$ )	$\rho_o$ ( $kg/m^3$ )	$\mu_o$ ( $Pa.s$ )	$D$ (m)
Chakrabarti et al. (2005)	0	787	$1.2 \times 10^{-3}$	0.0254
Vielma et al. (2008)	0	860	$1.8 \times 10^{-2}$	0.0508
Vuong et al. (2009)	0	884	1.07	0.0508
Atmaca et al. (2009)	2	850	$1.5 \times 10^{-2}$	0.0508

Table 5-2: Key pipe variables and fluid properties from experiments of (Chakrabarti, Das and Ray, 2005; Vielma et al., 2008; Atmaca et al., 2009; Vuong et al., 2009).

As shown in Figure 5-4 and Figure 5-5, the results for the newly proposed pressure gradient developed from this study and pressure gradient models from (Elseth, 2001) and (Shi, Jepson and Rhyne, 2003) are respectively presented. Similar to the experimental results of the studied work, the homogeneous models from literature underestimate the true pressure value of a liquid-liquid multiphase flow system because the interaction between fluid types and pipe geometry is not considered. Additionally, the newly developed pressure gradient performs well under a wide combination of fluid properties and pipeline variables.

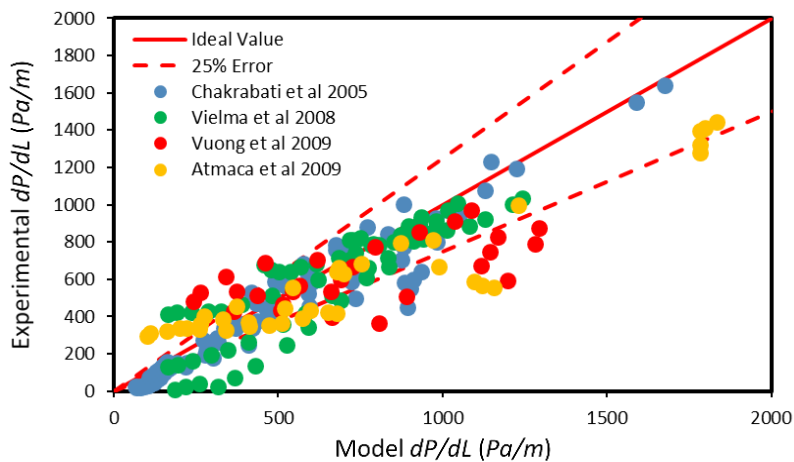


Figure 5-4: Newly proposed pressure gradient correlation vs measured pressure. Experimental data and measured pressure split between (Chakrabarti, Das and Ray, 2005; Vielma et al., 2008; Atmaca et al., 2009; Vuong et al., 2009).

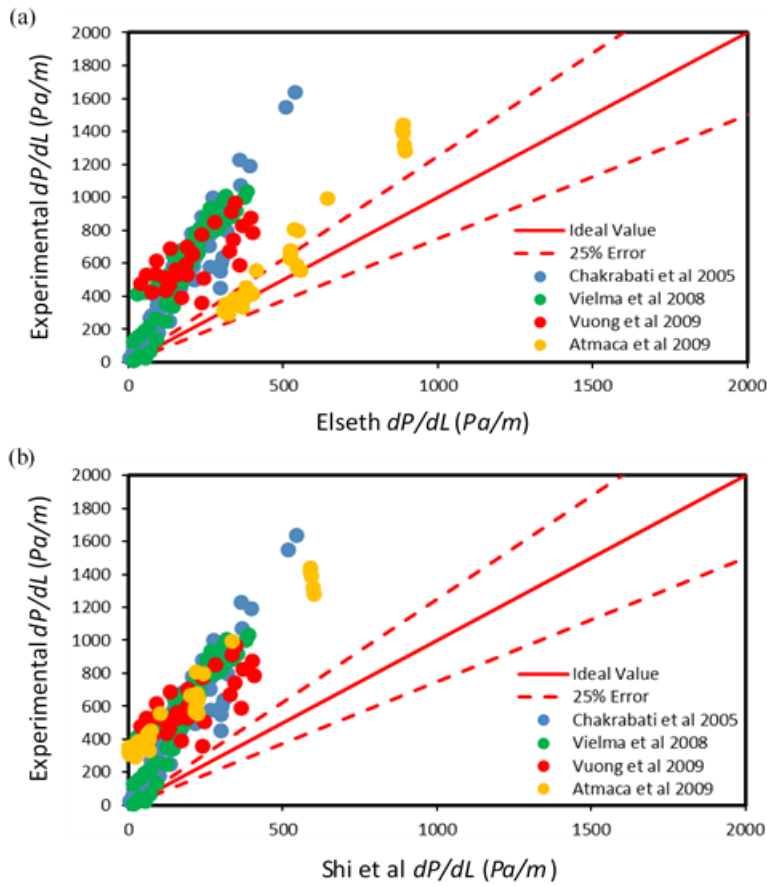


Figure 5-5: (a) (Elseth, 2001) pressure gradient correlation and (b) (Shi, Jepson and Rhyne, 2003) pressure gradient correlation vs measured pressure. Experimental data and measured pressure split between (Chakrabarti, Das and Ray, 2005; Vielma et al., 2008; Atmaca et al., 2009; Vuong et al., 2009).

## 5.2 Hold-up Prediction

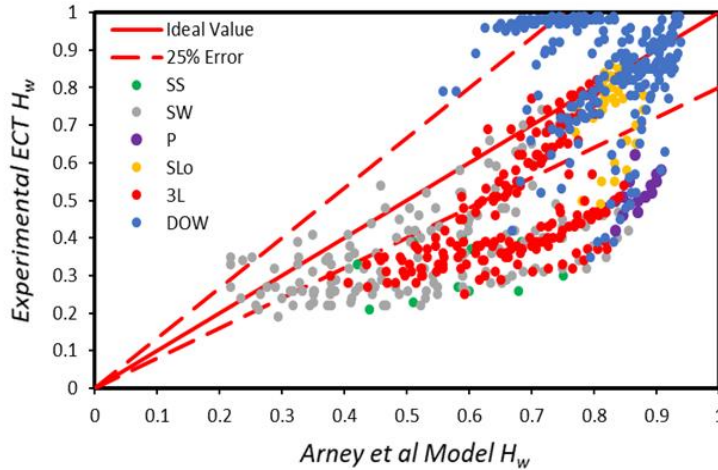
### 5.2.1 Example of Current Hold-up Model

Hold-up correlations are generally formed by ratios between separate phase velocities, volumes or flowrates. One distinct example from literature is the hold-up prediction from Arney et al. (1996), where the water cut from Eq. (5-7) is utilised across a parabolic platform as shown in Eq. (5-9):

$$H_w = C_w [1 + 0.35(1 - C_w)] \quad (5-9)$$

However, typical hold-up correlations do not consider the other key multiphase flow attributes such as pipe geometry and fluid properties. Similar to that of the pressure gradient analysis in section 5.1, the hold-up correlations are assessed based on the accuracy of experimental results.

In the case of the hold-up analysis, the ECT data is used for each individual flow condition. *Figure 5-6* shows this study's experimental data and the Arney et al. (1996) correlation.



*Figure 5-6: Water hold-up correlation from (Arney et al., 1996) vs measured water hold-up. All experimental data from this study is separated into flow regimes.*

The results show that the Arney et al. (1996) correlation at lower water hold-up (or lower superficial velocity combinations) for a dual-incompressible flow system does not perform well. This is considered for flow regimes such as stratified and intermittent flows. However, dispersed flow regimes seem to work generally better, which include regions of flow regimes that neighbour dispersed flow around the constituent transition boundary, such as slug and three-layered flow. This is because the trend of the correlation acts exponentially. Implying that flow regimes which are formed at higher combinations of superficial velocities are typically more accurate. Therefore, the accuracy of the hold-up diminishes as the mixture flowrate decreases.

### 5.2.2 Mathematical Development of New Hold-up Model

Similar to that of the newly developed pressure gradient correlation, the newly proposed hold-up analysis is developed from other correlations in literature. In this case, Arney et al. (1996) is utilised. However, the difference between this approach is the manner in which the formula's overall structure is initially developed. The overall trend of the data gathered from the experiments conducted in this study are subjected to Eq. (5-9) for trend analysis. As shown in *Figure 5-7*, the real ECT hold-up data against the Arney et al. (1996) correlation is reconstructed to evaluate the data across a wide range of variable combinations of all experimental conditions. It was found that the best fit for the overall data series was an exponential formation.

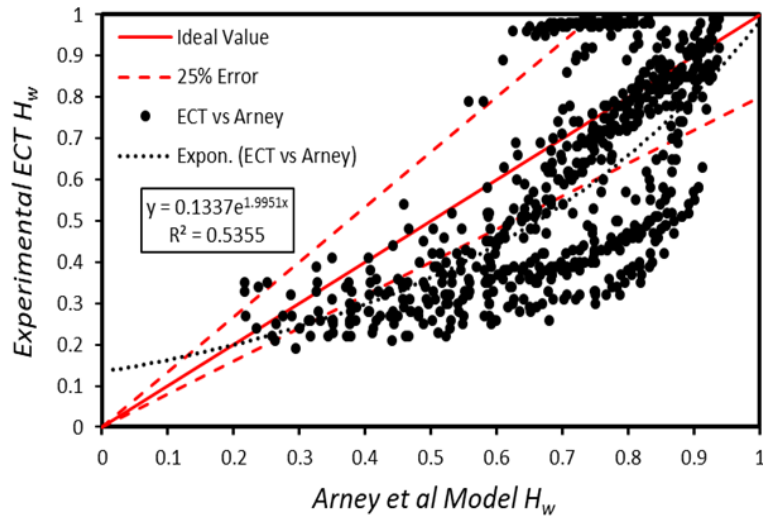


Figure 5-7: Water hold-up correlation from (Arney et al., 1996) vs measured ECT water hold-up. All experimental data from this study is combined.

Pipe inclination, fluid viscosity, fluid density and flowrates must all be incorporated within the new equation to be applicable for a larger range of fluid liquid-liquid flow system combinations. However, as hold-up values are normalised dimensionless parameters, in order to fulfil a balanced equation, four aspects must be considered. (1) It is essential that the equation utilises ratios for fluid properties between the corresponding phases and the hydrodynamic forces induced upon the phases. This is because the most influential parameter towards the hold-up must be present within the exponential term of the formula. The two most dominant parameters for the hold-up are the phase density differential between the two constituent fluids as this determines the interface between the two fluids during segregation, while the phase velocity determines the degree each phase enters and travels through the pipe, altering the hold-up accordingly which can be determined through the water cut.

$$H_w \rightarrow \left( \frac{\mu_o}{\mu_w + \mu_o} \right) e^{\left( \frac{C_w \rho_w \sqrt{\frac{\rho_o}{\rho_w - \rho_o}}}{\rho_o} \right)}$$

(2) As the hold-up parameter is based on a normalised 2D construction, length-based parameters such as pipe geometry (e.g. pipe length and diameter sizes) are not considered to be part of the equation. (3) Pipe inclinations can be incorporated but must be valid to be applicable to limits for when there is no inclination to not force the correlation to zero.

$$H_w \rightarrow [1 - \sin(\theta)] \left( \frac{\mu_o}{\mu_w + \mu_o} \right) e^{\left( \frac{C_w \rho_w \sqrt{\frac{\rho_o}{\rho_w - \rho_o}}}{\rho_o} \right)}$$

(4) Additional constants for each term must be incorporated similar to that of the pressure gradient to balance the equation under different conditions. Hence, considering these points in constructing the hold-up correlation for liquid-liquid multiphase flow, the model is as follows:

$$H_w = K_{H_w} [1 - \sin(\theta) K_\theta] \left( \frac{\mu_o K_\mu}{\mu_w + \mu_o} \right) e^{\left( \frac{C_w \rho_w \sqrt{\frac{\rho_o}{\rho_w - \rho_o}}}{\rho_o K_\rho} \right)} \quad (5-10)$$

where;  $K_{H_w}$  is the water hold-up constant. With a similar approach as the pressure gradient correlation, the constants are interchangeable due to the equation being subject to inaccuracy at various lower flowrate conditions, which cause different levels of mixing as the dual-liquid phases such as oil and water are miscible. Hence, Eq. (5-11) is used to determine what condition of mixing the system is under based on key fluid property ratios of density and viscosity, along with the superficial velocity ratio between oil and water. The correlation must maintain the condition of multiphase flow and hence, the pressure correlation is applicable for when  $0.01 < C_w < 0.99$ .

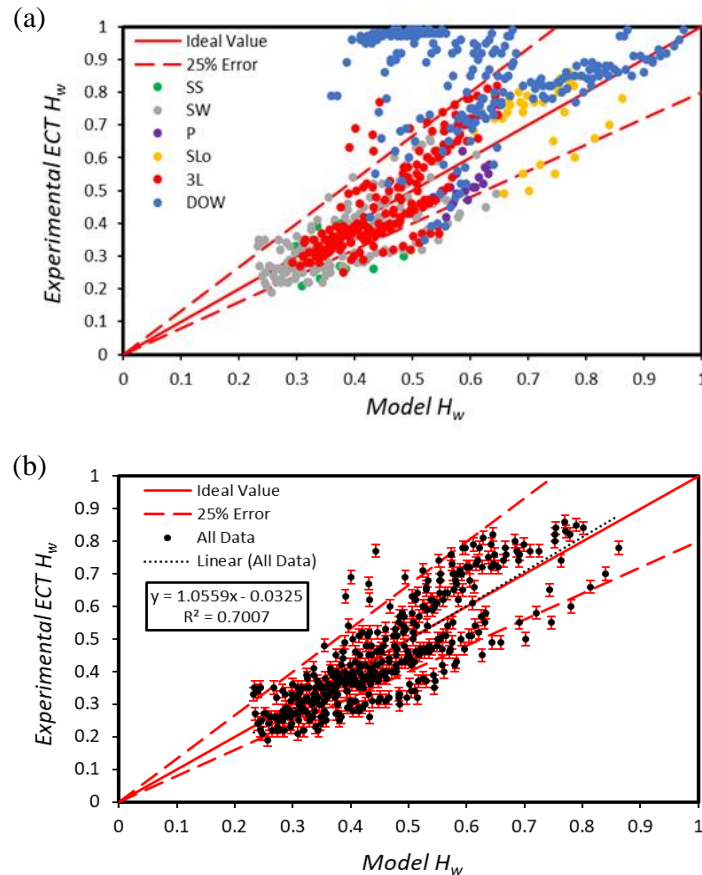
$$\alpha_{H_w} = \frac{v_{sw} \rho_w \mu_w}{v_{so} \rho_o \mu_o} \quad (5-11)$$

where;  $\alpha_{H_w}$  is considered, the hold-up mixing ratio between the two constituent liquid phases of the oil-water multiphase flow system. For when  $\alpha_{H_w} \geq 0.04$  the multiphase flow is under a high mixing while  $\alpha_{H_w} < 0.04$  results in a lower form of mixing. As a result, the hold-up correlation constants change accordingly, as shown in *Table 5-3*. However, one main limitation of the mixing analysis is, if the oil density is far greater than the water density, the equation will not be able to accurately distinguish between the mixing types. Additionally, a further condition must be implemented where the mixing equation is not applicable at  $\mu_o \gg \mu_w$  typically in two orders of magnitude greater.

Mixing Condition	$K_{H_w}$	$K_\theta$	$K_\mu$	$K_\rho$
$\alpha_{H_w} \geq 0.04$	0.081	0.1	2.6	1.8
$\alpha_{H_w} < 0.04$	0.045	0.1	1.4	0.5

*Table 5-3: Water hold-up correlation constant changes between mixing conditions.*

Similarly to that of Eq. (5-6), limits are again implemented for the water cut towards Eq. (5-10) to maintain the conditions of multiphase flow and hence, the hold-up correlation is applicable for when  $0.01 < C_w < 0.99$ . Based on the newly proposed correlation, the data developed from this experimental study is subject to the new correlation for analysing the degree of accuracy for predicting liquid-liquid hold-up, as demonstrated in *Figure 5-8*.



*Figure 5-8: Newly proposed hold-up correlation vs measured ECT hold-up. (a) Experimental data from this study are segregated based on flow regimes and (b) experimental data is combined while excluding the exception of the DOW data. Experimental uncertainty of absolute hold-up at  $\pm 0.02$ .*

The results strongly suggest a significant improvement in predicting oil-water hold-up. However, in some cases, the dispersed flow regime ECT data is not considered to be accurate because the ECT sensors will not be able to measure the small droplet formations, which results in overestimating the water hold-up. Hence, the newly developed hold-up correlation can be considered accurate for dispersed flow regimes when considering combinations of the limitations from the experimental set-up and the resulting data. Overall, with the exception of dispersed flow, the newly proposed hold-up correlation performs consistently well with other flow regimes such as stratified flow, intermittent flow and three-layered flow.

### 5.2.3 Hold-up Comparison in Literature

Similarly to assessing the pressure gradient correlation, measures hold-up data (which is not calculated from other correlation sources, but rather experimental-based measurements are used. The experiments that will be used to test the correlation are the same data from the studies used in the pressure gradient comparison. The following experiments that have been used for the hold-up comparison are; (Vielma et al., 2008; Atmaca et al., 2009; Vuong et al., 2009). Figure 5-9 shows the correlation performance of the experimental data while also demonstrating the comparison of the Arney et al. (1996) approach.

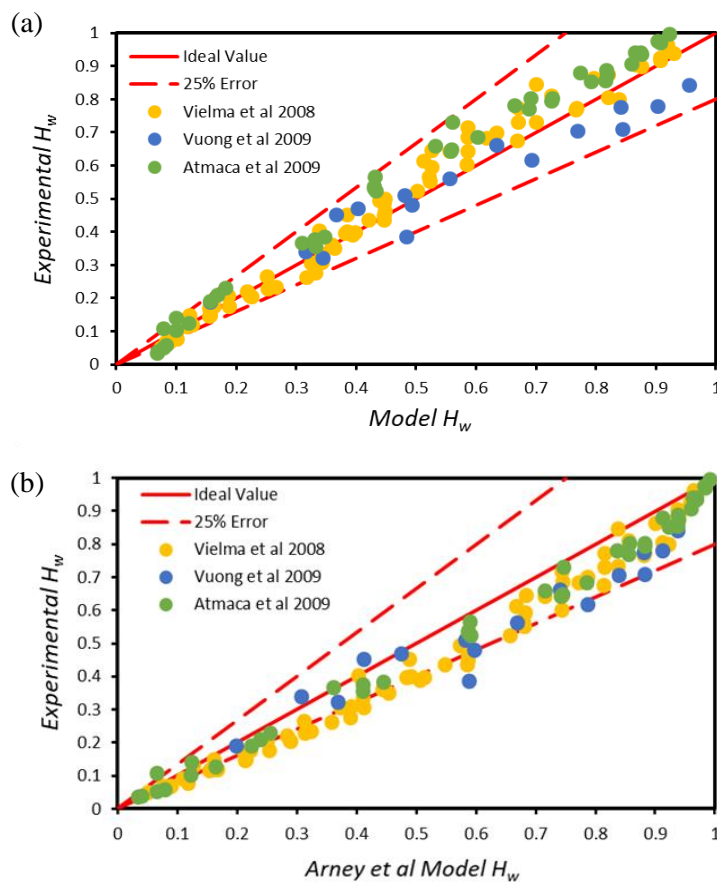


Figure 5-9: (a) Newly proposed hold-up correlation vs experimentally measured hold-up and (b) (Arney et al., 1996) hold-up correlation vs experimentally measured hold-up. Experimental data and measured hold-up arranged between (Vielma et al., 2008; Atmaca et al., 2009; Vuong et al., 2009).

Based on the correlation comparisons between this work and that of the Arney et al. (1996) approach, it is clearly shown that the newly proposed hold-up correlation analysis works extremely well for a wide range of oil property combinations, as well as slightly induced pipe inclinations. In addition, the Arney et al. (1996) approach also performed well in the cases of the



---

respective studies utilised for this analysis but still demonstrates its limitations where the approach can accurately predict hold-up values at high and low extremes of the normalised distribution; an example such as for when  $0.1 < H_w < 0.9$ . Hence, the Arney et al. (1996) correlation still overestimates the hold-up values between the extremes. The newly proposed correlation eliminates this factor when incorporating the correct trend type into the model.

### ***5.3 Correlation Limitations***

The correlation limitations for the newly proposed pressure gradient and hold-up are similar due to both incorporating identical variable terms, as each respective variable is dedicated to a specific degree of equation dominance. There are five key limitations of the newly proposed correlations. (1) The correlation cannot accurately predict multiphase flow in microtubes or porous media. This is because the physics behind micro-fluidics is mainly found under laminar flow conditions, which will result in very small values for the Reynolds number throwing friction factor values off because the main dominating force for micro-channels is the surface tension. The correlation pairs do not include surface tension within the formulae mainly because when considering pipelines at a macro-scale, the surface tensions between the fluids and inner pipe walls are considered negligible. (2) The correlations may not be able to work accurately under very low flowrates. This is because when the mixture flowrate is low enough to the degree that the pressure and hold-up will have no significant difference to when the system is stationary, which may result in inaccurate predictions. This is because the gravitational force during this period is much greater than the inertial forces and will result in an imbalanced assessment of variables for the correlations. (3) Very heavy oils can not be accurately measured for pressure gradient and hold-up because it would far exceed the water property base values creating irregular ratios between density and viscosity, which will cause the constant selection equations to be inaccurate, hindering the performance of the correlations. (4) When a multiphase flow system is found to have a pressure or hold-up threshold point that is very close or equal to 1 or 0.04 respectively, the accuracy of the correlations can be questioned. This is because the correlation thresholds only consider the major parameters of a multiphase flow system to group a system accordingly to utilise the respective constants. However, if the forces acting upon the less dominant phases such as pipe roughness and interfacial tension can shift the system between threshold conditions. (5) Finally, the degree of inclination on the accuracy of the models is unknown despite slightly inclined pipes being considered no greater than  $5^\circ$  from the horizontal. However, downward pipe inclinations cannot be accurately used because the changes in significant gravitational dominance are not considered.

# CHAPTER 6

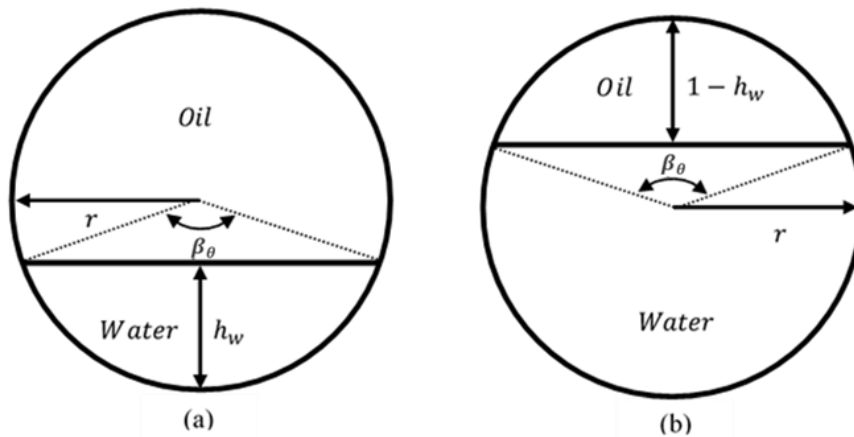
## DIMENSIONLESS GROUPING

### ***6.1 Mathematical Development of Grouping Model***

One of the many new developments carried out to grasp an improved understanding of multiphase flow is the grouping of flow regimes to develop better predictions of mapping sequences through dimensionless analysis rather than utilising conventionally measured parameters such as phase velocity and/or other dimensional parameters. Such an approach can better predict and identify possible developments of different flow regimes under a vast range of multiphase configurations by simultaneously grouping multiple forces involved in a particular multiphase system. This work will focus on the dimensional analysis of the liquid-liquid multiphase flow correspondence to the Froude number by assessing a newly proposed approach to use this dimensionless set-up by allowing the equation to fully segregate the constituent phases. The Froude number is not commonly used to quantify the state of an oil-water system through dimensionless analysis (McKibben, Gillies and Shook, 2000a). However, this allows for the individual phases to be assessed in terms of separate phase dynamics, such as superficial velocity and density while incorporating the effects of the gravitational forces between the two phases.

Initially developed by Zapke and Kröger (2000) for analysing gas-liquid flow, two separate Froude numbers are identified based on the conditions of the individual phases and are graphically combined. It can also be adapted to utilise dual incompressible flow. In the case of oil-water flows, as previously shown, the Froude numbers are expressed in Eqs. (2-73) and (2-74). Evaluating both Froude numbers, when considering the current state of  $Fr_o$  and  $Fr_w$ , their purpose is to assess both phases separately. However, the diameter, in this case, is considered equal, yet each phase does not occupy the entire pipeline, nor does it rarely occupy the same amount of volume. Hence, the hydraulic diameter of both fluids are used in place of the internal pipe diameter. The hydraulic diameter varies depending on the height of the fluid interface between

the top and bottom walls of the pipeline, where the phase of interest surrounds the section of the pipe. Since the Froude number is the dimensionless ratio of the inertial forces over the gravitational forces, it would be the optimal dimensionless parameter to incorporate the hydraulic diameter to develop the dimensionless grouping analysis. Utilising other dimensionless parameters such as the Reynolds number which is the inertial forces over the viscous forces would limit the grouping analysis to not consider fluid phase segregation which is a major aspect of the hydraulic diameter. *Figure 6-1* shows examples of oil and water under different levels of phase occupancy of the entire pipe cross-section and hence the wetted perimeter. Incorporating the perimeter and the cross-sectional area of the pipe for the assessment of individual phase diameters in contrast to only using the actual pipe diameter has the advantage of fully segregating each constituent fluid for its analysis while having the proportions to maintain the conservation of momentum. Two conditions are considered during the flow of both oil and water because the approach of exploiting the hydraulic diameter alters under different fluid levels. Using the water as the initial reference fluid, the conditions are considered to be (1) when the reference fluid occupies less than half of the area of the pipe cross-section and (2) when the reference fluid is equal to or greater than half the area of the pipe cross-section.



*Figure 6-1: Hydraulic diameter cross-section examples (a) the heavier fluid (water) occupies less than half of the pipe as the lighter fluid contains the rest of the remaining area (b) the heavier fluid (water) equals or more than half-filled in the pipe as the lighter fluid (oil) contains the rest of the area.*

The hydraulic diameter for a given cross-section of a circular pipe is expressed as the area over the perimeter where the fluid occupies the space in the pipe.

$$D_H = \frac{4A_{\alpha\beta}}{p_{\alpha\beta}} \quad (6-1)$$

---

Where  $D_H$  is the hydraulic diameter and  $p_{\alpha\beta}$  is the respective perimeter of the phase. Starting with the initial condition of the water-oil interface to be lower than half of the pipe. The area and perimeter used to estimate the hydraulic diameter are respectively defined as:

$$A_{\alpha\beta} = \frac{r^2[\beta_\theta - \sin(\beta_\theta)]}{2} \quad (6-2)$$

$$p_w = r\beta_\theta \quad (6-3)$$

Where,  $\beta_\theta$  is the angle from the centre point of the pipe which forms between the endpoints of the multiphase interface and is always expressed as:

$$\beta_\theta = 2 \cos^{-1} \left( \frac{r - h_w}{r} \right) \quad (6-4)$$

where  $h_w$  is the height of the reference phase between the bottom of the pipe and the interface (in this case, water) and  $r$  is the inner pipeline radius. When considering the way at which the height of the fluid is assessed, under lower flowrates of laminar conditions, the height can be translated from hold-up values which occupy the pipe cross-section by incorporating the diameter.

$$h_w = DH_w \quad (6-5)$$

Considering when the water-oil interface is equal to or above half of the pipe midsection, the following expressions for the area and perimeter are respectively:

$$A = \pi r^2 - \frac{r^2[\beta_\theta - \sin(\beta_\theta)]}{2} \quad (6-6)$$

$$p_w = 2\pi r - r\beta_\theta \quad (6-7)$$

Hence, combining Eqs. (6-1) - (6-5), the reference modified Froude numbers for complete separate assessment of only water in a multiphase flow system is:

$$Fr_{wn} = \frac{v_{sw} \sqrt{\rho_w \cos^{-1} \left( \frac{r - DH_w}{r} \right)}}{\sqrt{4\Delta\rho gr \left\{ 2 \cos^{-1} \left[ \frac{r - DH_w}{r} \right] - \sin \left[ 2 \cos^{-1} \left( \frac{r - DH_w}{r} \right) \right] \right\}}} \quad (6-8)$$

To assess the oil phase, Eqs. (6-6) and (6-7) are used in place of Eqs. (6-2) and (6-3), respectively, as in this case, the oil phase occupies equally or more than half the cross-sectional area.

$$Fr_{on} = \frac{v_{so} \sqrt{\rho_o \left[ \pi - \cos^{-1} \left( \frac{r - DH_w}{r} \right) \right]}}{\sqrt{\Delta \rho g r \left\{ 2\pi - \left\{ 2 \cos^{-1} \left[ \frac{r - DH_w}{r} \right] - \sin \left[ 2 \cos^{-1} \left( \frac{r - DH_w}{r} \right) \right] \right\} \right\}}} \quad (6-9)$$

When the interface is equal to or above the midpoint of the pipe, Eqs. (6-8) and (6-9) are interchanged between the modified Froude numbers for oil and water,  $Fr_{on}$  and  $Fr_{wn}$  respectively.

## 6.2 Grouping Experimental Data

Figure 6-2 shows the implementation of the modified Froude number against the experimental data from this work. The analysis is split between the experiments with only horizontal pipe orientation and a combination of all data, which include inclined pipe orientation. This was done to observe the effects of the test section inclination and if the newly proposed method applies to inclined multiphase flow systems. The results of the compiled experimental data sequences show that the modified Froude number can generally execute good flow regimes grouping stratified, three-layered, intermittent and dispersed flows of an oil-water multiphase system for up to medium-heavy oil types ( $\rho_o \ll \rho_w$ ). This is strongly supported by the estimated transition boundaries containing a large majority of each flow regime experimental data point within their respective regions. With regards to other flow regime data points that do not comply with the estimated boundary positions, it can be suggested that these flow regimes are a result of either being under the transition between two flow regimes or the flow regimes not being considered into sub-categories and have been grouped generally such as stratified flows.

Regardless of the different conditions between the results found from each study, there is a clear transition boundary between the neighbouring flow regimes. This indicates that the modified Froude number can be used to aid in identifying flow regimes between constituent transition boundaries rather than relying upon the conventional subjective methods based on observation and probability grouping techniques, particularly within the regions of transition. However, incorporating inclined data does have some drawbacks within the transition regions, particularly between intermittent and three-layered flow regimes. For example, in the region  $Fr_{on} = 0.2 - 0.9$  and  $Fr_{wn} = 0.8 - 3$  significant overlapping occurs within areas of intermittent flow from the three-layered regimes from the EDM250 oil experiment for a  $5^\circ$  pipe incline. This effect is mostly found within a localised section in which other flow regime points also exist.

Indicating that the region previously stated within the dimensionless log-scaled Froude chart is a converging point where intermittent flow is connected through a four-way boundary layer.

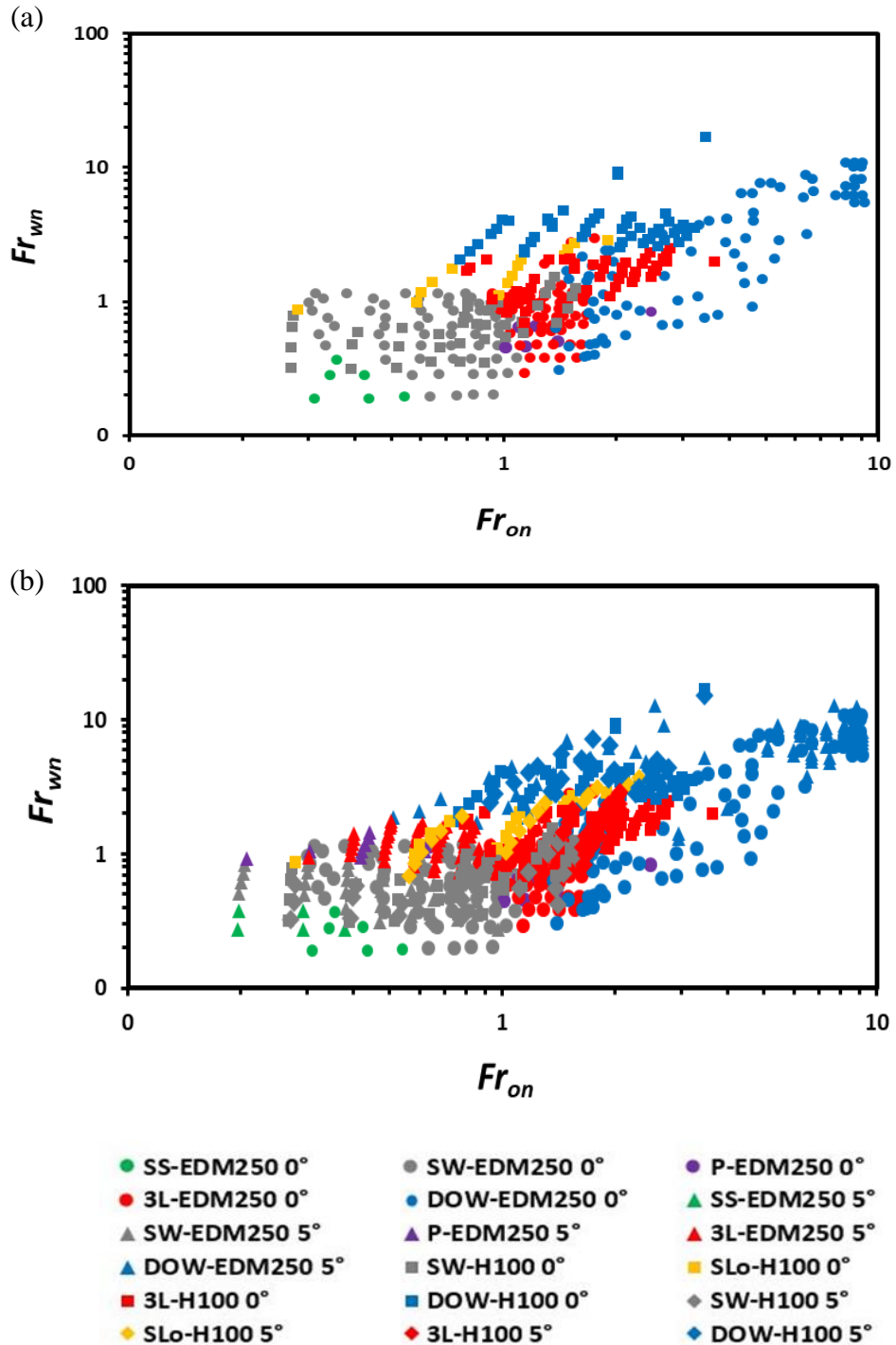
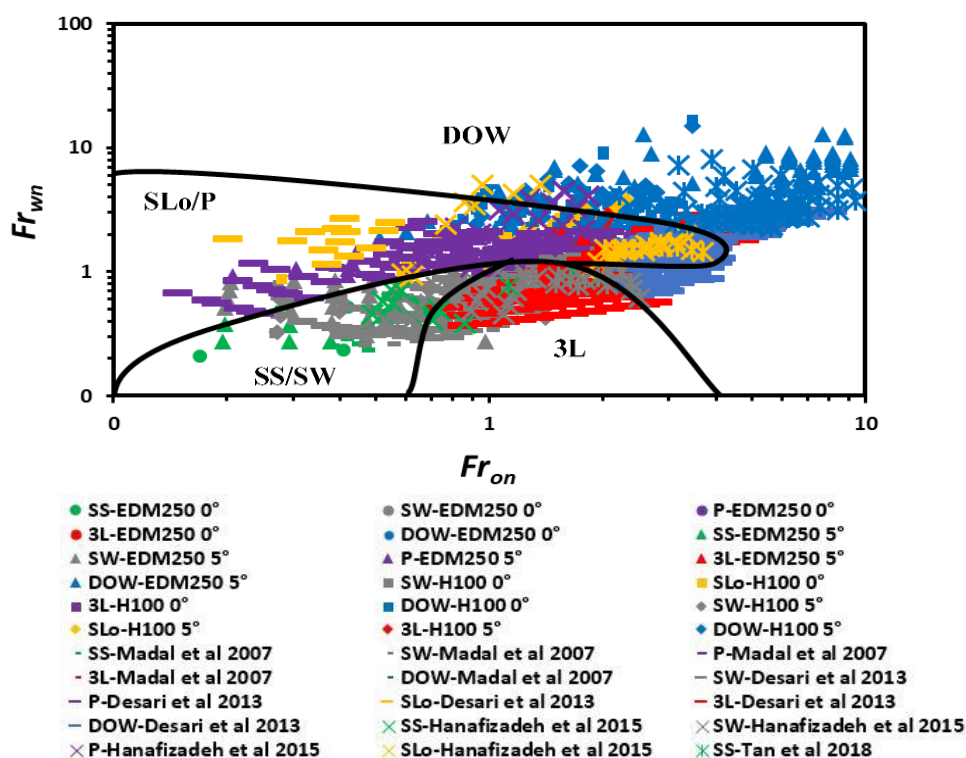


Figure 6-2: Modified Froude number grouping comparison between (a) only 0° inclined experimental data from this study and (b) all experimental data from this study. Intermittent flows are plugs (P) and Slugs (SLo).

### 6.3 Grouping Literature Data

The newly proposed liquid-liquid flow regimes grouping model will now be tested against other suitable data from literature. The experiments are selected based on data availability, experiment type diversity and the presence of intermittent flow. Furthermore, constituent boundary flow regimes are also added to the data set to ensure that a wider scale is considered and tested. Only non-inclined (horizontal) experimental data was used due to the lack of data availability of inclined pipe experiments from literature. The experiments from literature that have been utilised and superimposed on the experimental data from this work are; Mandal, Chakrabarti and Das (2007); Hanafizadeh, Hojati and Karimi (2015); and Tan et al. (2018). All key experimental data properties and details for each studying can be revisited in section 2.8.4 *Table 2-3*. *Figure 6-3* exhibits the final flow regime group mapping of the modified Froude number analysis.



*Figure 6-3: Modified Froude number grouping comparison between experiments by (Mandal, Chakrabarti and Das, 2007; Hanafizadeh, Hojati and Karimi, 2015; Tan et al., 2018) and this study, focusing on pipe internal diameter sizes between 0.012m and 0.0254m.*

The overall results suggest that the modified Froude number can segregate key flow regime types across a wide range of experimental systems within small pipe diameters between 0.012m and 0.0254m. The implemented boundary layers clarify the segregation occurring between each flow regime. Additionally, as stated in section 6.2, there is a clear four-way boundary between (1) stratified, (2) intermittent, (3) three-layered and (4) dispersed flow regimes. It is also noticeable

---

that some flow regime points intrude into the constituent neighbouring flow regime envelope, which can be explained through multiple factors such as (1) the flow regime is identified incorrectly under a transitioning state, (2) limitations of the modified Froude number of not being able to group inclined pipeline data from certain flow regimes accurately (from this experiment), (3) a combination of data errors such as anomalies, calibration and slight mismeasurement of key variables such as superficial phase velocity, oil properties causing the data points to marginally deviate accordingly.

Despite intermittent flow being a very uncommon flow regime and difficult to identify, the intermittent phase boundary envelope stretches across a wide range of oil and water Froude number parameters from various published studies which show a consistent connection within the constituent flow regime envelope. Hence, this strongly proves the existence of dual-incompressible intermittent flow regimes such that plug and slug flow and transition between with other conventional flow patterns. When considering pipe design, the chart can be used as an initial estimate to predict the probable condition to when an undesired flow regime can develop. For example, if the fluid properties are known, a desired hold-up is set according to the respective correlation and a constant target superficial velocity is established, the correct pipe diameter can be selected accordingly.

## 6.4 Grouping Limitations

The key assumption made while applying the hydraulic diameter to the Froude number is that the fluids are to be fully segregated under a non-mixed state. Furthermore, the newly proposed Froude number is still applicable for flow regimes with more dynamic interfaces with a small degree of mixing occurring, such as wavy stratified flow or three-layered flow. This is because the hold-up that was integrated to represent the height acts as an averaging factor, yet the curved surface tension is not accounted for. However, in contrast to using this approach with other more unstable flow regimes, such as dispersed flow, the modified Froude number may be limited due to the absence of a well-pronounced interface. Other limitations that can be found are the presence of other oil-water flow parameters such as test oil type, where flow regimes such as core-annular flow may only be identified when the multiphase system contains very heavy to extra heavy oils ( $\rho_o \geq \rho_w$ ) which fluctuates in the hydrodynamic configuration, leading to different transition boundaries. Similar to the statements made in section 5.3, the modified Froude number is also limited to not functioning under smaller pipe formations. Additionally, larger diameter pipes may not be applicable because flow regimes become more unstable in larger diameter pipes and tend to show more dispersed flow characteristics.



# CHAPTER 7

## SCALE-UP ANALYSIS

### *7.1 Scale-Up Methodology*

Scaling is a process in which known data of a system of some size is utilised to predict unknown data from a similar system of a larger or smaller scale. In the case of this study, the scaling direction will be of a scale-up approach to assess and predict the developments of liquid-liquid multiphase flow in multiple larger pipe diameters to that of the experimental 1-inch data gathered from this work. Hence, dimensionless analysis is needed to scale the two size contrasting systems in accordance with the known data. However, even in literature, limited studies have successfully applied dimensionless analysis to multiphase flow because of the vast variety of dimensionless groups that can be created while combining a series of key parameters in an unlimited number of ways. This is particularly the case for the scale-up methods because the multiphase flow correlation-based models have been very limited and therefore inaccurate to use across larger scales due to inadequate or unidentified extrapolation properties.

There are some methods, particularly for gas-liquid flows of dimensionless analysis, such as the Buckingham Pi theorem, the synthesis method, the matrix method and Rayleigh's method. All presented methods are explained in more detail by Sharp (1981). Utilising the Buckingham (1914) approach, the Pi theorem for defining dimensionless parameters outlines dimensional homogeneity to be satisfied by some physical process (in this case, dual incompressible fluid flow) involving a series of constituent independent and dependent variables of some quantity. Hence, the process can be reduced to a series of dimensionless parameters. There are three fundamental requirements for scaling to be successfully achieved where the larger and small system sizes must abide by similar conditions: (1) The two systems for scaling comparisons, one being the known model and the other as the scaled prototype, must have satisfied geometric similarities, such that selection coordinates between the two relevant systems for scaling, both

---

must possess the same length-scale ratio. (2) Since the model and the scaled prototype must have the same length scale, the two systems must also have the same time-scale ratio. This will therefore result in the same kinematic consideration (Langhaar, 1951), which would therefore require the phase velocities to be scaled accordingly. (3) Finally, dynamic considerations are similar when considering all variables that vary with time between motion, forces and material/fluid properties. Hence the model against the prototype scale has satisfied all time-scale, length-scale and force/mass-scale ratio similarities.

When considering that in long-distance transportation of oil and water, the thermodynamic influences associated have no significant effect on the hydrodynamic forces upon the multiphase flow system; hence, this study will only focus on the hydrodynamic effects of multiphase flow and will not take into account heat transfer as it is considered negligible. However, temperature and pressure-dependent parameters such as density and viscosity are still included in the scale-up process. When an oil-water multiphase system is fully developed and under a steady-state condition while the pipe is inclined, there are 11 main variables to consider, which can be segregated under three conditions:

- i. Pipe properties (three variables): Internal pipe diameter, roughness and inclination.
- ii. Fluid properties of oil and water (six variables): Density and viscosity of both oil and water. The interfacial tension between the phases and the internal wall of the pipe.
- iii. Applied kinematic forces (two variables): Superficial velocities of oil and water.

In contrast, other variables can be considered in the dimensionless scaling approach, such as pipeline wall wetting and various surface chemical properties. However, these specific variables are not considered part of the scaling analysis because they are uncommonly used in dimensionless analysis. Furthermore, its individual analysis may vary depending on different systems, which would unnecessarily overcomplicate the scaling process between multiple systems. The Buckingham Pi theorem states that the number of dimensionless parameters is equal to the number of main variables minus the three independent variables which are time, length and mass. Thus, since there are 11 main variables and 3 independent variables, a total of 8 dimensionless variables can be used for scaling. In addition, for theoretical perfect scaling, all dimensionless parameters must be incorporated. However, attempting to match all dimensionless parameters is extremely difficult because of the operational limitations within flow loops and industrial pipelines (Farokhpoor et al., 2020). Hence, the main idea is to conduct a process of

---

elimination to determine which parameters must be maintained as the most influential variable while neglecting less significant parameters to simplify the scaling process. The following scaling process was developed on the basis of gas-liquid multiphase flow. However, liquid-liquid flows would also be applicable to be used if not better suited for accuracy because of the incompressibility between the two test fluids. Inferring that pressure would not be an important factor in the hold-up alterations when pipe diameters change and can be directly normalised. Hence, dimensionless scale-up analysis can be separately conducted between pressure, hold-up and flow regimes for each scaled model. The scale-up rules and inputs for the following dimensionless parameters are considered:

- 1) The test section inclination angle is an important part of altering flow regimes with respect to comparing the scaled pipe orientation similarities.
- 2) The density ratio between oil and water ( $r_\rho$ ) must also be considered, as shown:

$$r_\rho = \frac{\rho_o}{\rho_w} \quad (7-1)$$

- 3) Hydrodynamic modelling is needed to be preserved as this is the most important parameter in the multiphase flow system. Since gravity also plays a key role in the system hydrodynamics, the most optimum method is to use the Froude number. It is assumed that the squared Froude number, as shown in Eq. (7-2), where the scaled target value of the superficial oil velocity can be extrapolated by equating the dimensionless Froude parameters between the experimental data and the prototype model.

$$Fr_o^2 = \frac{\rho_o v_{so}^2}{(\rho_w - \rho_o)gD} = \frac{r_\rho v_{so}^2}{(1 - r_\rho)gD} \quad (7-2)$$

- 4) The superficial velocity ratio ( $r_{v_{sw}}$ ) between oil and water, as shown in Eq. (7-3), is needed to identify the kinematic comparisons between the systems under the scale-up analysis. This is combined with point (3) to find the scaled target value of the superficial water velocity accordingly.

$$r_{v_{sw}} = \frac{v_{sw}}{v_{so}} \quad (7-3)$$

- 
- 5) As the target values for the water and oil superficial velocities are found, the inverse Reynolds number for oil and water ( $Re_o^{-1}$  and  $Re_w^{-1}$ , respectively) can now be used to identify the individually scaled phase viscosities for oil and water accordingly, as shown in Eqs. (7-4) and (7-5) respectively.

$$Re_o^{-1} = \frac{\mu_o}{\rho_o v_{so} D} \quad (7-4)$$

$$Re_w^{-1} = \frac{\mu_w}{\rho_w v_{sw} D} \quad (7-5)$$

- 6) The inverse Weber number ( $We^{-1}$ ) which represents the cohesion force over drag force, can also be used to determine the target value of the surface tension of the oil phase when scaling, as shown in Eq. (7-6).

$$We^{-1} = \frac{C_D \pi D \sigma}{\frac{\rho_o v_{so}^2}{2} 8 C_D \pi \frac{D^2}{4}} = \frac{8 C_D \pi D \sigma}{\rho_o v_{so}^2 8 C_D \pi D^2} = \frac{\sigma}{\rho_o v_{so}^2 D} \quad (7-6)$$

- 7) Finally, the ratio between the roughness and diameter ( $\epsilon/D$ ) is also another parameter that can be analysed.

Despite presenting all possible analysis techniques to evaluate a wide scope of parameters for the scale-up process, taking the experimental and even larger industrial limitations into account, when gathering data for scaling, it is still difficult to find a multiphase system which would satisfy all scaling requirements. Therefore, for the purpose which would best fit the set-up of the entire experimental investigation of this work, the density ratio will be prioritised as this main matching factor. This would mean both the light and heavy oils will be separately scaled-up accordingly. Furthermore, through the process of elimination of the least effective parameters for the scale-up, points 5, 6 and 7 are all assumed to be negligible.

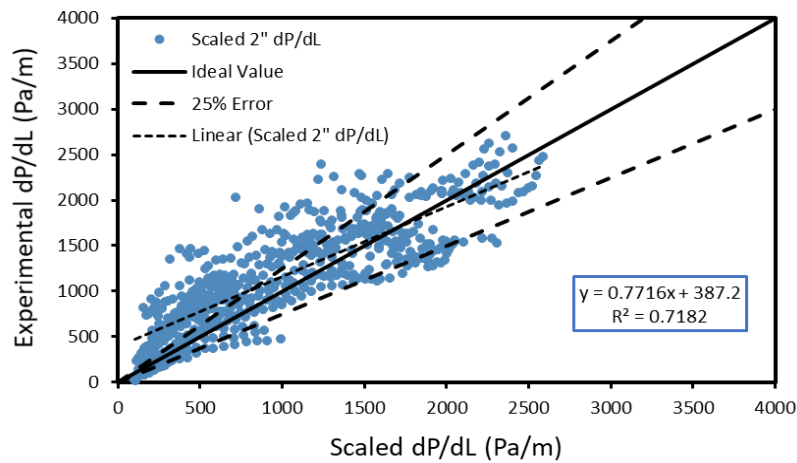
## 7.2 *Prototype Scaling*

Utilising the correlations developed for liquid-liquid multiphase flow as shown throughout chapter 5, along with the scaling procedures explained previously in section 7.1, the prototype scaling is a means of predicting a direct scale-up of a relevant system. For example, the EDM250 and H100 oils tested in the 1-inch experiment flow loop rig can be separately scaled-up to any desired pipe diameter. However, only the required superficial velocities of oil and water phases

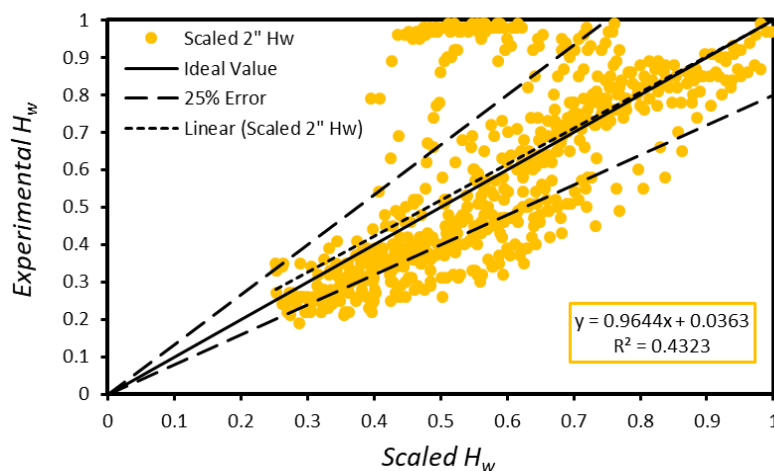
will be needed to undergo a scale-up analysis to satisfy the current hold-up and pressure from the 1-inch rig data. Hence, a 2-inch (0.0508m); and an industrial-scale 42-inch (1.0668m) pipe diameters will be used to test the scaling proficiency of the correlations while analysing how the change in oil type (density and viscosity) and pipeline inclination is affected by larger pipes.

### 7.2.1 2-Inch Pipe Scaling

As shown between *Figure 7-1* and *Figure 7-6*, the graphs represent the resulting prototype scaling of a 2-inch diameter pipeline with reference to the 1-inch flow loop data. Pressure and hold-up are analysed while focusing on the oil type (density ratio) and pipeline inclination parameters.



*Figure 7-1: 2-inch diameter pipeline prototype scale-up analysis of pressure between all the 1-inch experimental data from this work.*



*Figure 7-2: 2-inch diameter pipeline prototype scale-up analysis of water hold-up between all the 1-inch experimental data from this work.*

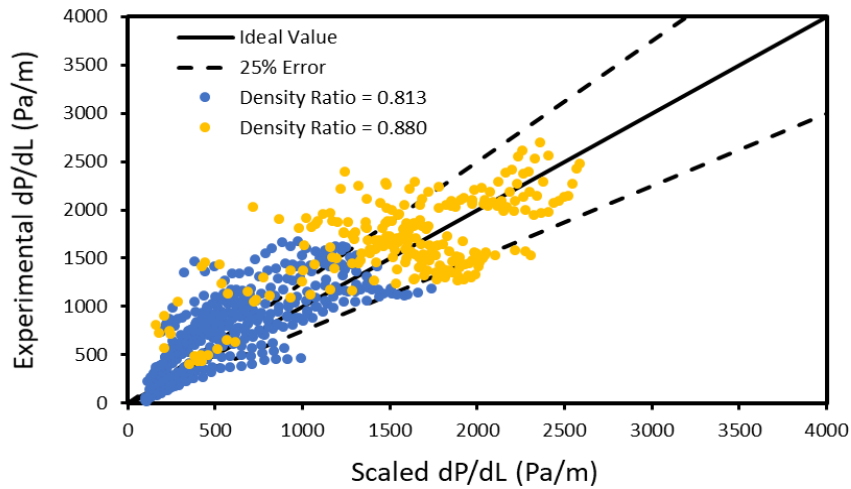


Figure 7-3: 2-inch diameter pipeline prototype scale-up analysis of pressure between all the 1-inch experimental data from this work which have been separated between oil types with density ratios of EDM250 oil = 0.813 and H100 oil = 0.880.

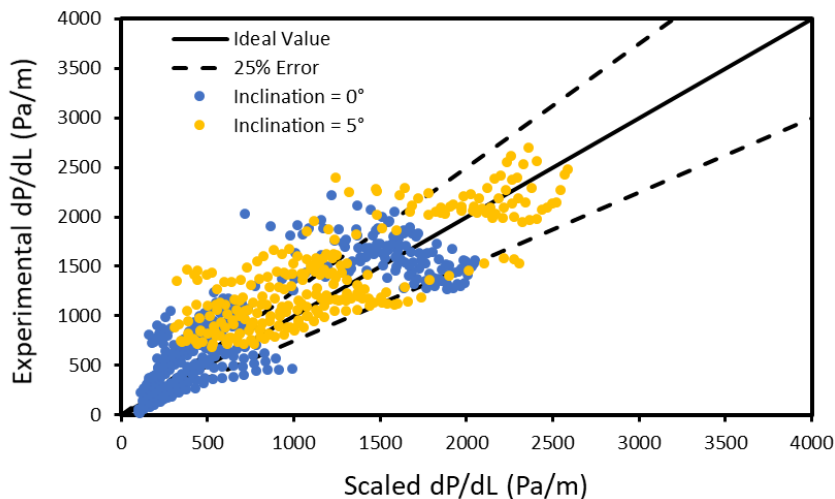


Figure 7-4: 2-inch diameter pipeline prototype scale-up analysis of pressure between all the 1-inch experimental data from this work which have been separated between pipeline inclinations of 0° and 5° upwards from the horizontal.

The scale-up protocol for the 2-inch pipeline prototype demonstrates consistent agreement between pressure and hold-up across all constituent variables when the pipe diameter has doubled. However, the condition where the data points are not located within the 25% error region from the ideal value between the scaled pressure and the experimental pressure is possibly due to the minute pressure fluctuations when measuring over an average period.

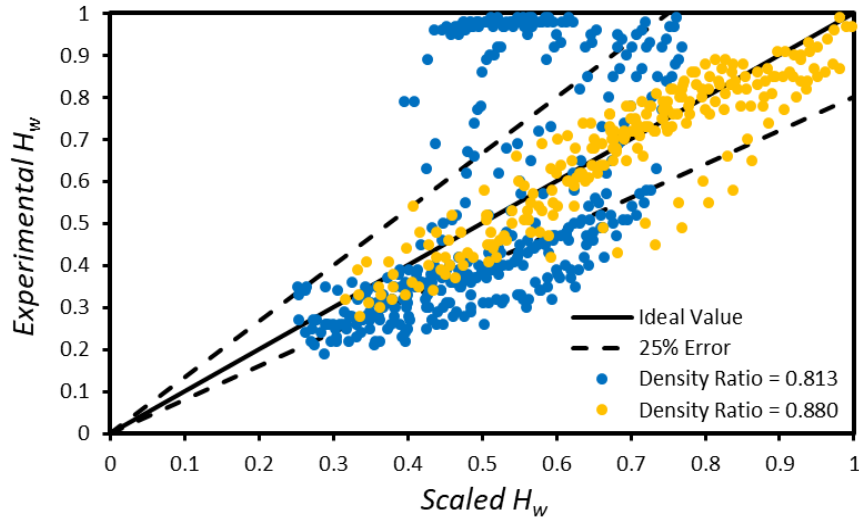


Figure 7-5: 2-inch diameter pipeline prototype scale-up analysis of hold-up between all the 1-inch experimental data from this work which have been separated between oil types with density ratios of EDM250 oil = 0.813 and H100 oil = 0.880.

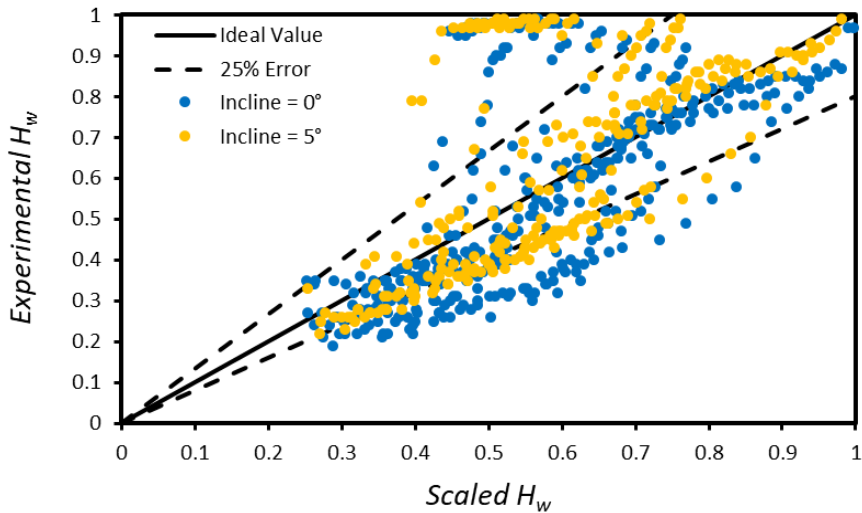
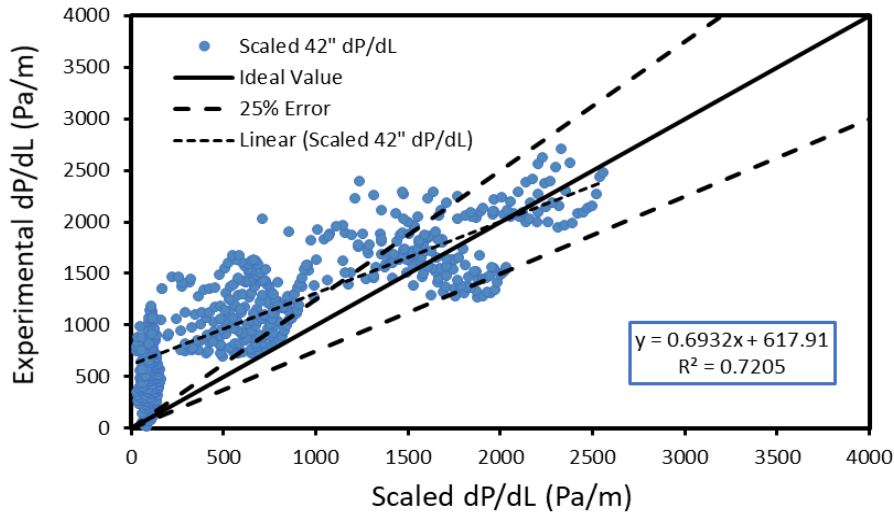


Figure 7-6: 2-inch diameter pipeline prototype scale-up analysis of hold-up between all the 1-inch experimental data from this work which have been separated between pipeline inclinations of  $0^\circ$  and  $5^\circ$  upwards from the horizontal.

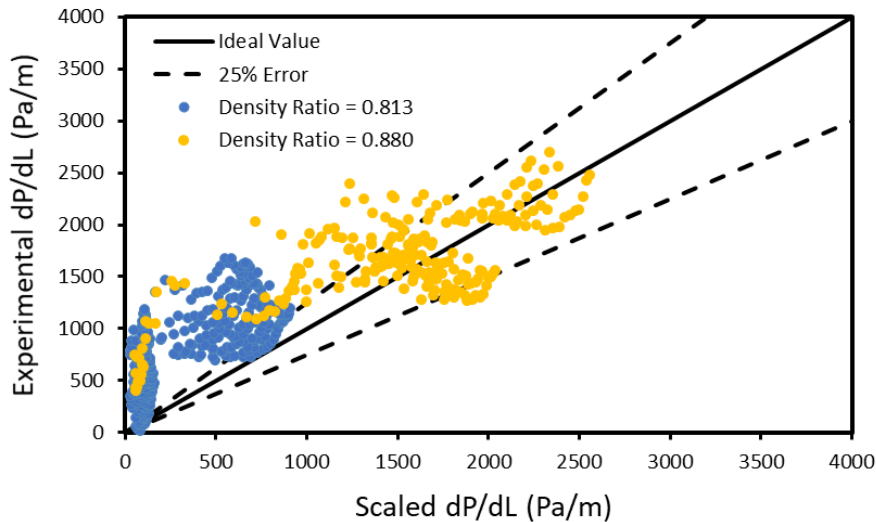
Similar to the pressure, the scaled hold-up also generally matches the original data; however, the multiphase conditions that are outside of the error region from the ideal value are usually due to the incompatibility between measuring equipment and flow regimes. For example, one key issue is dispersed flow; when directly measuring hold-up from the ECT system, the small oil droplets cannot be scanned by the sensors causing an overestimation in water hold-up.

## 7.2.2 Industrial Pipe Scaling

As shown between *Figure 7-7* and *Figure 7-9*, the graphs represent the resulting prototype scaling of an industrial-scaled export pipeline which was deemed to be 42-inch in diameter with regards to the 1-inch flow loop data. As previously explored in section 7.2.1, the pressure and hold-up correlations are used to compare the scaled data from the original 1-inch data at a 42:1 scale.

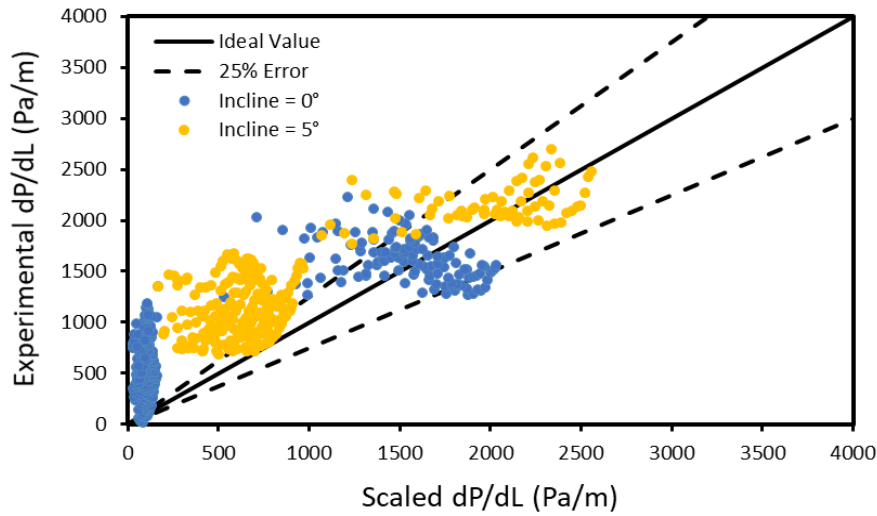


*Figure 7-7: 42-inch diameter pipeline prototype scale-up analysis of pressure between all the 1-inch experimental data from this work.*



*Figure 7-8: 42-inch diameter pipeline prototype scale-up analysis of pressure between all the 1-inch experimental data from this work which have been separated between oil types with density ratios of EDM250 oil = 0.813 and H100 oil = 0.880.*





*Figure 7-9: 42-inch diameter pipeline prototype scale-up analysis of pressure between all the 1-inch experimental data from this work which have been separated between pipeline inclinations of 0° and 5° upwards from the horizontal.*

The scale-up protocol for the 42-inch pipeline prototype demonstrates a worse performance than the 2-inch pipe prototype in specific areas of the pressure data series. The scaling model seems to consistently underestimate the pressure gradient for systems containing light oil types due to the significant contrast between the density ratio and pipe diameter index. In contrast, heavy oils perform extremely well with the scale-up model. Yet, pipe inclination has no significant importance over the scaling performance of the prototype, particularly when attempting to scale at very large pipe diameters. There are no major performance alterations when scaling the hold-up of a multiphase flow system, even in an extreme case when the prototype is at an industrial scale. This is due to the correlation normalising the hold-up values, as this follows the dimensionless scaling according to the correlation, which has no direct relation with the pipe diameter. In fact, the hold-up scaling analysis graphs of the 42-inch diameter prototype are identical to that of the 2-inch prototype in *Figure 7-2*, *Figure 7-5* and *Figure 7-6*.

Additionally, similar to the pressure gradient, the hold-up scaling analysis is better suited with the heavier oil type, and inclination has no significant bearing on the scaling outcome. The applicable uses of the scale-up protocol can be found in industrial-sized pipelines that typically transport heavy oil phases over large distances. This implies that the scaling protocol presented in this section can be applicable and consistent in industrial scaled systems at a large range of high viscous oil-water multiphase systems. However, as mentioned in previous chapters of this thesis, correlation and scaling limitations are still present. Such changes in fluid properties and the density ratio limiting factor must be considered for the analysis to perform at its optimal.

---

### 7.3 Literature Data Scaling

Utilising the same approach as the previous section, large pipe diameter data from literature will be used in accordance with the hold-up, pressure gradient and flow regime data generated from the 1-inch experiment from this work to identify the accuracy of the scale-up protocol. The experimental work from literature that will be used is the same from chapter 5, where the work of Vielma et al. (2008); Atmaca et al. (2009); and Vuong et al. (2009) will again be utilised along with additional work from Esther (2014). As previously shown in *Table 5-2*, all key information of the reoccurring studies can be revisited. All literature-based studies have an internal pipe diameter of 2-inches (0.0508m). As for Esther (2014), the key constant data is as follows; the internal pipe diameter is 4-inches (0.1016m); the inclination of the pipeline is 0° from the horizontal, while the oil density and viscosity are 811kg/m<sup>3</sup> and 0.007Pa.s respectively. Furthermore, the same EDM250 oil used in this work was also used in the Esther study. Since data already exists for these studies, scaling against the 1-inch experimental data from this work must be carefully selected. As there are four separate studies from this work, each study from literature must be scaled against one of the four experimental data. Which is selected by means of similarity between the system set-ups in terms of fluid properties and pipe inclination. The best scale-up pairings between the selected literature studies and this work are shown in *Table 7-1*.

Current Experiments	Literature Experiments
H100 0°	Vielma et al. (2008)
H100 0°	Vuong et al. (2009)
H100 5°	Atmaca et al. (2009)
EDM250 0°	Esther (2014)

*Table 7-1: List of selected Scale-up compatibilities between selected studies from literature and experimental data from the current work.*

As shown in *Figure 7-10* and *Figure 7-11*, superimposed graphs of the hold-up and pressure gradient correlation scale-up analysis of multiple studies from literature are constructed, respectively. This aims to demonstrate the validity of the scale-up protocol when combined with the newly developed correlations while incorporating validated literature data. Furthermore, the diverse range of combinations between fluid properties and pipe dimensions and orientation will also aid in identifying the limits of this approach.

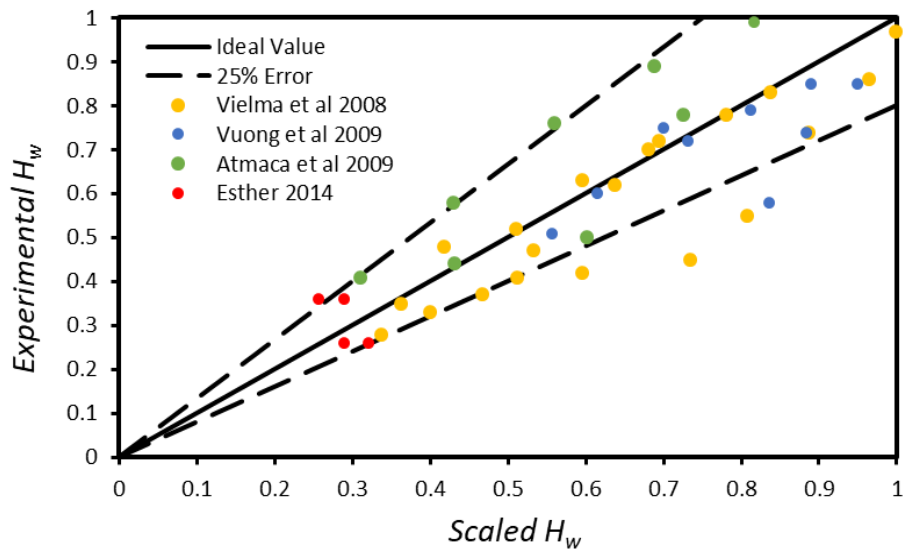


Figure 7-10: Superimposed hold-up scale-up correlation vs measured hold-up. Experimental data and measured hold-up were split between multiple experiments from (Vielma et al., 2008; Atmaca et al., 2009; Vuong et al., 2009; Esther, 2014).

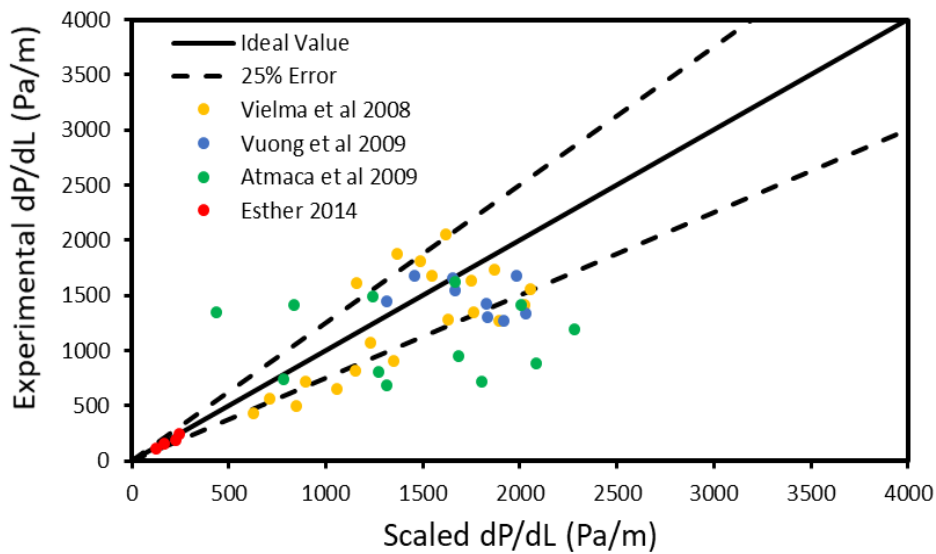
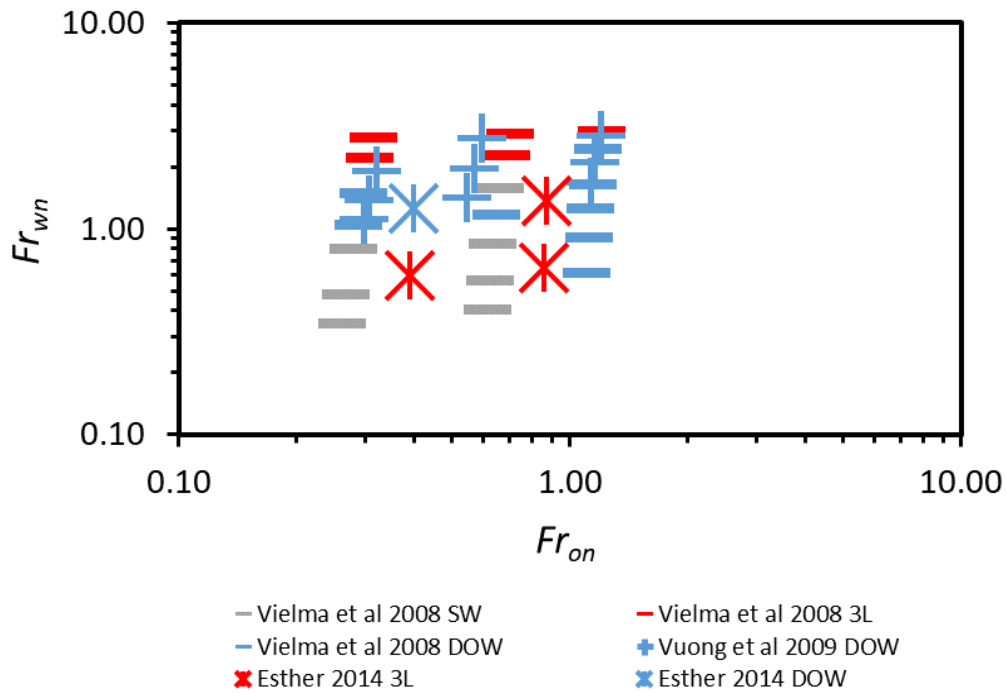


Figure 7-11: Superimposed pressure gradient scale-up correlation vs measured pressure gradient. Experimental data and measured pressure were split between multiple experiments from (Vielma et al., 2008; Atmaca et al., 2009; Vuong et al., 2009; Esther, 2014).

The results suggest that despite non-perfect scaling was conducted to validate the pressure gradient and hold-up scale-up analysis, the dimensionless scale-up approach works to the degree where the general data series of all the experiments are found within or in close proximity to the 25% error margin where the general trend of the data series are consistent between both the scaling analysis and correlations. It is also important to note that the dimensionless scaling approach of

the 1-inch experimental data is not a perfect scaled representation of the larger scaled data from literature, leading to some errors. The scaled-up data was also applied to the modified Froude number; (review chapter 6 for further information), where the dimensionless grouping was applied to the respective flow regimes to identify any changes from the 1-inch data series. The dimensionless grouping graph for the respective flow regimes is depicted in *Figure 7-12*.



*Figure 7-12: Superimposed scaled-up dimensionless Froude number grouping of flow regimes between multiple experiments from (Vielma et al., 2008; Vuong et al., 2009; Esther, 2014).*

The flow regimes that were presented in literature have all developed from pipe diameters that are 2-inches or larger. Therefore, the flow regime development per combination of oil and water Froude numbers would not be akin to the 1-inch data. This is because larger pipes tend to develop more dispersed dominant flow regimes, which force flow patterns such as slug and plug flow to instantaneously breakup before fully developing due to the spacing between the top and bottom pipe walls. Overall, the pressure gradient and hold-up scaling approach with the newly developed correlations work well to predict the dimensionless scaled values. The scale-up protocol for flow regimes is not as constructive to utilise because the flow regime envelopes are significantly affected by pipe diameter. However, flow regimes that develop under a lower mixture flowrate, such as stratified flow, are consistently found in the same Froude log-scale region in the 1-inch flow regime grouping analysis from *Figure 6-3*. Hence, further experimentation with large pipelines is needed to obtain a better dimensionless grouping of the scaled data.

# CHAPTER 8

## FUTURE WORK, RECOMMENDATIONS AND CONCLUSION

### 8.1 *Main Conclusions*

In conclusion, steady-state or pseudo steady-state oil-water intermittent flow regimes such as plug and slug flow patterns can develop in export pipelines if favourable conditions are present within the multiphase system. The transition of intermittent flow has been conventionally attributed from stratified wavy conditions as the most consistent path of development. During an increasing surge of water velocity, wave amplitudes are escalated towards the top of the pipe segment. Until the water peaks begin to come in contact with the upper section of the pipeline, the waves of the water phase will cause a blockage for the upper oil streamline to flow and cause deterioration within the oil layer to progress in intermittent flow regimes. This demonstrates the shift in dominance from gravitational to inertial forces. Furthermore, intermittent flow regime developments are found more frequently under narrow pipelines, which is likely to be attributed due to the shorter distance between the top segment of the inner pipe walls and the interface between the two fluid phases. Hence, it would require less amount of water velocity for the peak water amplitude to ascend to the top of the pipeline, which will initiate slug flow. This, in turn, indicates the reason as to why slug flow is not commonly documented in oil-water export pipelines.

Despite large pipes being advantageous in eliminating the intermittent flow envelope, other combinations of system parameters have a key impact on the development of intermittent flow. Generally, the intermittent flow regimes show a tendency to develop under the conditions of low oil velocity in conjunction with a moderate rate of water velocity, which would be the equivalent of a superficial phase velocity ratio of around 1:4, respectively. Plug flow regimes generally develop in more localised conditions than slug flow, as slug flow can develop under a wider range

---

of oil and water velocity configurations. Furthermore, heavier oils have a greater tendency to develop intermittent flows and have a larger flow regime envelope due to the fluid properties of countering gravitational and inertial forces to stabilise intermittent formations. Additionally, when pipelines are slightly orientated upwards (up to  $+5^\circ$ ) in the direction of the flow, the transition boundary for intermittent flows such as slug flow expands. For downward angled pipelines (up to  $-5^\circ$ ), this configuration suppresses all intermittent flow regimes and revitalises the transition boundary at much smaller oil and water phase velocities, allowing for stable flow regimes such as stratified flows to dominate.

Flow travelling upwards is more unstable than downwards flow, as this phenomenon occurs due to gravitational forces acting against or with the travelling streamline fluids, respectively. However, identifying dual-incompressible intermittent flow regimes are far more difficult than that of gas-liquid flows because the two constituent phases are of the same phase type and are miscible, as mixing can be found between oil and water. Altering the fluid properties of the two phases and making flow regime characterisation more difficult. Intermittent flow regimes can be identified by conducting a PDF analysis of the real-time hold-up data. If a bi-modal distribution is present, then the flow regime strongly indicates the presence of intermittent flow. For slug flow regimes, the hold-up bi-modal peaks are more spread-out across the extremes of the hold-up limits, whereas plug flow regimes are more localised. An analysis of the intermittent flow hold-up frequencies through an FFT analysis shows that plug flow regimes are more stable similar to stratified flow due to a near-zero dominant frequency. In contrast, slug flow regimes are consistently unstable, with dominant frequencies always exceeding the stability threshold of  $0.1\text{Hz}$ . When pipelines are slightly inclined, further instabilities are formed, creating a further separation of the bi-modal distribution crests. Slightly inclined pipe orientations at  $+5^\circ$  from the horizontal create further instabilities to intermittent flow regimes, particularly to plug flow, causing this formation to exceed the  $0.1\text{Hz}$  stability threshold. In addition, the inclination process also averts mixing between oil and water, creating a more pronounced intermittent flow regime structure to form across the pipeline.

The shape and size of the individual intermittent oil patterns are found to be mainly controlled by the oil flowrate. Higher to lower oil velocities will progressively narrow the slug/plug sizing, causing more of a spherical formation. This work has also developed a flow regime grouping method where the newly proposed modified Froude number can provide a good estimation of flow regime mapping for oil-water multiphase flow systems, with the condition of oil types to be no more than medium-heavy ( $\rho_o \ll \rho_w$ ). The newly proposed dimensionless parameter can be used as an inspection tool to better assess flow regimes that are not visually

---

clear and are typically seen around transition boundaries. However, it is limited to mainly horizontal flows and possibly very small inclinations (up to 2° incline) and internal pipe diameters around 1-inch because the transition boundaries of the flow regimes change depending on the diameter size. In contrast, despite the limitations of the dimensionless grouping method, it clearly shows that steady-state intermittent flow strongly exists consistently among oil-water multiphase flow, with consistent grouping being found across a wide variety of studies. Further to the proposed dimensionless grouping, oil-water flow correlations of pressure gradient and hold-up were developed to conduct a scale-up analysis on larger theoretical prototypes and other experimental work that has conducted oil-water flow tests in larger pipes of 2-inch or greater. The proposed pressure gradient and hold-up correlations in a majority of cases are very accurately estimated to the corresponding variables. It has also proven to work across a range of different experimental studies from literature. However, when conducting a scale-up analysis with the newly developed correlation via a prototype industrial scale of a 42-inch pipeline, the results suggest that under large diameter pipes, the pressure correlation is not sufficiently accurate when analysing oil-water systems that contain light oil types.

Overall, the hold-up correlation is consistent throughout the prototype and literature scale-up analysis, and the pressure correlation scaling is relatively consistent for a majority of the data series. Finally, a scale-up of the flow regimes was also conducted on the same set of scaled literature data by again utilising the dimensionless grouping method of the modified Froude number. It was found that there were no similarities in flow regime grouping when scaling as the transition boundaries for oil-water flow regimes significantly alter as the pipe diameter enlarges as it becomes a more dispersed dominated flow regime. A final remark, the contribution of knowledge from this work emphasises the existence of steady-state liquid-liquid multiphase flow for intermittent flows such as slug flow to a degree where the hydrodynamic and terrain-induced behaviours are now better understood and presented as strong evidence.

## ***8.2 Contribution to Knowledge***

Based on the research developed from experimental and literature analysis, along with additional observations conducted in this work; a series of contributions to knowledge are made. Hence a series of recommendations can be made particularly towards the petroleum industry for preventing and mitigating oil-water multiphase intermittent flow for export pipelines. The development of the pressure gradient and hold-up correlations along with the use of the modified Froude number and scaling techniques for the use of pipeline design and operational management can enable the following advancements:

- 
- i. In general, large pipelines that exceed 0.3m in diameter do not typically produce oil-water slug or plug flow regimes because the larger size of the pipeline prevents the induction of water and oil phases from overlapping each other to create intermittent characteristics across the pipeline. However, it may still form under very strict conditions such that the oil-to-water superficial velocity ratios must not be a ratio of around 1:4.
  - ii. Prevent rapidly closing and lowering one of the inlets of the oil and water phases as this will cause overlapping of the phases through instantaneous slippage, which in turn will create intermittent flow regimes.
  - iii. When developing export pipeline systems, as a design consideration, when constructing long-distance horizontal systems, it is better to have the pipeline orientated slightly downward (no more than 0.1°) rather than upward to prevent further induction of intermittent flows.
  - iv. Heavy oils typically induce larger flow regime envelopes for intermittent patterns. Unless required, avoid transporting heavy oils of at least 960kg/m<sup>3</sup> to preserve the prevention of intermittent flow developments.
  - v. As an operational suggestion, when oil production is too low to sustain at higher velocities, to prevent slug and plug developments, increasing the water flowrate would sustain a more water-dominated flow regime resulting in a breakdown in oil phases while still maintaining the required production speed.
  - vi. Regular pipeline cleaning such as pigging is required to ensure the internal diameter of the pipeline is not reduced due to emulsification or waxing.
  - vii. As it is not generally feasible to insulate an entire export pipeline system, it is suggested to insulate the regions where the pipeline slightly orientates upwards from the horizontal to ensure that the combination of inclined pipeline and heavier oil properties do not develop intermittent flow regimes during colder weather periods.

### **8.3 *Attainment Against Objectives***

This work aimed to predict the development of liquid-liquid intermittent flow patterns and process parameters within export pipelines and identify which combination of controllable variables such as pipeline design, operational inputs and fluid properties influences these flow behaviours. The



---

aim was achieved through the attainment of the flowing objectives. (1) The effects of horizontal and slightly inclined pipe orientations of  $0^\circ$  and  $5^\circ$  inclination were discovered to have a significant effect on the intermittent flow envelope of all test conditions. (2) By comparing the effects of oil property/type alterations on oil-water intermittent flows and their flow regime envelope boundaries, it was found that changes in oil property, predominantly density and viscosity significantly affect the flow regime envelop of intermittent flow. This was shown in the comparison between resulting flow regime maps from the light and heavy oil experimental studies. (3) Through the use of an FFT analysis of the hold-up data gathered from the ECT results of individual intermittent flow conditions maintained at steady-state (or pseudo steady-state), were used to assess the frequency of the interchanging phases between the continuous phase and the slug/plug formation for each experimental condition. (4) The newly proposed correlations for pressure gradient and hold-up and the dimensionless grouping analysis of the modified Froude number can be used to predict the range of conditions oil-water intermittent flow regimes develop. (5) Finally, scaling analysis was conducted to observe the effects of pipe diameter from a laboratory to an industrial scale intermittent flow.

#### **8.4 Key Limitations of Work**

Limitations of this study must be considered to develop and improve future studies of identical or similar work. The first limitation is the experimental analysis and the realism it reflects towards larger scale industrial applications. The controlled conditions of the experimental studies do not consider the much greater operational pressure extremes and fluctuations, radical temperature changes and occasional alternating fluid properties found within larger pipelines. Between both scenarios, the extreme environmental difference that the multiphase flow system is found in can potentially result in changes in flow regime behaviour. The developed pressure and hold-up correlations along with the dimensionless grouping proposals also have limitations to the degree that it cannot accurately consider all limits of liquid-liquid multiphase flow systems. For example, the correlation thresholds only consider major parameters to group a system accordingly and utilise the respective constants. However, if less dominant forces are of greater effect such as pipe roughness and interfacial tension, this can shift the system between threshold conditions and inaccurately predict pressure, hold-up and hence flow regime grouping. The final key limitation is the scaling analysis, which is based on experimentations from a single pipe diameter rather than multiple pipe diameter experiments. The advantage of multiple pipe diameter experimentations can allow for extrapolation of the multiphase flow behaviour as pipe diameter increases so the scaling analysis would be developed accordingly.

---

## 8.5 *Future Work*

The future work that this thesis strongly suggests exploring is four of the following concepts; (1) improvements to the current developed work that was not possible due to time and budget constraints in terms of experimental analysis, (2) creating new correlations and methods for multiphase flow; (3) additional experiments and methods of measuring data which will provide further information and insight onto the phenomenon of oil-water multiphase flow and (4) further investigation of the new models and correlations presented in this work. Hence, the following future works this thesis suggests are the following:

- i. Additional experiments of various larger flow loop diameters are required to be constructed and executed according to what was conducted from the 1-inch flow loop rig in this study. Furthermore, the larger flow loop pipelines must be constructed in accordance with the pipe diameter scaling of the 1-inch flow loop such that the length distribution of the test section, pressure transducers and ECT sensors must all be located accordingly to the diameter scale. This is to ensure perfect scaling can be conducted when testing against the different experiments. The scaled pipe diameter flow loops that are suggested to be constructed and tested are 3-inch (0.0762m) and 4-inch (0.1016m) flow loops. Larger-sized flow loops are more desirable, however, from a practical point of view, constructing larger flow loops would cause issues such as maintenance, safety, space, budget and time.
- ii. The correlation constants for the hold-up and pressure gradient must be further developed such that an investigation as to why these values are required for different combinations of fluid properties and phase velocities. Hence, an improved and more accurate correlation can be developed, eliminating the need for alternating constants. Additionally, the limits of fluid properties can also be better considered for correlation to function across a wider range of parameter combinations.
- iii. An industrial scaled experiment is required to compare the true scale-up components of the scaling protocol. An exact scaled replica of the 1-inch flow loop will not be required as long as the data is gathered in accordance with a similar assessment from the 1-inch tests.
- iv. An experimental improvement would be to incorporate more ECT sensors downstream of the main flow line to assess the development of the hold-up as the multiphase travels through the pipeline. This would also help to accurately measure a better hold-up average across the entire pipeline for each respective flow regime during testing.

- 
- v. The transitioning state of slug and plug flow patterns between neighbouring flow regimes should be analysed to a degree where smaller sub-flow regimes are developed within the main flow regimes before settling into a fully developed flow. This can help better understand the transition boundary, allowing a better mapping analysis of the flow regimes and leading to incorporating transition regions.
  - vi. Operational experimentations can also be conducted to assess the development of intermittent flow regimes when phase injection is instantly closed and compared against gradually closed. Hence, transient state flow data could be developed into new flow regime maps that can be compared to steady-state (or pseudo steady-state) conditions.
  - vii. Further frequency analysis of the intermittent flow regimes can be developed such that an equation can be established in two forms. One for predicting the alternating phase frequencies and a separate correlation to predict the presence of intermittent flow within a liquid-liquid multiphase flow system.
  - viii. Internal pipe wetting should be considered where the pipeline can be initially filled with water or oil and then instantaneously injecting the opposite phase.

# REFERENCES

- Al-Awadi, H. (2011) *Multiphase Characteristics of High Viscosity Oil*. Ph.D, Cranfield University.
- Al-Otaibi, A. M. and Habib, M. A. (2015) *Impact of Different Parameters on Flow-Patterns of Two-Phase Flow: Oil-Water Flowing in Pipelines*. Lambert Academic Publishing.
- Al-Wahaibi, T., Al-Wahaibi, Y., Al-Ajmi, A., Al-Hajri, R., Yusuf, N., Olawale, A. S. and Mohammed, I. A. (2014) 'Experimental Investigation on Flow Patterns and Pressure Gradient Through Two Pipe Diameters in Horizontal Oil–Water Flows', *Journal of Petroleum Science and Engineering*, 122(1), pp. 266–273. doi: 10.1016/j.petrol.2014.07.019.
- Al-Wahaibi, T., Smith, M. and Angeli, P. (2007) 'Effect of Drag-reducing Polymers on Horizontal Oil–Water Flows', *Journal of Petroleum Science and Engineering*, 57(4), pp. 334–346. doi: 10.1016/j.petrol.2006.11.002.
- Alagbe, S. O. (2013) *Experimental and Numerical Investigation of High Viscosity Oil-Based Multiphase Flows*. PhD Cranfield University. Available at: [http://link.springer.com/10.1007/978-1-349-95810-8\\_377](http://link.springer.com/10.1007/978-1-349-95810-8_377).
- Alboudwarej, H., Felix, J., Taylor, S., Badry, R., Bremner, C., Brough, B., Skeates, C., Baker, A., Palmer, D., Pattison, K., Beshry, M., Krawchuk, P., Brown, G., Calvo, R., Triana, J. a C., Hathcock, R., Koerner, K., Hughes, T., Kundu, D., De Cárdenas, J. L. and West, C. (2006) 'Highlighting Heavy Oil', *Oilfield Review*, 18(2), pp. 34–53. Available at: [https://www.slb.com/resources/publications/industry\\_articles/oilfield\\_review/2006/or2006sum03\\_highlighting\\_heavyoil.aspx%0Ahttp://www.scopus.com/inward/record.url?eid=2-s2.0-33750047195&partnerID=40&md5=76213b2719151416f2ba741951baf65b](https://www.slb.com/resources/publications/industry_articles/oilfield_review/2006/or2006sum03_highlighting_heavyoil.aspx%0Ahttp://www.scopus.com/inward/record.url?eid=2-s2.0-33750047195&partnerID=40&md5=76213b2719151416f2ba741951baf65b).
- Angeli, P. and Hewitt, G. . (2000) 'Flow Structure in Horizontal Oil–Water Flow', *International Journal of Multiphase Flow*, 26(7), pp. 1117–1140. doi: 10.1016/S0301-9322(99)00081-6.
- Angeli, P. and Hewitt, G. F. (1998) 'Pressure Gradient in Horizontal Liquid–liquid Flows', *International Journal of Multiphase Flow*, 24(7), pp. 1183–1203. doi: 10.1016/S0301-9322(98)00006-8.
- Arirachakaran, S., Oglesby, K. D., Malinowsky, M. S., Shoham, O. and Brill, J. P. (1989) 'An analysis of Oil-Water flow phenomena in horizontal pipes', in *SPE Production Operations Symposium*. Oklahoma City, Oklahoma, USA: Society of Petroleum Engineers, pp. 155–167. doi: 10.2118/18836-MS.
- Arney, M. S., Bai, R., Guevara, E., Joseph, D. D. and Liu, K. (1993) 'Friction factor and holdup studies for lubricated pipeline', *International Journal of Multiphase Flow*, 19(6), pp. 1061–1076.
- Arney, M. S., Ribeiro, G. S., Guevara, E., Bai, R. and Joseph, D. D. (1996) 'Cement-lined pipes for water lubricated transport of heavy oil', *International Journal of Multiphase Flow*, 22(2), pp. 207–221. doi: 10.1016/0301-9322(95)00064-X.

- 
- Atmaca, S., Sarica, C., Zhang, H.-Q. and Al-Sarkhi, A. S. (2009) 'Characterization of oil-water flows in inclined pipes', *SPE Projects, Facilities & Construction*, 4(2), pp. 41–46. doi: 10.2118/115485-PA.
- Bai, R., Chen, K. and Joseph, D. D. (1992) 'Lubricated pipelining: Stability of core-annular flow. Part 5. Experiments and comparison with theory', *Journal of Fluid Mechanics*, 240(1), pp. 1–88. doi: 10.1017/S0022112092000041.
- Barajas, A. M. and Panton, R. L. (1993) 'The effects of contact angle on two-phase flow in capillary tubes', *International Journal of Multiphase Flow*, 19(2), pp. 337–346. doi: 10.1016/0301-9322(93)90007-H.
- Barnea, D. and Taitel, Y. (1994) 'Structural stability of stratified flow—the two-fluid model approach', *Chemical Engineering Science*, 49(22), pp. 3757–3764. doi: 10.1016/0009-2509(94)00185-5.
- Barrett, N. and King, D. (1998) 'Oil-water slugging of horizontal wells - Symptom, cause and design', in *SPE Annual Technical Conference and Exhibition*. New Orleans, Louisiana, USA: Society of Petroleum Engineers, pp. 461–469. doi: 10.2118/49160-MS.
- Beggs, D. H. and Brill, J. P. (1973) 'A Study of Two-Phase Flow in Inclined Pipes', *Journal of Petroleum Technology*, 25(05), pp. 607–617. doi: 10.2118/4007-PA.
- Beretta, A., Ferrari, P., Galbiati, L. and Andreini, P. A. (1997) 'Horizontal oil-water flow in small diameter tubes - Pressure drop', *International Communications in Heat and Mass Transfer*, 24(2), pp. 231–239. doi: 10.1016/S0735-1933(97)00009-2.
- Brauner, N. (2003) 'Experimental investigation of viscous oil-water flows in pipeline', *Journal of Petroleum Science and Engineering*, 1(1), pp. 1–59. doi: 10.1016/j.petrol.2016.05.010.
- Brauner, N., Moalem Maron, D. and Rovinsky, J. (1998) 'A two-fluid model for stratified flows with curved interfaces', *International Journal of Multiphase Flow*, 24(6), pp. 975–1004. doi: 10.1016/S0301-9322(98)00005-6.
- Brauner, N. and Ullmann, A. (2002) 'Modeling of phase inversion phenomenon in two-phase pipe flows', *International Journal of Multiphase Flow*, 28(7), pp. 1177–1204. doi: 10.1016/S0301-9322(02)00017-4.
- Brennen, C. E. (2005) *Fundamentals of Multiphase Flow*. New York, USA: Cambridge University Press.
- Brill, J. P. and Mukherjee, H. (1999) *Multiphase Flow in Wells*. Pennsylvania, USA: Society of Petroleum Engineers.
- Brookfield Engineering Laboratories Inc. (2020) *Enhanced UL Adapter Assembly & Operating Instructions*. Middleborough, Massachusetts, USA. Available at: [https://www.brookfieldengineering.com/-/media/ametekbrookfield/manuals/lab\\_accessories/ula\\_ula\\_ez\\_instructions.pdf](https://www.brookfieldengineering.com/-/media/ametekbrookfield/manuals/lab_accessories/ula_ula_ez_instructions.pdf).
- Buckingham, E. (1914) 'On Physically Similar Systems; Illustrations of the Use of Dimensional Equations', *Physical Review*, 4(4), pp. 345–376. doi: 10.1103/PhysRev.4.345.

- 
- Chakrabarti, D. P., Das, G. and Ray, S. (2005) 'Pressure drop in liquid-liquid two phase horizontal flow: Experiment and prediction', *Chemical Engineering & Technology*, 28(9), pp. 1003–1009. doi: 10.1002/ceat.200500143.
- Charles, M. E., Govier, G. W. and Hodgson, G. W. (1961) 'The horizontal pipeline flow of equal density oil-water mixtures', *The Canadian Journal of Chemical Engineering*, 39(1), pp. 27–36. doi: 10.1002/cjce.5450390106.
- Charles, M. E. and Lilleleht, L. V. (1966) 'Correlation of pressure gradients for the stratified laminar-turbulent pipeline flow of two immiscible liquids', *The Canadian Journal of Chemical Engineering*, 44(1), pp. 47–49. doi: 10.1002/cjce.5450440110.
- Clayton, C. G., Clarke, W. E. and Ball, A. M. (1960) 'The accurate measurement of turbulent flow in pipes using the isotope velocity method and the effect of some restrictions on optimum operation', in *Symposium on Flow Measurement in Closed Conduits. National Engineering Laboratory*, pp. 555–578.
- Dasari, A., Desamala, A. B., Dasmahapatra, A. K. and Mandal, T. K. (2013) 'Experimental studies and probabilistic neural network prediction on flow pattern of viscous oil–water flow through a circular horizontal pipe', *Industrial & Engineering Chemistry Research*, 52(23), pp. 7975–7985. doi: 10.1021/ie301430m.
- Van Duin, E., Henkes, R. and Ooms, G. (2018) 'Influence of oil viscosity on oil-water core-annular flow through a horizontal pipe', *Petroleum xxx*, 1(1), pp. 1–7. doi: 10.1016/j.petlm.2018.01.003.
- Edomwonyi-Otu, L. C. and Angeli, P. (2015) 'Pressure drop and holdup predictions in horizontal oil–water flows for curved and wavy interfaces', *Chemical Engineering Research and Design. Institution of Chemical Engineers*, 93(1), pp. 55–65. doi: 10.1016/j.cherd.2014.06.009.
- Elseth, G. (2001) *An experimental study of oil/water flow in horizontal pipes*. PhD, Telemark University College.
- Escojido, D., Urribarri, O. and Gonzalez, J. (1991) 'Part 1: Transportation of Heavy Crude Oil and Natural Bitumen', in *13th World Petroleum Congress*. Buenos Aires, Argentina, pp. 15–22. doi: WPC-24203.
- Esther, B. (2014) *Oil / Water Two Phase Flow in Horizontal Pipes*. MSc, Cranfield University.
- Fairuzov, Y. V., Arenas-Medina, P., Verdejo-Fierro, J. and Gonzalez-Islas, R. (2000) 'Flow pattern transitions in horizontal pipelines carrying oil-water mixtures: Full-scale experiments', *Journal of Energy Resources Technology*, 122(4), pp. 169–176. doi: 10.1115/1.1318204.
- Falcone, G., Hewitt, G. . and Alimonti, C. (2009) *Multiphase flow metering*. Boston, Massachusetts, USA: Elsevier.

- 
- Farokhpoor, R., Liu, L., Langsholt, M., Hald, K., Amundsen, J. and Lawrence, C. (2020) 'Dimensional analysis and scaling in two-phase gas–liquid stratified pipe flow–Methodology evaluation', *International Journal of Multiphase Flow*, 122, p. 103139. doi: 10.1016/j.ijmultiphaseflow.2019.103139.
- Ferrell, J. K. and McGee, J. W. (1965) 'An accurate one-shot gamma attenuation technique for measuring void fractions', in *Proceedings of the Conference on Application of High Temperature Instrumentation to Liquid-Metal Experiments*. Chicago, pp. 247–269.
- Ghosh, S., Mandal, T. K., Das, G. and Das, P. K. (2009) 'Review of oil water core annular flow', *Renewable and Sustainable Energy Reviews*, 13(8), pp. 1957–1965. doi: 10.1016/j.rser.2008.09.034.
- Govier, G. W. and Aziz, K. (1972) *The flow of complex mixtures in pipes*. 1st edn. New York, USA: Van Nostrand Reinhold.
- Grassi, B., Strazza, D. and Poesio, P. (2008) 'Experimental validation of theoretical models in two-phase high-viscosity ratio liquid–liquid flows in horizontal and slightly inclined pipes', *International Journal of Multiphase Flow*, 34(10), pp. 950–965. doi: 10.1016/j.ijmultiphaseflow.2008.03.006.
- Green, R. G. and Cunliffe, J. M. (1983) 'A frequency-modulated capacitance transducer for on-line measurement of two-component fluid flow', *Measurement*, 1(4), pp. 191–195. doi: 10.1016/0263-2241(83)90005-2.
- Guzhov, A., Grishin, A., D., Medredev, V. F. and Medredeva, O. P. (1973) 'Emulsion formation during the flow of two immiscible liquids.', *Neft. Choz.*, 8(1), pp. 58-61 (In Russian).
- Hagedorn, A. R. and Brown, K. E. (1965) 'Experimental study of pressure gradients occurring during continuous two-phase flow in small-diameter vertical conduits', *Journal of Petroleum Technology*, 17(4), pp. 475–484. doi: 10.2118/940-PA.
- Hanafizadeh, P., Hojati, A. and Karimi, A. (2015) 'Experimental investigation of oil–water two phase flow regime in an inclined pipe', *Journal of Petroleum Science and Engineering*, 136(1), pp. 12–22. doi: 10.1016/j.petrol.2015.10.031.
- Hasson, D., Mann, V. and Nir, A. (1970) 'Annular flow of two immiscible liquids I. Mechanisms', *The Canadian Journal of Chemical Engineering*, 48(5), pp. 514–520. doi: 10.1002/cjce.5450480507.
- Ibarra, R. J. (2017) *Horizontal and low-inclination oil-water flow investigations using laser-based diagnostic techniques*. PhD, Imperial College London.
- Ibarra, R., Markides, C. N. and Matar, O. K. (2015) 'A review of liquid-liquid flow patterns in horizontal and slightly inclined pipes', *Multiphase Science and Technology*, 26(3), pp. 171–198. doi: 10.1615/MultScienTechn.v26.i3.10.
- Ibarra, R., Matar, O. K. and Zadrazil, I. (2015) 'An experimental study of oil-water flows in pipes', *BHR Group*, 1(1), pp. 1–15.

- 
- Ibarra, R., Zadrazil, I., Matar, O. K. and Markides, C. N. (2018) 'Dynamics of liquid–liquid flows in horizontal pipes using simultaneous two–line planar laser–induced fluorescence and particle velocimetry', *International Journal of Multiphase Flow*, 101(1), pp. 47–63. doi: 10.1016/j.ijmultiphaseflow.2017.12.018.
- Ismail, A. S. I., Ismail, I., Zoveidavianpoor, M., Mohsin, R., Piroozian, A., Misnan, M. S. and Sariman, M. Z. (2015) 'Review of oil–water through pipes', *Flow Measurement and Instrumentation*, 45(1), pp. 357–374. doi: 10.1016/j.flowmeasinst.2015.07.015.
- John, H., Reimann, J. and Müller, U. (1984) 'Test of Two-Phase Mass Flow Rate Instrumentation in Transient Steam-Water Flow', in *Measuring Techniques in Gas-Liquid Two-Phase Flows*. Heidelberg: Springer Berlin Heidelberg, pp. 677–694. doi: 10.1007/978-3-642-82112-7\_32.
- Joseph, D. D., Bai, R., Chen, K. P. and Renardy, Y. Y. (1997) 'Core-annular flows', *Annual Review Fluid Mechanics*, 29(1), pp. 65–90.
- Joseph, D. D., Bannwart, A. C. and Liu, Y. J. (1996) 'Stability of annular flow and slugging', *International Journal of Multiphase Flow*, 22(6), pp. 1247–1254. doi: 10.1016/0301-9322(96)00048-1.
- Kays, W. M. and Crawford, M. E. (1993) *Convective Heat and Mass Transfer*. 3rd Editio. New York, USA: McGraw-Hill.
- Kumara, W. A. S., Halvorsen, B. M. and Melaaen, M. C. (2009) 'Pressure drop, flow pattern and local water volume fraction measurements of oil–water flow in pipes', *Measurement Science and Technology*, 20(11), pp. 1–18. doi: 10.1088/0957-0233/20/11/114004.
- Kumara, W. A. S., Halvorsen, B. M. and Melaaen, M. C. (2010) 'Particle image velocimetry for characterizing the flow structure of oil–water flow in horizontal and slightly inclined pipes', *Chemical Engineering Science*, 65(15), pp. 4332–4349. doi: 10.1016/j.ces.2010.03.045.
- Kurban, A. P. A. (1997) *Stratified liquid-liquid flow*. Imperial College London.
- Langhaar, H. L. (1951) *Dimensional Analysis and Theory of Models*. 1st edn. New York, USA: Wiley.
- Liu, Y., Zhang, H., Wang, S. and Wang, J. (2008) 'Prediction of pressure gradient and holdup in small eötvös number liquid-liquid segregated Flow', *Chinese Journal of Chemical Engineering*, 16(2), pp. 184–191. doi: 10.1016/S1004-9541(08)60060-9.
- Lockhart, R. W. and Martinelli, R. C. (1949) 'Proposed Correlation of Data for Isothermal Two-Phase, Two-Component Flow in Pipes', *Chemical Engineering Progress*, 45(1), pp. 39–48.
- Lovick, J. and Angeli, P. (2004) 'Experimental studies on the dual continuous flow pattern in oil–water flows', *International Journal of Multiphase Flow*, 30(2), pp. 139–157. doi: 10.1016/j.ijmultiphaseflow.2003.11.011.
- Lum, J. Y.-L., Al-Wahaibi, T. and Angeli, P. (2006) 'Upward and downward inclination oil–water flows', *International Journal of Multiphase Flow*, 32(4), pp. 413–435. doi: 10.1016/j.ijmultiphaseflow.2006.01.001.



- 
- Luo, X., Lü, G., Zhang, W., He, L. and Lü, Y. (2017) 'Flow structure and pressure gradient of extra heavy crude oil-water two-phase flow', *Experimental Thermal and Fluid Science*, 82(1), pp. 174–181. doi: 10.1016/j.expthermflusci.2016.11.015.
- Mandal, T. K., Chakrabarti, D. P. and Das, G. (2007) 'Oil water flow through different diameter pipes', *Chemical Engineering Research and Design*, 85(8), pp. 1123–1128. doi: 10.1205/cherd06036.
- Mandal, T. K., Das, G. and Das, P. K. (2010) 'An appraisal of liquid–liquid slug flow in different pipe orientations', *International Journal of Multiphase Flow*, 36(8), pp. 661–671. doi: 10.1016/j.ijmultiphaseflow.2010.04.002.
- Martínez-Palou, R., Mosqueira, M. de L., Zapata-Rendón, B., Mar-Juárez, E., Bernal-Huicochea, C., de la Cruz Clavel-López, J. and Aburto, J. (2011) 'Transportation of heavy and extra-heavy crude oil by pipeline: A review', *Journal of Petroleum Science and Engineering*. Elsevier B.V., 75(4), pp. 274–282. doi: 10.1016/j.petrol.2010.11.020.
- McKibben, M. J., Gillies, R. G. and Shook, C. A. (2000a) 'A laboratory investigation of horizontal well heavy oil-water flows', *The Canadian Journal of Chemical Engineering*, 78(4), pp. 743–751. doi: 10.1002/cjce.5450780417.
- McKibben, M. J., Gillies, R. G. and Shook, C. A. (2000b) 'Predicting pressure gradients in heavy oil-water pipelines', *The Canadian Journal of Chemical Engineering*, 78(4), pp. 752–756. doi: 10.1002/cjce.5450780418.
- Morgan, R. G., Ibarra, R., Zadrazil, I., Matar, O. K., Hewitt, G. F. and Markides, C. N. (2017) 'On the role of buoyancy-driven instabilities in horizontal liquid–liquid flow', *International Journal of Multiphase Flow*, 89(1), pp. 123–135. doi: 10.1016/j.ijmultiphaseflow.2016.07.009.
- Morgan, R. G., Markides, C. N., Hale, C. P. and Hewitt, G. F. (2012) 'Horizontal liquid-liquid flow characteristics at low superficial velocities using laser-induced fluorescence', *International Journal of Multiphase Flow*, 43, pp. 101–117. doi: 10.1016/j.ijmultiphaseflow.2012.01.013.
- Morgan, R. G., Markides, C. N., Zadrazil, I. and Hewitt, G. F. (2013) 'Characteristics of horizontal liquid–liquid flows in a circular pipe using simultaneous high-speed laser-induced fluorescence and particle velocimetry', *International Journal of Multiphase Flow*. Elsevier Ltd, 49(1), pp. 99–118. doi: 10.1016/j.ijmultiphaseflow.2012.09.004.
- Morgan, R. G., Sharaf, S., Zadrazil, I., Hewitt, G. F. and Markides, C. N. (2012) 'Experimental investigations of two-phase liquid-liquid horizontal flows through orifice plates', *9th International Conference on Heat Transfer, Fluid Mechanics and Thermodynamics*, 9(1), pp. 1631–1639.
- Mukherjee, H., Brill, J. P. and Beggs, H. D. (1981) 'Experimental study of oil-water flow in inclined pipes', *Journal of Energy Resources Technology*, 103(1), pp. 56–66. doi: 10.1115/1.3230815.

- 
- Nädler, M. and Mewes, D. (1997) 'Flow induced emulsification in the flow of two immiscible liquids in horizontal pipes', *International Journal of Multiphase Flow*, 23(1), pp. 55–68. doi: 10.1016/S0301-9322(96)00055-9.
- Norato, M. A., Tavlarides, L. L. and Tsouris, C. (1998) 'Phase inversion studies in liquid-liquid dispersions', *The Canadian Journal of Chemical Engineering*, 76(3), pp. 486–494. doi: 10.1002/cjce.5450760319.
- Nossen, J., Liu, L., Skjæraasen, O., Tutkun, M., Amundsen, J. E., Sleipnæs, H. G., Popovici, N., Hald, K., Langsholt, M. and Ibarra, R. (2017) 'An experimental study of two-phase flow in horizontal and inclined annuli', in *18th International Conference on Multiphase Production Technology*. Oslo, Norway, pp. 87–102.
- Oddie, G., Shi, H., Durlflosky, L. J., Aziz, K., Pfeffer, B. and Holmes, J. A. (2003) 'Experimental study of two and three phase flows in large diameter inclined pipes', *International Journal of Multiphase Flow*, 29(4), pp. 527–558. doi: 10.1016/S0301-9322(03)00015-6.
- Oglesby, K. D. (1979) *An experimental study on the effects of oil viscosity, mixture velocity and water fraction on horizontal oil-water flow*. MSc, University of Tulsa.
- Ooms, G., Segal, A., van der Wees, A. J., Meerhoff, R. and Oliemans, R. V. A. (1984) 'A theoretical model for core-annular flow of a very viscous oil core and a water annulus through a horizontal pipe', *International Journal of Multiphase Flow*, 10(1), pp. 41–60. doi: 10.1016/0301-9322(83)90059-9.
- Pilehvari, A., Saadevandi, B., Halvaci, M. and Clark, P. E. (1988) 'Oil/Water Emulsions for Pipeline Transport of Viscous Crude Oils', in *SPE Annual Technical Conference and Exhibition*. Houston: Society of Petroleum Engineers. doi: 10.2118/18218-MS.
- Prieto, L., Muñoz, F., Pereyra, E. and Ratkovich, N. (2018) 'Pressure gradient correlations analysis for liquid-liquid flow in horizontal pipes', *Journal of Petroleum Science and Engineering*, 169(1), pp. 683–704. doi: 10.1016/j.petrol.2018.04.001.
- Raj, T. S., Chakrabarti, D. P. and Das, G. (2005) 'Liquid-liquid stratified flow through horizontal conduits', *Chemical Engineering & Technology*, 28(8), pp. 899–907. doi: 10.1002/ceat.200500067.
- Ramey, H. J. J. (1973) 'Correlations of surface and interfacial tensions of reservoir fluids', *SPE General*, 4429-MS, 1(1), pp. 1–27.
- Rodriguez, O. M. H. and Castro, M. S. (2014) 'Interfacial-tension-force model for the wavy-stratified liquid-liquid flow pattern transition', *International Journal of Multiphase Flow*, 58(1), pp. 114–126. doi: 10.1016/j.ijmultiphaseflow.2013.09.003.
- Rodriguez, O. M. H. and Oliemans, R. V. A. (2006) 'Experimental study on oil-water flow in horizontal and slightly inclined pipes', *International Journal of Multiphase Flow*, 32(3), pp. 323–343. doi: 10.1016/j.ijmultiphaseflow.2005.11.001.
- Russell, T. W. F. and Charles, M. E. (1959) 'The effect of the less viscous liquid in the laminar flow of two immiscible liquids', *The Canadian Journal of Chemical Engineering*, 37(1), pp. 18–24. doi: 10.1002/cjce.5450370105.

- 
- Selker, A. H. and Sleicher, C. A. (1965) 'Factors affecting which phase will disperse when immiscible liquids are stirred together', *The Canadian Journal of Chemical Engineering*, 43(6), pp. 298–301. doi: 10.1002/cjce.5450430606.
- Sharp, J. J. (1981) *Hydraulic Modelling*. 1st edn. London, UK: Butterworths.
- Shi, H., Jepson, W. P. and Rhyne, L. D. (2003) 'Segregated modelling of oil–water flows', in *SPE Annual Technical Conference*. Colorado, USA: SPE 84232, pp. 1–10.
- Shi, J. (2015) *A study on high-viscosity oil-water two-phase flow in horizontal pipes*. PhD, Cranfield University.
- Shi, J. and Yeung, H. (2017) 'Characterization of liquid-liquid flows in horizontal pipes', *AIChE Journal*, 63(3), pp. 1132–1143. doi: 10.1002/aic.15452.
- Shu, M. T., Weinberger, C. B. and Lee, Y. H. (1982) 'A simple capacitance sensor for void fraction measurement in two-phase flow', *Industrial & Engineering Chemistry Fundamentals*, 21(2), pp. 175–181. doi: 10.1021/i100006a013.
- Sinclair, A. R. (1970) 'Rheology of viscous fracturing fluids', *Journal of Petroleum Technology*, 22(6), pp. 711–719. doi: 10.2118/2623-PA.
- Smith, J. E. (1978) 'Gyroscopic/Coriolis Mass Flow Meter', *Canadian Controls and Instruments*, 29(101), pp. 29–31.
- Soleimani, A., Al-Sarkhi, A. and Hanratty, T. J. (2002) 'Effect of drag-reducing polymers on pseudo-slugs—interfacial drag and transition to slug flow', *International Journal of Multiphase Flow*, 28(12), pp. 1911–1927. doi: 10.1016/S0301-9322(02)00110-6.
- Sotgia, G., Tartarini, P. and Stalio, E. (2008) 'Experimental analysis of flow regimes and pressure drop reduction in oil–water mixtures', *International Journal of Multiphase Flow*, 34(12), pp. 1161–1174. doi: 10.1016/j.ijmultiphaseflow.2008.06.001.
- Stapelberg, H. H. and Mewes, D. (1994) 'The pressure loss and slug frequency of liquid-liquid-gas slug flow in horizontal pipes', *International Journal of Multiphase Flow*, 20(2), pp. 285–303. doi: 10.1016/0301-9322(94)90083-3.
- Strazza, D., Grassi, B., Demori, M., Ferrari, V. and Poesio, P. (2011) 'Core-annular flow in horizontal and slightly inclined pipes: Existence, pressure drops, and hold-up', *Chemical Engineering Science*. Elsevier, 66(12), pp. 2853–2863. doi: 10.1016/j.ces.2011.03.053.
- Taitel, Y. and Barnea, D. (1990) 'Two-Phase Slug Flow', *Advances in Heat Transfer*, 20, pp. 83–132. doi: 10.1016/S0065-2717(08)70026-1.
- Taitel, Y. and Dukler, A. E. (1976) 'A model for predicting flow regime transitions in horizontal and near horizontal gas-liquid flow', *AIChE Journal*, 22(1), pp. 47–55. doi: 10.1002/aic.690220105.
- Tan, J., Jing, J., Hu, H. and You, X. (2018) 'Experimental study of the factors affecting the flow pattern transition in horizontal oil–water flow', *Experimental Thermal and Fluid Science*, 98(8), pp. 534–545. doi: 10.1016/j.expthermflusci.2018.06.020.

- 
- Taylor, G. I. (1954) 'The dispersion of matter in turbulent flow through a pipe', *Proceedings of the Royal Society of London. Series A. Mathematical and Physical Sciences*, 223(1155), pp. 446–468. doi: 10.1098/rspa.1954.0130.
- Theissing, P. (1980) 'A generally valid method for calculating frictional pressure drop in multiphase flow', *Chemie Ingenieur Technik*, 52, pp. 344–345 (In German).
- Torres, C. F., Mohan, R. S., Gomez, L. E. and Shoham, O. (2015) 'Oil–water flow pattern transition prediction in horizontal pipes', *Journal of Energy Resources Technology*, 138(2), pp. 1–11. doi: 10.1115/1.4031608.
- Trallero, J. L. (1995) *Oil-water flow patterns in horizontal pipes*. PhD, University of Tusla.
- Trallero, J. L., Sarica, C. and Brill, J. P. (1997) 'A study of oil-water flow patterns in horizontal pipes', *SPE Production & Facilities*, 12(3), pp. 165–172. doi: 10.2118/36609-PA.
- Vedapuri, D. (1999) *Studies on oil-water flow in inclined pipelines*. MSc, Ohio University.
- Vedapuri, D., Bessette, D. and Jepson, W. P. (1997) 'A Segregated Flow Model To Predict Water Layer Thickness In Oil-Water Flows In Horizontal And Slightly Inclined Pipelines', in *BHR Group Multiphase*.
- Veil, J. A., Quinn, J. J. and Garcia, J. P. (2009) 'Water Issues Relating to Heavy Oil Production', in *SPE Americas E and P Environmental and Safety Conference*. San Antonio: Society of Petroleum Engineers, pp. 116–126. doi: 10.2118/120630-MS.
- Vielma, M., Atmaca, S., Sarica, C., Zhang, H.-Q. and Al-Sarkhi, A. (2008) 'Characterization of Oil Water Flows in Inclined Pipes', in *SPE Annual Technical Conference and Exhibition*. Anaheim, California, USA: Society of Petroleum Engineers, pp. 1–14. doi: 10.2118/115485-MS.
- Vuong, D. H., Zhang, H.-Q., Sarica, C. and Li, M. (2009) 'Experimental Study on High Viscosity Oil/Water Flow in Horizontal and Vertical Pipes', in *SPE Annual Technical Conference and Exhibition*. New Orleans, Louisiana, USA: Society of Petroleum Engineers, pp. 1–10. doi: 10.2118/124542-MS.
- Wang, W. and Gong, J. (2009) 'Experiment Research of Phase Inversion in Mineral Oil-Water Two-Phase Flow in Horizontal Pipe', *Journal of Energy Resources Technology*, 131(4), pp. 1–6. doi: 10.1115/1.4000324.
- Weisman, J. and Kang, S. Y. (1981) 'Flow pattern transitions in vertical and upwardly inclined lines', *International Journal of Multiphase Flow*, 7(3), pp. 271–291. doi: 10.1016/0301-9322(81)90022-7.
- Wong, S. F., Lim, J. S. and Dol, S. S. (2015) 'Crude oil emulsion: A review on formation, classification and stability of water-in-oil emulsions', *Journal of Petroleum Science and Engineering*, 135(1), pp. 498–504. doi: 10.1016/j.petrol.2015.10.006.
- Xu, X.-X. (2007) 'Study on oil–water two-phase flow in horizontal pipelines', *Journal of Petroleum Science and Engineering*, 59(2), pp. 43–58. doi: 10.1016/j.petrol.2007.03.002.

- 
- Yeo, L. Y., Matar, O. K., Perez de Ortiz, E. S. and Hewitt, G. F. (2002) 'A simple predictive tool for modelling phase inversion in liquid–liquid dispersions', *Chemical Engineering Science*, 57(6), pp. 1069–1072. doi: 10.1016/S0009-2509(01)00443-2.
- Yusuf, N., Al-Wahaibi, Y., Al-Wahaibi, T., Al-Ajmi, A., Olawale, A. S. and Mohammed, I. A. (2012) 'Effect of oil viscosity on the flow structure and pressure gradient in horizontal oil–water flow', *Chemical Engineering Research and Design*. Institution of Chemical Engineers, 90(8), pp. 1019–1030. doi: 10.1016/j.cherd.2011.11.013.
- Zapke, A. and Kröger, D. G. (2000) 'Countercurrent gas–liquid flow in inclined and vertical ducts — I: Flow patterns, pressure drop characteristics and flooding', *International Journal of Multiphase Flow*, 26(9), pp. 1439–1455. doi: 10.1016/S0301-9322(99)00097-X.
- Zigrang, D. J. and Sylvester, N. D. (1982) 'Explicit approximations to the solution of Colebrook's friction factor equation', *AIChE Journal*, 28(3), pp. 514–515. doi: 10.1002/aic.690280323.

---

# APPENDICES

## *Appendix A Operational and Health & Safety Information (1-Inch Rig)*

### *A.1 Safety for Operators*

All operators must be authorised PSE Lab users and have undergone a full Health & Safety induction which covers the general School of Water, Environment & Energy and specific PSE Lab procedures to be followed in an emergency. Specific training for the 1-inch facility is also provided to the user by the lab manager before taking the lead in an experiment. To reduce the likelihood of accidents, the supervisor must ensure that all staff and researchers who will operate the rig:

- Have received comprehensive training to operate the facility
- Have an understanding of the content of the general risk assessment.
- Use the Personal Protective Equipment (PPE) detailed in the general risk assessment when working on the test rig.
- Use the PPE detailed in the relevant COSHH form when handling any of the substances used in the test rig.

### *A.2 Regular Checks*

A visual inspection of the rig area should always be performed before rig start-up, at regular intervals during operation, and after shutdown to detect any leaks and defects promptly. If any leakage or spill is detected, it should be cleaned up immediately, following the normal PSE Lab procedures. A spill kit for minor spills must be readily accessible and regularly checked to ensure supplies are topped up.

### *A.3 Waste Disposal*

Liquid waste generated during the experiments (i.e. oil-contaminated water) will be put into designated containers for temporary storage. The technicians will advise which container(s) are currently in use. The waste will be disposed of using the university's approved waste contractors.

---

#### ***A.4 Pre-Test Checks***

Before undertaking any new experiments, the following checks must be conducted:

- i. A visual inspection of the test sections for defects. Any defects must be rectified and inspected again.
- ii. Always ensure all valves are initially closed, RV-1 is turned to zero, and all PCP dial controls are set to minimum before opening the corresponding valves and pumps for each desired flow type.
- iii. Test the water pump by opening BV-1 and DV-1 and turn on the water pump isolation switch to initiate PCP-1. Allow the pump to circulate the water within the water tank. Allow the pump to circulate the oil within the oil tank.
- iv. Test the oil pump by opening BV-2, DV-5, and BV2W-1 returning to the tank and turn on the oil pump isolation switch to initiate PCP-2. Allow the pump to circulate the oil within the oil tank.
- v. Check if the DAS is running correctly against all connected measurement instruments.
- vi. Adjust the height of the oil return pump within the separator under the water and oil combined volume. For best separation, ensure the intake of the oil return pump is above the oil-water interface by approximately 0.05m.

#### ***A.5 Normal Operating Procedure***

The normal operations of the 1-inch rig are as follows:

1. Switch on the computer and operate the LabVIEW® software to monitor all individual phase flowrates and automatically activate SV-1 on the airline.
2. To flow air:
  - a. Switch on the air electrical isolator and then switch on the laboratory air compressor.

- 
- b. Open the following valves in the airflow line to inject air through the test section, BV-6 (gradually), BV-7, BV-8, BV-9, set RV-1 between 2-3 barg, BV-12, DV-7, BV-5, and BVW2-2 towards BV-5.
  - c. Set the valve appropriately, based on **ONLY ONE** of the airflow requirements for the corresponding experiment.
    - i. For air, the flowrate ranges from  $3 - 100m^3/h$ ; adjust BV-10 in the 1-inch flow line to inject the required flowrate.
    - ii. For air, the flowrate ranges from  $0 - 3m^3/h$ ; adjust BV-11 in the 0.5-inch airflow line to inject the required flowrate.
  - c. Adjust to the desired air flowrate using NV-1 and use the DAS software to read the air flowrate as a reference.
  - d. Record data from the DAS.
3. To flow water:
- a. Set the valves in the water flow line and test section appropriately to loop water around the rig: Open BV-1, BV-5, DV-2, DV-3, DV-4 and BVW2-2 towards BV-5.
  - b. Switch on the water electrical isolator to switch on PCP-1.
  - c. Adjust the desired water flowrate through the corresponding pump dials and use the DAS software to read the water flowrate as a reference.
  - d. Record data from the DAS.
  - e. Return the water from the separator to the water tank by switching on PCP-3.



- 
4. To flow oil:
    - a. Turn on the mixer and chiller as it is submersed in the oil tank to alter/maintain oil temperature and viscosity if required. Depending on the oil type and desired temperature, wait for several minutes to several hours to take effect.
    - b. To flow oil with other fluids or on its own within the test section: Open BV-2, BV-5, DV-6, BV2W-1 (to test section) and BVW2-2 (to BV-5).
    - f. Switch on the oil electrical isolator to switch on PCP-2.
    - g. Adjust the desired oil flowrate through the corresponding pump dials and use the DAS software to read the oil flowrate as a reference.
    - h. Record data from the DAS.
    - i. Return the oil from the separator to the oil tank using PCP-4.

### ***A.6 In-situ Water Hold-up Measurement Procedure***

In-situ water hold-up sampling starts after the data collection from the pressure transducers is recorded and finalised before the test is shut down.

1. Open the sampling port by opening BV2W-2, immediately followed by closing BV-5.
2. Open BV-4 to let fluids flow out into a 1000ml graduated cylinder.
3. After a majority of the fluids are removed from the closed-off section, use the 1/4-inch air lines to flush the remaining fluids out into the cylinder.
4. Switch on the air electrical isolator and then switch on the laboratory air compressor.
5. Open the following valves in the airflow line to inject air through the closed-off section, BV-6 (gradually), BV-7, BV-8, BV-9, set RV-1 between 2-3 barg, BV-13 and BV-14.
6. Close BV-6 (gradually), BV-7, BV-8, BV-9, RV-1, BV-13 and BV-14.
7. Conduct hold-up measurements, and record the data.
8. Open valves BV-5 and switch BVW2-2 to flow towards BV-5.

---

## ***A.7 ECT Configuration and Analysis***

The ETC and its constituent DAS unit are used to perform this specific data collection. The following must be completed before using the ECT.

1. Ensure the MMTC software is installed on a device that is connected to the ECT DAS unit via a high-speed USB 2.0 connection.
2. Ensure all program extensions and files are saved in a single spot for data import and export within the software.
3. Ensure the ECT sensor cables are correctly connected to the ECT DAS unit.
4. Turn on the DAS unit and leave it on for at least 30 minutes before use.
5. Before using the ECT, fluid capacitance calibrations must be set for each fluid configuration in use. This step only needs to be conducted once, and the calibration file can be repeatedly used for the same test fluids:
  - a. Fill the entire test section pipeline with water at the lowest possible flowrate and record the highest capacitance range. Ensure no bubbles or foreign bodies are present within the stream.
  - b. Fill the entire test section pipeline with oil at the lowest possible flowrate and record the lowest capacitance range. Ensure no bubbles or foreign bodies are present within the stream.
6. Set calibration conditions per the test specifications of the experiment and save the calibration file in the same folder location as the extension files.
7. Once steps 1-6 are complete, the ECT can be used in parallel with the DAS recordings during the experiment.
8. Once the recording is completed, the respective ECT data is then viewed/analysed via the Toolsuite software. This only requires the data file to function (ECT – DAS unit connection is not required). Images and videos can be developed from this.

---

## **A.8 Sample Collection**

Fluid samples can be gathered during the operational procedure upstream or downstream of the test section by opening one of the BV-3 and/or BV-4, respectively and contain the fluids through a graduated cylinder. Close the selected valves after a required amount of sample is collected.

## **A.9 Normal Shutdown Procedure**

Once the required data has been collected after a successful run completion, and a shutdown is required, perform the following steps in chronological order:

1. Stop data recording.
2. If running, switch off PCP-2 and close BV-2.
3. Allow water to run through the test section for 5 minutes to wash away the other fluids from the internal walls of the test pipe. If the water is not running, refer to A.5 (3a-3c).
4. Switch off PCP-1 and close BV-1.
5. Allow air to run through the test section for 5 minutes to wash away the other fluids from the internal walls of the test pipe to remove any water droplets from the internal walls of the test pipe. If the air system is not running, refer to A.5 (2a-2d).
6. Switch off the compressor and close all gas valves by turning off BV-6, BV-7, BV-8, BV-9 or BV-10, BV-11, NV-1, DV-7, and set RV-1 to *0barg*.
7. Ensure all the test fluids are located back in their constituent storage tanks and large volumes of these test fluids are not present in the separator by running PCP-3 and PCP-4 for water and oil, respectively. **IMPORTANT:** Ensure PCP-4 is adjusted beforehand to compensate for any changes in the interface height.
8. Switch off PCP-3 and PCP-4.
9. Switch off the chiller and mixer within the oil tank and close all remaining valves and electrical isolators.
10. Switch off the DAS and computer.
11. Check the test facility for any leaks/spills. If any are found, fix/clean it up.

---

### ***A.10 Emergency Shutdown Procedure***

In the instance of any abnormal or dangerous facility behaviour is present which will compromise the rig safety for the operator and others within the lab, the following steps should be carried out:

1. Push the emergency stop button. This is located near the main DAS for the 1-inch rig on the electrical box. Once activated, this will cut out all electrical power to pumps and the solenoid valve to completely restrict all fluid flow of the rig.
2. Report the incident to the laboratory technicians or authorised coordinator.

### ***A.11 Additional References***

The following list is a reference to the additional required safety and technical information found in the university archives.

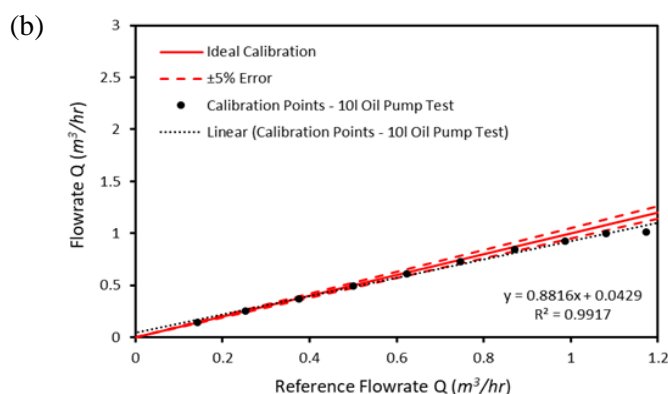
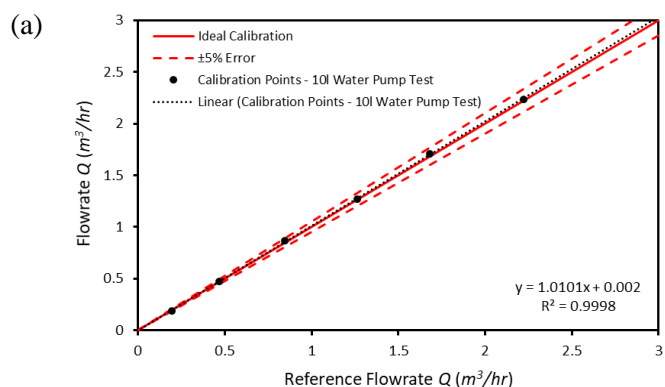
1. ITS M3000 V2.9 Manual.
2. ITS Toolsuite V7.4 Manual.
3. Cranfield University Health & Safety Induction.
4. Working in the PSE Laboratory guide.
5. RA-2479-0920 Operation of 1-inch multiphase rig in PSE Lab.
6. COSHH-1919-0920 Experimental use of EDM250 and H100 oils within the 1-inch multiphase rig (PSE Lab).

Please refer to the laboratory manager, online search or university online portals to source all required documentation or other oil COSHH documents not stated.

## Appendix B PCP Calibrations (1-Inch Rig)

To calibrate the oil and water pumps that deliver the constituent test fluids around the flow loop, a calibration check must be made to ensure incorrect flowrates and superficial velocities are not established. The flow loop separator was used to measure the volume of the fluids displaced during testing, where predetermined volume lines in increments of 10l were implemented on the viewing window of the separator. Between six to ten random speeds are tested where a stopwatch was used to time how long it would require each variable speed to displace 10l of fluid. Hence, the theoretical flowrate could then be determined by the amount of fluid over the time required to displace the focused volume. Furthermore, the DAS flowrate is also used as a reference to determine the offset of the output data. Finally, to avoid the possibility of human error, the oil test was repeated while increasing the timed volume displacement requirement from 10l to 20l because of the ongoing changes in fluid properties due to temperature. Additionally, readings from the individual flowmeter and DAS outputs were used as references.

### B.1 Oil and Water PCP Calibration (10l Test)



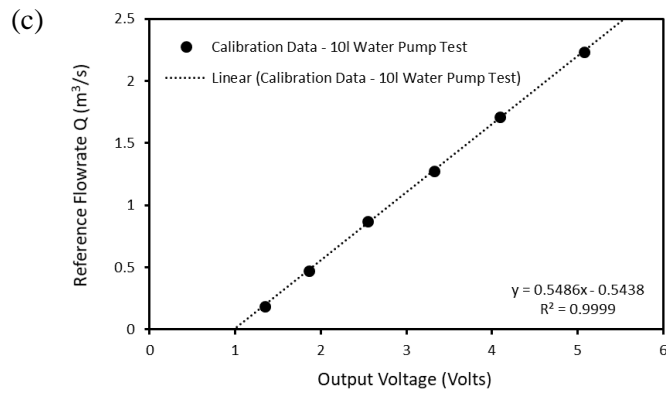


Figure Apx B-1: (a) Water PCP-1 Calibration at 10l sequences for each flowrate test (b) oil PCP-2 Calibration at 10l sequences for each flowrate test and (c) voltage output for water PCP-1 calibration at 10l sequences for each flowrate.

## B.2 Oil PCP Calibration (20 l Test)

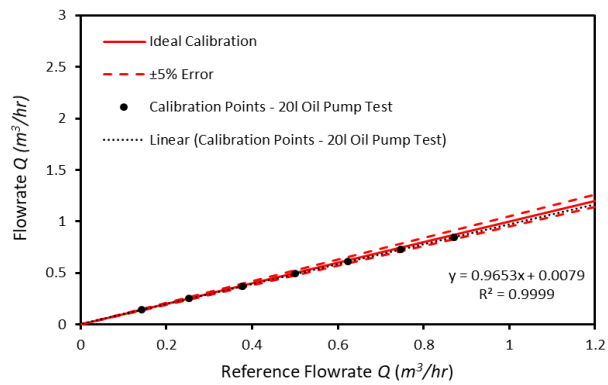


Figure Apx B-2: Oil PCP-2 Calibration at 20l sequences for each flowrate test.

## Appendix C Pressure Transducer Calibrations

The pressure transducers were tested against a reference transducer which was recalibrated accordingly for accurate analysis. Each DAS cable for each transducer is connected to a pressure calibrator where the required pressure is incrementally set based on the limits of the pressure transducer and split evenly between a single volt. The output voltage is recorded through the DAS and plotted against the calibration to determine any offsets of the pressure outcome.

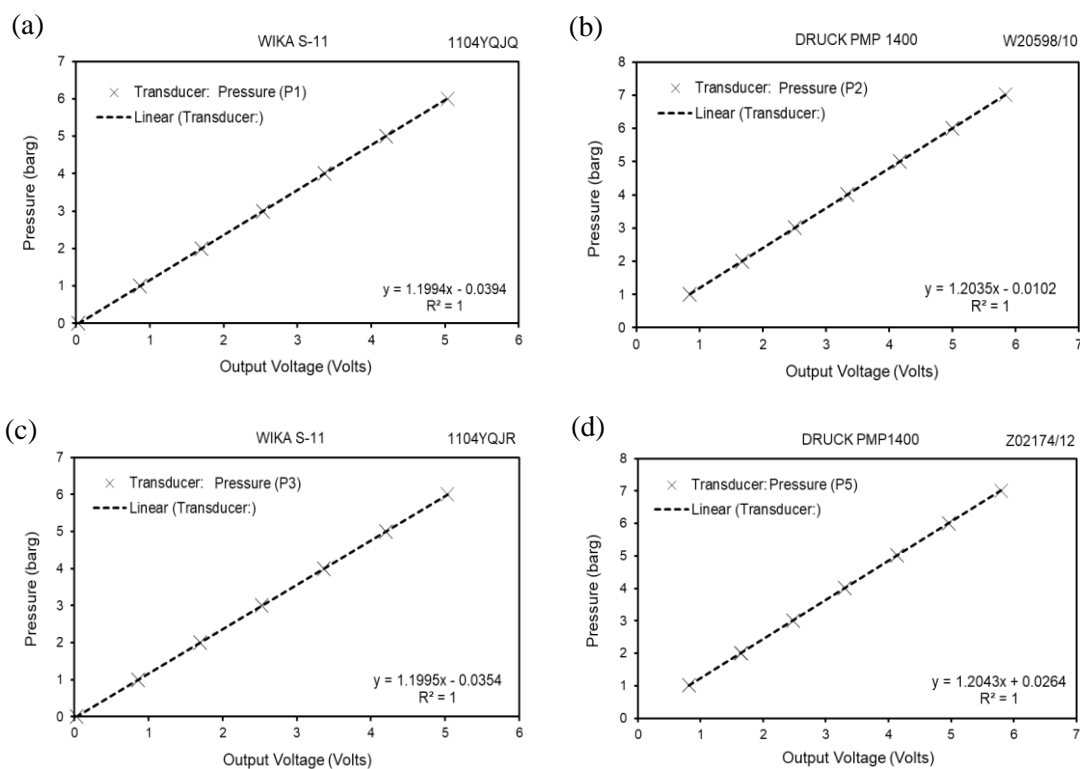


Figure Apx C-1: (a) P1 WIKA S-11 pressure transducer calibration, (b) P2 DRUCK PMP1400 pressure transducer calibration, (c) P3 WIKA S-11 pressure transducer calibration and (d) P5 DRUCK PMP1400 pressure transducer calibration.

---

## Appendix D Remaining FFT Analysis Graphs Intermittent Flows

As previously shown in section 4.6, the FFT frequency analysis was partially shown for comparative analysis of the plug and slug flow regimes. All FFT analysis tables for each intermittent flow regime found within this study are presented.

### D.1 EDM250 0° Pipe Incline

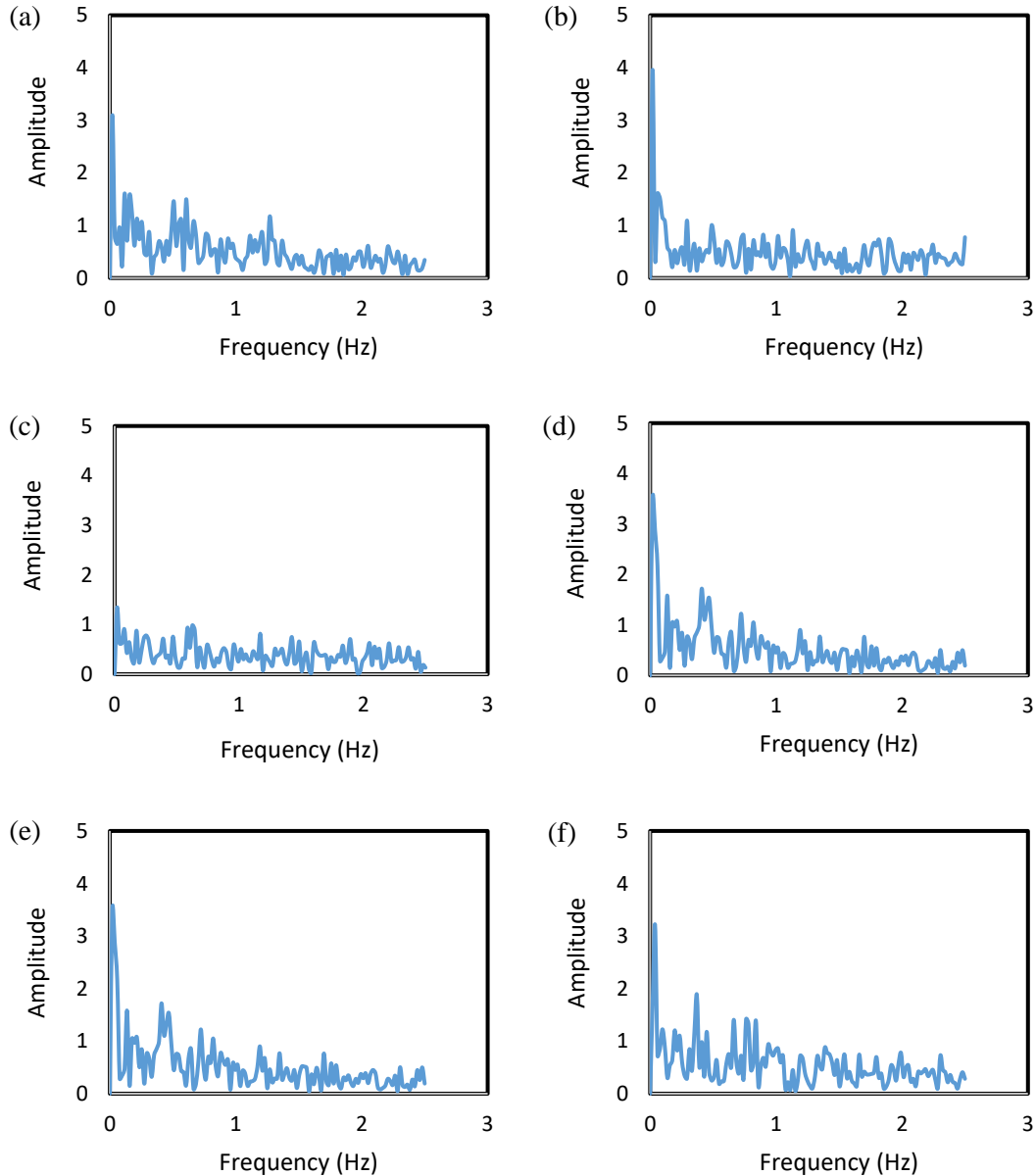
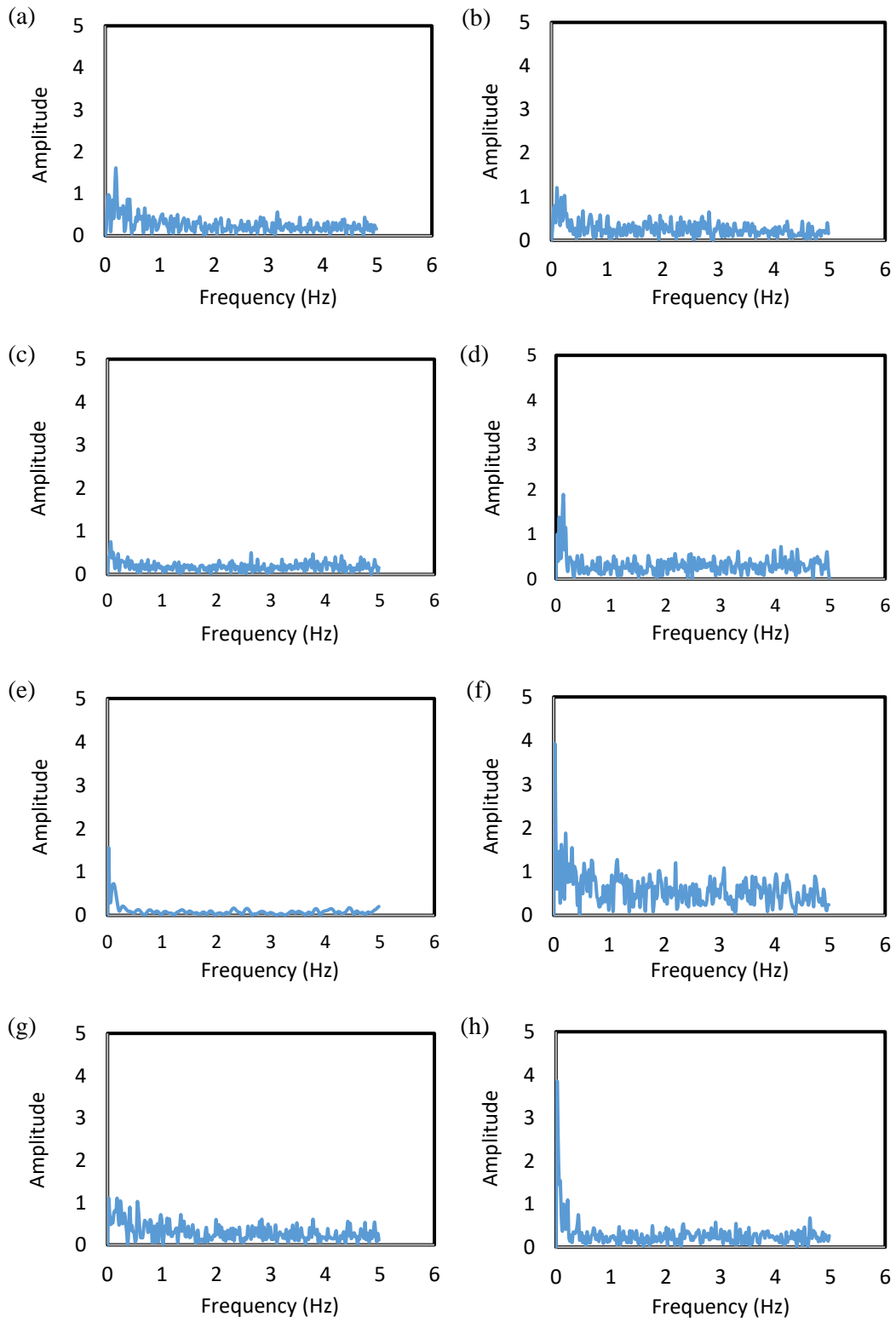


Figure Apx D-1: Intermittent flow frequency analysis of EDM250 (light oil) at 0° pipe inclination at experimental conditions of, (a)  $v_{sw} = 0.45\text{m/s}$   $v_{so} = 0.10\text{m/s}$ , (b)  $v_{sw} = 0.50\text{m/s}$   $v_{so} = 0.10\text{m/s}$ , (c)  $v_{sw} = 0.55\text{m/s}$   $v_{so} = 0.10\text{m/s}$ , (d)  $v_{sw} = 0.60\text{m/s}$   $v_{so} = 0.10\text{m/s}$ , (e)  $v_{sw} = 0.50\text{m/s}$   $v_{so} = 0.15\text{m/s}$  and (f)  $v_{sw} = 0.55\text{m/s}$   $v_{so} = 0.15\text{m/s}$ .



---

## D.2 EDM250 5° Pipe Incline



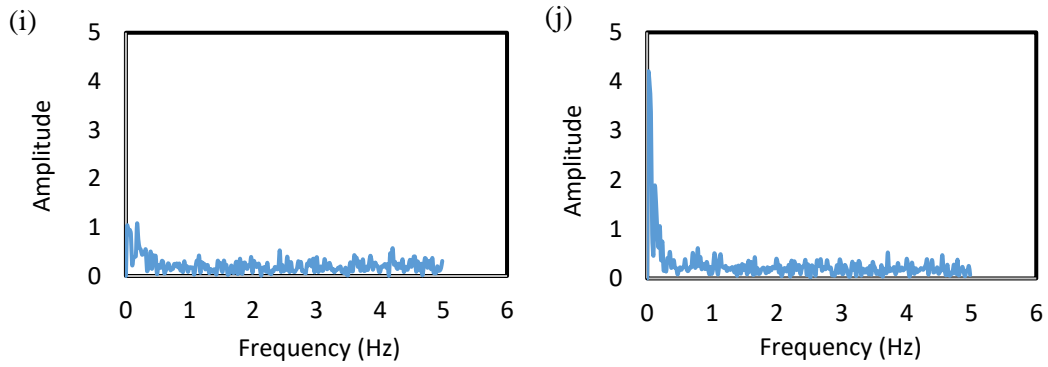
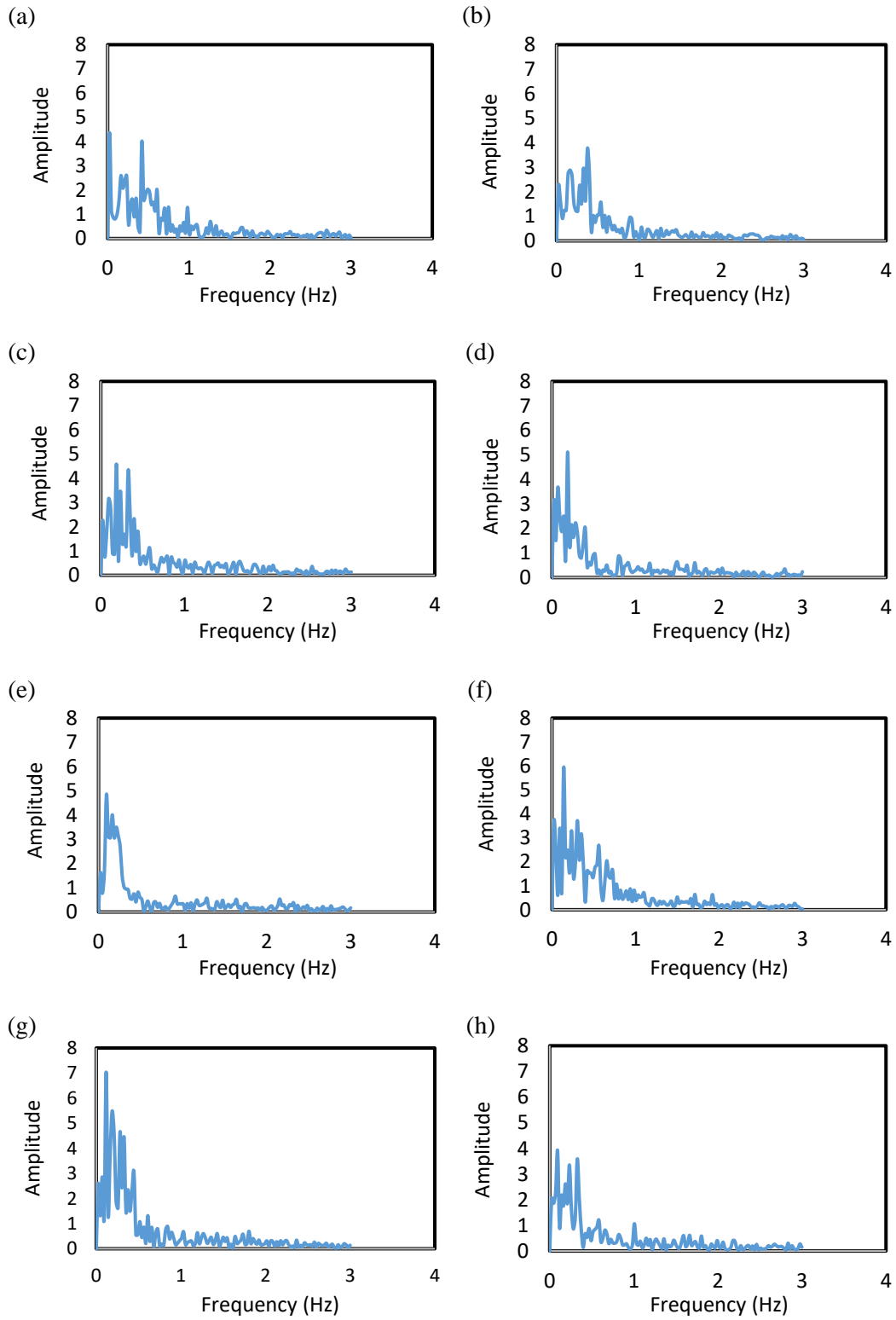


Figure Apx D-2: Intermittent flow frequency analysis of EDM250 (light oil) at 5° pipe inclination at experimental conditions of, (a)  $v_{sw} = 0.40\text{m/s}$   $v_{so} = 0.10\text{m/s}$ , (b)  $v_{sw} = 0.45\text{m/s}$   $v_{so} = 0.10\text{m/s}$ , (c)  $v_{sw} = 0.50\text{m/s}$   $v_{so} = 0.10\text{m/s}$ , (d)  $v_{sw} = 0.55\text{m/s}$   $v_{so} = 0.10\text{m/s}$ , (e)  $v_{sw} = 0.60\text{m/s}$   $v_{so} = 0.10\text{m/s}$ , (f)  $v_{sw} = 0.65\text{m/s}$   $v_{so} = 0.10\text{m/s}$ , (g)  $v_{sw} = 0.45\text{m/s}$   $v_{so} = 0.15\text{m/s}$ , (h)  $v_{sw} = 0.50\text{m/s}$   $v_{so} = 0.15\text{m/s}$ , (i)  $v_{sw} = 0.55\text{m/s}$   $v_{so} = 0.15\text{m/s}$  and (j)  $v_{sw} = 0.60\text{m/s}$   $v_{so} = 0.15\text{m/s}$ .

---

### D.3 H100 0° Pipe Incline



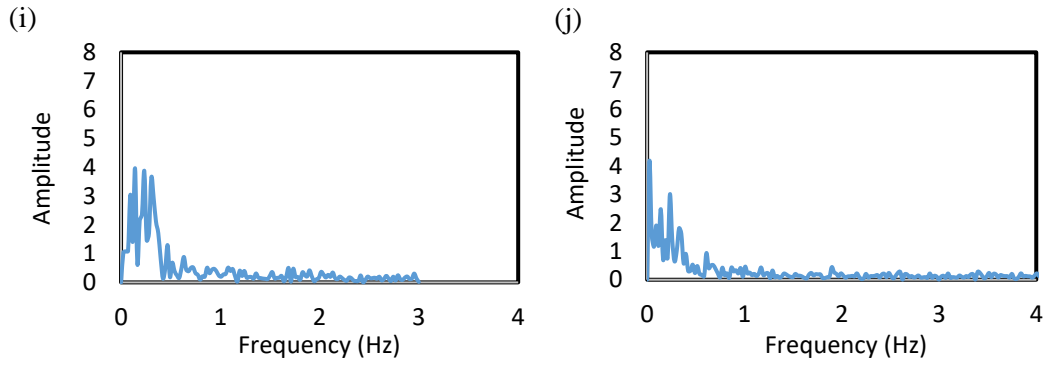
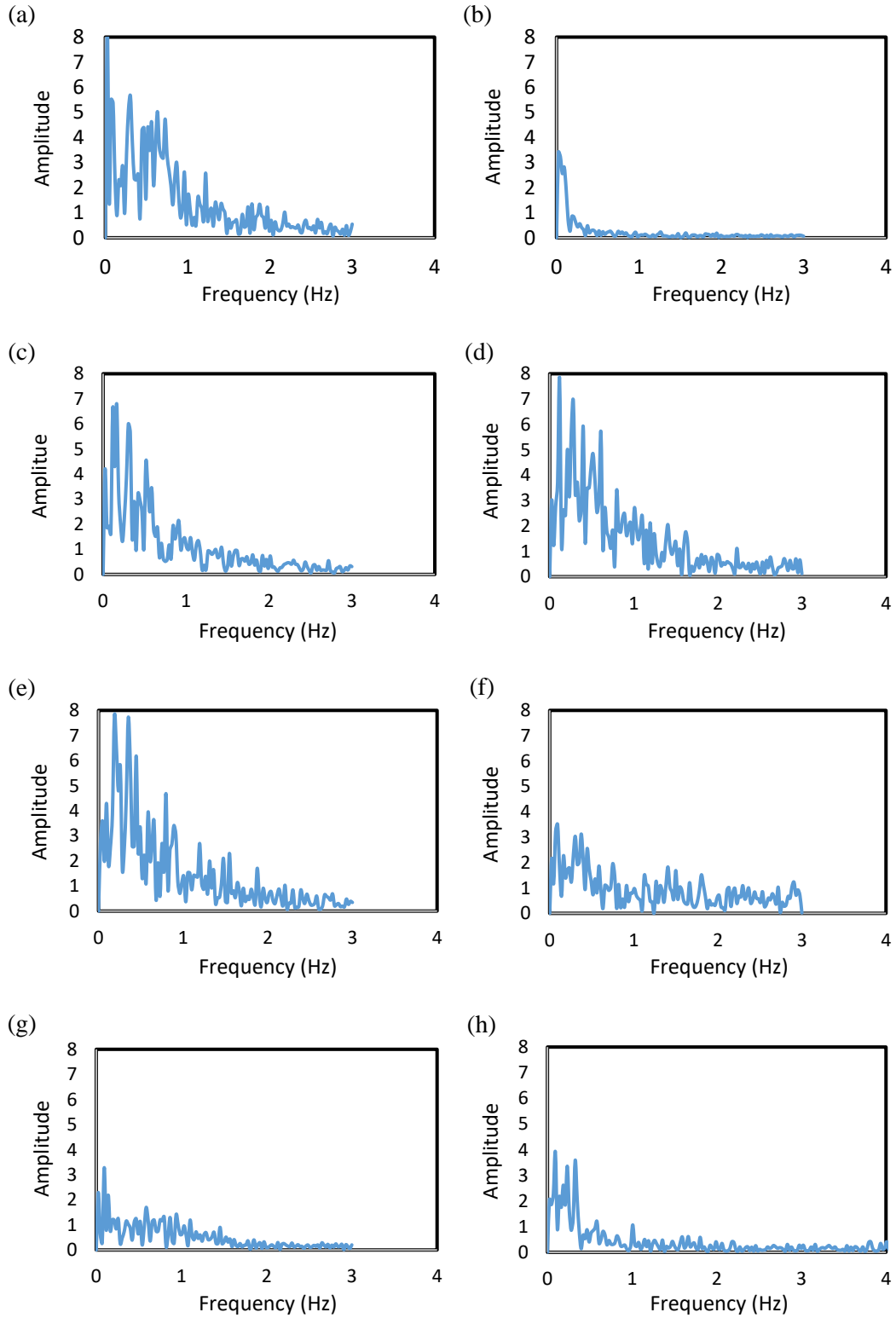
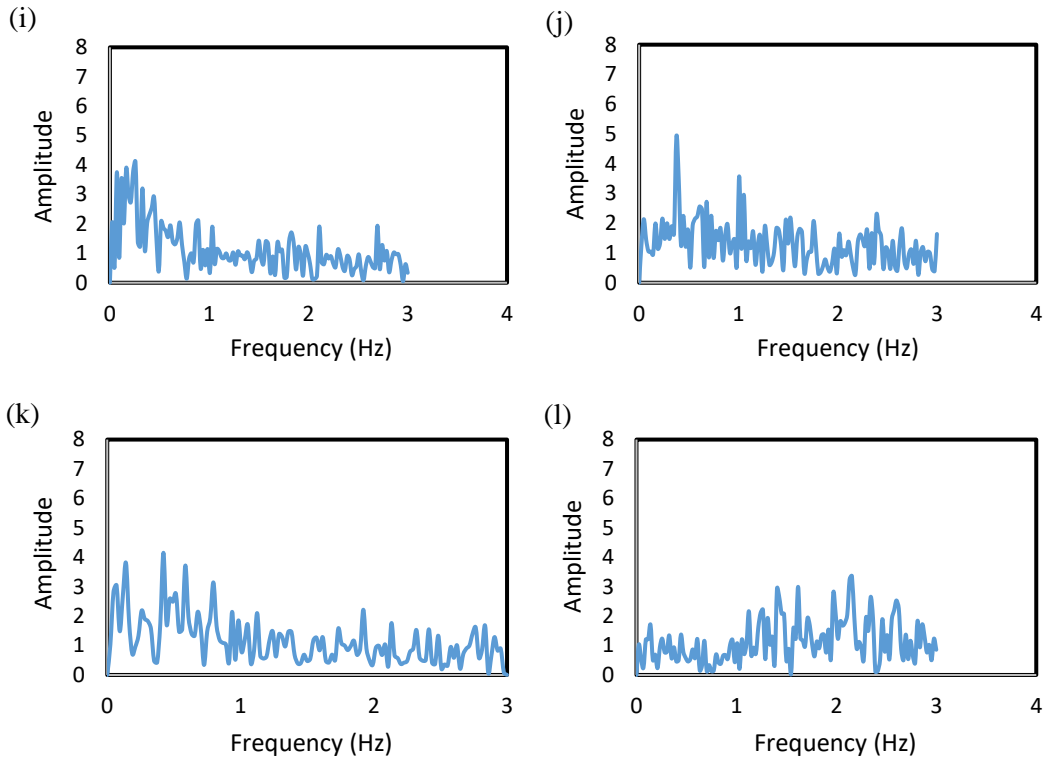


Figure Apx D-3: Intermittent flow frequency analysis of H100 (heavy oil) at  $0^\circ$  pipe inclination at experimental conditions of, (a)  $v_{sw} = 0.30\text{m/s}$   $v_{so} = 0.10\text{m/s}$ , (b)  $v_{sw} = 0.34\text{m/s}$   $v_{so} = 0.10\text{m/s}$ , (c)  $v_{sw} = 0.40\text{m/s}$   $v_{so} = 0.10\text{m/s}$ , (d)  $v_{sw} = 0.45\text{m/s}$   $v_{so} = 0.10\text{m/s}$ , (e)  $v_{sw} = 0.50\text{m/s}$   $v_{so} = 0.10\text{m/s}$ , (f)  $v_{sw} = 0.34\text{m/s}$   $v_{so} = 0.15\text{m/s}$ , (g)  $v_{sw} = 0.40\text{m/s}$   $v_{so} = 0.15\text{m/s}$ , (h)  $v_{sw} = 0.45\text{m/s}$   $v_{so} = 0.15\text{m/s}$ , (i)  $v_{sw} = 0.51\text{m/s}$   $v_{so} = 0.15\text{m/s}$  and (j)  $v_{sw} = 0.55\text{m/s}$   $v_{so} = 0.15\text{m/s}$ .

---

## D.4 H100 5° Pipe Incline





*Figure Apx D-4: Intermittent flow frequency analysis of H100 (heavy oil) at 5° pipe inclination at experimental conditions of, (a)  $v_{sw} = 0.25\text{m/s}$   $v_{so} = 0.10\text{m/s}$ , (b)  $v_{sw} = 0.30\text{m/s}$   $v_{so} = 0.10\text{m/s}$ , (c)  $v_{sw} = 0.35\text{m/s}$   $v_{so} = 0.10\text{m/s}$ , (d)  $v_{sw} = 0.40\text{m/s}$   $v_{so} = 0.10\text{m/s}$ , (e)  $v_{sw} = 0.45\text{m/s}$   $v_{so} = 0.10\text{m/s}$ , (f)  $v_{sw} = 0.50\text{m/s}$   $v_{so} = 0.10\text{m/s}$ , (g)  $v_{sw} = 0.30\text{m/s}$   $v_{so} = 0.15\text{m/s}$ , (h)  $v_{sw} = 0.35\text{m/s}$   $v_{so} = 0.15\text{m/s}$ , (i)  $v_{sw} = 0.40\text{m/s}$   $v_{so} = 0.15\text{m/s}$ , (j)  $v_{sw} = 0.45\text{m/s}$   $v_{so} = 0.15\text{m/s}$ , (k)  $v_{sw} = 0.50\text{m/s}$   $v_{so} = 0.15\text{m/s}$  and (l)  $v_{sw} = 0.55\text{m/s}$   $v_{so} = 0.15\text{m/s}$ .*